



# CENTER FOR INFRASTRUCTURE ENGINEERING STUDIES

## **Masonry Reinforced with FRP Systems**

By

**Stefano Secondin**

University of Missouri-Rolla

**CIES  
03-43**

### Disclaimer

The contents of this report reflect the views of the author(s), who are responsible for the facts and the accuracy of information presented herein. This document is disseminated under the sponsorship of the Center for Infrastructure Engineering Studies (CIES), University of Missouri -Rolla, in the interest of information exchange. CIES assumes no liability for the contents or use thereof.

The mission of CIES is to provide leadership in research and education for solving society's problems affecting the nation's infrastructure systems. CIES is the primary conduit for communication among those on the UMR campus interested in infrastructure studies and provides coordination for collaborative efforts. CIES activities include interdisciplinary research and development with projects tailored to address needs of federal agencies, state agencies, and private industry as well as technology transfer and continuing/distance education to the engineering community and industry.

Center for Infrastructure Engineering Studies (CIES)

University of Missouri-Rolla  
223 Engineering Research Lab  
1870 Miner Circle  
Rolla, MO 65409-0710  
Tel: (573) 341-6223; fax -6215  
E-mail: [cies@umr.edu](mailto:cies@umr.edu)  
[www.cies.umr.edu](http://www.cies.umr.edu)

## ABSTRACT

The worldwide engineering community has identified failures of URM walls as one of the major causes of material damage and loss of human life due to seismic events. Therefore, the development of effective and affordable retrofitting techniques for masonry members is an urgent need. Fiber Reinforced Polymer (FRP) composites provide solutions for the strengthening of URM walls subjected to in-plane and out-of-plane overstresses caused by high wind pressures or earthquake loads. The presented research, part of the effective collaboration between the Department of Construction and Transportation (DCT) of University of Padua (Italy) and the Center for Infrastructure Engineering Studies (CIES) of University of Missouri-Rolla (U.S.A.), deals with the mechanical behavior of masonry walls strengthened with FRP composites with the technique NSM and subjected to out-of-plane and in-plane loading. Two series of walls were tested for this research study. The first series studied the behavior of masonry wallettes under out-of-plane loads; the second series analyzed the performance in terms of shear capacity of masonry panels. FRP composites in the form of rectangular and circular cross section bars were used as strengthening materials. The results showed that both flexural and shear capacity of masonry walls can be notably increased by strengthening with FRP composites.

Analytical models to predict the behavior of strengthened walls, as well as provisional guidelines to design the FRP strengthening for shear and flexure are also presented. Finally, conclusions are provided and future research needs on the area of masonry strengthening are outlined.

## RIASSUNTO

La maggioranza degli ingegneri ha identificato il crollo dei muri in muratura non rinforzati (URM) come una delle cause principali per danni e perdita di vita umana durante un evento sismico. Per questo motivo, è necessario lo sviluppo di una tecnica di rinforzo murario efficace ed affidabile. I materiali compositi fibro rinforzati a matrice polimerica (FRP) forniscono una vasta gamma di soluzioni nel campo del rinforzo strutturale di pannelli murari URM, sottoposti a carichi di tipo in-plane e out-of-plane, dovuti ad elevate condizioni di vento o terremoti.

Questa ricerca si pone come sviluppo di un programma iniziato qualche anno fa grazie alla collaborazione tra l'Università degli Studi di Padova e l'Università del Missouri-Rolla sull'utilizzo di materiali compositi FRP nel rinforzo murario con la tecnica del Near Surface Mounted. Due serie di muri sono stati testati in questo programma sperimentale: la prima studiava il comportamento di provini soggetti a taglio, la seconda a flessione. Come rinforzo sono state usate barre di FRP al Carbonio e al Vetro, a sezione circolare (diametri 5, 6 e 9 mm) e rettangolare (15 per 2 mm). Sono stati presi in considerazione diversi tipi di mattone (argilla e cemento) e diversi materiali da incasso (materiali che hanno il compito di legare la barra alla muratura: pasta epossidica e pasta cementizia) e diverse scanalature.

I risultati hanno mostrato buoni incrementi in termini di resistenza al taglio e ottimi in termini di resistenza a flessione. I modelli analitici di progetto adottati hanno mostrato risultati ragionevoli e conservativi. Infine, vengono presentate conclusioni sui dati sperimentali e suggerimenti per eventuali sviluppi futuri.

# TABLE OF CONTENTS

ABSTRACT .....	1
TABLE OF CONTENTS .....	3
ACKNOWLEDGEMENTS .....	7
DEFINITIONS .....	9
NOTATIONS .....	13
UNITS OF MEASUREMENT .....	15
1. MASONRY .....	17
1.1 BACKGROUND .....	18
1.2 MASONRY IN THE UNITED STATES .....	23
1.2.1 Masonry in Backup Walls .....	23
1.3 MASONRY BUILDING SYSTEMS .....	26
1.3.1 Single-Story Loadbearing Buildings .....	26
1.3.2 Multistory Loadbearing Buildings .....	26
1.3.3 Hybrid Buildings .....	28
1.3.4 Panel, Curtain and Bearing Walls .....	28
1.4 MECHANICS PROPERTIES OF MASONRY ASSEMBLAGES .....	30
1.4.1 Axial Compression .....	30
1.4.2 Shear Strength along Mortar Bed Joint .....	31
1.4.3 In-plane Tensile Strength .....	33
1.4.4 Shear Strength for Out-of-Plane Loads .....	34
1.5 TRADITIONAL REPAIRING TECHNIQUES .....	35
1.5.1 Repointing .....	35
1.5.2 Grout Injection .....	36
1.5.3 Grout Filling of Hollow and Cavity Walls .....	36
1.5.4 External Reinforcing Overlay .....	37
1.5.5 Internal Steel Reinforcing .....	38
1.5.6 External Steel Plate Reinforcing .....	40
2. COMPOSITE MATERIALS .....	41
2.1 FRP STRUCTURE .....	42
2.1.1 Introduction .....	42
2.1.2 Resin Systems .....	46
2.1.3 Reinforcements .....	52
2.1.4 Manufacturing Processes .....	63
2.2 REINFORCEMENTS FORMS .....	66
2.2.1 Internal Reinforcement .....	67
2.2.2 External Reinforcement .....	70
2.3 PHYSICAL AND MECHANICAL PROPERTIES .....	74
2.3.1 Introduction .....	74
2.3.2 FRP Rebars .....	76
2.3.3 FRP Laminates, Sheets and Fabrics .....	80
2.3.4 Durability of FRP Composites .....	83
2.4 CONCLUSIONS .....	94
3. MATERIALS USED IN THE EXPERIMENTAL PROGRAM .....	97
3.1 INTRODUCTION .....	98
3.2 MASONRY UNITS .....	99
3.2.1 6 in.-Concrete Block (in-plane and out-of-plane tests) .....	100
3.2.2 4 in.-Concrete Block (out-of-plane test) .....	102
3.2.3 Clay Bricks Named “c11” .....	104

3.2.4 Clay Brick Named “cl2” .....	105
3.3 MORTAR.....	107
3.4 REINFORCING MATERIALS.....	109
3.4.1 Primer, Putty, Saturant, Paste.....	109
3.4.2 C, A and G FRP Laminates.....	110
3.4.3 GFRP Circular Cross Section Bars .....	111
3.4.4 GFRP Smooth Rods .....	113
3.4.5 GFRP Rectangular Bar (tape) .....	113
3.4.6 CFRP Rectangular Bar (tape) .....	115
3.4.7 Stainless Steel Rods .....	116
3.4.8 Internal Steel Wires.....	118
3.5 EPOXY PASTE, CEMENTITIOUS PASTE .....	120
3.5.1 Epoxy-Based Paste.....	120
3.5.2 Cementitious-Based Paste.....	120
3.5.3 Comparison.....	121
4. SHEAR STRENGTHENING OF MASONRY WALLS .....	125
4.1 INTRODUCTION .....	126
4.1.1 Infill walls .....	126
4.1.2 Failures Modes of URM Walls.....	130
4.2 EXPERIMENTAL PROGRAM .....	132
4.2.1 Test Specimens .....	132
4.2.2 Strengthening Procedure.....	134
4.2.3 Test Setup.....	136
4.2.4 Results: GT-3 and GT-5.....	137
4.2.5 Results: GSR-3 and GSR-7.....	144
4.2.6 Summary .....	147
4.3 COMPARISON WITH PREVIOUS TESTS.....	149
4.4 ANALYTICAL WORK.....	151
4.4.1 FRP Bars Strengthening Computation.....	151
4.4.2 Computation of $V_f$ .....	151
4.4.3 Computation of $V_m$ .....	154
4.4.4 Theoretical / Experimental Results.....	155
4.4.5 FRP Laminates Strengthening Computation.....	157
4.4.6 Evaluation of new Coefficients for FRP Systems.....	158
4.4.7 Comparison Based on Pseudo-Ductility .....	161
4.5 DESIGN.....	165
4.5.1 Shear Strength Design.....	165
4.5.2 Example of Calculation of Nominal Shear Strength.....	165
4.6 PRELIMINARY CONCLUSIONS .....	168
5. FLEXURAL STRENGTHENING OF MASONRY WALLS .....	171
5.1 INTRODUCTION .....	172
5.2 TEST MATRIX .....	174
5.3 SPECIMEN PREPARATION .....	177
5.3.1 Application of the Strain Gages.....	177
5.3.2 Strengthening Procedure.....	177
5.4 TEST SETUP.....	179
5.5 TEST RESULTS.....	182
5.5.1 Sigle used and summary of the main materials.....	182
5.5.2 Glass and Carbon FRP Rectangular Bars .....	183
5.5.3 Glass FRP Rods #2 Embedded with Epoxy Paste in a Groove 2.25 Times the Rod Diameter.....	187

5.5.4 Glass FRP Rods #3 Embedded with Cementitious Modified Paste in a Groove 2.25 Times the Rod Diameter .....	189
5.5.5 Glass FRP Rods #2 Displaced Along the Mortar Joints .....	192
5.5.6 Glass FRP Rods #2 Displaced Along the Blocks .....	195
5.6 PREVIOUS RESULTS.....	197
5.7 MODES OF FAILURE.....	200
5.8 ANALYTICAL WORK.....	203
5.8.1 Computation of the maximum moment .....	203
5.8.2 Computation of the shear capacity in the blocks .....	208
5.8.3 Estimation of the shear strength in the joints (sliding-shear).....	212
5.8.4 Design Method.....	220
5.9 PRELIMINARY CONCLUSIONS .....	229
6. CONCLUSIONS AND FUTURE WORKS.....	231



## **ACKNOWLEDGEMENTS**

The author would like to acknowledge the Department of Structural and Transportations Engineering, Università degli Studi di Padova (Italy), and the Center for Infrastructures Engineering Studies, University of Missouri-Rolla (USA), that supported this study.

It has been a honour to work beside Dr. Antonio Nanni, Dr. Claudio Modena, Eng. Maria R. Valluzzi, Eng. Nestore Galati, Dr. Jaime Gustavo Tuliaman, Mr. Harold Martin, Mr. Jason Cox, Miss Abbiegayle Sherman.

Finally, he would to express his sincere gratitude to his parents, Virginia and Guerino, and to Rossella.

## ***RINGRAZIAMENTI***

*L'autore desidera ringraziare il Dipartimento di Costruzioni e Trasporti dell'Università degli Studi di Padova (Italia) e il Center for Infrastructures Engineering Studies, University of Missouri Rolla (USA), che hanno permesso e finanziato questa tesi.*

*E' stato un piacere e un onore lavorare al fianco dei proff. Antonio Nanni e Claudio Modena, degli ingegneri Maria Rosa Valluzzi, Nestore Galati e Jaime Gustavo Tuliaman, del prof. Harold Martin, nonché del signor Jason Cox e di Abbiegayle Sherman.*

*Vorrebbe infine esprimere la sua più sincera gratitudine ai genitori Virginia e Guerino, e a Rossella.*



## DEFINITIONS

The following definitions clarify terms that are not commonly used in reinforced concrete practice.

-A-

AFRP — Aramid-fiber-reinforced polymer.

Alkalinity — The condition of having or containing hydroxyl (OH<sup>-</sup>) ions; containing alkaline substances. In concrete, the initial alkaline environment has a pH above 12.

-B-

Bar, FRP — A composite material formed into a long, slender structural shape suitable for the internal reinforcement of concrete and consisting of primarily longitudinal unidirectional fibers bound and shaped by a rigid polymer resin material. The bar may have a cross section of variable shape (commonly circular or rectangular) and may have a deformed or roughened surface to enhance bonding with concrete.

Bidirectional laminate — Reinforced-polymer laminate with the fibers oriented in two directions in its plane; a cross laminate.

-C-

CFRP — Carbon-Fiber-Reinforced Polymer.

Coefficient of Thermal Expansion (CTE) — a measure of the relative change in linear dimension in a material based on a unit increase in temperature of that material. Note: Due to the anisotropy of FRPs, the CTE in the longitudinal direction of the rod is likely to be different from that measured in the transverse direction.

Composite — A combination of one or more materials differing in form or composition on a macroscale. Note: The constituents retain their identities; that is, they do not dissolve or merge completely into one another, although they act in concert. Normally, the components can be physically identified and exhibit an interface between one another.

Creep — Time dependent accumulation of strain under constant stress.

Cure — To irreversibly change the properties of a thermosetting resin by chemical reaction, such as, condensation, ring closure, or addition. Note: Cure can be accomplished by adding curing (cross-linking) agents with or without heat and pressure.

-D-

Debonding — A separation at the interface between the substrate and the reinforcing layer.

Deformability — The ratio of energy absorption (area under the moment-curvature curve) at ultimate strength level to the energy absorption at service level.

Delamination — A separation along a plane parallel to the surface, as in the separation of the layers of the FRP laminate from each other.

Development length — length of embedded reinforcement required to develop the tensile capacity.

Durability — The ability of a material to resist weathering action, chemical attack, abrasion, and other conditions of service.

-E-

E-glass — A family of glass with a calcium alumina borosilicate composition and a maximum alkali content of 2.0%. A general-purpose fiber that is used in reinforced polymers.

Epoxy — A thermosetting polymer that is the reaction product of epoxy resin and an amino hardener. (See also Epoxy resin.)

Epoxy resin — A class of organic chemical-bonding systems used in the preparation of special coatings or adhesives for concrete as binders in epoxy-resin mortars and concretes.

-F-

Fatigue life — The number of cycles of deformation or load required to bring about failure of a material, test specimen, or structural member.

Fatigue strength — The greatest stress that can be sustained for a given number of load cycles without failure.

Fiber — Any fine thread-like natural or synthetic object of mineral or organic origin. Note: This term is generally used for materials whose length is at least 100 times its diameter.

Fiber, aramid — Highly oriented organic fiber derived from polyamide incorporating into aromatic ring structure.

Fiber, carbon — Fiber produced by heating organic precursor materials containing a substantial amount of carbon, such as rayon, polyacrylonitrile (PAN), or pitch in an inert environment.

Fiber, glass — Fiber drawn from an inorganic product of fusion that has cooled without crystallizing.

Fiber content — The amount of fiber present in a composite. Note: This is usually expressed as a percentage volume fraction or weight fraction of the composite. Due to differing constituent densities, weight fractions and volume fractions of fibers are not the same.

Fiber-Reinforced Polymer (FRP) — Composite material consisting of continuous fibers impregnated with a fiber-binding polymer then molded and hardened in the intended shape.

Fiber volume fraction — The ratio of the volume of fibers to the volume of the composite.

Fiber weight fraction — The ratio of the weight of fibers to the weight of the composite.

-G-

Gauge length — Also gage length; the distance between two gauge points on the test section, over which the percentage of elongation is determined (used for tensile tests).

GFRP — Glass-Fiber-Reinforced Polymer (see glass fiber).

Glass fiber — An individual filament made by drawing or spinning molten glass through a fine orifice. A continuous filament is a single glass fiber of great or indefinite length. A staple fiber is a glass fiber of relatively short length, generally less than 17 in. (0.43 m), the length related to the forming or spinning process used.

Glass fiber, types — Alkali resistant (AR-glass), general purpose (E-glass), high strength (S-glass).

Glass transition temperature (T<sub>g</sub>) — The midpoint of the temperature range over which an amorphous material changes from (or to) a brittle, vitreous state to (or from) a plastic state.

-H-

Hybrid — A combination of two or more different fibers, such as carbon and glass or carbon and aramid, into a structure.

-I-

Impregnate — In the case of fiber-reinforced polymers, to saturate the fibers with resin.

-J- -K- -L- -M-

Matrix — In the case of fiber-reinforced polymers, the polymeric materials that serve to bind the fibers together, transfer load to the fibers, and protect them against environmental attack and damage due to handling.

-N- -O- -P-

Polymer — A high molecular weight organic compound, natural or synthetic, containing repeating units.

Pultrusion — A continuous process that combines pulling and extrusion for manufacturing composite sections that typically have a constant cross-sectional shape; the process consists of pulling a fiber material through a resin bath and then through a heated shaping die where the resin is cured.

-Q- -R-

Relaxation — The reduction of stress (or load) in a material under a constant state of strain (or deformation).

Relaxation rate — The absolute value of the slope of the relaxation curve at a given time. In particular, the relaxation value after 1 million hours is referred to as the million-hour relaxation rate.

Resin — A natural or synthetic, solid or semisolid, organic material of indefinite and often high molecular weight having a tendency to flow under stress, usually has a softening or melting range, and usually fractures conchoidally. Resin often refers to the mixed polymer component or matrix of the FRP.

Resin content — The amount of resin in a laminate, expressed as either a percentage of total mass or total volume.

Rod, FRP — Resin-bound construction mostly made of continuous fibers in the shape of a bar or tendon used to reinforce concrete uniaxially.

-S-

Sheet, FRP — FRP sheets are a major component of FRP system suitable for external strengthening of concrete structures. Sheets come in the physical form of dry, prepreg, and procured materials.

-T-

Tensile capacity — The maximum tensile load carried by test specimen prior to failure.

Thermoplastic — Resin that is not cross-linked; it generally can be repeatedly remelted and reshaped by the application of heat.

Thermoset — Resin that is formed by cross-linking polymer chains. Note: A thermoset cannot be melted and reshaped because the polymer chains form a three-dimensional network.

-U-

Ultimate strain — The change in length per unit length corresponding to the tensile capacity.

-V-

Vinyl esters — A class of thermosetting resins containing ester of acrylic, methacrylic acids, or both, many of which have been made from epoxy resin.

-W- -X- -Y- -Z-

## NOTATIONS

$A_f$	= cross-sectional area of FRP bar, mm <sup>2</sup>
$A$ or $A_m$	= net or gross (gross if not specified) cross-sectional area of masonry, mm <sup>2</sup>
$A_{mv}$	= net area for the horizontal section of the wall, mm <sup>2</sup> or also sq-in <sup>2</sup>
$b$	= width of the specimen, mm
$b_w$	= overall width of concrete or clay in a generic cross section of a masonry hollow wall
$c$	= distance from extreme compression fiber to neutral axis, mm
$C_d$	= shear strength coefficient (Unified Building Code, 1997)
$C_E$	= environmental reduction factor (ACI-440, 2000)
$d$	= in the in-plane test walls, distance between the two points, on the wall diagonal, considered in the pseudo-ductility computation, mm
$d$	= in the out-of-plane walls distance FRP reinforcement-extreme compression fiber, mm
$d_b$	= diameter of reinforcing bar, mm
$E_m$	= modulus of elasticity of the masonry, MPa
$E$ or $E_f$	= modulus of elasticity of FRP, MPa
$f_c$	= compressive stress in concrete or in masonry, MPa
$f'_c$	= maximum compressive strength of concrete, corresponding to $\epsilon'_c$ , MPa
$f'_d$	= diagonal stress of in-plane tensile strength, MPa
$f_f$	= stress in the FRP reinforcement in tension, MPa
$f_{fu}$	= allowable tensile strength of the FRP bar, $f_{fu} = k C_E f_{fu}^*$ , MPa
$f_{fu}^*$	= guaranteed ultimate tensile strength of the bar as reported by the manufacturer, MPa
$f'_m$	= specified compressive strength of masonry, estimated on the net area (concrete blocks) or on the gross area (clay bricks), MPa
$h$	= specimen length, mm
$h/t_m$	= slenderness ratio (wall height-to-wall thickness)
$k'$	= empirical ratio $E_m / f'_m$
$k$ or $k_m$	= bond dependent coefficient (from 0 to 1) used to limit the allowable FRP strain in the out-of-plane loads design
$l$	= length of the specimen, mm
$L_e$	= length at which the rod breaks, in the computation of $V_f$ , mm
$L_{TOT}$	= overall length of every bar in the $V_b$ computation, mm
$M_n$	= nominal flexural capacity
$M_u$	= flexural demand based on factored loads
$P$	= external load applied, kN
$P_{exp,u}$	= ultimate reached external applied load, kN
$P_{th,u}$	= theoretical ultimate load capacity, kN
$r_f$	= overall number of rod in a shear wall
$r_b$	= number of the rods in the bond-controlled region
$r_t$	= number of the rods in the rupture-controlled region
$SD$	= standard Deviation
$t$ or $t_m$	= overall thickness of a flexural member, mm
$T_g$	= glass transition temperature, °C or F
$V$	= shear, kN
$V_b$	= part of $V_f$ due to the bond-controlled region
$V_f$	= shear capacity provided by the reinforcement, kN

$V_{FRP}$	=	shear capacity provided by FRP laminates, kN
$V_m$	=	shear capacity provided by the masonry, kN
$V_n$	=	overall shear capacity of the system wall-reinforcement, theoretical or experimental (if experimental obtained dividing by 1.414 the external applied load), kN
$V_t$	=	part of $V_f$ due to the rupture-controlled region, kN
$V_{th,u}$	=	theoretical ultimate shear capacity, kN
$w$	=	width, mm
$x$	=	distance from the support, out-of-plane tests, mm
$\alpha_L, \alpha_T$	=	longitudinal and transverse coefficient of thermal expansion, 1/°C
$\alpha$	=	stress block width factor (by using the stress/strain parabola)
$\beta$	=	stress block depth factor (by using the stress/strain parabola)
$\delta_u, \delta_y$	=	horizontal displacements at ultimate and “yielding” point, mm (or in)
$\varepsilon_\theta$	=	strain associated to the wall compressed diagonal in in-plane tests, mm/mm (=in/in)
$\varepsilon_{90}$	=	strain associated to the wall tensile diagonal in in-plane tests, mm/mm (=in/in)
$\varepsilon_c$	=	strain in the concrete or in a compressive fiber, mm/mm (=in/in)
$\varepsilon_{c,u}$	=	maximum usable strain at the extreme compressive fiber, mm/mm (=in/in)
$\varepsilon'_c$	=	strain corresponding to the maximum compressive strain $f'_c$ in the parabola, mm/mm
$\varepsilon_c^*$	=	strain in the top fiber in a flexural member, mm/mm (=in/in)
$\varepsilon_f$	=	strain in the FRP reinforcement
$\varepsilon_{f,u}^*$	=	rupture strain of FRP reinforcement as reported by the manufacturer
$\varepsilon_{f,u}$	=	design rupture strain of FRP reinforcement
$\varepsilon_s$	=	strain in the centroid of tension reinforcement in a flexural member, mm/mm (=in/in)
$\varepsilon_u$	=	ultimate strain of FRP bar
$\Phi$	=	safety or reduction factor (value between 0 and 1)
$\kappa$ or $\kappa_m$	=	bond dependent coefficient (from 0 to 1); used to limit the allowable FRP strain in the in-plane loads design
$\gamma_u, \gamma_y$	=	shear strain at ultimate and at “yielding” point, mm/mm (=in/in)
$\mu$	=	coefficient of friction in the Mohr-Coulomb law
$\mu$	=	ductility and pseudo ductility of in-plane walls
$\rho_f$	=	ratio of FRP flexural reinforcement
$\sigma_n$	=	compressive stress normal to the bed joint in the Mohr-Coulomb law, MPa
$\tau$	=	bond or joint shear stress, MPa
$\tau_\theta$	=	shear bond strength in the Mohr-Coulomb law, MPa
$\tau_b$	=	pull-off bond strength between FRP bar and masonry, MPa
$\tau_{bl}$	=	allowable bond strength, $k \tau_b$ , MPa
$\gamma$	=	multiplier on $f'_m$ to determine the intensity of an equivalent block stress for masonry
$\omega$ or $\omega_f$	=	FRP reinforcement index

## UNITS OF MEASUREMENT

### CONVERSION FACTORS:

length	$1 \text{ cm} = 0.394 \text{ in}$ $1 \text{ m} = 3.28 \text{ ft}$ $1 \text{ m} = 1.094 \text{ yd}$ $1 \text{ km} = 0.621 \text{ mi}$	$1 \text{ in} = 25.4 \text{ cm}$ $1 \text{ ft} = 30.48 \text{ cm}$ $1 \text{ yd} = 91.444 \text{ cm}$ $1 \text{ mi} = 1609.34 \text{ m}$
mass	$1 \text{ g} = 0.0353 \text{ oz}$ $1 \text{ kg} = 2.205 \text{ lb}$	$1 \text{ oz} = 28.35 \text{ g}$ $1 \text{ lb} = 453.51 \text{ g}$
volume	$1 \text{ l} = 0.264 \text{ gal}$	$1 \text{ gal} = 3.7854 \text{ l}$
force	$1 \text{ N} = 0.2248 \text{ lbf}$ $1 \text{ kN} = 0.2248 \text{ kips}$	$1 \text{ lbf} = 4.44822 \text{ N}$ $1 \text{ kip} = 4.44822 \text{ kN}$
moment	$1 \text{ kNm} = 0.7376 \text{ k-ft}$	$1 \text{ k-ft} = 1.3558 \text{ kNm}$
stress	$1 \text{ MPa} = 145.04 \text{ psi}$ $1 \text{ MPa} = 0.145 \text{ ksi}$	$1 \text{ psi} = 6894.76 \text{ Pa}$ $1 \text{ ksi} = 6.89476 \text{ MPa}$
temperature	$^{\circ}\text{C} = ( ^{\circ}\text{F} - 32 ) / 1.8$	$^{\circ}\text{F} = 32 + 1.8 ( ^{\circ}\text{C} )$



# 1. MASONRY

Masonry constitutes approximately 70% of the existing building inventory in USA, and 70% of people in the world live in or use masonry buildings. 30% of those people live in seismic regions.



*Figure 1 Earthquake Damages in a Masonry Building, Turkey 1999*

## 1.1 BACKGROUND

Masonry has been and still is one of the most widely used types of construction system in the world, due to its advantages, like aesthetic, architectural appearance, effective heat and sound isolation, fire resistance and economical construction.

On the other hand, it offers low out-of-plane loading strength, besides a brittle and weak behavior, and therefore easily crumbles during the intense shaking of an earthquake.



*Figure 2 In-plane Collapse of Bearing Wall; San Francisco , U.S.A., Feb 1989, Magnitude (Ms): 7.1*

In the past centuries, many traditional buildings were designed using the weight of the floors and the massive walls to prevent tensile stresses caused by eccentricity of vertical loads and by lateral loads. Achieving lateral stability by gravity alone, however, places a practical economic limit on the size of loadbearing masonry structures. This has led designers and builders to seek ways to decrease wall thickness while maintaining structural stability.

The significant improvements in masonry materials and advances in manufacturing, design methods, and construction techniques have contributed to the growth of masonry as a cost-efficient contemporary building system. High-strength units are now available with a variety of shapes, colours, and textures. Moisture, sound, and thermal characteristics have been improved and ready-mix mortars and grout are available for better quality control and speed of construction. The development of reinforced masonry has contributed significantly to the use of this system in areas of high seismic activity and to efficient use in many general applications.

But overloading, dynamic vibrations, settlement, and in-plane and out-of-plane deformations can cause failure of masonry structures. Unreinforced masonry (URM) buildings have features that can threaten human lives. These include unbraced parapets, inadequate connections to the roof, and the brittle nature of the URM elements. As a matter of fact, organizations such as The Masonry Society

(TMS) and the Federal Emergency Management Agency (FEMA), have identified that failures of URM walls result in more material damage and loss of human life during earthquakes than any other type of structural element. This was evident from the recent post-earthquake observation in Turkey.

Nowadays, in the United States, large investments are being directed to retrofitting projects. It is estimated that the national average spending on reconstruction is about 25% of new construction investment (U.S. Census Bureau 1998). For example, under the URM Building Law of California, passed in 1986, approximately 25500 URM buildings were inventoried throughout the state. Even though this number is relatively small percentage of the total building inventory in California, it includes many cultural icons and historical buildings. The building evaluation showed that 96% of the URM buildings in California needed to be retrofitted. To date, it has been estimated that only half of the owners have taken remedial actions, which may be attribute to the retrofitting cost. Thereby, the development of effective and affordable retrofitting techniques for masonry elements is an urgent need.

Seismic loadings induce *out-of-plane* bending of walls between the restraining floors. Analysis of the failure modes must take into account many different factors, such as boundary conditions, wall compressive strengths, joint tensile strengths, wall stiffness, and applied loadings. Walls will typically remain stable under dead load and after cracking if they are within the specified height-to-thickness ratio. In the slenderness ratio is exceeded, the wall needs bracing by either a horizontal brace or vertical columns. Parapets, chimneys, and similar elements extending above the topmost line of restraint are most vulnerable to out-of-plane forces.



*Figure 3 Out-of-Plane Collapse of Bearing Walls  
Umbria, Italy, 1997*

*In-plane* resistance of unreinforced masonry walls is based on mortar strength and brick proportions. If the forces are strong enough to exceed the in-plane strength capacity of the wall, a shear failure will occur. This failure mode is characterized by brittle tensile cracking through the mortar and the masonry unit and a sudden loss of lateral load capacity.

Earthquake forces cause walls to push against and pull away from the floors that they are connected to. Failure to have a secure connection between the two elements can cause failure by falling brick as well as floor collapse. This type of problem can be corrected and work can be performed while the building is occupied.



*Figure 4 In-Plane Failures of Load-Bearing Walls  
Umbria, Italy, September 1997*

Current methods of *retrofitting* masonry structures have proved to be effective, but have many drawbacks. These methods usually include the addition of framing elements such as steel columns, pilasters, beams, or surface treatments such as shotcrete or ferrocement to increase the strength and ductility of the walls. Such procedures are often time consuming to apply, not cost-effective, add significant mass to the structure, encroach upon available working space, and adversely affects the aesthetics of the repaired area and in many cases the building as a whole. The extra mass added to the structure can also increase the earthquake-induced inertia forces and may require strengthening of the footing as well.

These problems may be overcome by using fiber reinforced polymers (FRP) reinforcement instead of the conventional methods. Because of the corrosion of metal reinforcement in concrete structures, alternative procedures are being studied and FRP products have proved to be a successful solution. Supporting research and development in the use of FRP for reinforcement, repair and strengthening was conducted for reinforced concrete applications, especially in United States and Japan for the last 20 years.

While extensive research was conducted and reported for reinforced and prestressed concrete structures, much less has been reported for masonry structures.

#### Objectives and scope

Summarizing, many failures can occur in unreinforced masonry (URM) buildings when they are subjected to dynamic or static actions such as those caused by moderate earthquakes, high speed winds, deterioration, construction or design mistakes. During a seismic event, walls located at the bottom story of the building may be overstressed because the shear forces at that level are larger than any other story. On the other hand, walls located at the upper stories are prone to fail under out-of-plane loading because the maximum seismic accelerations occur at those levels.

This research, as a part of the collaboration between University of Missouri-Rolla, U.S.A., and University of Padua, Italy, investigates the mechanical behavior of masonry walls reinforced with FRP composites (in particular, rods, tapes and laminates) and subjected to out-of-plane and in-plane loading.

The first series of walls deals with the flexural behavior of members strengthened with FRP laminates and with high height/thickness ratios. Different widths of reinforcement are evaluated and depending of the amount of FRP applied remarkable differences in the mode of failure are observed.

In the second series of walls a new technique, called “structural repointing”, less intrusive in terms of aesthetics, has been explored; variables such as different configurations of strengthening and masonry typologies are investigated.

For both of the series static load tests to failure are performed in order to understand the behavior of the specimens.

Because of the urgent need of an international code for the design of FRP reinforcement for masonry structures, one of the most important goals of this study is to provide provisional design guidelines to be implemented by practitioners when retrofitting URM walls.

## 1.2 MASONRY IN THE UNITED STATES

Masonry constitutes approximately 70% of the existing building inventory in the United States. Most of these buildings are constituted by unreinforced masonry, in special to the east of the Rocky Mountains. During the formation of the United States as a new nation, bearing unreinforced masonry walls were a very common form of construction. These walls had thickness ranging from 30 to 100 cm (12 to 40 inches), and were multi-wythe walls, where sometimes rubble was used for the interior wythes. The walls were commonly built with hand-made and fired clay units, bonded by sand-lime mortar.

The transition from traditional to modern methods was a consequence of the severe damage to URM walls due to the earthquake of 1933 in Long Beach, California. This seismic event forced to take preventive actions for future earthquakes. Through the California's Field Act, the use of masonry was prohibited in all the public buildings throughout the state of California. In the late 1940's and early 1950's, the masonry construction was revitalized in California. It was required that new masonry edifications complied with the newly developed Uniform Building Code, which was based on the reinforced concrete design practice of the time. Those provisions required that minimum seismic lateral forces be considered in the design of masonry elements, that tensile stresses in masonry be resisted by reinforcement; and that at least a minimum percentage of horizontal and vertical reinforcement be used.

In contemporary North American commercial construction, masonry walls include panel, curtain, and bearing walls, which can be unreinforced or reinforced (Klingner, 1994).

### 1.2.1 Masonry in Backup Walls

Commonly two different masonry units are found in backup or inner walls, clay tiles and concrete units. Structural clay tile has been first manufactured in the United States approximately since 1875. A clay tile is a hollow unit, which is characterized by possessing parallel cores and thin webs and face shells. In the beginning, structural tile was used in building floors and as a fireproofing material for steel frame construction. Owing to its lightweight, large unit size and ease of handling during construction, the use of clay tiles was extended to load-bearing walls, wall facings, silos, columns, etc. In the early 1900's, structural clay tiles were used in infill walls throughout the United States. Some notable structures where it is possible to observe this kind of construction are

the New York Chrysler Building, Los Angeles City Hall Building, and the Oakland City Hall Building in California, which is considered a historic structure.

Figure 5 illustrates information, made available by the U.S. Department of Commerce Census of Manufacturers, on the production of clay tile in the 20th century. As can be observed, the maximum peak in the production of clay tiles was in the 1920's. As a consequence of the Great Depression, the production suffered a dramatic decrease. As World War II began, the economy was revitalized and large public works were performed. Some of military facilities built primarily with clay tiles included Fort Benning in Georgia, and the Women's Army Auxiliary Corps Barracks in Iowa. From the same figure, it is observed that the production of clay tiles decreased during the 1960's, when concrete units began to be widely used.

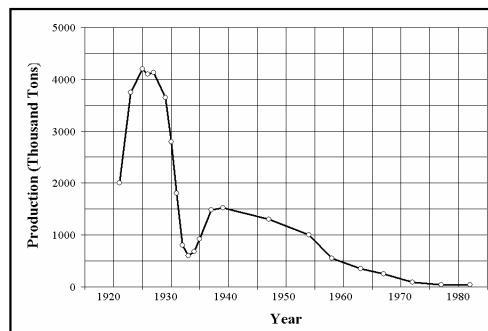


Figure 5 Production of Clay Tile During the 20th Century

It is important to point out that the use of concrete units was not new in the United States. Concrete blocks were first manufactured in the United States at about the turn of the 20<sup>th</sup> century in small one-at-a-time machines that could be operated by hand and purchased from Sears and Roebuck catalogs. Using this kind of machines, the production was limited to 10 blocks per man-hour. Due to manufacturing and aesthetic limitations, and because the architects preferred the use of stone because of its integrity, the use of concrete units was limited. The concrete block were not widely used until the 1920's when the manufacturing processes were improved; however due to the big recession many plants had to close or merge. It was not until the 1960's that the market started to change. This change is attributed to the automation of plant equipment, which increased the production capability of concrete blocks. The increase in production capability led to low unit cost and increased available quantity. In addition, the manufacturing process of concrete units allowed a better quality control of the products. For instance, concrete units show more uniformity since they are not fired during their manufacture process. Also, due to the brittle characteristics of clay tiles when being handled and transported, made that the demand of concrete units was increased.

Another cause for the decrease of clay tiles production was the efforts driven by the Environmental Protection Agency (EPA) to reduce the environmental costs associated with the manufacture of clay masonry units. This led to the closing of many old plants where the kilns generated emissions above the standards.

## **1.3 MASONRY BUILDING SYSTEMS**

### **1.3.1 Single-Story Loadbearing Buildings**

Single-story buildings make up the majority of loadbearing masonry construction in the USA. This type of building has thin walls for economic reasons and, since unreinforced free-standing thin walls have negligible stability, they must be laterally supported in some way. Stability is achieved by using end wall, intermediate cross walls, supports along the top edge of the wall, or a combination of these. Lateral support along the top edge of the wall is usually provided by the roof or ceiling system. In residential construction, a drywall ceiling is sufficiently strong in its own plane to give support to the outside wall by spanning between cross walls.

Wind pressures (or suction) acting on the exterior walls are transferred to lateral supports provided by the floor, roof, end walls, and cross walls. The portion of load transferred to the roof level is in turn transferred by the roof or ceiling system, acting as a diaphragm in its own plane, to the cross walls and end walls. The components of load distributed to the end walls and cross walls are then transmitted through these walls, by shearing action, to the foundation.

With lightweight roof construction and reduced weight of thin walls, out-of-plane vertical bending in tall walls may produce tensile stresses that require the wall to be reinforced. Axial compressive loads and horizontal shear are usually small in single-story buildings and can easily be resisted even though thin walls are used.

### **1.3.2 Multistory Loadbearing Buildings**

Many conventional low-rise and high-rise masonry buildings were designed and built utilizing their self-weight to counteract tensile stresses from lateral loads. The tallest was the Monadnock Building erected in Chicago from 1889 to 1891. This 16-story building had an internal pin-jointed iron frame (unbraced) and exterior walls of solid loadbearing masonry. It was noted for the simplicity of its architectural elevation treatment. However, the walls were nearly 1.8 m (6 ft) thick at the foundations, occupying valuable floor space and imposing a heavy load on the foundations, and by 1940 had settled 0.5 m (20 in) into the soft clay soil.



*Figure 6 Monadnock Building, Chicago 1889-91*

It was the last high-rise loadbearing masonry building constructed in Chicago for many decades. Steel-framed buildings, which had been introduced a few years earlier, and later concrete frames, took over as the structural element of multistory buildings. Masonry cladding, now supported by the frame, acted as a weather barrier and provided an aesthetic effect. Frames were designed to be structurally sufficient by themselves.

It was not generally recognized until the 1930s that infill brickwork within a steel frame acted as a shear panel to resist the lateral distortion of the frame in its own plane. Twenty years later, it was realized that masonry cross walls in a multistory building would act as shear walls whether or not a steel frame was present. Thus, in the 1960s, many multistory loadbearing buildings were constructed in several countries using masonry shear walls instead of concrete or steel frames to achieve lateral stability. In this construction, masonry walls support a concrete floor, which in turn supports the next story of masonry walls placed directly in line with those below. The concrete floor slabs act as rigid diaphragms to distribute the lateral load to the shear walls, which in turn transmit them to the foundation.

The overturning effect of wind on a traditional, loadbearing, multistory masonry building is resisted by the walls facing the wind. Contemporary loadbearing masonry construction resists overturning by walls placed parallel to the wind load direction.

Stability must be provided against wind or earthquake from all directions. This is usually attained by using a system of internal shear walls in both longitudinal and transverse directions. Because of their increased structural efficiency, modern loadbearing buildings have thinner walls than traditional buildings.

### 1.3.3 Hybrid Buildings

Masonry can be used with other materials to form a hybrid composite building system. Loadbearing masonry shear walls have been utilized in steel framing systems as service cores and stairways as well as to carry lateral shear loads. Another example is infill frame buildings where masonry infill provides stiffness to control building drift. Great care is necessary in detailing and construction to allow for the long-term differential movements of the masonry and framework that can lead to overstressing and failure. Masonry infill elements should be properly designed to carry loads, otherwise they can crack, thereby greatly reducing their stiffness, and resulting in increased deformations and stresses in the framing system.

### 1.3.4 Panel, Curtain and Bearing Walls

Panel walls are single-story walls meant to primarily resist out-of-plane loads generated by either earthquakes or wind; and vertical loads primarily due to self-weight. Panel walls are a common façade element in buildings conformed by frames of steel or reinforced concrete. This kind of walls may consist of two wythes separated by at least 5 cm (2 in) air space, commonly referred as to cavity walls. Panel walls may also consist of single wythe or multiple wythes in contact with each other. In the latter case are also denominated composite walls. When built within steel or RC frames these walls are called infill walls, and are commonly found forming the envelope of the building to protect the interior from the external environment; for this reason are also called barrier walls. Infill walls can be subjected to in-plane loads caused by their interaction with the surrounding frame. Due to vertical spans of 3.6 m (12 ft) or less, panel walls can satisfactorily resist out-of-plane loading and are generally unreinforced.

Curtain walls are multi-story walls that also resist out-of-plane loads due to earthquakes or wind. If a single wythe is used, horizontal steel, in the form of welded reinforcement, is placed in the mortar joints to increase the wind resistance. This kind of construction is commonly referred to as “partially reinforced”.

Bearing walls are arranged at a fairly uniform spacing to resist out-of-plane loads, in-plane loads (traditionally called “shear walls” when having this function); and vertical loads from self-weight and upper tributary floor areas. Cavity and composite walls can also lie on this category. Depending on the load solicitations bearing walls can be unreinforced or reinforced.

In the United States, differences of masonry systems can be categorized according to the geographical region. Thus, in contrast to the eastern United States, masonry in the western United

State has been primarily developed for earthquake resistance criteria, and secondarily for architectural and fire resistance criteria. Because of the seismic considerations the majority of the masonry construction in that part of the country consists of reinforced and fully grouted walls built with concrete masonry units (CMU), which are meant to act as shear and bearing elements.

## 1.4 MECHANICS PROPERTIES OF MASONRY ASSEMBLAGES

A masonry assemblage is an element composed of some or all of the constituent masonry materials: units, mortar, grout, and reinforcement. Knowledge of the interaction between these materials and of other factors affecting the physical and mechanical properties of the composite is needed to understand the fundamental behavior of masonry.

### 1.4.1 Axial Compression

With the modern use of high strength materials and thinner elements, compressive strength is often of prime importance in loadbearing structures. Compression tests of masonry prisms are used as the basis for assigning design stress and, in some cases, as a quality control measure.

The compressive strength of the solid prism depends in general by the compressive strength of the brick/block and of the mortar, by the joint thickness, by the shape of the brick/block, and by the materials constituting the brick/block.

Obviously the compressive strength of the masonry,  $f'_m$ , varies for different kind of blocks, as well as stress-strain curve; but it is important to underline that generally the compressive strain at peak stress for clay masonry (about 0.3%) is higher than for concrete masonry (about 0.2%), as well as the ultimate strain.

Because of the nonlinear shape of the stress-strain curve, the modulus of elasticity can be defined as the chord modulus for a line drawn from the curve at 5% of the maximum compressive stress to 33% of the maximum compressive stress. This region usually lies well within the reasonably linear part of the curve.

Traditionally, the modulus of elasticity for masonry,  $E_m$ , is calculated by the equation  $E_m = k' f'_m$ , where  $k' = 700$  to  $1000$ , and  $f'_m =$  specified compressive strength. The MSJC code specifies to take  $k' = 700$  for clay masonry and  $k' = 900$  for concrete masonry; the UBC specifies that  $k'$  should be taken equal to  $750$  for both clay and concrete masonry.

It has to be underlined that as in the case for concrete, long-term deformation of clay and concrete masonry due to creep may be significant and should be considered in design. The MSJC code specifies creep coefficients (long-term deformation due to creep per unit compressive stress) of  $0.36$

$\times 10^{-4}$  per MPa ( $0.7 \times 10^{-7}$  per psi) for clay masonry and  $0.1 \times 10^{-4}$  per MPa ( $2.5 \times 10^{-7}$  per psi) for concrete masonry.

This research has assumed the stress-strain curve to be equal to the one, for reinforced concrete members, given by the ACI code:

$$f_c = f'_m \times \left[ 2 \frac{\varepsilon_c}{\varepsilon'_c} - \left( \frac{\varepsilon_c}{\varepsilon'_c} \right)^2 \right]$$

This curve was adopted either for the concrete or the clay walls. Indeed, like other researches suggested (prof. Ayman S. Mosallam, California State Univ.), a different parabolic curve was also tried in the clay brick masonry computing, but the results were similar to the ones obtained with the RC curve (see 5.8.1).

#### 1.4.2 Shear Strength along Mortar Bed Joint

Masonry shear walls are intended to resist shear forces from to in-plane lateral loads plus the effects of axial load and bending. Depending on the form of construction and the combined effects of axial load and bending, the shear failure mode is characterized by shear slip along the bed joints, diagonal tension cracking, or shear compression failure.

Tests to measure the shear strength along mortar bed joints have not been standardized and, as a result, many variations have been developed. In our test we have used the triplet test.

Naturally, increased shear strength corresponds with increased compression force normal to the bed joints. This increased shear capacity can be thought of as being similar to an increased frictional resistance due to compression. The slope for low axial compression equates to the coefficient of friction and is often greater than one for low compressive stresses. For normal compressive stress ( $>0.3 f'_m$ ), the change to decreasing shear strength corresponds to the change to a compression splitting failure mode. This behavior is also observed for grout-filled hollow masonry.

For shear failures, experimental investigations have shown that the shear strength corresponding to slip along one or more bed joints is strongly related to the combined shear and compressive stresses. The relationship most commonly adopted to model this phenomenon is a Coulomb friction relationship. This assumes that the joint shear strength is composed of initial shear bond strength between the mortar and the masonry unit plus a shear friction capacity, which is considered to be proportional to the compressive stress applied normal to the bed joints. This relationship is

expressed as  $\tau = \tau_o + \mu \sigma_n$ , where  $\tau$  = joint shear strength;  $\tau_o$  = shear bond strength for  $\sigma_n = 0$ ;  $\mu$  = coefficient of friction  $\sigma_n = 0$ ;  $\sigma_n$  = compressive stress normal to the bed joints.

The test results indicate the validity of this concept at low levels of compression (approximately  $\sigma_n < 10$  MPa ). However, this formulation does not apply to failure modes other than slip along the mortar joints.

One might anticipate that many of the factors affecting the flexural tensile bond between mortar and masonry units also affect the shear slip strength along mortar bed joint. However, little research has been done on this topic. Test results show that shear bond strength for solid masonry is affected by the surface condition and initial rate of absorption of the units. Values ranging from 0.24 to 0.69 MPa (35 to 100 psi) are reported but with high coefficients of variation similar to those for flexural tensile bond. The MSJC code specifies an allowable in-plane shear of 0.26 MPa (37 psi) for solid or hollow masonry. No strong correlation is evident between mortar or prism compressive strength and shear bond strength.

Filling the cells of hollow masonry with grout has been found to significantly increase the shear strength along the bed joints. The magnitude of this increased strength is influenced by the tensile strength of the grout and the percent solid of the units (at a net-to-gross area ratio of about 0.6, an increase in average shear strength ranging from 50 to 100% can be achieved by grouting the cores). The MSJC code specifies a 62% increase in allowable in-plane shear stress for grouted hollow masonry compared to hollow or solid masonry. Therefore, grouting is a very effective means of improving the shear capacity along the bed joints as the increased shear resisting area also increases the shear capacity.

Test results typically indicate average coefficients of friction ranging from 0.6 to 1.0 depending on material properties and surface roughness. Currently, masonry codes specify allowable shear bond stress in terms of mortar type and an added component due to friction ranging from 0.2 to 0.45 times the normal compressive stress due to dead loads.

Following initial slip along the bed joint, the friction component of shear resistance remains nearly constant, although usually at a lower value than calculated from capacities prior to slip. This is important for modelling the shear force-displacement behavior of unreinforced solid and hollow masonry walls under reserved cyclic loading. A steady-state value of the residual shear resistance is reached that is not significantly affected by the number of cycles of loading. For reinforced masonry, the residual friction following slip is useful for calculating the shear friction associated with the clamping (dowel) action of the reinforcement resulting from the slip along the bed joints.

### 1.4.3 In-plane Tensile Strength

The combination of relatively low tensile strength and brittle behavior results in masonry being susceptible to tensile cracking. In fact, the cause of most masonry structural failures is tensile cracking. In loadbearing masonry structural buildings, shear walls carry vertical loads and resist the lateral in-plane loads due to wind or earthquakes. This combined loading creates principal tension stresses in the wall leading to tensile cracking when the tensile strength of the masonry is exceeded. In addition to the potential for developing horizontal or vertical cracks corresponding to tension normal or parallel to the bed joints, various forms of diagonal cracking can occur. Therefore, it is important that this type of failure is predictable for various combinations of principal stress, orientation of principal stress with respect to the mortar joints, and various combinations of material properties. Although in-plane tension normal to bed or head joints can result from in-plane flexure or from axial restraint to shrinkage and thermal movements, the main emphasis of this section relates to principal tension resulting from combined in-plane shear and axial loads.

Test methods.

ASTM describes two test methods to determine the capacity of masonry under conditions that can produce diagonal cracking. The diagonal compression test is based on subjecting a 1.2 m (4 ft) square section of wall to diagonal compression through steel shoes (loading plates) on two diagonally opposite corners of the specimen, as described in ASTM C1391. These samples usually fail by forming diagonal cracks parallel to the line of action of the compression force. The diagonal tensile stress,  $f'_d$  is calculated from the equation:

$$f'_d = \frac{0.707P}{A}$$

where  $P$  is the applied load, and  $A$  is the average gross or net area of the wall cross section. Axial load normal to the bed joints can also be applied.

A difficulty with the diagonal tension test is that the stress field tends to force the cracks to follow the line of action of the compression load. This may not be the path of least resistance for other boundary conditions. In addition, the loading shoes on opposite ends of the diagonal can transfer compression load through a fairly large compression strut can carry higher loads than those required to produce diagonal cracking. Alternatively, local compression failures may prevent actual shear failure.

The difficulty of relating the strength and behavior of diagonal tests to diagonal cracking in walls has resulted in an alternate test, the ASTM E72 racking test method. Results obtained from this test are only relevant for the particular loading conditions and wall geometry used in the test. However,

they can be used to confirm shear capacity provisions in codes, at least for cases similar to the test conditions.

Failure modes.

We expect both the orientation of the principal tension stress and the relative magnitudes of the principal stresses to affect the in-plane tensile cracking requires many large test specimens. Therefore, a compromise between direct representation and practicality has led to use of the splitting tension test to provide reasonable approximations of strength and failure modes.

#### **1.4.4 Shear Strength for Out-of-Plane Loads**

Shear stress, for walls under out-of-plane loading, should not exceed allowable shear stresses specifies in building codes for working stress design. The MJSC code specifies allowable shear for flexural members not to exceed  $0.083 \sqrt{f'_m}$  MPa ( $\sqrt{f'_m}$  psi) or 0.35 MPa (50 psi), whichever is less. It is seldom that shear stresses exceed code allowable stresses. In such a case, increasing wall thickness or increasing compressive strength will be required because shear reinforcement is difficult to provide in flexural walls.

## 1.5 TRADITIONAL REPAIRING TECHNIQUES

In this section, the most common retrofitting techniques are reviewed.

### 1.5.1 Repointing

Over time, mortar joints may spall or erode due to freeze-thaw cycles or water drainage paths or the joints may not have been well filled or not filled with durable mortar. Also, debonding and separation cracks along the joints may occur due to differential movement. In most cases, deteriorated or unsatisfactory mortar joints can be repaired by repointing. Note that the term “repointing” is not applied consistently across the masonry industry and in some geographic areas may be taken to mean simply replacing missing mortar. The cutting out, filling, and retooling of masonry joints is sometimes called tuck pointing.

A common practice is to hose down the wall about one hour before repointing to remove debris and to wet masonry units. The fresh mortar, matching the original material as closely as possible, is placed in layers and tooled when thumb print hard. The new mortar should match as closely as possible the existing mortar in color, texture, and physical properties. In major restoration projects of historic buildings, comprehensive investigations may be justified to ensure the compatibility and long term durability of the repaired joints (see figure 7).

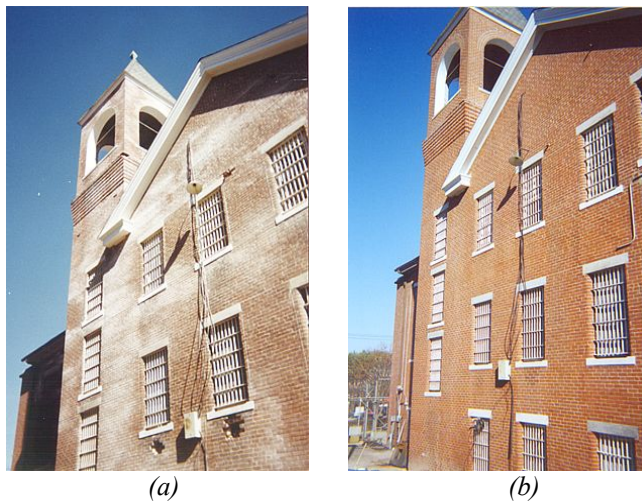


Figure 7 A Masonry Facade Before (a) and After (b) a Repointing Application

### 1.5.2 Grout Injection

Grout can be injected into walls to anchor other components or to strengthen and stiffen a wall by solidly filling hollow masonry. Whether using a non-shrink Portland cement grout (preferably an expanding grout) or an epoxy or polymer-modified grout, it is important to ensure complete filling and avoid later shrink-back as water is adsorbed from the grout. Experience has shown that the effectiveness depends on the compatibility of physical, chemical, and mechanical properties of the original masonry and the injected material (Binda et al. 1993).

The grout material should be selected to maximize the following desirable properties:

- high water retentivity
- minimum shrinkage or even slight expansion
- highly fluid grout but not subjected to segregation of constituent materials
- high tensile strength (greater than standard mortars)
- high bond to mortar and units (greater than bond of standard mortars)

### 1.5.3 Grout Filling of Hollow and Cavity Walls

Filling the cells of hollow units with grout increases the compressive capacity and, because of the greater tensile strength of grout compared to mortar bond, also produces a significant improvement in flexural and in-plane shear capacities. Filling voids with grout can also improve the resistance to water penetration, particularly for single-wythe construction. Except for very large cells or cavity widths, gravity placement of grout is typically not reliable due to obstructions from mortar fins and droppings and because of the difficulty of providing vibration for consolidation. Therefore, pressure grouting from the bottom up is usually the most reliable method for achieving complete filling. The vertical spacing is limited by the ability of the masonry to withstand internal pressure, by the capacity of the pump, and by the desire to limit the height of lifts to allow for some consolidation due to water absorption and compaction of the grout. Fine grout, often incorporating a plasticizer, is typically used and commercially available products that also recommended to avoid shrink-back of the grout and creation of voids in the grout or between the grout and the masonry.

### 1.5.4 External Reinforcing Overlay

Prawel et al. (1985) conducted an investigation on masonry panels retrofitted with ferrocement overlays. Ferrocement is an orthotropic composite material, which consists of a high-strength cement mortar matrix and layers of fine steel wires configured in the form of a mesh. The overall thickness usually varies between 1 and 2.5 cm (0.5 and 1 in). The tensile strength of the ferrocement layer ranges from 3.5 to 14 MPa (500 to 2000 psi), and it is dependable on mesh type, and the amount and orientation of the reinforcement. These overlays are used to increase in-plane and out-of-plane resistance. This study was focused on masonry specimens subjected to in-plane loading. The specimens consisted of 65 by 65 cm (25.5 by 25.5 in) brick panels laid in a stack bond pattern, having a thickness of 20 cm (8 in). A 1.27 cm (0.5 in) -wide layer of ferrocement, with different amounts of reinforcement, were attached to both sides of the masonry to increase the shear strength. The specimens were subjected to diagonal in-plane loading. Two modes of failure were observed, a ductile one caused by yielding of the steel wire and a brittle failure caused by debonding of the ferrocement overlay from the masonry surface. The experimental results indicated that the strength and ductility were almost doubled in the coated walls compared to the unstrengthened wall. Figure 8 illustrates the test results of three specimens. In the testing of panel 2, which had a 1.27 cm (0.5 in) mesh wire spacing, it was observed that the layer of ferrocement debonded from masonry after substantial cracking. In contrast, in panel 3, with a mesh wire spacing of 0.32 cm (0.125 in), complete yielding and tensile failure of the mesh was observed.

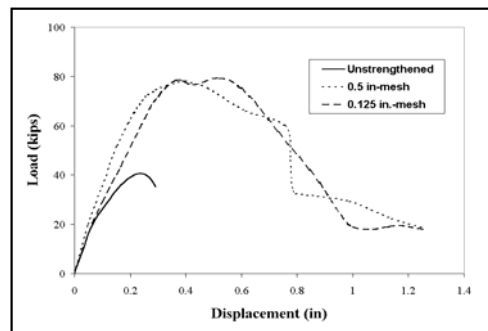
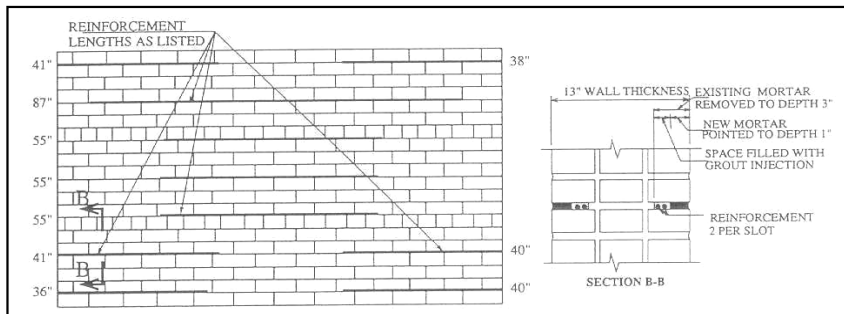


Figure 8 Test Results-External Reinforcing Overlay

**1.5.5 Internal Steel Reinforcing**

Manzouri et.al. (1996) evaluated the efficiency of repairing URM walls by grout injection in combination with horizontal and vertical steel reinforcement. URM walls were built in three whites with clay bricks for an overall dimension of 258 by 152 cm (8 ft.-6 in by 5 ft). The walls were tested under in-plane loading. First, the behavior of the walls in their original condition was investigated. Then, the walls were retrofitted to be tested once again. All the retrofitted walls were injected with grout. The severely damaged areas were repaired by replacement with similar materials. Crack widths larger than 1.5 mm (0.06 in) were injected with a coarse aggregate; whereas, crack widths ranging between 0.2 to 1.5 mm (0.008 to 0.06 in) were injected with a fine grout. Steel ties for use as dry-fix remedial anchor were placed as vertical reinforcement used for the pinning of the wythes in the toe area; and horizontal reinforcement as can be observed in Figure 9. The ties were made of Type 304 stainless steel with a helical design, similar to a self-tapping screw, which cuts a spiral groove as it is tapped into a pilot hole. The installation procedure included cutting of certain bed joints to a depth of 8 cm (3 in) followed by placement of the tie in the slot and sealing with mortar.



*Figure 9 Location of Horizontal Reinforcement-Internal Steel Reinforcing*

The test results demonstrated that the injection of grout accompanied by repair of localized damaged areas can restore the original strength and stiffness of retrofitted walls. The introduction of horizontal reinforcement increased the strength and ductility of the wall system, since shear failure was prevented. It was also observed that the vertical reinforcement increased the lateral resistance and ductility.

Figure 10 illustrates the test results for a wall before and after being strengthened.

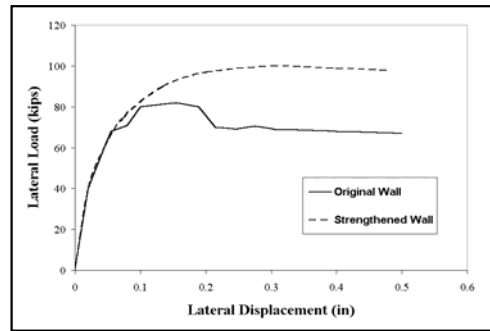


Figure 10 Test Results-Internal Steel Reinforcing

In old structures, load bearing masonry elements are prone to vertical cracking due to the combined effect of the gravitational sustained load and cyclic loads. This phenomenon has been observed in masonry towers and pillars throughout Europe, and can eventually lead to the collapse of the structure. Binda et al. (1999) investigated a technique to repair and strengthen masonry elements subjected to the aforementioned mechanism. This technique consisted of grooving the bed joints, placing of mortar along with the steel reinforcement (bars or plates) as shown in Figure 11.

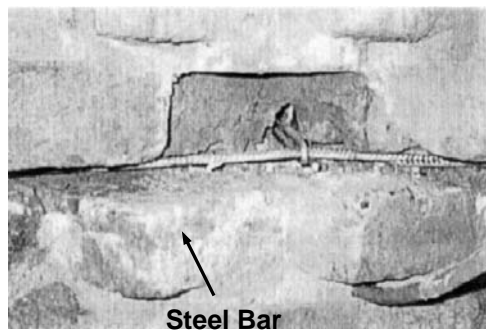


Figure 11 Internal Reinforcement

25x50x112 cm (10x20x44 in) panels were built for this research program. Initially, the specimens were pre-cracked by compressive loads representing the 80% of their capacity. After this, the specimens were repaired by placing two #6 bars every three bed joints in grooves 6 cm (2.5 in)-deep grooves. The test results of the repaired specimens showed that the strength was not improved. However, significant results in terms of deformation were attained, which was evident from the reduced cracking observed. In the repaired walls, reductions in the strains ranging between 40% and 50% were recorded. It was concluded that the structural degradation process of a masonry element can be detained; especially if the overall conditions are improved by other strengthening techniques such as injections and replacement of damaged sections.

### 1.5.6 External Steel Plate Reinforcing

Taghdi et al. (2000) proposed a strengthening method which consisted of placing diagonal and vertical steel strips on both sides of lightly reinforced masonry walls, as illustrated in figure 12.

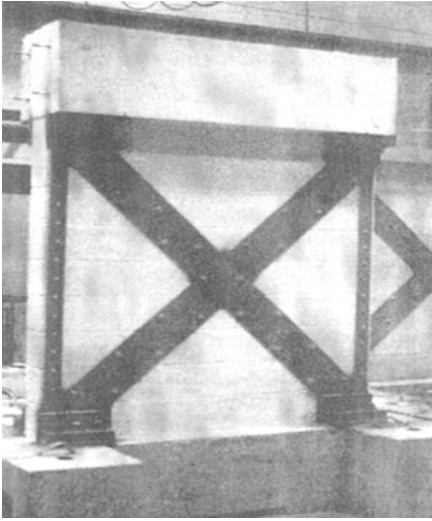


Figure 12 Steel Plate Reinforcing

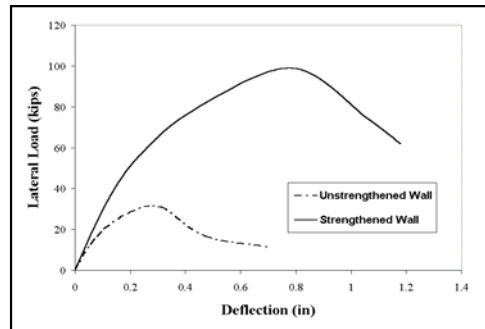


Figure 13 Test Results-Internal Steel Reinforcing

The walls were built with standard concrete masonry units, being their overall dimensions 183 by 183 cm (72 by 72 in). The walls were internally reinforced with No.8 gauge ladder reinforcement every 2 courses and Canadian M15 vertical steel placed at the edges and at the centre of the wall. The retrofitting strategy consisted of two 23 cm (9 in) wide diagonal steel strips with a thickness of 0.4 cm (0.15 in). The diagonal steel strips were welded at the intersection. Structural steel bolts were used to fasten the steel strips to the walls. Also, steel angles and high strength anchors connected the strips to the floor to prevent sliding of the walls. Figure 13 illustrates the test results of an unstrengthened wall and a wall strengthened with the described method. Although the primary objective of this experimental program was to study the in-plane behavior of strengthened walls, it was suggested that the proposed technique could also be effective for walls subjected to out-of-plane loading. A shear failure with crushing of the masonry diagonal struts was observed in the unstrengthened wall. In the strengthened wall, the diagonal steel strips delayed the crushing of masonry until excessive yielding, which led to buckling in the strips, occurred. It was observed that the vertical strips provided a ductile flexural behavior to the walls; and the steel strip system prevented the development of rigid body rotation and allowed cracks to spread the cracks.

## 2. COMPOSITE MATERIALS

In the U.S.A., cost estimates for maintenance of highway bridge decks composed of steel-reinforced concrete are up to \$90 billion/year.

Fiber Reinforced Polymer (FRP) is a relatively new class of composite material manufactured from fibers and resins and has proven efficient and economical for the development and repair of new and deteriorating structures in civil engineering.



*Figure 14 Common FRPs Used in Structural Engineering*

## 2.1 FRP STRUCTURE

### 2.1.1 Introduction

To fully appreciate the role and application of composite materials to a structure, an understanding is required of the component materials themselves and of the ways in which they can be processed. This chapter looks at basic composite theory, properties of materials used, various processing techniques commonly found and applications of composite products.

In its most basic form a composite material is one which is composed of at least two elements working together to produce material properties that are different to the properties of those elements on their own. In practice, most composites consist of a bulk material (the 'matrix'), and a reinforcement of some kind, added primarily to increase the strength and stiffness of the matrix. This reinforcement is usually in fibre form. Today, the most common man-made composites can be divided into three main groups:

**Polymer Matrix Composites (PMC's).** These are the most common and will be the main area of discussion in this chapter. Also known as FRP - Fibre Reinforced Polymers (or Plastics) - these materials use a polymer-based resin as the matrix, and a variety of fibres such as glass, carbon and aramid as the reinforcement.

**Metal Matrix Composites (MMC's)** - Increasingly found in the automotive industry, these materials use a metal such as aluminium as the matrix, and reinforce it with fibres such as silicon carbide.

**Ceramic Matrix Composites (CMC's)** - Used in very high temperature environments, these materials use a ceramic as the matrix and reinforce it with short fibres, or whiskers such as those made from silicon carbide and boron nitride.

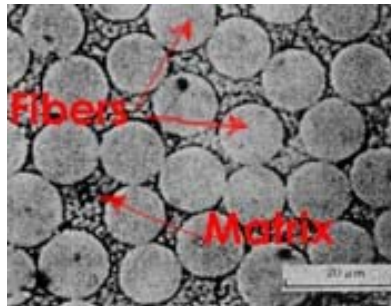


*Figure 15 Electron Micrograph of Partial cross Section of GFRP Composite*

## Polymer Matrix Composites

Resin systems such as epoxies and polyesters have limited use for the manufacture of structures on their own, since their mechanical properties are not very high when compared to, for example, most metals. However, they have desirable properties, most notably their ability to be easily formed into complex shapes.

Materials such as glass, aramid and boron have extremely high tensile and compressive strength but in 'solid form' these properties are not readily apparent. This is due to the fact that when stressed, random surface flaws will cause each material to crack and fail well below its theoretical 'breaking point'. To overcome this problem, the material is produced in fibre form, so that, although the same number of random flaws will occur, they will be restricted to a small number of fibres with the remainder exhibiting the material's theoretical strength. Therefore a bundle of fibres will reflect more accurately the optimum performance of the material. However, fibres alone can only exhibit tensile properties along the fibre's length, in the same way as fibres in a rope.

It is when the resin systems are combined with reinforcing fibres such as glass, carbon and aramid, that exceptional properties can be obtained. The resin matrix spreads the load applied to the composite between each of the individual fibres and also protects the fibres from damage caused by abrasion and impact. High strengths and stiffnesses, ease of moulding complex shapes, high environmental resistance all coupled with low densities, make the resultant composite superior to metals for many applications.

Since Polymer Matrix Composites combine a resin system and reinforcing fibres, the properties of the resulting composite material will combine something of the properties of the resin on its own with that of the fibres on their own.

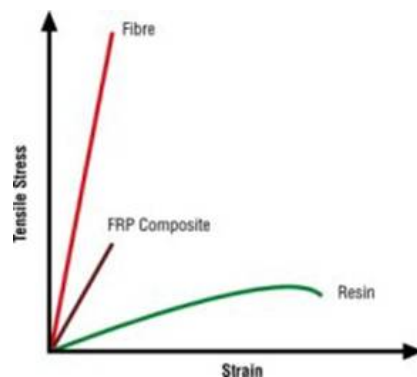


Figure 16 Stress/Strain Behavior: Comparison Between the Components of a FRP

Overall, the properties of the composite are determined by:

- The properties of the fibre
- The properties of the resin
- The ratio of fibre to resin in the composite (Fibre Volume Fraction)
- The geometry and orientation of the fibres in the composite

The first two will be dealt with in more detail later. The ratio of the fibre to resin derives largely from the manufacturing process used to combine resin with fibre, as will be described in the section on manufacturing processes. However, it is also influenced by the type of resin system used, and the form in which the fibres are incorporated. In general, since the mechanical properties of fibres are much higher than those of resins, the higher the fibre volume fraction the higher will be the mechanical properties of the resultant composite. In practice there are limits to this, since the fibres need to be fully coated in resin to be effective, and there will be optimum packing of the generally circular cross-section fibres. In addition, the manufacturing process used to combine fibre with resin leads to varying amounts of imperfections and air inclusions. Typically, with a common hand lay-up process as widely used in the boat-building industry, a limit for Fibre Volume Fraction is approximately 30-40%. With the higher quality, more sophisticated and precise processes used in the aerospace industry, Fibre Volume Fractions approaching 70% can be successfully obtained.

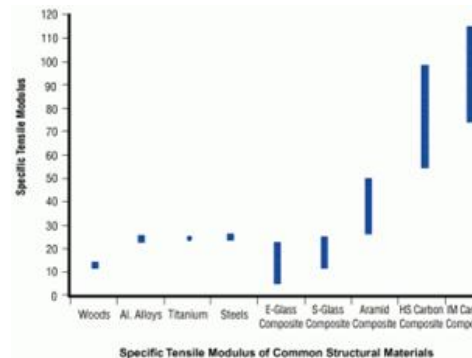
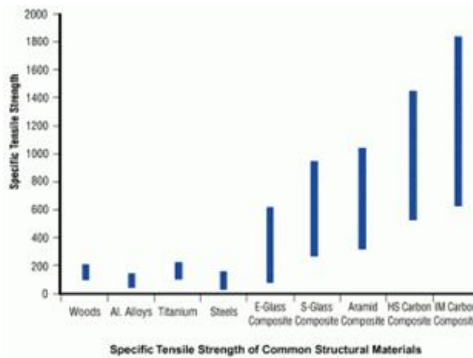
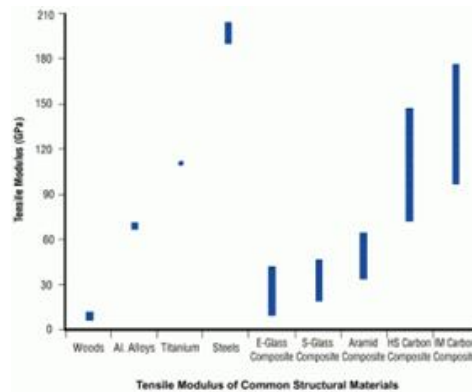
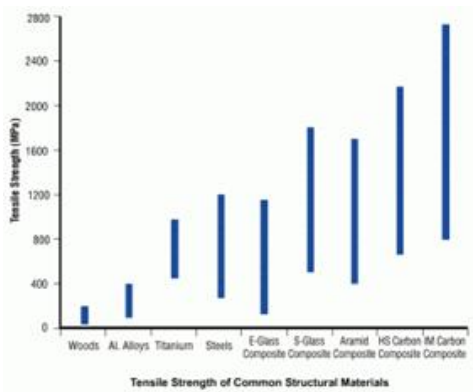
The geometry of the fibres in a composite is also important since fibres have their highest mechanical properties along their lengths, rather than across their widths. This leads to the highly anisotropic properties of composites, where, unlike metals, the mechanical properties of the composite are likely to be very different when tested in different directions. This means that it is very important when considering the use of composites to understand at the design stage, both the magnitude and the direction of the applied loads. When correctly accounted for, these anisotropic properties can be very advantageous since it is only necessary to put material where loads will be applied, and thus redundant material is avoided.

It is also important to note that with metals the properties of the materials are largely determined by the material supplier, and the person who fabricates the materials into a finished structure can do little to change those 'in-built' properties. However, a composite material is formed at the same time as the structure is itself being fabricated. This means that the person who is making the structure is creating the properties of the resultant composite material, and so the manufacturing processes they use have an unusually critical part to play in determining the performance of the resultant structure.

Comparison with Other Structural Materials

Due to the factors described above, there is a very large range of mechanical properties that can be achieved with composite materials. Even when considering one fibre type on its own, the composite properties can vary by a factor of 10 with the range of fibre contents and orientations that are commonly achieved. The comparisons that follow therefore show a range of mechanical properties for the composite materials. The lowest properties for each material are associated with simple manufacturing processes and material forms (e.g. spray lay-up glass fibre), and the higher properties are associated with higher technology manufacture (e.g. autoclave moulding of unidirectional glass fibre prepreg), such as would be found in the aerospace industry.

For the other materials shown, a range of strength and stiffness (modulus) figures is also given to indicate the spread of properties associated with different alloys, for example.



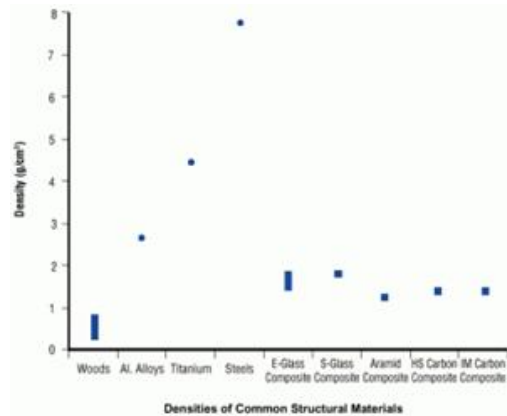


Figure 17 Comparison with Other Structural Materials

The above figures clearly show the range of properties that different composite materials can display. These properties can best be summed up as high strengths and stiffnesses combined with low densities. It is these properties that give rise to the characteristic high strength and stiffness to weight ratios that make composite structures ideal for so many applications. This is particularly true of applications which involve movement, such as cars, trains and aircraft, since lighter structures in such applications play a significant part in making these applications more efficient.

The strength and stiffness to weight ratio of composite materials can best be illustrated by the following graphs that plot 'specific' properties. These are simply the result of dividing the mechanical properties of a material by its density. Generally, the properties at the higher end of the ranges illustrated in the previous graphs are produced from the highest density variant of the material. The spread of specific properties shown in the following graphs takes this into account.

Further comparisons between laminates made from the different fibre types are given later in this guide in the section on 'Reinforcements' (2.1.3).

### 2.1.2 Resin Systems

Any resin system for use in a composite material will require the following properties:

- Good mechanical properties
- Good adhesive properties
- Good toughness properties
- Good resistance to environmental degradation

Mechanical Properties of the Resin System

The figure below shows the stress / strain curve for an 'ideal' resin system. The curve for this resin shows high ultimate strength, high stiffness (indicated by the initial gradient) and a high strain to failure. This means that the resin is initially stiff but at the same time will not suffer from brittle failure.

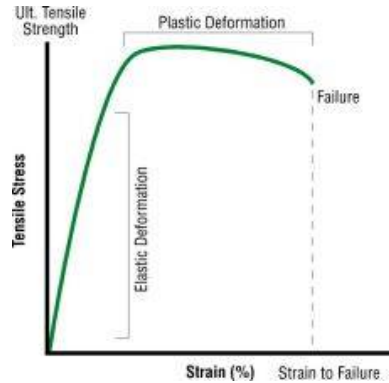


Figure 18 Stress/Strain Curve for an Ideal Resin System

It should also be noted that when a composite is loaded in tension, for the full mechanical properties of the fibre component to be achieved, the resin must be able to deform to at least the same extent as the fibre. The figure below gives the strain to failure for E-glass, S-glass, aramid and high-strength grade carbon fibres on their own (i.e. not in a composite form). Here it can be seen that, for example, the S-glass fibre, with an elongation to break of 5.3%, will require a resin with an elongation to break of at least this value to achieve maximum tensile properties.

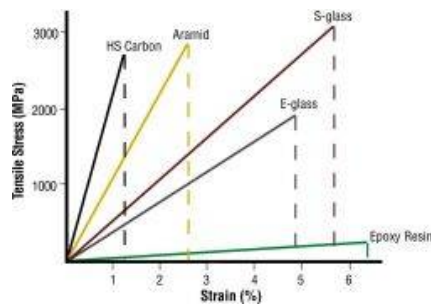


Figure 19 Yungh Modulus Comparison Between FRPs

Adhesive Properties of the Resin System

High adhesion between resin and reinforcement fibres is necessary for any resin system. This will ensure that the loads are transferred efficiently and will prevent cracking or fibre / resin debonding when stressed.

### Toughness Properties of the Resin System

Toughness is a measure of a material's resistance to crack propagation, but in a composite this can be hard to measure accurately. However, the stress / strain curve of the resin system on its own provides some indication of the material's toughness. Generally the more deformation the resin will accept before failure the tougher and more crack-resistant the material will be. Conversely, a resin system with a low strain to failure will tend to create a brittle composite, which cracks easily. It is important to match this property to the elongation of the fibre reinforcement.

### Environmental Properties of the Resin System

Good resistance to the environment, water and other aggressive substances, together with an ability to withstand constant stress cycling, are properties essential to any resin system. These properties are particularly important for use in a marine environment.

### Resin Types

The resins that are used in fibre reinforced composites can also be referred to as 'polymers'. All polymers exhibit an important common property in that they are composed of long chain-like molecules consisting of many simple repeating units. Man-made polymers are generally called 'synthetic resins' or simply 'resins'. Polymers can be classified under two types, 'thermoplastic' and 'thermosetting', according to the effect of heat on their properties.

Thermoplastics, like metals, soften with heating and eventually melt, hardening again with cooling. This process of crossing the softening or melting point on the temperature scale can be repeated as often as desired without any appreciable effect on the material properties in either state. Typical thermoplastics include nylon, polypropylene and ABS, and these can be reinforced, although usually only with short, chopped fibres such as glass.

Thermosetting materials, or 'thermosets', are formed from a chemical reaction in situ, where the resin and hardener or resin and catalyst are mixed and then undergo a non-reversible chemical reaction to form a hard, infusible product. In some thermosets, such as phenolic resins, volatile substances are produced as by-products (a 'condensation' reaction). Other thermosetting resins such as polyester and epoxy cure by mechanisms that do not produce any volatile by products and thus are much easier to process ('addition' reactions). Once cured, thermosets will not become liquid again if heated, although above a certain temperature their mechanical properties will change significantly. This temperature is known as the Glass Transition Temperature ( $T_g$ ), and varies widely according to the particular resin system used, its degree of cure and whether it was mixed

correctly. Above the  $T_g$ , the molecular structure of the thermoset changes from that of a rigid crystalline polymer to a more flexible, amorphous polymer. This change is reversible on cooling back below the  $T_g$ . Above the  $T_g$  properties such as resin modulus (stiffness) drop sharply, and as a result the compressive and shear strength of the composite does too. Other properties such as water resistance and colour stability also reduce markedly above the resin's  $T_g$ .

Although there are many different types of resin in use in the composite industry, the majority of structural parts are made with three main types, namely polyester, vinylester and epoxy.

### Epoxy Resins

The large family of epoxy resins represent some of the highest performance resins of those available at this time. Epoxies generally out-perform most other resin types in terms of mechanical properties and resistance to environmental degradation, which leads to their almost exclusive use in aircraft components. As a laminating resin their increased adhesive properties and resistance to water degradation make these resins ideal for use in applications such as boat building. Here epoxies are widely used as a primary construction material for high-performance boats or as a secondary application to sheath a hull or replace water-degraded polyester resins and gel coats.

The term 'epoxy' refers to a chemical group consisting of an oxygen atom bonded to two carbon atoms that are already bonded in some way. The simplest epoxy is a three-member ring structure known by the term 'alpha-epoxy' or '1,2-epoxy'. The idealised chemical structure is shown in the figure below and is the most easily identified characteristic of any more complex epoxy molecule.



Idealised Chemical Structure of a Simple Epoxy (Ethylene Oxide)

*Figure 20 Idealised Chemical Structure of a "Epoxy Chemical Group"*

Usually identifiable by their characteristic amber or brown colouring, epoxy resins have a number of useful properties. Both the liquid resin and the curing agents form low viscosity easily processed systems. Epoxy resins are easily and quickly cured at any temperature from 5°C to 150°C, depending on the choice of curing agent. One of the most advantageous properties of epoxies is their low shrinkage during cure which minimises fabric 'print-through' and internal stresses. High adhesive strength and high mechanical properties are also enhanced by high electrical insulation and good chemical resistance. Epoxies find uses as adhesives, caulking compounds, casting

compounds, sealants, varnishes and paints, as well as laminating resins for a variety of industrial applications.

Epoxy resins are formed from a long chain molecular structure similar to vinyl ester with reactive sites at either end. In the epoxy resin, however, these reactive sites are formed by epoxy groups instead of ester groups. The absence of ester groups means that the epoxy resin has particularly good water resistance. The epoxy molecule also contains two ring groups at its centre which are able to absorb both mechanical and thermal stresses better than linear groups and therefore give the epoxy resin very good stiffness, toughness and heat resistant properties.

The figure below shows the idealised chemical structure of a typical epoxy. Note the absence of the ester groups within the molecular chain.

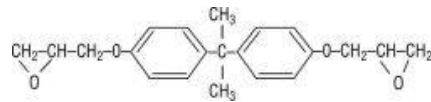


*Figure 21 Idealised Chemical Structure of a Typical Epoxy Molecule*

Epoxy resins differ from polyester resins in that they are cured by a 'hardener' rather than a catalyst. The hardener, often an amine, is used to cure the epoxy by an 'addition reaction' where both materials take place in the chemical reaction. The chemistry of this reaction means that there are usually two epoxy sites binding to each amine site. This forms a complex three-dimensional molecular structure.

Since the amine molecules 'co-react' with the epoxy molecules in a fixed ratio, it is essential that the correct mix ratio is obtained between resin and hardener to ensure that a complete reaction takes place. If amine and epoxy are not mixed in the correct ratios, unreacted resin or hardener will remain within the matrix which will affect the final properties after cure. To assist with the accurate mixing of the resin and hardener, manufacturers usually formulate the components to give a simple mix ratio which is easily achieved by measuring out by weight or volume.

### Resin Comparison Summary

The polyesters, vinyl esters and epoxies discussed here probably account for some 90% of all thermosetting resin systems used in structural composites. In summary the main advantages and disadvantages of each of these types are:

### Polyesters

Advantages:

- Easy to use
- Lowest cost of resins available (U.S. \$ 1.5-3 /kg)

Disadvantages:

- Only moderate mechanical properties
- High styrene emissions in open moulds
- High cure shrinkage Limited range of working times

### Vinylesters

Advantages:

- Very high chemical/environmental resistance
- Higher mechanical properties than polyesters

Disadvantages:

- Postcure generally required for high properties
- High styrene content
- Higher cost than polyesters (U.S. \$ 3-6 /kg)
- High cure shrinkage

### Epoxies

Advantages:

- High mechanical and thermal properties
- High water resistance
- Long working times available
- Temperature resistance can be up to 140°C wet / 220°C dry
- Low cure shrinkage

Disadvantages:

- More expensive than vinylesters (U.S. \$ 4.5-22 /kg)
- Critical mixing
- Corrosive handling

### 2.1.3 Reinforcements

The role of the reinforcement in a composite material is fundamentally one of increasing the mechanical properties of the neat resin system. All of the different fibres used in composites have different properties and so affect the properties of the composite in different ways. The properties and characteristics of common fibres are explained below.

However, individual fibres or fibre bundles can only be used on their own in a few processes such as filament winding (described later). For most other applications, the fibres need to be arranged into some form of sheet, known as a fabric, to make handling possible. Different ways for assembling fibres into sheets and the variety of fibre orientations possible lead to there being many different types of fabrics, each of which has its own characteristics. These different fabric types and constructions are explained later.

#### Properties of Reinforcing Fibres

The mechanical properties of most reinforcing fibres are considerably higher than those of unreinforced resin systems. The mechanical properties of the fibre/resin composite are therefore dominated by the contribution of the fibre to the composite.

The four main factors that govern the fibre's contribution are:

- The basic mechanical properties of the fibre itself.
- The surface interaction of fibre and resin (the 'interface').
- The amount of fibre in the composite ('Fibre Volume Fraction').
- The orientation of the fibres in the composite.

The basic mechanical properties of the most commonly used fibres are later. The surface interaction of fibre and resin is controlled by the degree of bonding that exists between the two. This is heavily influenced by the treatment given to the fibre surface, and a description of the different surface treatments and 'finishes' is also given here.

The amount of fibre in the composite is largely governed by the manufacturing process used. However, reinforcing fabrics with closely packed fibres will give higher Fibre Volume Fractions (FVF) in a laminate than will those fabrics which are made with coarser fibres, or which have large gaps between the fibre bundles. Fibre diameter is an important factor here with the more expensive smaller diameter fibres providing higher fibre surface areas, spreading the fibre/matrix interfacial loads. As a general rule, the stiffness and strength of a laminate will increase in proportion to the amount of fibre present. However, above about 60-70% FVF (depending on the way in which the

fibres pack together) although tensile stiffness may continue to increase, the laminate's strength will reach a peak and then begin to decrease due to the lack of sufficient resin to hold the fibres together properly.

Finally, since reinforcing fibres are designed to be loaded along their length, and not across their width, the orientation of the fibres creates highly 'direction-specific' properties in the composite. This 'anisotropic' feature of composites can be used to good advantage in designs, with the majority of fibres being placed along the orientation of the main load paths. This minimises the amount of parasitic material that is put in orientations where there is little or no load.

Basic Properties of Fibres and Other Engineering Materials

Material Type	Tensile Str. (MPa)	Tensile Modulus (GPa)	Typical Density (g/cc)	Specific Modulus
Carbon HS	3500	160 - 270	1.8	90 - 150
Carbon IM	5300	270 - 325	1.8	150 - 180
Carbon HM	3500	325 - 440	1.8	180 - 240
Carbon UHM	2000	440+	2.0	200+
Aramid LM	3600	60	1.45	40
Aramid HM	3100	120	1.45	80
Aramid UHM	3400	180	1.47	120
Glass - E glass	2400	69	2.5	27
Glass - S2 glass	3450	86	2.5	34
Glass - quartz	3700	69	2.2	31
Aluminium Alloy (7020)	400	1069	2.7	26
Titanium	950	110	4.5	24
Mild Steel (55 Grade)	450	205	7.8	26
Stainless Steel (A5-80)	800	196	7.8	25
HS Steel (17/4 H900)	1241	197	7.8	25

Table 1 Basic Properties of Fibres and Other Engineering Materials

Laminate Mechanical Properties

The properties of the fibres only show part of the picture. The properties of the composite will derive from those of the fibre, but also the way it interacts with the resin system used, the resin properties itself, the volume of fibre in the composite and its orientation. The following diagrams show a basic comparison of the main fibre types when used in a typical high-performance unidirectional epoxy prepreg, at the fibre volume fractions that are commonly achieved in aerospace components.

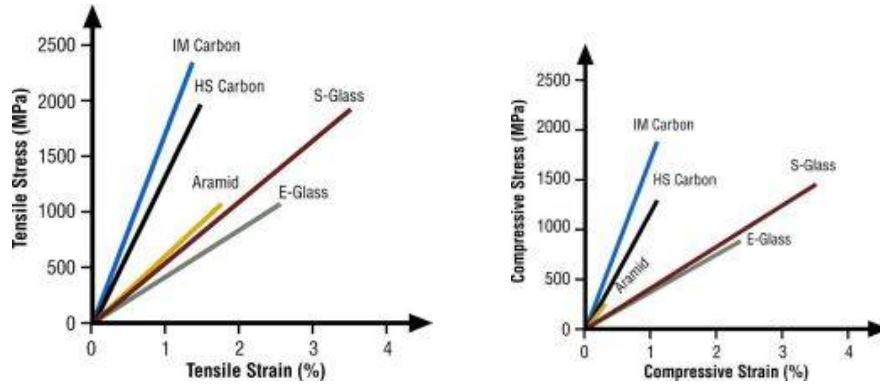


Figure 22 FRP: Tensile and Compressive Stress/Strain Curve

These graphs show the strengths and maximum strains of the different composites at failure. The gradient of each graph also indicates the stiffness (modulus) of the composite; the steeper the gradient, the higher its stiffness. The graphs also show how some fibres, such as aramid, display very different properties when loaded in compression, compared with loading in tension.

Laminate Impact Strength

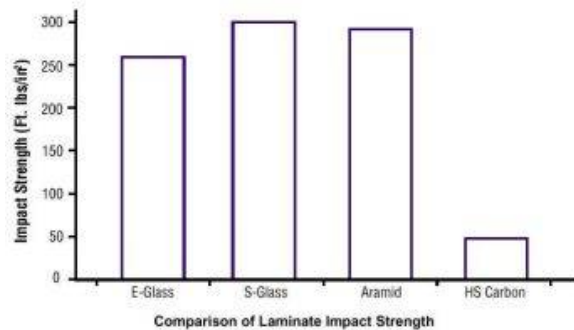


Figure 23 Comparison of Laminate Impact Strength

Impact damage can pose particular problems when using high stiffness fibres in very thin laminates. In some structures, where cores are used, laminate skins can be less than 0.3 mm thick. Although other factors such as weave style and fibre orientation can significantly affect impact resistance, in impact-critical applications, carbon is often found in combination with one of the other fibres. This can be in the form of a hybrid fabric where more than one fibre type is used in the fabric construction. These are described in more detail later.

Comparative Fibre Cost

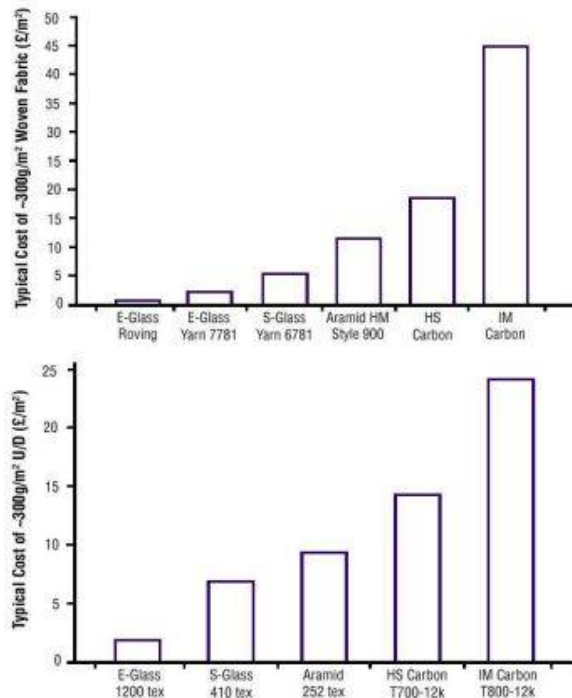


Figure 24 Comparison of Fibre Cost (2002)

The figures above are calculated on a typical price of a 300 g woven fabric. Most fibre prices are considerably higher for the small bundle size (tex) used in such lightweight fabrics. Where heavier bundles of fibre can be used, such as in unidirectional fabrics, the cost comparison is slightly different.

Glass Fiber

By blending quarry products (sand, kaolin, limestone, colemanite) at 1600°C, liquid glass is formed. The liquid is passed through micro-fine bushings and simultaneously cooled to produce glass fibre filaments from 5-24 m in diameter. The filaments are drawn together into a strand (closely associated) or roving (loosely associated), and coated with a “size” to provide filament cohesion and protect the glass from abrasion.

By variation of the “recipe”, different types of glass can be produced. The types used for structural reinforcements are as follows:

- E-glass (electrical) - lower alkali content and stronger than A glass (alkali). Good tensile and compressive strength and stiffness, good electrical properties and relatively low cost, but impact resistance relatively poor. Depending on the type of E glass the price ranges from

about U.S. \$ 1.5-3 /kg. E-glass is the most common form of reinforcing fibre used in polymer matrix composites.

- C-glass (chemical) - best resistance to chemical attack. Mainly used in the form of surface tissue in the outer layer of laminates used in chemical and water pipes and tanks.
- R, S or T-glass – manufacturer's trade names for equivalent fibres having higher tensile strength and modulus than E glass, with better wet strength retention. Higher ILSS and wet out properties are achieved through smaller filament diameter. S-glass is produced in the USA by OCF, R-glass in Europe by Vetrotex and T-glass by Nittobo in Japan. Developed for aerospace and defence industries, and used in some hard ballistic armour applications. This factor, and low production volumes mean relatively high price. Depending on the type of R or S glass the price ranges from about U.S. \$ 18-30 /kg.

### E Glass Fibre Types

E Glass fibre is available in the following forms:

- Strand - a compactly associated bundle of filaments. Strands are rarely seen commercially and are usually twisted together to give yarns.
- Yarns - a closely associated bundle of twisted filaments or strands. Each filament diameter in a yarn is the same, and is usually between 4-13m. Yarns have varying weights described by their 'tex' ( the weight in grammes of 1000 linear metres) or denier ( the weight in lbs of 10000 yards), with the typical tex range usually being between 5 and 400.
- Rovings - a loosely associated bundle of untwisted filaments or strands. Each filament diameter in a roving is the same, and is usually between 13-24 m. Rovings also have varying weights and the tex range is usually between 300 and 4800. Where filaments are gathered together directly after the melting process, the resultant fibre bundle is known as a direct roving. Several strands can also be brought together separately after manufacture of the glass, to give what is known as an assembled roving. Assembled rovings usually have smaller filament diameters than direct rovings, giving better wet-out and mechanical properties, but they can suffer from catenary problems (unequal strand tension), and are usually higher in cost because of the more involved manufacturing processes.



*Figure 25 Glass fiber*

It is also possible to obtain long fibres of glass from short fibres by spinning them. These spun yarn fibres have higher surface areas and are more able to absorb resin, but they have lower structural properties than the equivalent continuously drawn fibres.

#### Aramid Fibre / Aramid Fiber

Aramid fibre is a man-made organic polymer (an aromatic polyamide) produced by spinning a solid fibre from a liquid chemical blend. The bright golden yellow filaments produced can have a range of properties, but all have high strength and low density giving very high specific strength. All grades have good resistance to impact, and lower modulus grades are used extensively in ballistic applications. Compressive strength, however, is only similar to that of E glass.



*Figure 26 Aramid fiber*

Although most commonly known under its Dupont trade name 'Kevlar', there are now a number of suppliers of the fibre, most notably Akzo Nobel with 'Twaron'. Each supplier offers several grades of aramid with various combinations of modulus and surface finish to suit various applications. As well as the high strength properties, the fibres also offer good resistance to abrasion, and chemical and thermal degradation. However, the fibre can degrade slowly when exposed to ultraviolet light.

Aramid fibres are usually available in the form of rovings, with texes ranging from about 20 to 800. Typically the price of the high modulus type ranges from U.S. \$ 22-to U.S. \$ 40 per kg.

#### Carbon Fibre/ Carbon Fiber

Carbon fibre is produced by the controlled oxidation, carbonisation and graphitisation of carbon-rich organic precursors which are already in fibre form. The most common precursor is polyacrylonitrile (PAN), because it gives the best carbon fibre properties, but fibres can also be made from pitch or cellulose. Variation of the graphitisation process produces either high strength fibres (at  $\sim 2600^{\circ}\text{C}$ ) or high modulus fibres (at  $\sim 3000^{\circ}\text{C}$ ) with other types in between. Once formed, the carbon fibre has a surface treatment applied to improve matrix bonding and chemical sizing which serves to protect it during handling.



Figure 27 Carbon Fiber

When carbon fibre was first produced in the late sixties the price for the basic high strength grade was about U.S. \$ 300 /kg. By 1996 the annual worldwide capacity had increased to about 7000 tonnes and the price for the equivalent (high strength) grade was U.S. \$ 22-60 /kg. Carbon fibres are usually grouped according to the modulus band in which their properties fall. These bands are commonly referred to as: high strength (HS), intermediate modulus (IM), high modulus (HM) and ultra high modulus (UHM). The filament diameter of most types is about 5-7 mm. Carbon fibre has the highest specific stiffness of any commercially available fibre, very high strength in both tension and compression and a high resistance to corrosion, creep and fatigue. Their impact strength, however, is lower than either glass or aramid, with particularly brittle characteristics being exhibited by HM and UHM fibres.

**Strength and Modulus Figures for Commercial PAN-based Carbon Fibres**

Grade	Tensile Modulus (GPa)	Tensile Strength (GPa)	Country of Manufacture
<b>Standard Modulus (&lt;265GPa) (also known as 'High Strength')</b>			
T300	230	3.53	France/Japan
T700	235	5.3	Japan
HTA	238	3.95	Germany
UTS	240	4.8	Japan
34-700	234	4.5	Japan/USA
AS4	241	4.0	USA
T650-35	241	4.55	USA
Panex 33	228	3.6	USA/Hungary
F3C	228	3.8	USA
TR50S	235	4.83	Japan
TR30S	234	4.41	Japan
<b>Intermediate Modulus (265-320GPa)</b>			
T800	294	5.94	France/Japan
M30S	294	5.49	France
IMS	295	4.12/5.5	Japan
MR40/MR50	289	4.4/5.1	Japan
IM6/IM7	303	5.1/5.3	USA
IM9	310	5.3	USA
T650-42	290	4.82	USA
T40	290	5.65	USA
<b>High Modulus (320-440GPa)</b>			
M40	392	2.74	Japan
M40J	377	4.41	France/Japan
HMA	358	3.0	Japan
UMS2526	395	4.56	Japan
MS40	340	4.8	Japan
HR40	381	4.8	Japan
<b>Ultra High Modulus (&gt;440GPa)</b>			
M46J	436	4.21	Japan
UMS3536	435	4.5	Japan
HS40	441	4.4	Japan
UHMS	441	3.45	USA

Information from manufacturer's datasheets

Table 2 Comparison of E and f' of Various C-FRP

Fibre Type Comparisons

Comparing the properties of all of the fibre types with each other, shows that they all have distinct advantages and disadvantages. This makes different fibre types more suitable for some applications than others. The following table provides a basic comparison between the main desirable features of generic fibre types. 'A' indicates a feature where the fibre scores well, and 'C' indicates a feature where the fibre is not so good.

Property	Aramid	Carbon	Glass
High Tensile Strength	B	A	B
High Tensile Modulus	B	A	C
High Compressive Strength	C	A	B
High Compressive Modulus	B	A	C
High Flexural Strength	C	A	B
High Flexural Modulus	B	A	C
High Impact Strength	A	C	B
High Interlaminar Shear Strength	B	A	A
High In-plane Shear Strength	B	A	A
Low Density	A	B	C
High Fatigue Resistance	B	A	C
High Fire Resistance	A	C	A
High Thermal Insulation	A	C	B
High Electrical Insulation	B	C	A
Low Thermal Expansion	A	A	A
Low Cost	C	C	A

Table 3 Comparison of A,C,G -FRP Properties

Other Fibres

There are a variety of other fibres which can be used in advanced composite structures but their use is not widespread. These include:

Polyester

A low density, high tenacity fibre with good impact resistance but low modulus. Its lack of stiffness usually precludes it from inclusion in a composite component, but it is useful where low weight, high impact or abrasion resistance, and low cost are required. It is mainly used as a surfacing material, as it can be very smooth, keeps weight down and works well with most resin types.

Polyethylene

In random orientation, ultra-high molecular weight polyethylene molecules give very low mechanical properties. However, if dissolved and drawn from solution into a filament by a process called gel-

spinning, the molecules become disentangled and aligned in the direction of the filament. The molecular alignment promotes very high tensile strength to the filament and the resulting fibre. Coupled with their low S.G. ( $<1.0$ ), these fibres have the highest specific strength of the fibres described here. However, the fibre's tensile modulus and ultimate strength are only slightly better than E-glass and less than that of aramid or carbon. The fibre also demonstrates very low compressive strength in laminate form. These factors, coupled with high price, and more importantly, the difficulty in creating a good fibre/matrix bond means that polyethylene fibres are not often used in isolation for composite components.

#### Quartz

A very high silica version of glass with much higher mechanical properties and excellent resistance to high temperatures ( $1000^{\circ}\text{C}+$ ). However, the manufacturing process and low volume production lead to a very high price (14 mm - U.S. \$ 110 /kg, 9 mm - U.S. \$ 180 /kg).

#### Boron

Carbon or metal fibres are coated with a layer of boron to improve the overall fibre properties. The extremely high cost of this fibre restricts its use to high temperature aerospace applications and in specialised sporting equipment. A boron/carbon hybrid, composed of carbon fibres interspersed among 80-100 mm boron fibres, in an epoxy matrix, can achieve properties greater than either fibre alone, with flexural strength and stiffness twice that of HS carbon and 1.4 times that of boron, and shear strength exceeding that of either fibre.

#### Ceramics

Ceramic fibres, usually in the form of very short 'whiskers' are mainly used in areas requiring high temperature resistance. They are more frequently associated with non-polymer matrices such as metal alloys.

#### Natural

At the other end of the scale it is possible to use fibrous plant materials such as jute and sisal as reinforcements in 'low-tech' applications. In these applications, the fibres' low S.G. (typically 0.5-0.6) mean that fairly high specific strengths can be achieved.

#### Fibre Finishes

Surface finishes are nearly always applied to fibres both to allow handling with minimum damage and to promote fibre/matrix interfacial bond strength. With carbon and aramid fibres for use in

composite applications, the surface finish or size applied usually performs both functions. The finish is applied to the fibre at the point of fibre manufacture and this finish remains on the fibre throughout the conversion process into fabric. With glass fibre there is a choice of approach in the surface finish that can be applied.

#### Glass Fibre Finishes

Glass fibre rovings that are to be used in direct fibre processes such as prepregging, pultrusion and filament winding, are treated with a 'dual-function' finish at the point of fibre manufacture.



*Figure 28 Glass Fibre Finishes*

Glass fibre yarns, however, when used for weaving are treated in two stages. The first finish is applied at the point of fibre manufacture at quite a high level and is purely for protection of the fibre against damage during handling and the weaving process itself. This protective finish, which is often starch based, is cleaned off or 'scoured' after the weaving process either by heat or with chemicals. The scoured woven fabric is then separately treated with a different matrix-compatible finish specifically designed to optimise fibre to resin interfacial characteristics such as bond strength, water resistance and optical clarity.

#### Carbon Fibre Finishes

Finishes, or sizes, for carbon fibres used in structural composites are generally epoxy based, with varying levels being used depending on the end use of the fibre. For weaving the size level is about 1-2 % by weight whereas for tape prepregging or filament winding (or similar single-fibre processes), the size level is about 0.5-1 %. The chemistry and level of the size are important not only for protection and matrix compatibility but also because they effect the degree of spread of the fibre. Fibres can also be supplied unsized but these will be prone to broken filaments caused by general handling. Most carbon fibre suppliers offer 3-4 levels of size for each grade of fibre.

#### Aramid Fibre Finishes

Aramid fibres are treated with a finish at the point of manufacture primarily for matrix compatibility. This is because aramid fibres require far less protection from damage caused by fibre handling. The main types of fibre treatment are composite finish, rubber compatible finish (belts

and tyres) and waterproof finish (ballistic soft armour). Like the carbon fibre finishes, there are differing levels of composite application finish depending on the type of process in which the fibre will be used.

### Fabric Types and Constructions

In polymeric composite terms, a fabric is defined as a manufactured assembly of long fibres of carbon, aramid or glass, or a combination of these, to produce a flat sheet of one or more layers of fibres. These layers are held together either by mechanical interlocking of the fibres themselves or with a secondary material to bind these fibres together and hold them in place, giving the assembly sufficient integrity to be handled.

Fabric types are categorised by the orientation of the fibres used, and by the various construction methods used to hold the fibres together.

The four main fibre orientation categories are: Unidirectional, Woven, Multiaxial, and Other/random. These are described in the following pages.

### Unidirectional Fabrics

A unidirectional (UD) fabric is one in which the majority of fibres run in one direction only. A small amount of fibre or other material may run in other directions with the main intention being to hold the primary fibres in position, although the other fibres may also offer some structural properties. Some weavers of 0/90° fabrics term a fabric with only 75% of its weight in one direction as a unidirectional, whilst for others the unidirectional designation only applies to those fabrics with more than 90% of the fibre weight in one direction. Unidirectionals usually have their primary fibres in the 0° direction (along the roll a warp UD) but can also have them at 90° to the roll length (a weft UD).

True unidirectional fabrics offer the ability to place fibre in the component exactly where it is required, and in the optimum quantity (no more or less than required). As well as this, UD fibres are straight and uncrimped. This results in the highest possible fibre properties from a fabric in composite component construction. For mechanical properties, unidirectional fabrics can only be improved on by prepreg unidirectional tape, where there is no secondary material at all holding the unidirectional fibres in place. In these prepreg products only the resin system holds the fibres in place.

### Unidirectional Construction

There are various methods of maintaining the primary fibres in position in a unidirectional including weaving, stitching, and bonding. As with other fabrics, the surface quality of a unidirectional fabric is determined by two main factors: the combination of tex and thread count of the primary fibre and the amount and type of the secondary fibre. The drape, surface smoothness and stability of a fabric are controlled primarily by the construction style, while the area weight, porosity and (to a lesser degree) wet out are determined by selecting the appropriate combination of fibre tex and numbers of fibres per cm.

Warp or weft unidirectionals can be made by the stitching process (see information in the 'Multiaxial' section of this publication). However, in order to gain adequate stability, it is usually necessary to add a mat or tissue to the face of the fabric. Therefore, together with the stitching thread required to assemble the fibres, there is a relatively large amount of secondary, parasitic material in this type of UD fabric, which tends to reduce the laminate properties. Furthermore the high cost of set up of the 0° layer of a stitching line and the relatively slow speed of production means that these fabrics can be relatively expensive.

### Woven Fabrics

For applications where more than one fibre orientation is required, a fabric combining 0° and 90° fibre orientations is useful.

Woven fabrics are produced by the interlacing of warp (0°) fibres and weft (90°) fibres in a regular pattern or weave style. The fabric's integrity is maintained by the mechanical interlocking of the fibres. Drape (the ability of a fabric to conform to a complex surface), surface smoothness and stability of a fabric are controlled primarily by the weave style.

## 2.1.4 Manufacturing Processes

Taking composite materials as a whole, there are many different material options to choose from in the areas of resins, fibres and cores, all with their own unique set of properties such as strength, stiffness, toughness, heat resistance, cost, production rate etc.. However, the end properties of a composite part produced from these different materials is not only a function of the individual properties of the resin matrix and fibre (and in sandwich structures, the core as well), but is also a function of the way in which the materials themselves are designed into the part and also the way in which they are processed. This section compares a few of the commonly used composite production

methods and presents some of the factors to be borne in mind with each different process, including the influence of each process on materials selection.

### Pultrusion

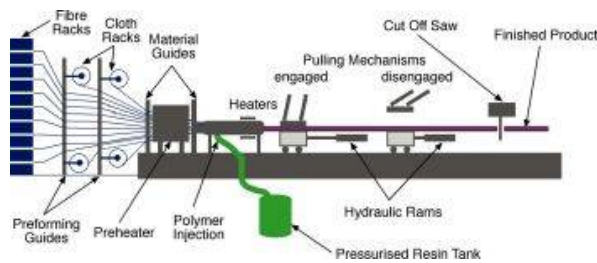


Figure 29 Pultrusion Scheme

### Description

Fibres are pulled from a creel through a resin bath and then on through a heated die. The die completes the impregnation of the fibre, controls the resin content and cures the material into its final shape as it passes through the die. This cured profile is then automatically cut to length. Fabrics may also be introduced into the die to provide fibre direction other than at  $0^\circ$ . Although pultrusion is a continuous process, producing a profile of constant cross-section, a variant known as 'pulforming' allows for some variation to be introduced into the cross-section. The process pulls the materials through the die for impregnation, and then clamps them in a mould for curing. This makes the process non-continuous, but accommodating of small changes in cross-section.

### Materials Options:

- Resins: Generally epoxy, polyester, vinylester and phenolic.
- Fibres: Any.
- Cores: Not generally used.

### Main Advantages:

- This can be a very fast, and therefore economic, way of impregnating and curing materials.
- Resin content can be accurately controlled.
- Fibre cost is minimised since the majority is taken from a creel.
- Structural properties of laminates can be very good since the profiles have very straight fibres and high fibre volume fractions can be obtained.
- Resin impregnation area can be enclosed thus limiting volatile emissions.

Main Disadvantages:

- Limited to constant or near constant cross-section components
- Heated die costs can be high.

Typical Applications:

Beams and girders used in roof structures, bridges, ladders, frameworks.

## 2.2 REINFORCEMENTS FORMS

Currently, many FRP products are available to build or repair civil engineering structures. These include:

- New structural shapes applied to beams for bridge decks
- Bridge deck panels and pedestrian bridge systems
- FRP rebars and tendons for concrete reinforcement
- FRP composite systems for repair, strengthening, seismic retrofit for beams, columns and walls



*Prefabricated Superdeck™ is installed using minimal equipment*



*Use of Carbon FRP as reinforcement of a concrete slab*

*Figure 30 Use of Carbon FRP as Reinforcement of a Concrete Slab*

As partially mentioned, reasons for the use of FRP in concrete structures are its:

- Corrosion resistance
- Low weight
- High tensile strength
- Low mechanical relaxation
- Good toughness
- High fatigue resistance
- Dimensional stability
- Stiffness
- Magnetic permeability
- Electrical conductivity
- Easy installation

A slight disadvantage of FRP today is its initial costs. A perfection of the manufacturing process and the development of new application methods and a therefore wider use will decrease these costs in the future. There are two mainly important types of reinforcements:

- INTERNAL
- EXTERNAL

### 2.2.1 Internal Reinforcement

This is the most known use of FRP, due to the characteristics of the material with which FRP is made. A smaller concrete cover is needed because of its non-corrosiveness, which allows the construction of thinner members. Furthermore, it can be used for structures in high chloride environments. Due to its non-magnetic properties, FRP is used as reinforcement in hospitals and in free-access floors, as well as in sensitive structures such as scientific laboratories and observatories. Relating to one/two/three-dimensional features of the composite, there are three different typologies of products:

- Rebars
- Grids
- Cages
- Prestressing Tendons

#### Rebars

They are fabricated in the Pultrusion process. Hereby, the fibers are pulled through a resin bath, the forming guide and cured in the heated die. The most important issue to be addressed is the bond between the rebars and the concrete. Bars fabricated in the pultrusion process have a smooth surface. Nowadays two different surface treatments are used to give rebars the necessary grip.

One is to wrap the rebar with an additional resin impregnated fiber strand while the resin of the bar is still uncured to obtain a profile. Furthermore, a sand coating is applied. The other possibility is to stamp ribs on the rebar. Rebars with an untreated surface require special anchoring devices. They are mainly used in prestressing applications.

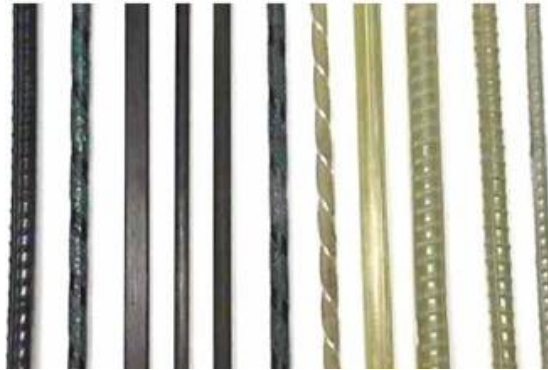


Figure 31 Rebars with Different Surfaces

### Grids

FRP composites are nowadays widely used to form 2-D reinforcing systems such as panels, grids or gratings. The method of production is a batch process. A series of continuous fibers is dispensed from individual creels by a mechanical system through a wet-bath to be deposited by two orthogonal traveling (winding) heads in a grid pattern.

The heads move at synchronized speeds that define the size of the grid. Successive movement of the heads results in fiber cross-over and the placement of interlocking layers until the desired content/cross-sectional area is achieved. 2-D FRP reinforcing systems are available in various surfaces patterns, thickness and colors (figure 32)



Figure 32 FRP Grids

Grids are used in tunnels, runways and aprons for airstrips/tarmacs, roads, buildings, channels, rehabilitation, and for general architectural elements. They are often used as lightweight reinforcement in building fascia and curtain walls, where the lower requirements for cover applications result in thinner and lighter panels. Grids can be used in the construction of floating foundation slabs, columns and column bases, walls and floors. Due to their excellent corrosion resistance, 2-D grids, especially carbon fiber reinforced, have been used extensively in marine

structures and reinforcements in systems for slope protections and stability. Some applications can be seen in figure 33.



*Figure 33 Applications of FRP Grids*

### Cages

They are ideal to reinforce complex concrete structures. Through the prefabrication, the installation time on the construction site is considerably decreased. Cages are made as a combination of pultrusion and filament winding: first the 2-D trusses are fabricated then these are combined into a 3-D cage by filament winding. Further complex shapes can be assembled by combining these elements. Fiber material, number of filaments and distance between rovings can be varied easily. Figure 29 shows an example for a GFRP cage.



*Figure 34 GFRP Cage*

### Prestressing Tendons

The interest in the use of FRP composites in prestressed concrete is mainly based on durability issues. Corrosion of prestressing steel tendons caused serious deterioration of infrastructure. Properties as high tensile strength and high resistance to corrosion would appear to make FRP

composites good candidates for prestressing tendons. A problem is that FRP materials are very time dependent. Under constant load they show varying degrees of creep deformation:

- CFRP does not creep
- GFRP shows a negligible creep
- AFRP is showing long-term deformations due to creep.

Furthermore, GFRP tendons exhibit premature tensile rupture under sustained loading. Carrying permanent tension, the tensile strength of GFRP drops to values as low as 20% what causes stress rupture. Because of these reasons CFRP seems to be the most suitable FRP for prestressing applications. Another problem, which needs to be addressed, is the anchorage of the tendons. Special devices are necessary due to the low transverse strength of the tendons. Examples for on the market available anchorage systems are shown in figure 35.



*Figure 35 Anchorage Systems for Prestressing Tendons  
(Leadline tendons, Parafil tendons, Carbon stress tendons)*

### 2.2.2 External Reinforcement

It is used for the strengthening of structures and for the seismic upgrade. The principles behind externally bonding FRP plates or wraps to concrete structures are very similar to the principles used in the application of bonded steel plates. In general, the member's flexural, shear, axial strength, or blast resistance, is increased or better mobilized by the external application of high tensile strength material (FIB – Federation Internationale du Beton – 2001, figure 36). Reasons for applying FRP systems as an external reinforcement for bridge structures include:

- Capacity upgrade due to a change in use of a structure
- Passive confinement to improve seismic resistance
- Crack control
- Strengthening around new openings in slabs
- Correction of a design deficiency

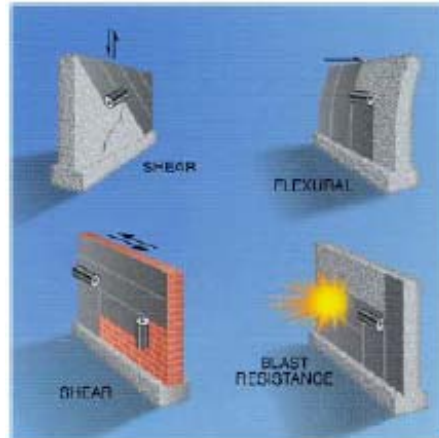


Figure 36 FRP Application on Walls

The following are some of the most important products available in commerce:

- Laminates
- Pre-cured elements
- Hand lay-up systems
- Near Surface Mounted bars
- FRP Spray-up

### Laminates

Laminates are made by stacking a number of thin layers (laminae) of fibers and matrix and consolidating them into the desired thickness. Fiber orientation in each layer, as well as the stacking sequence of the various layers, can be controlled to generate a range of physical and mechanical properties. Different systems of laminates exist, related to the constituent materials, the form and the technique of the FRP application. In general, these can be subdivided into “wet lay-up” (or “cured in-situ”) systems and “prefab” (or “pre-cured”) systems.

The most common form of fiber-reinforced composites used in structural applications is called a “laminate”. Two types of FRP laminates (GFRP and CFRP) are shown in figure 37.

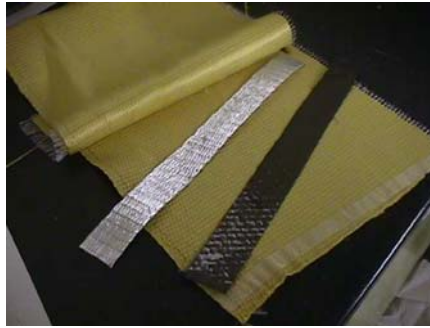


Figure 37 FRP Laminates

### Pre-Cured Systems

They consist of a wide variety of composite shapes manufactured in the system supplier's facility and shipped to the job site. They are typically in the form of thin ribbon strips or grids that may be delivered in a roiled coil. Normally strips are pultruded. Typically, an adhesive (e.g. epoxy) is used to bond the precured shapes to the concrete surface.

### Hand Lay-Up systems

The most interesting types related to this technique are the following:

Dry unidirectional fiber sheet and semi-unidirectional fabric, where fibers run predominantly in one direction partially or fully covering the structural element, and dry multidirectional fabric, where fibers run in at least two directions. Installation on the concrete surface requires saturating resin usually after a primer has been applied. Two different processes can be used to apply the fabric:

Formatted: Bullets and Numbering

- The fabric can be applied directly into the resin usually after a primer has been applied uniformly onto the concrete surface
- The fabric can be impregnated with the resin in a saturator machine and then applied wet to the sealed substrate

Resin pre-impregnated uncured unidirectional or multidirectional sheet or fabric, where fibres run predominantly in one direction. Installation may be done with or without additional resin.

Dry fibre tows (untwisted bundles of continuous fibres) that are wound or otherwise mechanically placed onto the concrete surface. Resin is applied to the fibre during winding.

Pre impregnated fibre tows that are wound or otherwise mechanically placed onto the concrete surface. Product installation may be executed with or without additional resin.



Figure 38 FRP Sheets

Near Surface Mounted Bars

This FRP-based strengthening technique is a valid alternative to externally bonded FRP laminates. Although the use of FRP rods for this application is very recent, Near Surface Mounted (NSM) steel rods have been used in Europe for strengthening of RC structures since the early 50's.

Nowadays, FRP rods (GFRP and CFRP) are used in place of steel and epoxy paste replaces cementitious mortar. The advantage is primarily the resistance of FRP to corrosion. This property is particularly important in this case due to the position of the rods very close to the surface, which exposes them to the environmental attacks (De Lorenzis, L., Nanni, A. – 1999).

The use of NSM FRP rods is an attractive method for increasing the flexural and the shear strength of deficient RC members and masonry walls and, in certain cases, can be more convenient than using FRP laminates. Furthermore, this technique becomes particularly attractive for strengthening in the negative moment regions of slabs and decks, where external reinforcement would be subjected to mechanical and environmental damage and would require protective cover which could interfere with the presence of floor finishes. Examples for the application of NSM bars are shown in figure 39.



Figure 39 Near Surface Mounted Bars

## 2.3 PHYSICAL AND MECHANICAL PROPERTIES

### 2.3.1 Introduction

Composites benefits

Composite materials have been used for centuries, such as bricks reinforced with straw, laminated iron-steel swords and gun barrels and concrete, etc. The oldest of all the resins commonly used in reinforced plastics are “phenolics”, having been known for over nine decades. They date commercially from about 1909 and were used first as wood lacquers rather than in composites, whereas polyesters have been used structurally in reinforced plastics since the 1940s. The benefits of using composite materials include:

- High strength
- Light weight
- Cost
- Design flexibility
- Corrosion resistance
- Durability

#### High Strength

Composite materials can be designed to meet the specific strength requirements of an application. A distinct advantage of composites, over other materials, is the ability to use many combinations of resins and reinforcements, and therefore custom tailor the mechanical and physical properties of a structure. The fiber reinforcements provide good damping characteristics and high resistance to fatigue and most resins provide very good resistance to chemicals and corrosion.

The fracture toughness of composites is better than aluminum castings: castings basically have built-in notches that can catastrophically fracture under impact. The fiber reinforcement of composites alters this failure sequence, resulting in an increased resistance to impact. This toughness of composites can be maximized by fiber selection, length of fiber and use of tougher resin such as thermoplastics.

### Light Weight

Composites offer materials that can be designed for both light-weight and high strength. In fact, composites are used to produce the highest strength-to-weight ratio structures known to man. A weight savings of 27% is attainable in most structures. This is due to the lower density of composites, which range (depending on material form) from 1246 kg/m<sup>3</sup> (0.045 lb/in<sup>3</sup>) to 1800 kg/m<sup>3</sup> (0.065 lb/in<sup>3</sup>) as compared to 2768 kg/m<sup>3</sup> (0.10 lb/in<sup>3</sup>) for aluminum.

### Cost

Tooling costs for high volume production of metals and composites parts are similar and also the production labor time is similar and the higher cost of composite parts is mostly due to high raw material costs. This means that high volume manufacturing methods are used to make composites cost competitive with metals: a reasonable selection of the optimal material for this part and of the suppliers can minimize the cost penalty.

### Design Flexibility

Composites have an advantage over other materials because they can be molded into complex shapes at relatively low cost. The flexibility offers designers a freedom, which is a hallmark of composites achievement. This transforms into a reduction of part count, fasteners and assembly time. The attachment areas of parts are where the majority of failures occur, due to high point loads and stress concentrations. Elimination of these interfaces improves the reliability of the structure. See figure 40 for an example of the underside of the pedestrian walkways on the LaSalle Street bridge: the walkways are supported by the original walkway cantilever girders (gray).



Figure 40 *Lasalle Street – Composite Pedestrian Walkway (Chicago, IL)*

### Corrosion Resistance

Composites provide long-term resistance to severe chemical and temperature environments. Composites are the material of choice for outdoor exposure, chemical handling applications and severe environment service.

### Durability

Composite structures have an exceedingly long lifespan. Coupled with low maintenance requirements, the longevity of composites is a benefit in critical applications. In a half-century of composites development, well-designed composite structures have yet to wear-out.

Nowadays, the composites industry continues to grow as a major provider of materials as more designers, engineers and manufacturers discover the benefits of these versatile materials.

In the normal reinforcing practice we can find many different types of composites:

- Injection of epoxy based resin
- Application of steel bars on the surface
- Repair and replacement of localized damaged areas
- FRP composites

In the passed thirty years, new composite materials appeared in the market: the fiber reinforced polymeric (FRP) materials.

In the following paragraphs a brief description of the main mechanical and physical properties for some kinds of FRP is presented. The properties of FRP bars and FRP laminates, sheets and fabrics are mainly analyzed.

### **2.3.2 FRP Rebars**

FRP rebars offer advantages over steel reinforcement because they are non-corrosive and non-conductive: As shown, the available FRP bars are made of aramid, carbon or glass. Factors, such as fiber volume, type of fiber, type of resin, fiber orientation, dimensional effects and manufacturing methods play a major role in establishing product characteristics.

The relative volume of fibers and resin in the product affects the properties of FRP rods: a usual fiber volume is between 0.5 and 0.7. Furthermore, the mechanical properties of FRP bars, like all structural materials, are affected by such factors as loading history and duration, temperature and moisture. FRP bars have a density ranging from four to six times smaller than that of steel. The reduced weight leads to lower transportation costs and decreased handling and installation time per bar on the job site. Before analyzing deeply the different properties, here is shown, in table 4, a summary of them (Fukuyama, H - 1999). [Note: 1 MPa = 145 psi]

Table 4 Properties of FRP Bars and Comparison with the Steel

	Steel	Fiber			
		Aramid (A)	Carbon (C)	Glass (G)	GC - Hybrid
Axial Fiber Volume %	-	43 – 69	43 – 66	40 – 68	40
Diameter mm (in)	-	3.0 - 21.8 (0.12 – 0.86)	3.0 - 40.0 (0.12 – 1.57)	2.4 - 19.4 (0.09 – 0.76)	7.1 - 23.8 (0.28 – 0.94)
Density g/cm <sup>3</sup> (p/in <sup>3</sup> )	7.8 (0.28)	1.2-1.5 (0.043–0.052)	1.3-1.6 (0.047–0.058)	1.5-2.0 (0.052–0.072)	1.7 (0.061)
Guarantied Tensile Str. MPa (ksi)	<b>483 - 690</b> (70 – 100)	1300 – 1830 (188 – 265)	<b>780 – 1800</b> (113 – 261)	<b>590 – 1130</b> (85 – 164)	530 (77)
E-Modulus 10 <sup>3</sup> MPa (10 <sup>3</sup> ksi)	<b>200</b> (29)	42 – 78 (6 – 11)	<b>73 – 210</b> (10 – 30)	<b>30 – 49</b> (4 – 7)	37 (5)
Yield Strain %	<b>0.14 - 0.25</b>	N/A	N/A	N/A	N/A
Rupt Str. %	<b>0.6 - 0.12</b>	0.5-1.7	<b>1.2-3.1</b>	<b>1.9-4.4</b>	1.4

#### Coefficient of thermal expansion and effects of high temperatures

The coefficients of thermal expansion of FRP bars vary in the longitudinal and transverse directions depending on the types of fiber, resin and volume fraction fiber. Table 5 (fiber volume fraction ranging from 0.5 to 0.7) lists the longitudinal and transverse coefficients of thermal expansion for typical FRP bars and steel bars (ACI Committee 440): note that a negative coefficient of thermal expansion indicates that the material contracts with increased temperature and expands with decreased temperature.

Table 5 Typical Coefficients of Thermal Expansion for Reinforcing Bars

Direction	Steel	AFRP	CFRP	GFRP
Long, $\alpha_L$	11.7x10 <sup>-6</sup> /°C (6.5x10 <sup>-6</sup> /°F)	-6 to 2x10 <sup>-6</sup> /°C (-3.3 to -1.1x10 <sup>-6</sup> /°F)	-2 to 0x10 <sup>-6</sup> /°C (-4 to 0 x10 <sup>-6</sup> /°F)	6 to 10x10 <sup>-6</sup> /°C (3.3 to 5.6 x10 <sup>-6</sup> /°F)
Trans, $\alpha_T$	11.7x10 <sup>-6</sup> /°C (6.5x10 <sup>-6</sup> /°F)	60 to 80x10 <sup>-6</sup> /°C (33.3 to 44.4x10 <sup>-6</sup> /°F)	23 to 32x10 <sup>-6</sup> /°C (41 to 58 x10 <sup>-6</sup> /°F)	21 to 23x10 <sup>-6</sup> /°C (11.7 to 12.8x10 <sup>-6</sup> /°F)

The use of FRP reinforcement is not recommended for structures in which fire resistance is essential to maintain structural integrity, because the polymers will soften due to the excessive heat. Beyond the glass-transition temperature, the elastic modulus of a polymer is significantly reduced due to changes in its molecular structure.

However, the tensile properties of the overall composite are reduced due to a reduction in force transfer between fibers through bond to the resin. Other properties more directly affected by the shear transfer through the resin, such as shear and bending strength, are reduced significantly at temperatures above the  $T_g$ .

#### Mechanical properties and behavior

##### Tensile behavior

Ultimate tensile strength of FRP bars is reached without exhibiting any plastic yielding: the tensile behavior is characterized by a linearly elastic stress-strain relationship until failure. Unlike steel bars, some FRP bars exhibit a substantial size effect: the fibers located near the center of the bar cross-section are subjected at less stress as for the fibers that are near the outer surface. This phenomenon results in reduced strength and efficiency in large diameter bars. Strength and stiffness variations will occur in bars with various fiber-volume fractions, even in bars with the same diameter, appearance, and constituents.

##### Compressive behavior

Compressive strengths of 55%, 78%, and 20% of the tensile strength have been reported for GFRP, CFRP, and AFRP, respectively. The compressive modulus of elasticity of FRP reinforcing bars appears to be smaller than its tensile modulus of elasticity; according to reports, the compressive modulus of elasticity is approximately 80% for GFRP, 85% for CFRP, and 100% for AFRP of the tensile modulus of elasticity for the same product.

Standard test methods are not yet established to characterize the compressive behavior of FRP bars; if the compressive properties of a particular FRP bar are needed, these should be obtained from the bar manufacturer. However it is not recommended to rely on FRP bars to resist compressive stresses.

#### Shear behavior

Most FRP bar composites are relatively weak in interlaminar shear where layers of unreinforced resin lie between layers of fibers, because there is usually no reinforcement across layers, and the interlaminar shear strength is governed by the relatively weak polymer matrix. This shortcoming can be overcome by orienting the FRP bars so that they resist the applied loads through axial tension.

#### Bond behavior

Bond performance of an FRP bar is dependent on the design, manufacturing process, mechanical properties of the bar itself, and the environmental conditions. The bond force of an embedded bar can be transferred by:

- Adhesion resistance of the interface, also known as chemical bond
- Frictional resistance of the interface against slip
- Mechanical interlock due to interface irregularity

#### Handling of FRP Rebars

FRP reinforcing bars are susceptible to surface damage and puncturing their surface can significantly reduce the strength capacity; in the case of glass FRP bars, the surface damage can cause a loss of durability due to infiltration of alkalis. The following handling guidelines are recommended to minimize damage to both the bars and the bar handlers:

- FRP-reinforcing bars should be handled with work gloves to avoid personal injuries from either exposed fibers or sharp edges
- FRP bars should not be stored on the ground, pallets should be placed under the bars to keep them clean and to provide easy handling
- High temperatures, ultraviolet rays, and chemical substances should be avoided
- When necessary, cutting should be performed with a high-speed grinding cutter or a fine blade saw. FRP bars should never be sheared. Dust masks, gloves, and glasses for eye protection are recommended when cutting because there is insufficient research available to make any recommendation on treatment of saw-cut bar ends.

**2.3.3 FRP Laminates, Sheets and Fabrics**

One of the best qualities of these materials is the thickness, because this property is often requested for rehabilitating or restoring the strength of a weakened structural element, or retrofitting or strengthening a sound structural element to resist increased loads due to changes in use of the structure. Some characteristics can be found in Table 6:

*Table 6 Main Characteristics and Typical Aspects of FRP (Basic Technique)*

	PRE-CURED (PREFAB)	CURED IN SITU (WET LAY- UP)
Shape	Strips or laminates	Sheets or fabrics
Thickness	About 1.0 to 1.5 mm (0.04 to 0.06 in)	About 0.1 to 0.5 mm (0.004 to 0.02 in)
Use	Simple bonding of the factory made elements with adhesives	Bonding and impregnation of the sheets or fabrics with resin (shaped and cured in-situ)
Typical application aspects	If not pre-shaped only for flat surfaces	Regardless of the shape, sharp corners should be rounded
	Thixotropic adhesive for bonding	Low viscosity resin for bonding and impregnation
	Normally 1 layer, multiple layers possible	Often multiple layers
	Stiffness of strip and use of thixotropic adhesive allow for certain surface unevenness	Often a putty is needed to prevent debonding due to unevenness
	Simple in use, higher quality guarantee (prefab system)	Very flexible in use, needs rigorous quality control
	Quality control (wrong application and bad workmanship = loss of composite action between FRP EBR and substrate/structure, lack of long term integrity of the system, ecc.)	

*Table 7 Properties of FRP Sheets*

Fibers	Area weight g/m <sup>2</sup> (lb/foot <sup>2</sup> )	Thickness mm (in)	Tensile Strength MPa (ksi)	E-Modulus 10 <sup>3</sup> MPa (10 <sup>3</sup> ksi)
High strength Carbon	200 – 400 (0.04 – 0.08)	0.1 - 0.2 (0.004 – 0.008)	<b>2900 – 3500</b> (421 – 507)	<b>230</b> (33)
High E-Modulus Carbon	200 – 300 (0.04 – 0.06)	0.1 - 0.2 (0.004 – 0.008)	<b>1960 – 2940</b> (284 – 426)	<b>370 – 640</b> (53 – 93)
High strength Aramid	235 – 525 (0.05 – 0.11)	0.2 - 0.4 (0.008 – 0.015)	2400 (348)	80 (12)
High E-Modulus Aramid	280 – 623 (0.06 – 0.13)	0.2 - 0.4 (0.008 – 0.015)	2100 (304)	120 (17)
Glass	300 (0.06)	0.2 (0.008)	<b>1470</b> (213)	<b>73</b> (10)

Material Properties sheets are shown in table 7 (Fukuyama, H – 1999). Hereby the numbers given do not take the resin properties into consideration, as, because of the application process, the exact amount of resin cannot be determined.

#### Coefficient of thermal expansion and effects of high temperatures

The coefficients of thermal expansion of unidirectional FRP materials differ in the longitudinal and transverse directions, depending on the types of fiber, resin, and volume fraction of fiber. Table 8 (fiber volume fraction ranging from 0.5 to 0.7) illustrates the typical coefficients of thermal expansion for unidirectional materials (ACI Committee 440).

*Table 8 Typical Coefficients of Thermal Expansion for Unidirectional FRP Materials*

Direction	Steel	AFRP	CFRP	GFRP
Long, $\alpha_l$	11.7x10 <sup>-6</sup> /°C (6.5x10 <sup>-6</sup> /°F)	-6 to 2x10 <sup>-6</sup> /°C (-3.3 to -1.1x10 <sup>-6</sup> /°F)	-1 to 0x10 <sup>-6</sup> /°C (0.6 to 0 x10 <sup>-6</sup> /°F)	6 to 10x10 <sup>-6</sup> /°C (3.3 to 5.6 x10 <sup>-6</sup> /°F)
Trans, $\alpha_T$	11.7x10 <sup>-6</sup> /°C (6.5x10 <sup>-6</sup> /°F)	60 to 80x10 <sup>-6</sup> /°C (33 to 44x10 <sup>-6</sup> /°F)	22 to 50x10 <sup>-6</sup> /°C (12 to 27 x10 <sup>-6</sup> /°F)	19 to 23x10 <sup>-6</sup> /°C (10.4 to 12.6x10 <sup>-6</sup> /°F)

When there is high temperature, beyond the  $T_g$ , the elastic modulus of a polymer is significantly reduced due to changes in its molecular structure; due to a reduction in force transfer between fibers through bond to the resin, the tensile properties of the overall composite are reduced. Test results have indicated that temperatures of 250°C (480 °F), much higher than the resin  $T_g$ , will reduce the tensile strength of GFRP and CFRP materials in excess of 20%. Other properties affected by the shear transfer through the resin, such as bending strength, are reduced significantly at lower temperatures.

#### Mechanical properties and behavior

##### Tensile behavior

The properties of an FRP system should be characterized as a composite, recognizing not just the material properties of the individual fibers but also the efficiency of the fiber-resin system and fabric architecture. The tensile properties of some commercially available FRP-strengthening systems are summarized in table 9.

Table 9 Properties of Some Commercially Available FRP Systems

FRP-system description (fiber type/saturating resin/fabric type)	Fabric weight		Ultimate strength <sup>(1)</sup>	
	g/m <sup>2</sup>	lb/foot <sup>2</sup>	kN/m	lb/in
General purpose carbon/epoxy/ unidirectional sheet	200	0.04	500	2850
	400	0.08	625	3562
High-strength carbon/epoxy/ unidirectional sheet	230	0.05	315	1795
	300	0.06	700	3990
	620	0.13	960	5472
High-modulus carbon/epoxy/ unidirectional sheet	300	0.06	600	3420
General-purpose carbon/epoxy/ balanced fabric	300	0.06	175	997
E-glass/epoxy/ unidirectional sheet	900	0.18	720	4104
	350	0.07	230	1311
E-glass/epoxy/ balanced fabric	300	0.06	120	684
Aramid/epoxy/ unidirectional sheet	415	0.08	700	3990
High-strength carbon/epoxy/ precured, unidir. laminate	2385	536.17	3300	18810
E-glass/vinyl ester/ precured, unidirectional shell	1695	381.05	1575	8977

<sup>(1)</sup> Ultimate tensile strength per unit of sheet or fabric

Table 10 shows the typical tensile properties of FRP laminates with fiber volumes between 40% to 60%.

Table 10 Tensile Properties of FRP Laminates with Fiber Volumes of 40% to 60%

FRP-system description (fiber orientation)	Young's modulus		Ultimate tensile strength		Rupture strain at 0 degrees
	Property at 0 degrees	Property at 90 degrees	Property at 0 degrees	Property at 90 degrees	
	GPa	MPa	MPa	MPa	
High-performance aramid/ epoxy, degrees					
0	48-68	2-7	700-1725	35-70	2.0-3.0
0/90	28-34	28-35	275-550	275-550	2.0-3.0
+45/-45	7-14	7-14	140-205	140-200	2.0-3.0
High-strength carbon/epoxy, degrees					
0	100-145	2-7	1025-2075	35-70	1.0-1.5
0/90	55-76	55-75	700-1025	525-1025	1.0-1.5
+45/-45	14-28	14-28	175-275	175-275	1.5-2.5
E-glass/epoxy, degrees					
0	20-40	2-7	525-1400	35-70	1.5-3.0
0/90	14-34	14-35	525-1025	525-1025	2.0-3.0
+45/-45	14-21	14-20	175-275	175-275	2.5-3.5

[zero degrees represent unidirectional fiber orientation, zero/ninety degrees (or  $\pm 45$  degrees) represents fiber balanced in two orthogonal directions, where zero degrees is the direction of the load]

#### Compressive behavior

Generally, compressive strength is higher for materials with higher tensile strengths except in the case of AFRP where the fibers exhibit nonlinear behavior in compression at relatively low levels of stress. For all other compressive behaviors, see the paragraph on FRP bars.

#### Handling of FRP laminates, sheets and fabrics

Each FRP-system-constituent material has different handling and storage requirements to prevent damage, so, the better way is to consult with the material manufacturer for guidance. There are precautions that should be observed when handling thermosetting resins and their component materials.

The workforce has to wear suits and gloves; disposable rubber or plastic gloves are recommended and should be discarded after each use. Gloves should be resistant to resins and solvents. Respiratory protection, such as dust masks or respirators, should be used when fiber fly, dust, or organic vapors are present.

### **2.3.4 Durability of FRP Composites**

Although FRP composites have been successfully used in the automotive, marine, industrial, and aerospace sectors, there are critical differences in loading, environment, and even the types of materials and processes used in these applications, as compared to the materials-process-load combinations that are likely to be used in civil infrastructure applications.

The durability of FRP composites is, obviously, one of the most important features we must take in consideration when we decide to apply these materials. FRP composites (and their constituents) can be affected by a variety of factors (including those related to the natural and surrounding environment), and the actual effect of each of these factors, or combinations thereof, can be substantially affected by the presence or absence of defects or other damage to the composite (or constituents thereof).

Durability of a material or structure can be defined as “its ability to resist cracking, oxidation, chemical degradation, delamination, wear, and / or the effects of foreign object damage for a

specified period of time, under the appropriate load conditions, under specified environmental conditions” (V.M. Karbhari).

There are different reasons for a lost in durability, the most significant are:

- Fatigue Resistance
- Creep - Relaxation
- Fire
- Thermal Effects
- Moisture (water)
- Alkaline Environment
- Agressive Chemical Solutions
- UV Exposure

Fatigue

Fatigue is generally defined as the physical phenomenon that causes a material, or component, to fail after the submission to an applied condition or conditions (cycles), even though the level of that condition (mechanical load, etc.) is not high enough to cause failure on the first cycle. Fatigue “life” is usually measured as the number of cycles to failure for a given applied level, as shown in figure 41 (A. Nanni, J. Lesko et al.). The loading may be mechanical (due to vehicle traffic, for example), thermal (from variations in temperature), or chemical (from seasonal road treatments, oxidation, water, etc.).

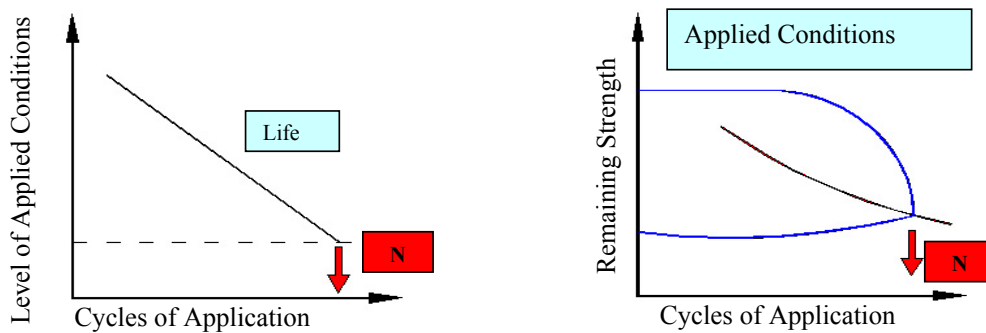


Figure 41 “Fatigue”Life Representation (left) and Remaining Strength (right)

If the material, or component, does not fail on the first application of load, then the level of applied load must be lower than the initial static strength. If the component does fail after many cycles of

application of the load (or other environment), then the strength at the time of that failure must be the same as the level of applied load, i.e., the strength of the material or component must have been reduced to the level of applied loading by some degradation process.

So the key to understanding fatigue of civil structures (or any other structure) is to understand the processes that reduce the strength of the material as a function of cycles of application of the applied environment. Figure 41 (A. Nanni, J. Lesko et al) shows the remaining strength after cycles of application.

In metals, many studies show that fatigue failure consists of crack initiation and growth. Crack initiation starts with a dislocation movement, then submicrocracks are formed at slip bands. They subsequently grow and merge to form a crack of detectable size to complete the crack initiation process. This is then followed by the growth of a single crack until final rupture. The period of crack initiation and submicrocrack growth covers most of the fatigue life (Pritchard, 1999).

In neat polymers, the fatigue failure process is quite similar. There are certain differences for some amorphous thermoplastics, such as polystyrene: phase crazes are formed during the initiation and then the subsequent fatigue crack propagation phase leads to final failure.

In short fiber reinforced composites, with aligned or randomly distributed fibers, cracks initiate at flaws, such as pores or in resin-rich areas with local strain in homogeneities caused by improper fiber alignment or at fiber ends. The local load transfer from the fiber into the matrix can lead to an overstressing of the matrix or a fiber/matrix debonding. After that, crack propagation can occur, but not as smooth as in metals.

In continuous fiber reinforced composites, the fatigue process is characterized by the initiation and multiplication of cracks, rather than propagation. Crack initiation occurs early in fatigue life, and coincides with the cracking of the weakest ply.

While in metals, crack growth accelerates during fatigue, crack multiplication in composites decelerates, resulting in uncontrolled final rupture of the composite, also called as *sudden death* (Pritchard, 1999).

FRP composites show significantly enhanced fatigue resistance over metallic materials. The fatigue life of FRP composites depends on various parameters such as frequency, amplitude ratio, specimen shape, load control, failure criteria. As a summary, some features are illustrated in table 11.

*Table 11 Properties of FRP Composites Fatigue Resistance*

	Fatigue Resistance related to prestressing steel	Dependency of stress level on the fatigue strength, related to prestressing steel	Endurance Limit at 2000000 cycles MPa (ksi) [*]
AFRP	Similar	Similar	700.5 (101.6)
CFRP	-	3 – 4 times higher	1500.9 (217.7)
GFRP	Low	Similar	500.5 (72.6)

[\*]: Curtis, 1989

Fatigue failure in FRP composites is usually initiated through fiber/matrix debonding and matrix micro cracking. Of all types of current FRP composites for infrastructure application, CFRP is generally thought to be the least prone to fatigue failure like E-glass and S-glass, but, for the last two types, environmental factors play an important role in the fatigue behavior due to their susceptibility to moisture, alkaline and acidic solutions. Aramid fibers, for which substantial durability data are available, appear to behave similarly to carbon and glass fibers in fatigue.

#### Creep and relaxation

FRP subjected to a constant load over time can suddenly fail after a time period called “the endurance time”. This phenomenon is known as creep rupture (or static fatigue). Creep rupture is not an issue with steel bars in reinforced concrete except in extremely high temperatures such as those encountered in a fire.

The creep rupture endurance time can also irreversibly decrease under sufficiently adverse environmental conditions, such as high temperature, ultraviolet radiation exposure, high alkalinity, wet and dry cycles, or freezing-thawing cycles and moisture. There are different behaviors for the three different types of FRP: in general, carbon fibers are the least susceptible to creep rupture. Aramid fibers are moderately susceptible, and glass fibers are the most susceptible to creep rupture (R. Morgan et al.)

On the other side carbon fibers exhibit no degradation with chemical-induced strength, but they have a larger spread in median failure times under stress rupture conditions. There have been studies (Chiao et al.) about Fiber Stress Rupture Level, as shown in table 12 (R. Morgan et al.), thanks to which we can know that:

- Aramid and glass fibers are very susceptible to alkali-induced, chemical-induced strength degradation, which, over long periods, will generally predominate over any fiber stress rupture attributes.

- Carbon fibers exhibit no chemical-induced strength degradation but exhibit a much larger spread in median failure times than aramid or glass fibers.
- The chemical-induced fiber strength degradation will be component specific and dependent on migration of moisture and alkali media to the fiber vicinity.

*Table 12 Fiber Stress Rupture Level for 10% Population Failures after 75 years Continuous Stress Exposure under Ambient Conditions*

Fiber Type	10% Failure Probability Stress Rupture Level after 75 years	Spread in Medium Time to fail in decades
Aramid	60%	3
Carbon	75%	6
Glass	50%	2.5

It's important to underline that the creep behavior of composites is strongly dependent on the fiber orientation of the system. The time dependency of creep compliance is less affected by the creep behavior of the matrix if the composite is loaded along the direction of the fiber. Overall, the shear creep modulus of the system is much smaller and exhibits much stronger time-dependency than the creep modulus in tension and compression along the fiber directions.

#### Fire and high thermal exposure

One of the most serious concerns in any application of organic matrix-based composites is the possibility that an accidental (or deliberate) fire may ignite the composite material, with a consequential release of heat and potentially toxic smoke. Besides, the composite can become the fuel for the fire, leading to a larger fire, and involving the whole structure.

Compared to other non-filled plastics, composites have a built-in advantage that helps resist the worst consequences (extensive fire involvement). This is a result of their non-combustible fiber content of as high as 70% by weight. The fibers displace polymer resin, making less fuel available to the fire. When the outermost layers of a composite lose their resin due to heat-induced gasification, they act as an insulating layer, slowing heat penetration and evolution of gases from the depth of the composite.

In critical applications, the FRP may be fireproofed with the use of special fire-resistant additives, intumescent coatings and the addition of inorganic fillers, but these increase the costs and, depending on the application, may not be possible. The usual method to achieve the necessary structural fire rating is to use the FRP reinforcement as supplemental reinforcement. With this concept, the existing structure will not be able to totally collapse with FRP reinforcement.

### Thermal Effects

FRP composites are subjected to thermal effects both during processing and throughout their lives.

There are mainly three thermal effects:

- Temperature above the cure temperature
- Freezing and freeze-thaw conditions
- Temperature variations and cycles

One of the most important aspects to be considered during design is about the coefficients.

*Table 13 Thermal Expansion Coefficients*

Material	Coefficient $10^{-6}$ 1/K	
	Longitudinal	Transverse
AFRP	-2.0 – -1.0	60 – 80
Aramid Fiber	-6.0 – -2.0	55 – 60
CFRP	-0.5 – 1.0	20 – 40
Carbon Fiber	-0.9 – 0.7	8 – 19
GFRP	7 – 12	9 – 20
Glass Fiber	5 – 15	5 – 15
Steel	6.5	
Resins	60 – 140	
Concrete	6 – 13	

In table 13 we can see that the coefficients of thermal expansion of GFRP are similar to that of concrete, whereas those of CFRP and AFRP are not. Also that the coefficients of adhesives can be orders of magnitude different from those of bulk resins and/or composites, and hence thermal gradients/exposure can cause premature debonding along the FRP composite-adhesive-concrete interfaces (not a sentence). Since the FRP composites are often used in conjunction with a concrete substrate in the form of external reinforcement, the response of both the resin and adhesive needs to be considered.

It is noted that resins and adhesives soften over a temperature range, which causes an increase in viscoelastic response, a consequent reduction in elastic mechanical performance levels, and, in a

number of cases, an increased susceptibility to moisture absorption. Prior researches have shown some general consequences, as reported in table 14.

*Table 14 Consequence of Temperature over FRP*

Temperature behavior	Consequence
Sub-zero	Composites are expected to withstand years of sub-zero conditions, but they can show matrix hardening, matrix microcracking, and fiber/matrix bond degradation
Freeze-thaw	Does not affect fibers although it can affect the resin and the fiber/resin interface
Freeze-thaw in the presence of salt	Accelerated degradation due to the formation and expansion of salt deposits in addition to effects of moisture induced swelling and drying
Temperature above that of processing	An initial post-cure followed by degradation due to thermal effects
Temperature exceeds the glass transition temperature ( $T_g$ )	FRP composite performance can be expected to drop
Thermal cycling	In general does not cause deleterious effects, although extended cycles of brittle resin systems can result in microcrack formation

The greatest concern with temperature effects on composite structures in civil engineering applications is that freeze-thaw conditions can potentially result in debonding of laminates, either from concrete, or from other FRP composite elements, particularly if there are gaps at the adhesive bond line.

Another important question is that FRP composites should not be used at temperatures above their glass transition temperatures. For purposes of design it is recommended that materials be chosen with a  $T_g$  at least 30°C (86 F) above the maximum use temperature (T. Juska et al.)

It must be noted that the synergistic effects of moisture and thermal effects can be substantially greater than those of each environment by itself. Due to effects related to glass transition temperature and viscoelasticity, possible loss in shear response of adhesives, and changes in response in sub-zero environments, the determination of effects and the durability of FRP systems in these environments is critical.

**Moisture (water)**

Moisture absorption in FRP composite depends on the type of resins, laminate composition, thickness, laminate quality, curing condition, fiber/resin interface and manufacturing process. In some applications, performance is improved with the use of a corrosion barrier.

The primary effect of the absorption is on the resin itself — through hydrolysis, plasticization, saponification, and other mechanisms — which causes both reversible and irreversible changes in

the polymer structure. In some cases, the moisture “walks” along the fiber-matrix interphase and has been shown to cause deleterious effects to the fiber-matrix bond, resulting in a loss of integrity at that level.

It is, however, possible to protect these fibers from rapid attack through the selection of appropriate resin systems, processing conditions, and the application of gel coats and protective coatings. In general, degradation is significantly retarded if the resin (and resulting composite) is completely cured prior to use in a service environment. FRP composite components used in civil infrastructure are often exposed to rain, humidity, moisture, or diffused solutions through other substrates (such as concrete). An example is shown in figure 42.



*Figure 42 Water Tank in Castiglione del Lago (Pg, Italy)*

In some cases, these components may even be immersed in aqueous solutions, as in the case of column jackets used for bridge columns in flood plains, structures used in harbors, or bridge decks that could have pounding or overflow in times of heavy rain. Most effects of moisture and solution-related deterioration/degradation are on the strength of a composite, with changes in modulus, in most cases, being very small, generally of the order of 10% over a period of 10-15 years. Based on the current state of knowledge and on several tests (D. Hunston et al.) over this problem, we can conclude that:

- Preference should be given to the use of appropriate epoxies and vinylesters
- Through the use of gel coats and surface scrim layers we can obtain an appropriate thickness of resin-rich surface in FRP composites and that the resin layer remaining uncracked through the period of intended use

- Due to the effect of moisture on glass transition temperature, composites must be cured such that the  $T_g$  achieved is significantly higher than the maximum service temperature (a minimum level of 30°C (86 F) above maximum service temperature is recommended).

However, we can note that in the absence of detailed test results and based on data from other areas of application (including factors of safety used routinely in boats of 4-6, and in tanks of 8-10), stress levels in the FRP composite should be limited under sustained loads, as shown in table 15 (D. Hunston et al.).

*Table 15 Advisable Stress levels*

FRP	Stress level
AFRP	less than 30% of ultimate design strength
CFRP	less than 40% of ultimate design strength if damage tolerance is considered
GFRP	less than 25% of ultimate design strength (due to stress rupture concerns)

#### Alkaline solutions

It is highly probable that FRP composite components will either be embedded, be bonded to, or placed adjacent to concrete, or have concrete encapsulated within. Although FRP composites can come in contact with alkaline media through interaction with a variety of sources, including alkaline chemicals, soil (or solutions diffusing through soil), and concrete, the main concern, at the present time, stems from the potential effects of degradation due to concrete pore water solution, which is known to have a high level of pH: concrete is known to have a pore water with pH level as high as 13.5.

Alkaline solutions, such as the pore water of concrete, have a high pH and high concentration of alkali ions. Alkaline ions and moisture can diffuse through the resin matrix to the fibers and damage the FRP composite through a variety of mechanisms that will change based on the type of application, fiber, resin, sizing, and even process used to fabricate the product.

Some researches (B. Benmokrane et al.) have shown that alkaline solutions and ions, combining in mechanisms ranging from pitting, hydroxylation, hydrolysis, and leaching, can cause severe degradation to bare glass fibers, and even to some polymer systems. Although the presence of resins in FRP composites around individual filaments can be expected to protect the fibers from such attack, the alkaline solutions can accelerate the degradation of bond and of some resins themselves, especially if not fully cured.

This combination has no relevant effect on carbon reinforcement but may lead to degradation at the resin matrix and/or interface levels (strength and stiffness have been reported to each decrease between 0-20%). Tensile strength reductions in GFRP bars ranging from zero to 75% of initial values have been reported in literature, while tensile stiffness reductions in GFRP bars range between zero and 20%.

Tensile strength and stiffness of AFRP rods in elevated temperature alkaline solutions, either with and without tensile stress applied, has been reported to decrease between 10-50% and 0-20% of initial values, respectively.

#### Aggressive chemical solutions

FRP composites generally exhibit a variable performance when exposed to solution such as acids or corrosives and the resin type primarily influences this performance. In the case of CFRP immersed in hydrochloric acid at the temperature of 80°C, the tensile strength reduced about 20% after 120 days.

Papers have reported that the tensile stress of glass fiber reduced rapidly with time when immersed in any of the solution (NaOH, HCl, H<sub>2</sub>O) at the temperature of 80°C and when immersed in sodium hydroxide (Uomoto et al., 1999). For the AFRP (Technora fiber), it has been reported that after immersing for 90 days, strength was reduced by about 80% in hydrochloric acid and about 45% in sodium hydroxide solution. However no particular sign of degradation were observed when the AFRP were immersed in distilled water at temperatures of 20, 40 and 80°C (68, 104, 176 F) (Uomoto et al. 1999).

#### Ultraviolet (UV) radiation

Ultraviolet radiation that reaches the earth's surface comprises about 6% of the total solar radiant flux and has wavelengths between 290 nm and 400 nm. Radiation below approximately 290 nm is effectively eliminated by stratospheric ozone, but the remainder of the solar radiation is composed of visible (52%) and infrared (42%) radiation.

It is a well-known fact that polymeric materials absorb in the ultraviolet region of the electromagnetic spectrum, and therefore are susceptible to reactions initiated by the absorption of ultraviolet energy: bond dissociation is initiated by the absorption of UV radiation, resulting in chain scission and/or crosslinking; subsequent reactions with oxygen result in the formation of functional groups such as carbonyl (C=O), carboxyl (COOH), or peroxide (O-O).

FRP composites are polymeric and are therefore prone to the same photochemical damage as unreinforced polymers and polymer coatings. Photochemical reactions in polymers, generally

limited to the topmost 50-100 microns (J.W. Chin et al.), increase the concentration of oxygen-containing functional groups and potentially lead to chain scission and/or crosslinking reactions. Chain scission reactions decrease the molecular weight of the surface polymers, allowing erosion of the low molecular weight fragments to occur.

Continued exposure and subsequent erosion results in substantial loss of resin from the polymer surface, and in the case of a FRP composite, the eventual uncovering of the underlying fibers. A common practice in outdoor applications of FRP composites is to use a gel coat or other protective coating to prevent the FRP surface from being directly exposed to UV radiation. The protective coating itself will eventually be degraded by UV radiation and will need to be maintained.

## 2.4 CONCLUSIONS

We can summarize the general properties of the FRP composites:

### High Strength and Stiffness Retention

composites can be designed to provide a wide range of mechanical properties including tensile, flexural, impact and compressive strengths. And, unlike traditional materials, composites can have their strengths oriented to meet specific design requirements of an application.

### Light Weight/Parts Consolidation

FRP composites deliver more strength per unit of weight than most metals. In fact, FRP composites are generally 1/5th the weight of steel. The composite can also be shaped into one complex part, often times replacing assemblies of several parts and fasteners. The combination of these two benefits makes FRP composites a powerful material system, structures can be partially or completely pre-fabricated, delivered on-site and installed.

### Creep (Permanent Deflection Under Long Term Loading)

The addition of the reinforcement to the polymer matrix increases the creep resistance of the properly designed FRP part.

### Resistance to Environmental Factors

Composites display excellent resistance to the corrosive effects of:

- Freeze-thaw: because composites are not attacked by galvanic corrosion and have low water absorption, they resist the destructive expansion of freezing water
- Weathering and Ultra-Violet Light: FRP composite structures designed for weather exposure are normally fabricated with a surface layer containing a pigmented gel coat or have an ultraviolet (UV) inhibitor included as an additive to the composite matrix.
- Chemicals and Temperature: Composites do not rust or corrode and can be formulated to provide long-term resistance to nearly every chemical and temperature environment. Of particular benefit, is composites ability to successfully withstand the normally destructive effects of de-icing salts and/or saltwater spray of the ocean

### Fire Performance of FRP Composites

FRP composites can burn under certain conditions. Composites can be designed to meet the most stringent fire regulations by the use of special resins and additives.

In any case we must note that there are significant gaps in durability data that need to be addressed. However, there is an important collection of studies to suggest that if the appropriate materials-process-design aspects are considered, FRP composite components can provide almost maintenance-free service in very harsh environments over extended periods of time.

It is also acknowledged that environments, which are typical in civil infrastructure, can cause significant degradation in FRP composites, and that there is in reality a lack of validated data and a comprehensive knowledge of lifetime durability related to some materials systems likely to be used in civil infrastructure.



### 3. MATERIALS USED IN THE EXPERIMENTAL PROGRAM

Failure of URM Walls is one of the main causes of material damages and loss of human life during a seismic event. Composite materials have shown a great potential for the strengthening of masonry structures in the forms of externally bonded fiber reinforced polymer (FRP) laminates or Near Surface Mounted (NSM) FRP bars.



*Figure 43 Bars used in this experimental program. From left: G-Circular bars:  $d=5, 6.3, 9.5\text{mm}$ ; C and G - FRP Rectangular Bars (15 by 2 mm).*

### **3.1 INTRODUCTION**

This section presents the properties of the materials used in the experimental program. These materials included concrete blocks and clay bricks, ash concrete mortar, G-FRP rods, stainless steel rods, C-FRP and G-FRP tape, epoxy paste and latex modified cementitious paste.

Standard tests were performed by previous researches in order to determine the compressive strength of mortar cubes and concrete blocks, the splitting tensile strength of the cementitious paste and epoxy paste, and the tensile strength of the FRP bars.

During this experimental program were executed just the tests on the new materials, such as the glass rectangular bar and the smooth circular bar.

## 3.2 MASONRY UNITS

The most common concrete masonry products are block and brick. Just as concrete has evolved as a modern construction material over the past 100 years, the history of concrete masonry products largely dates from this century; concrete brick, in fact, have been extensively used in North America since perhaps only the 1960s. Because the binder in concrete products is Portland cement, units derive their strength from the cement hydration process and much of concrete technology is applicable. In North America, concrete blocks are widely used in both loadbearing and nonloadbearing applications, where brick is commonly employed in nonloadbearing veneers and as pavers.

Concrete masonry products are defined as solid or hollow, depending on whether they contain 75% or more net solid horizontal cross-sectional area. In practice, hollow blocks are more frequently used because of their reduced weight, ease of handling, ease of reinforcing, and overall economy. The percent solid typically is in the range from 50 to 60%.

Concrete masonry units come in a large variety of sizes and shapes. Two and three-cell units are both common. The cells of hollow units are tapered and some molds also introduce flared webs and face shells. This facilitates stripping the molds and aids gripping the block during laying. The increased top area also is beneficial for mortar bedding.

The compressive strength of a concrete masonry unit is important from two points of view: first, the higher the strength, the better the durability under severe weathering conditions and, second, unit strength tests with mortar strength tests can serve as the basis for satisfying the required masonry compressive strength. Hollow blocks can be manufactured in strengths, ranging from 10 to 30 MPa (1500 to about 4000 psi) based on net area, to suit low-rise and high-rise construction.

Flexural tensile strength typically ranges between 10 and 20% of the unit compressive strengths. There is no widely accepted method for determining the tensile strength of concrete blocks. Splitting tensile strength tests across the face shells have shown that the ratio of splitting tensile strength to compressive strength ranges from 0.08 to 0.16.

The following paragraphs present different blocks and bricks, some used in this experimental program and some other, used in previous, similar, researches (Morbin, 01 and Turco, 02).

The specified dimensions of the blocks/bricks are ever 10 mm (3/8 in) less than the nominal values to allow for a standard mortar joint thickness. For every kind of block, following ASTM C1314 standard protocol, compression tests were performed, using a Tinius Olsen Universal Testing

Machine to apply the compression load. In order to create a uniform distribution of compression stresses on the edges of the specimens, two plywood strips were cut and inserted between the edges and the two cross-heads of the machine; in this manner, undesirable crushing failures at the borders were also prevented.

### 3.2.1 6 in.-Concrete Block (in-plane and out-of-plane tests)

This concrete block, named “bcb” (bigger concrete block) in the test matrix, was used for the specimens “bcb-gt-1” and “bcb-gt-2” in the out-of-plane tests, and for all the in-plane test specimens. Tables 16 and 17 report respectively the geometrical and the mechanical properties of this brick.

*Table 16 Unit Specifications*

Designation	Concrete hollow two-cells unit
Nominal dimensions - mm (in)	152x203x406 (6x8x16)
Real dimensions - mm (in)	142x93x396 (5.6x7.6x15.6)
Gross Area - mm <sup>2</sup> (in <sup>2</sup> )	54700 (84.89)
Net Area - mm <sup>2</sup> (in <sup>2</sup> )	35400 (54.89)
Percentage of solid	65 %

*Table 17 Compression Test Results (Morbin 01)*

Prism #	Compressive Strength $f'_m$ MPa (psi) -net area-
1	17.99 (2608)
2	15.36 (2230)
3	13.70 (1989)
4	19.90 (2889)
AVERAGE	16.73 (2429)
Standard Deviation	2.75 (398)

Modulus of elasticity:  $900 f'_m = 6267$  MPa (909 ksi) from Masonry Standard Joint Committee (MSJC) Code (1999).



Figure 44 Compression Test: Prism After Failure

In order to estimate shear stresses developed along bed mortar joints, five triplets were constructed as shown in figures 45 and 47. Cohesion and coefficient of friction according to Coulomb criterion expression:  $\tau = \tau_0 + \mu\sigma_n$  were calculated by means of linear interpolation of the data provided by the tests.

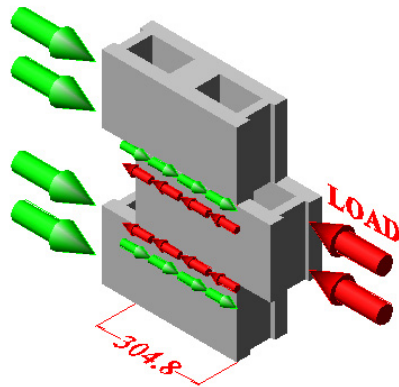


Figure 45 Scheme of Bed Joint Shear Test

The three confinement stresses resulted 0.5 (72), 1.0 (144), 1.5 MPa (216 psi) respectively. As shown in figure 46, it was obtained, according to Coulomb criterion:  $\tau = 0.396 + 0.668\sigma_n$  (MPa) for  $\sigma_n < 1.5$  MPa ( $\tau = 58.01 + 0.668\sigma_n$  [psi] for  $\sigma_n < 216$  psi).

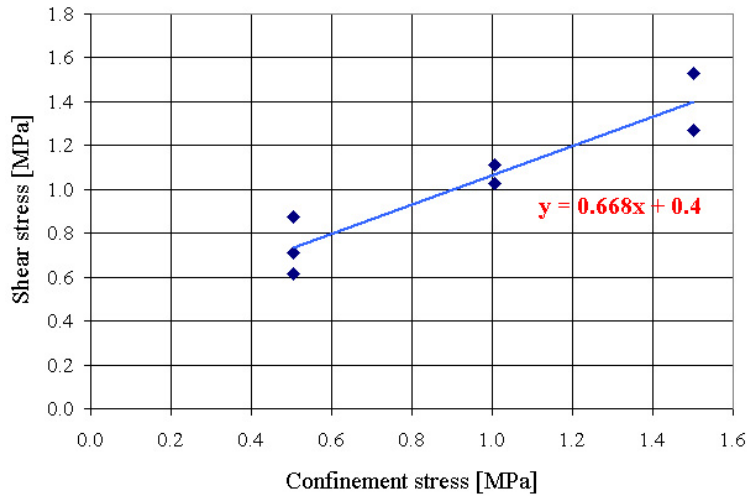


Figure 46 Test Results From Concrete Triplets



Figure 47 Concrete Block Triplet Under Loading

**3.2.2 4 in.-Concrete Block (out-of-plane test)**

This concrete block, named “cob” (concrete block), was widely used in the out-of-plane test program. Tables 18 and 19 report respectively the geometrical and the mechanical properties of this brick.



Figure 48 Concrete Unit

Table 18 Unit Specifications

Designation	Concrete Hollow Two-Cells unit
Nominal dimensions - mm (in)	102x203x305 [4x8x12]
Real dimensions - mm (in)	92x193x295 (3.6x7.6x11.6)
Gross Area - mm <sup>2</sup> (in <sup>2</sup> )	27337 (42.4)
Net Area - mm <sup>2</sup> (in <sup>2</sup> )	17904 (20.3)
Percentage of solid	65 %



Figure 49 Prism Test Setup

Table 19 Compression Test Results (Morbin 01)

Prism #	Compressive Strength $f'_m$ MPa [psi]
1	10.92 [1585]
2	8.19 [1189]
3	9.43 [1369]
4	10.42 [1513]
AVERAGE	9.74 [1414]
Standard Deviation	1.04 [151]

Modulus of elasticity:  $900 f'_m = 8770 \text{ MPa}$  (1270 ksi) from Masonry Standard Joint Committee (MSJC) Code (1999).

**3.2.3 Clay Bricks Named “c11”**

Two different kinds of clay bricks were used in the test program. The first kind, named “c11”, was used to build two specimens, c11-gt-1 and c11-gt-2, strengthened with glass rectangular bars and tested under out-of-plane load. Tables 20 and 21 report respectively the geometrical and the mechanical properties of this brick.

*Table 20 Unit Specifications*

Designation	Clay bricks – hollow 25%
Nominal dimensions - mm (in)	102x203x64 (4x8x2.5)
Real dimensions - mm (in)	92x193x54 (3.6x7.6x2.1)
Gross Area - mm <sup>2</sup> (in <sup>2</sup> )	17400 (27.0)
Net Area - mm <sup>2</sup> (in <sup>2</sup> )	13100 (20.3)
Percentage of solid	75 %



*Figure 50 Brick “c11”*

*Table 21 Compression Test Results*

Prism #	Compressive Strength $f'_m$ MPa (psi) -gross area-
1	20.10 (2915)
2	18.48 (2680)
3	19.71 (2859)
AVERAGE	19.43 (2818)
Standard Deviation	0.69 (100)

Modulus of elasticity:  $700 f'_m = 13600 \text{ MPa}$  (1973 ksi) from Masonry Standard Joint Committee (MSJC) Code (1999).

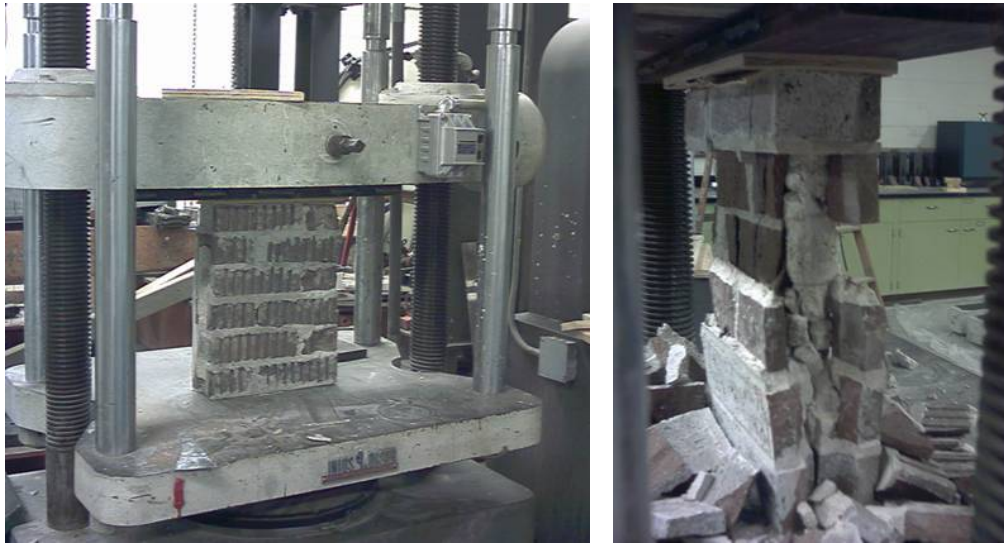


Figure 51 Compression Test: Specimen Before and After Failure

**3.2.4 Clay Brick Named “cl2”**

These bricks were used in this experimental program to build one specimen, cl2-ct-2, strengthened with carbon rectangular bars and tested under out-of-plane load. They were used also in previous researches (Morbin, 01). Tables 22 and 23 report respectively the geometrical and the mechanical properties of this brick.

Table 22 Unit Specifications

Designation	Clay bricks – hollow 16%
Nominal dimensions - mm (in)	102x203x64 (4x8x2.5)
Real dimensions - mm (in)	92x193x54 (3.6x7.6x2.1)
Gross Area - mm <sup>2</sup> (in <sup>2</sup> )	17800 (27.64)
Net Area - mm <sup>2</sup> (in <sup>2</sup> )	14200 (23.20)
Percentage of solid	84 %

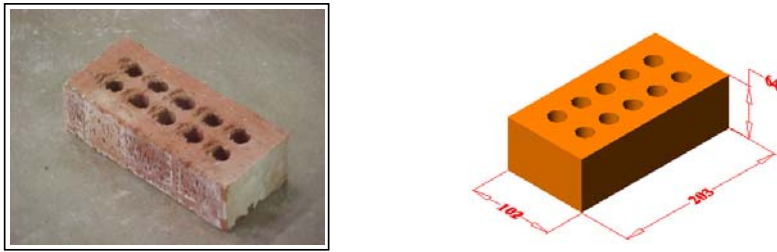


Figure 52 Clay Bricks (Dimensions in mm, 1 mm = 0.04 in)

Table 23 Compression Test Results (Morbin 01)

Prism #	Compressive Strength $f'_m$ MPa (psi) -net area-
1	17.93 (2601)
2	16.33 (2368)
3	10.02 (1454)
4	17.28 (2507)
5	17.34 (2515)
AVERAGE	15.78 (2289)
Standard Deviation	3.27 (474)

Modulus of elasticity:  $700 f'_m = 11047$  MPa (1602 ksi) from MSJC Code (1999)



Figure 53 Compression Test: Prism After Failure

### 3.3 MORTAR

Mortar, which gets its name from the Latin *mortarium* (the mason's trough), is used to provide uniform bearing between units and to bond individual masonry units into a composite assemblage that will withstand the imposed conditions of loads and weather. Mortar also serves to bond joint reinforcement and metal ties so that they can act integrally with masonry. The achievement of strength, durability, and weather tightness is the key requisite of hardened mortar. Mortar in its plastic state also facilitates ease of construction and allows for tolerances of units and dimensions.

The mortar used for the wallettes was available in bags in a dry premixed composition of cement and sand, and was classified as Type N according to the standard ASTM C270. Table 24 illustrates property specifications requirements for Type N masonry mortar.

*Table 24 Specifications for Type N Masonry Mortar*

Mortar	Type	Average Compressive Strength at 28 days MPa (psi)	Water Retention %	Air Content %
Masonry Cement	N	5.2 (750)	75	20

The characterization of the mortar was a part of another research (Morbin et al., 01). Mortar compressive strength is important because it has an influence on masonry compressive strength and because it is typically used as a measure of quality control. According to ASTM C1019, six cubes 5.8 by 5.8 by 5.8 cm (2x2x2 in) each were built using a special plastic grid.

The load was applied by means of a Tinius Olsen Machine: strain gages were bonded on the face shells of the cubes in order to estimate the vertical and horizontal strains when loading, and in ultimate analysis to calculate the Poisson ratio value. Test results are illustrates in table 25.

*Table 25 Compressive Test Results*

Prism #	Compression Strength $f'_m$ MPa (psi)
1	6.55 (950)
2	4.82 (700)
3	4.85 (705)
4	4.40 (638)
5	5.86 (850)
6	7.58 (1100)
S.D.	1.10 (161)
Average	5.67 (823)

As shown in table 25, large differences in values were observed. This may be explained because of different hand workers involved in the preparation of the specimens.

Besides, during the work, the mason can add water to do workable the mortar, and this is a great limit to consider uniform the joints.



(a)



(b)

Figure 54 (a) Mortar Cube Under Loading; (b) Failure



Figure 55 Typical Mode of Failure of Mortar Cube

### 3.4 REINFORCING MATERIALS

#### 3.4.1 Primer, Putty, Saturant, Paste

Here are shown the properties of all the materials used in the FRP sheets application (previous researches). Table 26 shows the physical properties of the resins (Mbrace, 1998). Table 27 shows their properties in tension.

*Table 26 Physical Properties of Epoxy Resins (Mbrace 98)*

Properties	Primer	Putty	Saturant	Paste
Color Part A	Amber	Tan	Blue	White
Color Part B	Clear	Charcoal	Clear	Black
Mixed	Amber	Tan	Blue	Gray
Mix Ratio by Volume Part A / Part B	3 / 1	3 / 1	3 / 1	2 / 1
Mix Ratio by Mass Part A / Part B	100 / 30	100 / 30	100 / 34	NA
Working time at 25 ° C (77° F) minutes	20	40	45	40

*Table 27 Resin Properties in Tension (Mbrace 98)*

Properties	Primer	Putty	Saturant	Paste
Tensile Strength MPa (psi)	12.41 (1800)	12.41 (1800)	54.47 (7900)	27.58 (4000)
Tensile Elastic Modulus kN (ksi)	467.1 (105)	1156.5 (260)	1957.3 (440)	NA
Tensile Strain %	3	1.5	2.5	1
Compressive Strength MPa (psi)	24.13 (3500)	24.13 (3500)	86.18 (12500)	86.18 (12500)
Compressive Modulus kN (ksi)	422.6 (95)	689.5 (155)	1690.3 (380)	2001.7 (450)
Poisson's Ratio	0.48	0.48	0.40	NA
Bond Strength MPa (psi)	NA	NA	NA	>13.79 (2000)

**3.4.2 C, A and G FRP Laminates**

Laminates were used by previous researches, in both out-of- and in-plane load tests. Mechanical properties provided by the manufacturers are presented in table 28.

*Table 28 Engineering Properties for FRP and GFRP Sheets*

Designation	Fiber Type	Tensile Strength MPa (ksi)	Tensile Elastic Modulus MPa (ksi)	Load per Sheet Width N/mm (lb/in)
CFRP – CF 130	Carbon	3789 (550)	227370 (33000)	626.9 (3580)
AFRP – AK60	Aramid	1998 (290)	117130 (17000)	560.0 (3190)
GFRP – EG900	Glass	1516 (220)	72345 (10500)	534.1 (3050)

In order to verify the mechanical properties provided by the manufacturers of the laminates, tensile tests on thin flat strip a of material having a constant rectangular cross section were performed in laboratory environment. All specimens were tested under displacement control with a constant loading speed of 2 mm/min (*ASTM 1995; Tarnopol'skii and Kincis 1985*). The results are presented in table 29.

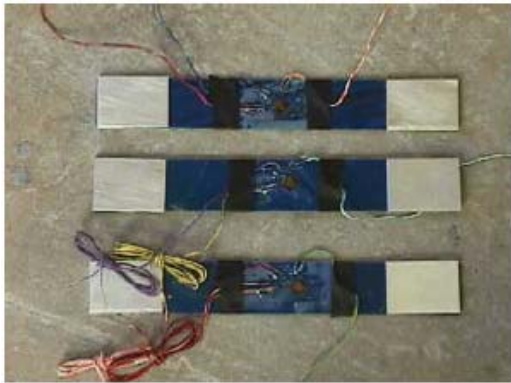


*Figure 56 C-FRP Specimens (Yang 02)*

Table 29 GFRP Laminates: Test Average Results (Morbin 01; Yang 02)

Designation	Maximum Strain %	Maximum Stress GPa (ksi)	Modulus of Elasticity GPa (ksi)
G-Lamin.	1.82	1.687 (244.7)	83.13 (12057)
C-Lamin.	1.47	3.942 (572)	264.0 (38290)
A-Lamin.	1.60	1.936 (281)	121.0 (17550)



Figure 57 Coupon Before (left) and After (right) Failure (Morbin 01)

**3.4.3 GFRP Circular Cross Section Bars**

Table 30 illustrates the mechanical properties of GFRP rods utilised as Near Surface Mounted (NSM) rods. As for laminates, the data were provided by the manufactures.

Table 30 Mechanical Properties of GFRP Rod #2

Bar size (mm) #	Cross-Sectional Area mm <sup>2</sup> (in <sup>2</sup> )	Nominal Diameter mm (in)	Tensile Strength MPa (ksi)	Tensile Modulus of Elasticity MPa (ksi)	Max Bond Stress to Concrete MPa (psi)
(6) 2	33.23 (0.0515)	6.35 (0.250)	760 (110)	40789 (5920)	11.57 (1679)

To verify the properties given from the manufactures, three GFRP bars #2 were tested (Turco 02).

Table 31 reports test data about the three rods.

Table 31 Tensile Test of GFRP rods #2 (Turco 02)

Specimen	Maximum strain %	Maximum stress MPa (ksi)	$E_f$ MPa (ksi)
Bar 1	1.63	820.6 (119.02)	48257.8 (6999.2)
Bar 2	1.89	827.2 (119.98)	43000.5 (6236.7)
Bar 3	1.85	825.4 (119.71)	59229.4 (8590.5)
AVERAGE	1.78	824.5 (119.6)	50162.8 (7275.5)
Standard Deviation	0.14	3.4 (0.49)	8280.4 (1200.9)

Figure 58 shows the graphics about the three specimens.

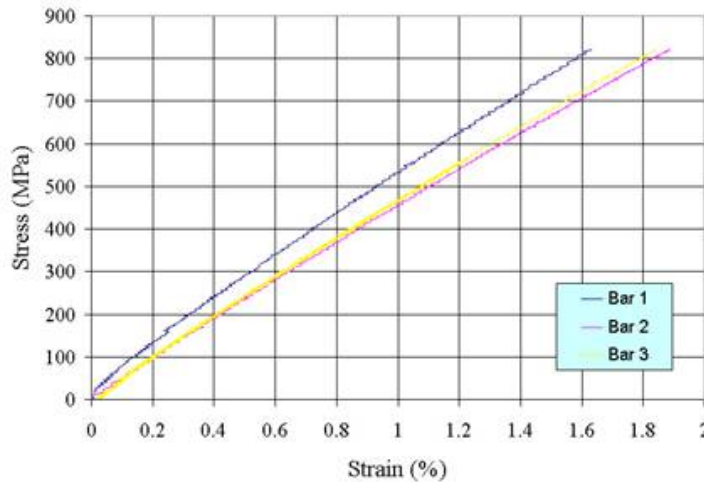


Figure 58 #2 GFRP Results

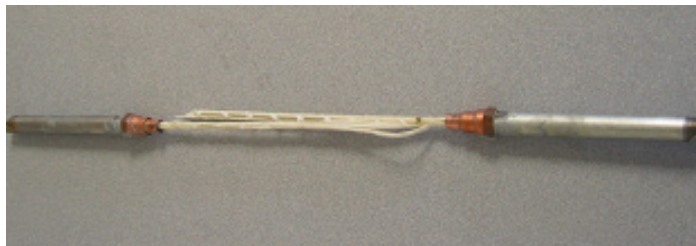


Figure 59 Failure of a Specimen

### 3.4.4 GFRP Smooth Rods

A new kind of rod was tested and used in the in-plane program: this is a circular cross section bar, with smooth coated surface and diameter equal to 5 mm. Table 32 illustrates the mechanical properties provided by the manufactures. Because of its smoothness, no tensile tests were performed in our laboratories.

*Table 32 Mechanical Properties of GFRP Smooth Rod Provided by the Manufactures*

Top coated Rod diameter	5.1 mm
Bare rod diameter	4.88 mm
Glass Content	79.3%
Maximum Strain	1.94 %
Maximum Stress	872 MPa
Modulus of Elasticity	53.54 GPa

### 3.4.5 GFRP Rectangular Bar (tape)

In order to find a better bond behavior, rectangular cross section bars were used. The dimensions were approximately 15 by 2 mm, and the surface was smooth. Also in this case tensile tests were performed in laboratory environment, following specifications provided by ASTM D3039, and the load was acquired by the built-in hydraulic pressure transducer of the INSTRON 4485 machine. In this testing frame, the loading head is rotationally self-aligning, which eliminates the potential of bending and twisting the specimen. The wedge grips are self-tightening, to keep a constant pressure, so the clamping conditions do not change due to laminate contraction. All specimens were tested under displacement control with a constant loading speed of 2mm/min (*ASTM 1995; Tarnopol'skii and Kincis 1985*). The results are shown in tables 33 and 34.



Figure 60 Specimens Before Failure

Table 33 Tensile Test Data

Test date	25 <sup>th</sup> Oct., 2002	
Interface type	4200	
Crosshead speed	0.0787 in/min	2 mm/min
Sample Rate	10.00 pts/sec	
Temperature	73 F	23°C
Humidity	68%	
Specimen Gauge Length (grip distance)	3.65 in	92.7 mm
Extensometer Gauge Length	1.00 in	25.4 mm
Width of specimen	0.599 in	15.21 mm
Thickness of specimen	0.081 in	2.06 mm
Area of specimen	0.04852 sq-in	31.30mm <sup>2</sup>

Table 34 Tensile Test Results

Designation	Maximum Strain mm/mm or in/in	Maximum Stress MPa (ksi)	Modulus of Elasticity GPa (ksi)
Tape1	0.0259	1118.5 (162.22)	43.2 (6259)
Tape2	0.0244	1144.0 (165.93)	46.9 (6801)
Tape3	0.0248	1042.6 (151.22)	42.0 (6085)
AVERAGE	0.02506	1101.7 (159.8)	44.0 (6382)
Standard Deviation	0.00078	52.74 (7.65)	2.57 (373)



*Figure 61 Specimens After Failure*

### 3.4.6 CFRP Rectangular Bar (tape)

This bar was used in this experimental program to strengthen the specimen called cl2-ct-2 and tested under out-of-plane load, and by a previous research (Grando 02) in in-plane load tests. Tests were conducted to determine the properties of the material. The results of these specimens are collected in table 35.

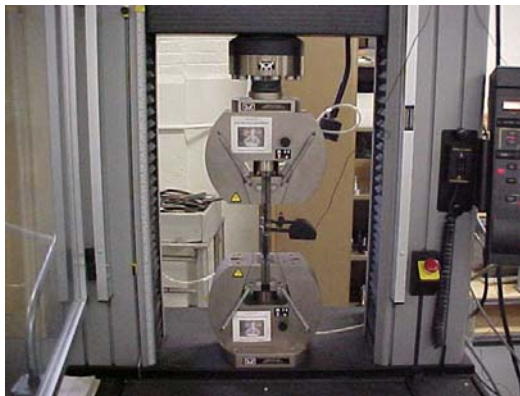


*Figure 62 Test Setup*

Table 35 Data for CFRP Tape Test (Grando 02)

Specimen	Maximum strain %	Maximum stress MPa (ksi)	Modulus of elasticity GPa (ksi)
C1	1.18	1370 (198.7)	133.8 (19420.1)
C2	0.86	1470 (213.1)	147.9 (21475.7)
C3	1.47	1360 (198.2)	142.2 (20632.8)
C4	0.88	1450 (210.6)	149.4 (21683.7)
C5	0.77	1270 (184.9)	144.9 (21041.4)
C6	0.91	1370 (198.4)	141.3 (20506.9)
C7	0.88	1420 (206.1)	141.1 (20477.2)
C8	0.87	1420 (205.9)	141.2 (20492.6)
AVERAGE	0.98	1392.4 (201.9)	142.74 (20702)
Standard Deviation	0.23	60 (8.9)	4.82 (702.7)



Figure 63 Failures of CFRP Tape

**3.4.7 Stainless Steel Rods**

These rods were used by previous programs in in-plane load tests in order to can compare the steel to the FRP. Tensile tests were performed to determine the mechanical properties of the stainless steel Helifix™: 5 specimens were prepared and tested; the results are shown in tables 36.

Table 36 Results for Ultimate Load Tests

Specimen	Maximum strain %	Maximum stress MPa (ksi)	Modulus of elasticity GPa (ksi)
S1	NA	943.9 (136.9)	NA
S2	15.03	904.6 (131.2)	120.45 (17470)
S3	15.59	865.9 (125.6)	119.97 (17400)
S4	15.61	979.7 (142.1)	118.22 (17146)
S5	18.30	999.7 (145.0)	117.03 (16974)
AVERAGE	16.133	938.9 (136.2)	118.918 (17225)
Standard Deviation	1.47	54.5 (7.9)	1.581 (229)



Figure 64 Four Specimens Ready to Be Tested



Figure 65 Failures

To estimate the area of the cross section of the bars, we used the Archimedes’s Theory: we plunged a piece of bar in a graduated cylinder to measure the different level of water, corresponding on the volume of the stainless steel rod (figure 66). Once we knew the volume, with the length of the little pieces, we could estimate the Area, as shown in table 37.



Figure 66 Graduated Cylinder and Steel Pieces Before (left) and During (right) Test

Table 37 Geometrical Properties of Stainless Steel Bars Cross Section

Specimen	Length mm (in)	Volume mm <sup>3</sup> (ounces)	Area mm <sup>2</sup> (in <sup>2</sup> )
A1	34.5 (1.36)	320 (0.011)	9.27 (0.0143)
A2	36.8 (1.45)	360 (0.012)	9.51 (0.0147)
A3	35.5 (1.39)	330 (0.011)	9.29 (0.0144)
A4	36.3 (1.43)	360 (0.012)	9.92 (0.0153)
A5	36.8 (1.45)	350 (0.012)	9.51 (0.0147)
A6	38.8 (1.53)	360 (0.012)	9.28 (0.0144)
AVERAGE	36.4 (1.43)	346 (0.012)	9.42 (0.0146)
Standard Deviation	1.4 (0.06)	17.5 (0.0005)	0.25 (0.0004)

3.4.8 Internal Steel Wires

Two walls, WI1 and WI 2 (Grando 02), were reinforced with a net made by a couple of steel wires, the geometrical dimensions of which are shown in figure 67.

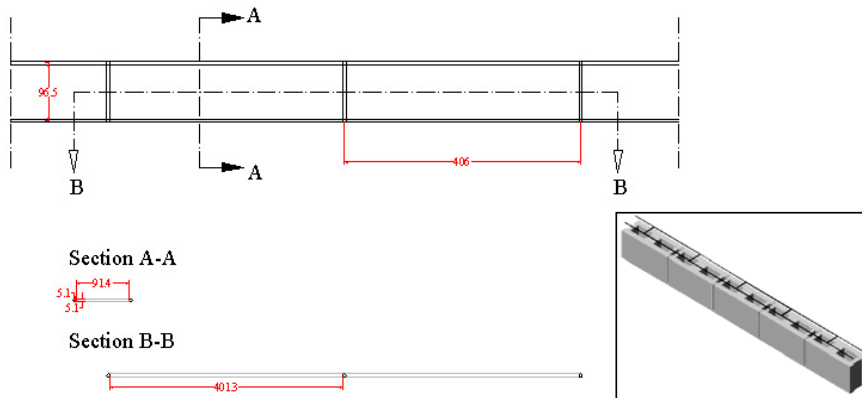


Figure 67 Geometrical Dimensions of Internal Steel Wires and Their Use (Dimensions in mm, 1 mm = 0.04 in)

The tested specimens had a length of 254 mm (10 in) between the top and the bottom of the vise, and a diameter of 5.31 mm (0.209 in). Tests were conducted to determine their properties. Test results are related in table 38.

Table 38 Tensile Test Results (Grando 02)

Specimen	Maximum strain %	Maximum stress MPa (ksi)	Modulus of elasticity GPa (ksi)
IW1	10.28	625.8 (90.7)	206.0 (29.8)
IW2	9.26	624.2 (90.5)	204.7 (29.7)
IW3	8.73	624.2 (90.5)	202.6 (29.4)
IW4	9.55	631.1 (91.5)	206.6 (29.9)
IW5	9.32	622.8 (90.3)	202.1 (29.3)
AVERAGE	9.43	625.6 (90.7)	204.4 (29646)
Standard Deviation	0.56	3.2 (0.5)	2.0 (0.2)



Figure 68 Test setup and Failure of the Specimens

Figure 69 shows a graphic with a comparison between the different specimens.

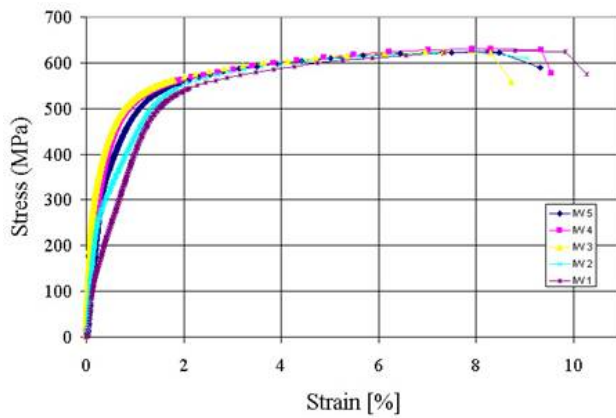


Figure 69 Stress Strain Behavior of Steel Wires

### 3.5 EPOXY PASTE, CEMENTITIOUS PASTE

The materials used to embed the NSM FRP reinforcement in the grooves and for the structural repointing were an epoxy-based paste and latex modified cementitious paste.

#### 3.5.1 Epoxy-Based Paste

This paste is commercially known as Concreative Paste LPL, manufactured by Master Builders Technologies. Table 39 shows the mechanical properties provided by the manufacturer.

*Table 39 Epoxy-Based Paste: Properties*

Properties	Relative ASTM Rule	Value
Tensile Strength - MPa (psi)	ASTM D 638	27.6 (4000)
Elongation at Break - %	-	1.0
Compressive Yield Strength – MPa (psi)	ASTM D 695	86.2 (12500)
Compressive Modulus – GPa (psi)	ASTM D 695	3.06 (450000)
Bond Strength (2 days cure) – MPa (psi)	ASTM C 882	>13.8 (2000)

#### 3.5.2 Cementitious-Based Paste

This paste is commercially known as Sonopatch 100, manufactured by Sonneborn Concrete Repair Systems. Table 40 reports the properties provided by the manufacturer.

*Table 40 Latex Modified Cementitious Paste*

Properties	Relative ASTM Rule	1 Day	28 Days
Compressive Strength – MPa (psi)	ASTM C109* modif.	5.5 (800)	34.5 (5000)
Modulus of Elasticity - GPa (psi)	ASTM C 215	19.0 (2800000)	
Splitting Tensile Strength – MPa (psi)	ASTM C 496	1.0 (140)	4.5 (650)
Flexural Strength – MPa (psi)	ASTM C 348* modif.	1.4 (200)	10.0 (1450)
Bond Strength – MPa (psi)	ASTM C 882* modif.	2.1 (300)	15.2 (2200)

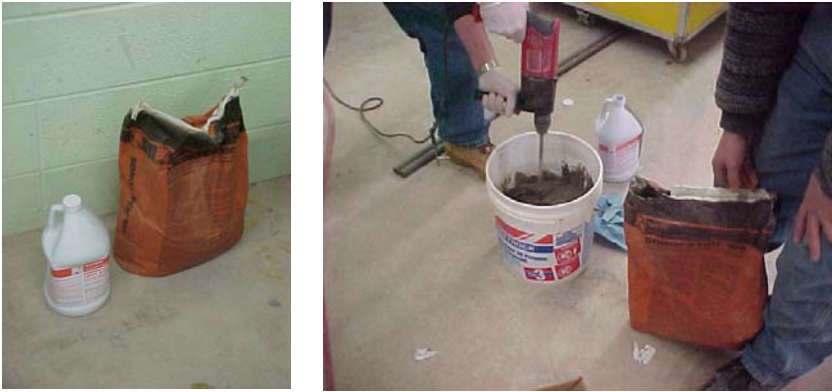


Figure 70 Preparation of the Paste: the Two Components (left), the Mix (right)

### 3.5.3 Comparison

Because the two embedding paste are differently based, the methods used by the manufacturers for the characterization were different and so not comparable. The principal objective of this experimental program was to compare the bond and the behavior under out-of-plane and in-plane loads using two different embedding pastes. Like with the G-FRP rebar and the steel rods, the most important mechanical properties that are used in design of RC structures and NSM reinforcement are the tensile properties. Therefore a splitting tensile test was performed for both materials following the ASTM C 496 (Splitting Tensile Test for Cylindrical Concrete Specimens): this method consists of applying a diametral compressive force along the length of a cylindrical specimen at a rate that is within a prescribed range until failure occurs.

#### Splitting Tensile Test (Turco 02)

Six specimens were prepared for each material. The dimension of the cylinders used was 2 in. (diameter) by 4 in. (length). They were allowed to cure for 7 and 28 days. Figure 74 shows specimens aligned prior to testing them.



Figure 71 LMCP Specimens

The Splitting Tensile Tests were performed by means of an Instron Machine. The data were recorded by a Labtech data acquisition system. The machine operated at a nominal crosshead speed of 8.45 kN (1.9 kips) / minute. The specimens were placed across the two cross-heads of the machine. One plywood strip was placed along the center of the lower bearing machine-block. Then the specimen was placed on the plywood strip and centered over it. A second strip was placed on the top of the cylinder aligned with the first. Figure 72 shows the test setup.



Figure 72 Splitting Tensile Test Setup

The load was applied continuously and without shock until failure. The loading induces compressive stresses in the same direction of the load and tensile stresses on the plane orthogonal to the applied load. The failure occurs rather than compressive failure because the areas of load application are in a state of triaxial compression, thereby allowing them to withstand much higher compressive stresses than would be indicated by a uniaxial compressive strength test result. Figures 73 a,b,c show cracks and a typical splitting failure. Tables 41 through 43 report the results of this test and the obtained average values.

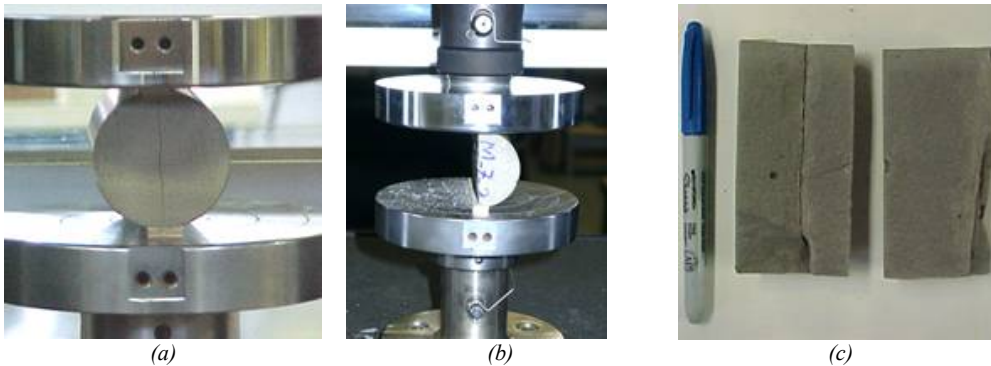


Figure 73 Splitting Failures: (a) Crack Forming, (b) Failure, (c) Specimen after Failure

Table 41 LMCP Results

Latex Modified Cementitious Paste		Maximum Load kN (kips)	Splitting Tensile Strength MPa (ksi)
7 Day	1	29.7 (6.687)	3.67 (0.532)
	2	28.2 (6.341)	3.5 (0.504)
	3	29 (6.505)	3.57 (0.518)
28 Days	1	45.3 (10.182)	5.59 (0.810)
	2	45.27 (10.177)	5.59 (0.810)
	3	45.3 (10.182)	5.59 (0.810)

Table 42 Epoxy Paste Results

Epoxy-Based Paste		Maximum Load kN (kips)	Splitting Tensile Strength MPa (ksi)
7 Day	1	130.64 (29.37)	16.13 (2.338)
	2	121 (27.19)	14.94 (2.165)
	3	144.1 (32.39)	17.79 (2.579)
28 Days	1	152 (34.16)	18.76 (2.720)
	2	150.1 (33.81)	18.57 (2.692)
	3	147.7 (33.29)	18.29 (3.650)

Table 43 Average Values

Material		Average Maximum Load - kN (kips)	Average Splitting Tensile Strength - MPa (ksi)
Latex Modified Cementitious Paste	7 Day	28.9 (6.511)	3.58 (0.518)
	28 Days	45.29 (10.18)	5.59 (0.810)
Epoxy-Based Paste	7 Days	132 (29.65)	16.3 (2.361)
	28 Days	150 (33.75)	18.54 (2.687)

From the obtained values some observations may be made:

- The splitting tensile strength was 1/3 higher after 28 days than after 7 days, while the epoxy paste tensile properties did not change considerably.
- The behavior of the LMCP under loading is much more homogeneous than that one of the epoxy paste.
- In the case of the epoxy paste, the range of ultimate loads obtained after 7 days was high. Instead, after 28 days, it was possible to calculate the exact splitting tensile strength.



## 4. SHEAR STRENGTHENING OF MASONRY WALLS

Controlling shear failure is a key issue in masonry strengthening because after the wall is cracked due to in-plane loads, it can easily collapse due to movement perpendicular to the plane and jeopardize human lives. This kind of behavior has been evident from post-earthquake observations.



*Figure 74 Specimen (GT-3) After the Failure*

This section presents an experimental program dealing with the shear behavior of URM concrete panels strengthened with FRP systems. The results of an experimental program conducted at the University of Missouri-Rolla have demonstrated the effectiveness of FRP to improve the structural performance of URM walls. FRP systems consisting of bars and laminates, and different strengthening configurations were investigated.

## 4.1 INTRODUCTION

The in-plane (shear) resistance in load-bearing unreinforced masonry (URM) walls is provided by the shear bond strength of the mortar and the friction shear due to the vertical load. The aging and often deteriorated mortar joints have little shear capacity. Under severe earthquake loads the shear capacity of the mortar is exceeded, resulting in failure of the wall. Those walls go under the name of infill panels.



*Figure 75 Shear Failure (Turkey 99)*

### 4.1.1 Infill walls

In general, infill walls can be grouped into two different categories: “isolated infill” and “regular infill” (sometimes referred to as shear infill). “Isolated infill” is a panel totally isolated from the confining frame at the top and on both sides. The isolation (gaps) between the infill and the frame must be greater than any possible deformation expected by the frame, thus prohibiting any infill/frame interaction. This infill is not considered structural elements.

Masonry infill panels should be evaluated in both the in-plane and out-of-plane direction while accounting for the effects of out-of-plane loading on in-plane capacity. This chapter focuses on the category of “regular” infill, where the panels act as part of the lateral force-resisting system of the structure, and analyse the effects of In-Plane loads.

The experimental program, conducted to study the in-plane behavior of masonry walls, investigated the shear behavior of masonry panels strengthened with FRP composites, which were intended to represent infill walls. These walls were tested at the RTI (Rolla Technical Institute), in the masonry class.

These tests had the objective to assess the behavior of URM panels similar to those found in infill walls. In particular, this work comes to become a sort of conclusion of other works conducted in the last two years, as shown in table 49 (page 149).

From the everyday experience, we know that an URM wall can fail mostly because of:

- Wrong design
- Structural weakness or overloading
- Differential settlements
- In-Plane and Out-of-Plane deformation
- Environmental conditions
- Earthquake loading

It is recognized that the behavior of these panels would be different in the presence of a surrounding structural frame. Masonry walls are commonly used as interior partitions or exterior walls, bound by steel or concrete frames conforming the building envelope. For the latter case, depending on the design considerations, the infill walls may or not may resist lateral and vertical loads.

In order to simplify the design, the potential interaction between the infill walls and the structural frame has been ordinarily ignored. Ignoring the contribution of the masonry infill walls does not always represent a conservative design. The presence of infill walls can lead to stiffening their frames and thereby cause a redistribution of lateral loads in the building plan.

The increase in stiffness of the frame can attract higher lateral loads than those expected according to the design. This may cause cracking of the wall and overstressing of the frame.

Previous investigations formed the basis for understanding and predicting infilled frame in-plane behaviour [Polyakov (1960) (work dating back to the early 1950s), Stafford-Smith (1962, 1966, 1969), Mainstone (1971), Klingner and Bertero (1976, 1978), to mention just a few]. Their experimental testing of infilled frames under lateral loads resulted in specimen deformation shapes similar to the one illustrated in figure 76.

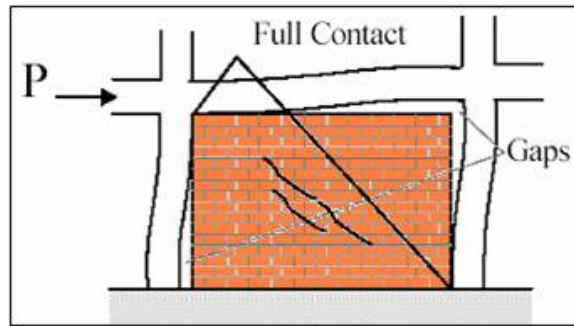


Figure 76 Specimen Deformation Shape

Sabnis (1976) has demonstrated that the composite action between the masonry infill and the surrounding frame is depending on the level of the in-plane load, bonding or anchorage at the interfaces, and geometry and stiffness of both the masonry infill and the structural frame.

At a very low level of in-plane loading, a full composite action between the infill wall and the frame is observed. Once the load increases, the infill wall and the frame are no longer in contact, except in surrounding areas of the two corners, where compression stresses are transmitted from the frame to the masonry, which lead to the formation of a diagonal compression strut (see figure 77).

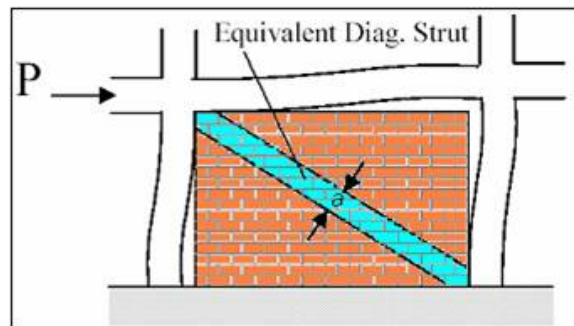


Figure 77 Equivalent Diagonal Strut

The equivalent masonry strut of width,  $a$ , with same net thickness and mechanical properties (such as the modulus of elasticity  $E_m$ ) as the infill itself, is assumed to be pinned at both ends to the confining frame.

This resulting structural system is usually analyzed as a truss. The stiffness of the infill starts decreasing once cracking is developed. At a stage when higher in-plane loads are present, the contribution of the compressive strut begins to reduce as further cracking is developed. Also, the gap separating masonry from frame is increased, which eventually leads to shear failure (diagonal tension) of masonry, as observed in figure 78, and flexure (yielding) failure of the columns.



*Figure 78 Diagonal Tension Failure (Umbria, September 26, 1997)*

Depending on the compressive strength of the masonry, the units in the corner areas may be crushed prior to developing diagonal cracking (see figure 79).



*Figure 79 Crushing of Infill Corners (Sakarya/Adapazari Turkey, 1999)*

Alternatively to the diagonal tension failure, a shear failure along a horizontal joint can be observed at a lower load level as compared to the load causing the latter mentioned failure. The resulting shear crack divides the infill in two parts, where the behavior is controlled by either the flexural or shear capacity of the columns. This failure mechanism is commonly known as Knee Brace or Joint-Slip (see figure 80).

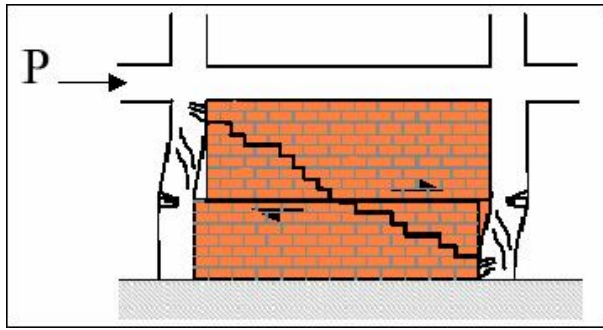


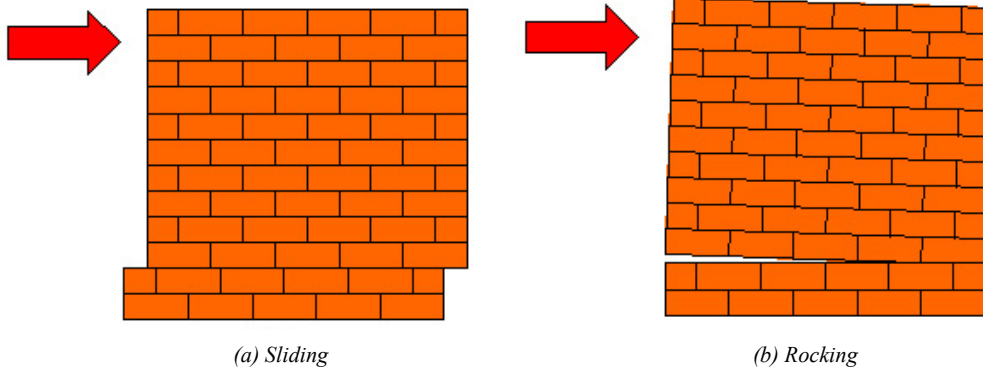
Figure 80 Joint-Slip Failure

#### 4.1.2 Failures Modes of URM Walls

Masonry is a non-homogeneous and anisotropic composite structural material, consisting of masonry unit and mortar. The behavior of masonry is complex. The accurate prediction of lateral load capacity of URM walls is difficult because of the complex brick-block mortar interaction behaviour.

The main in-plane failure mechanisms of URM walls subjected to earthquake actions are summarized as following:

- shear failure: this takes place when the principal tensile stresses, developed in the wall under the combination of the horizontal and vertical loads, exceed the tensile resistance of masonry materials. Just before the attainment of maximum lateral load, diagonal cracks are developed in the wall. These cracks are 45 degree sloped and, in case of strong bricks and weak mortars are “stair stepped”; in case of weak bricks and strong mortars they can pass through the bricks. For high axial loads explosive failure may happen.
- sliding mode: in the case of low vertical loads and/or low friction coefficient, which maybe due to poor quality mortar, horizontal crack in the bed joints will form. These cracks can form a sliding plane extending along the wall length as shown in figure 81a.
- flexural (rocking) mode: in case of high moment/shear ratio or improved shear resistance, crushing of the compressed zones at the edge of the wall may happen. Failure is obtained by overturning of the wall as shown in figure 81b.



(a) Sliding  
(b) Rocking  
Figure 81 Potential Failures in Walls with No Axial Load

The extent of existing infill damage can be determined by visual inspection of the infill. Existing panel damage (or cracking) must be classified as either: no damage, moderate damage, or severe damage as presented in figure 82.

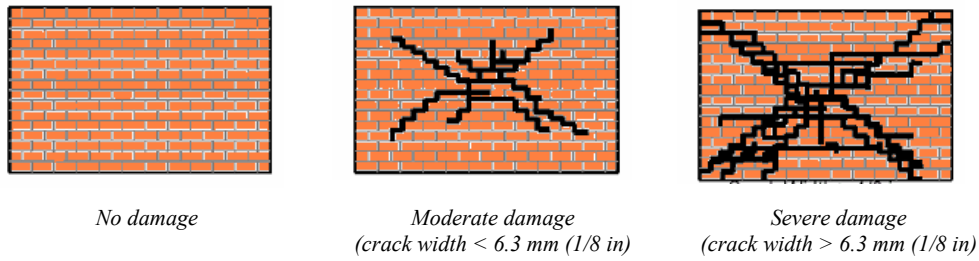
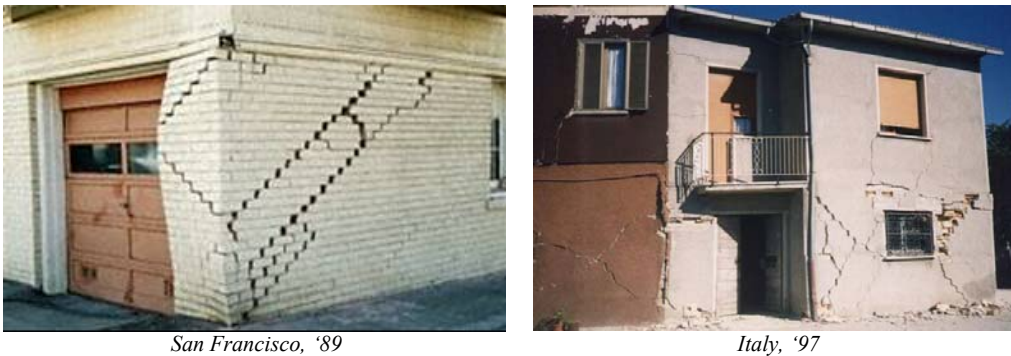


Figure 82 Visual Damage Classification

## 4.2 EXPERIMENTAL PROGRAM

### 4.2.1 Test Specimens

The objective of this section was to investigate the different behavior, resistance and failure of walls shear-reinforced with G-FRP rectangular bars, and G-FRP smooth circular bars, and to compare the results with the issues obtained from previous investigation with walls (same size) strengthened with FRP carbon tapes, laminates and rods, and steel.



*San Francisco, '89*

*Italy, '97*

*Figure 83 In-Plane Failures Due to Earthquakes*

Four masonry walls were manufactured for this experimental program. The nominal dimensions of each specimen were 1.6 m (64 in) high by 1.6 m (64 in) wide. The thickness was about 15 cm (6 in). The walls were constructed with concrete blocks using a Type N mortar (dimensions and properties reported in section 3.3 of this thesis). All the walls were built by a qualified mason to not introduce additional variables, such as handwork and different mortar workability that may arise from the construction of the specimens. All specimens were allowed to cure for at least 28 days after their building.

The first wall, named GT-3, was strengthened with 3 reinforcements made of glass FRP tape, one along the main diagonal, and two along the diagonals at 520.7 mm (20.5 in) from the corner. They were applied in the grooves filled up with epoxy-based paste.

The second one, named GT-5, was strengthened with tapes too, but this time 5 pieces of glass FRP tape were used, one along the main diagonal, two placed in the diagonals at 749.3 mm (29.5 in) from the corner, and two along diagonals at 342.9 mm (13.5 in).

The third wall, named GSR-3 had three Glass FRP smooth bars (having a diameter of 5 mm = 0.20 in), placed horizontally, one every two joints, embedded into an epoxy-based paste.

The last one, GSR-7, had seven Glass FRP smooth bars (having a diameter of 5 mm = 0.20 in), placed horizontally, every joint, embedded into an epoxy-based paste.

All the specimens were strengthened on one side. Table 44 explains the test matrix.

Table 44 Test Matrix for This Experimental Program

Specimen	Reinforcement
Wall WGSR-3	#2 GFRP bars + epoxy (4 bars)
Wall WGSR-7	#2 GFRP bars + epoxy (8 bars)
Wall WGT-3	Glass Tape (3 pieces)
Wall WGT-5	Glass Tape (5 pieces)

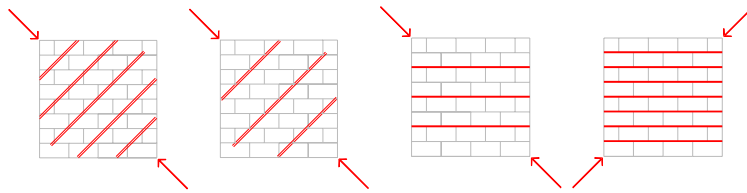


Figure 84. Strengthening Scheme for, From Left, the Walls GT-3, GT-5, GSR-3, GSR-7



Figure 85 Specimen W GT-5 Before the Test (Front Side)

One unreinforced wall was the control specimen for this test series (Tumialan 01).

To know the theoretical ultimate load it was used the formula from the 1997 Unified Building Code (UBC, 1997):

$$V_{th,u} = 10 \cdot A_{m,net} \cdot \sqrt{f'_m} \quad (\text{I.S. units of measurement});$$

$$V_{th,u} = 1.2 \cdot A_{m,net} \cdot \sqrt{f'_m} \quad (\text{American units of measurement});$$

where  $A_{m,net}$  is the “Net Area” along the horizontal section, and  $f'_m$  is the specified compressive strength of the masonry wall (calculated on the net area). Obtained values are shown in table 45.

Table 45 Values Used for Theoretical URM Concrete Wall

CONCRETE – W0 (control)	Wall dimensions mm (in)	$f'_m$ MPa (ksi)	$V_{th,u}$ kN (kips)	$P_{th,u} = 1.414V_{th,u}$ kN (kips)
	1625.6x1625.6x152.4 (64x64x6)	16.7 (2.43)	65.8 (14.8)	93.1 (20.9)

The walls were approximately 90-120 days old, and the epoxy paste was about 90 days old for the specimens GSR-3 and 7, 10 days old for the GT-3, 2 days old for the GT-5.

#### 4.2.2 Strengthening Procedure

Structural repointing offers advantages compared to the use of FRP laminates. The method itself is simpler since the surface preparation is not required. In addition the aesthetic of masonry is preserved. Figure 86 shows the strengthening procedure.

The diameter of the groove is limited by the thickness of the mortar joint when the bar is placed there (then horizontal), and by the thickness of the block when the bar is slanting.

Therefore the bars were placed using the following sequence:

- Cutting of the groove using a grinder (figure 86(a))
- Cleaning of the surface from the dust by means of an air blower (86(b))
- Applying a mask with a duck-tape (86(c))
- Filling the groove with the epoxy paste (86(d))
- Embedding of the bar in the groove (86(e))
- Levelling of the filled groove (86(f))
- Removing the mask (86(g))

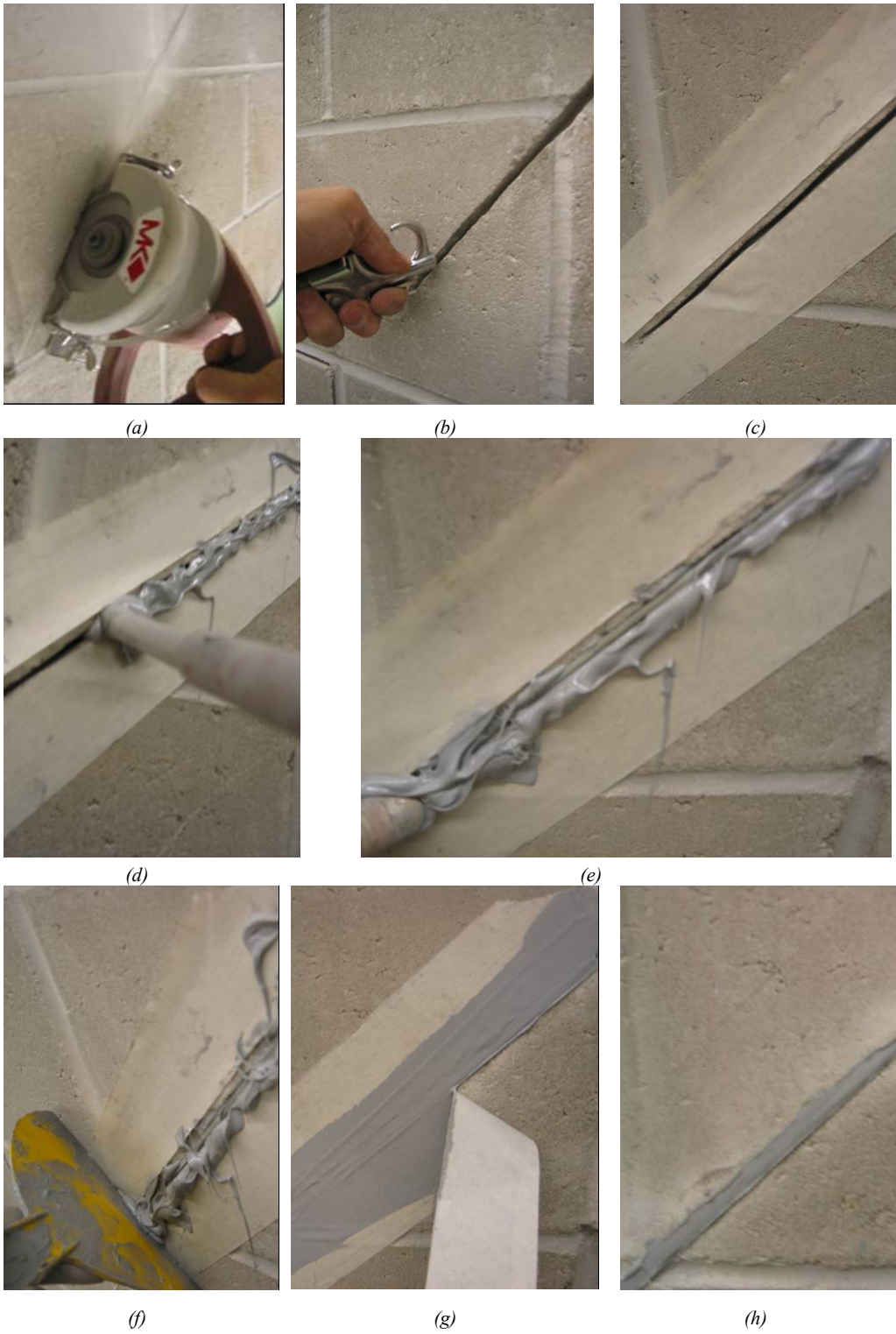


Figure 86 Strengthening Procedure Sequence

The dimension of the groove was about 3.5 x 17 mm (0.14 x 0.66 in) for the specimens strengthened with the rectangular bars, and 9 x 9 mm (0.35 x 0.35 in) for the two with the smooth bars.

Strain-gages were applied on the surface of the FRP tapes prior to their application. The purpose was to monitor the strain distribution along the bar during the test. The strain-gages used had a gage length of 9.5 mm (3/8 in) and they were placed along the loaded diagonal and close to the bed joint. No strain gages were applied on the surface of the smooth rods due to their dimensions.

#### 4.2.3 Test Setup

The specimens were tested in a closed loop fashion. Two 30-ton-capacity hydraulic jacks, activated by a manual pump, were used to generate the load along the diagonal of the wall being tested. When loading, the force was applied to the wall by steel shoes placed at the top corner, and transmitted to similar steel shoes at the bottom corner through high strength steel rods. Figure 87 illustrates the test setup.

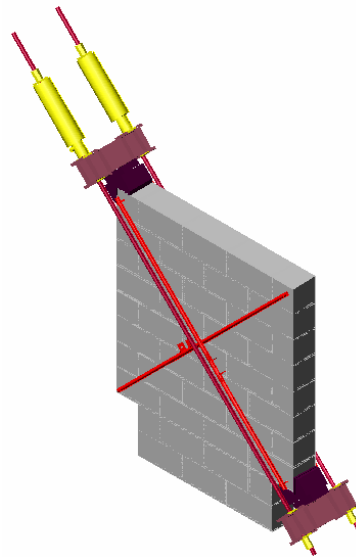


*Figure 87 Test Setup*

The load was applied in cycles of loading and unloading. An initial cycle for a low load was performed on every wall to verify that both the mechanical and electronic equipment were working properly. By applying the load in cycles, the stability of the system can be verified. The data acquired by the load cell and the Linear Variable Differential Transducers (LVDTs) were collected

by a DAYTRONIC data acquisition system at a frequency of one point per second. A total of four LVDTs were used to collect displacements in the walls. A couple of LVDTs were placed on each side of the walls; one oriented along the line force and the other perpendicular to the line. The latter one was placed to register the crack opening.

#### 4.2.4 Results: GT-3 and GT-5

The two specimens have exhibited a similar behavior during the entire test. In fact, in both the specimens, the peak load was reached at the first visible crack, that was running along the loaded diagonal on the mortar joints. The crack was more visible by the unstrengthened side. After these cracks, the wall has shown a very ductile behavior, the carried load was ever over 110 kN (25 kips, value reached by the control wall), and the test had to be stopped just because the slope towards the strengthened side was too high. There were no signs of debonding, in any tape. Table 46 and figures 88 through 92 show the results.

*Table 46 Peak Load and Reload Reached by the Specimens*

Wall	Peak Load $P$ (first crack) kN (kips)	Re-Load (successive cracks) kN (kips)
C-0-control	108 (24.3)	0
GT-3	157.5 (35.4)	126.3 (28.4)
GT-5	175.3 (39.4)	164.6 (37.0)

It should be noted that the load reported in the table refers to the value recorded by the load cell, then geometrically 1.414 times the shear value.

Figure 88 emphasizes the work of the bars at loading: they started working when the load was about 110 kN (25 kips; the maximum load reached by the control wall) and at the peak load the strain in the two lower bars reached up to 1% (strain gages were numbered from top left to down right).

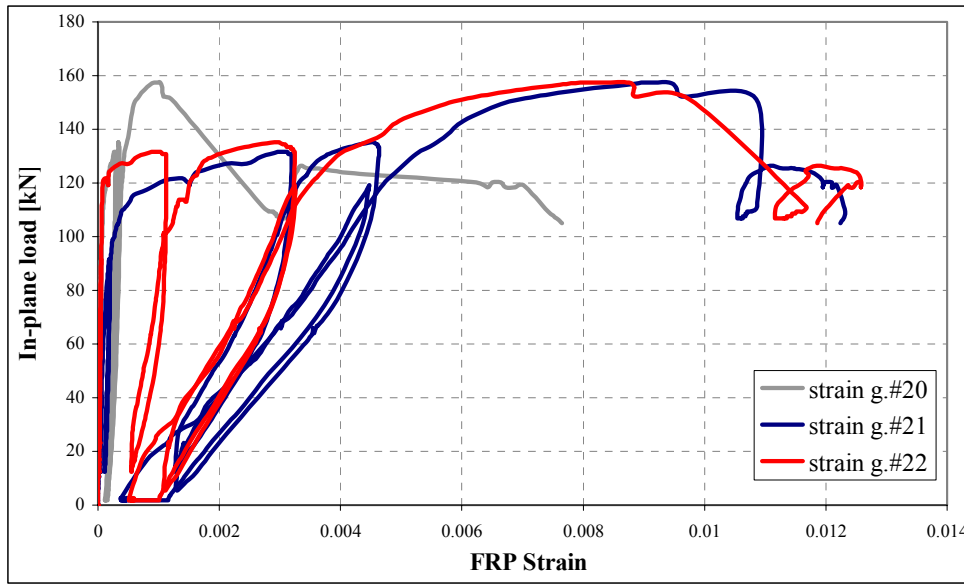


Figure 88 Wall GT-3: Load / Strain in the Three FRP Bars

Figure 89 shows the load-strain in FRP reinforcement ratio. Here the FRP started working at the peak load, allowing however the load to be almost invariable till the failure.

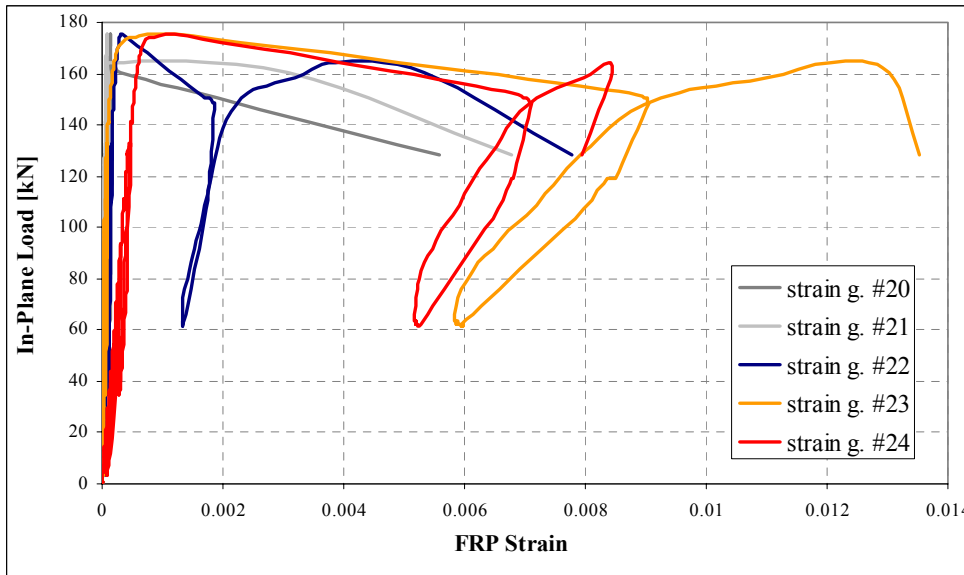


Figure 89 Wall GT-5: Load / Strain in the Three FRP Bars

Figure 90 reports the Applied Load Vs. Crack Opening of the two walls tested and the experimental behavior of the control one.

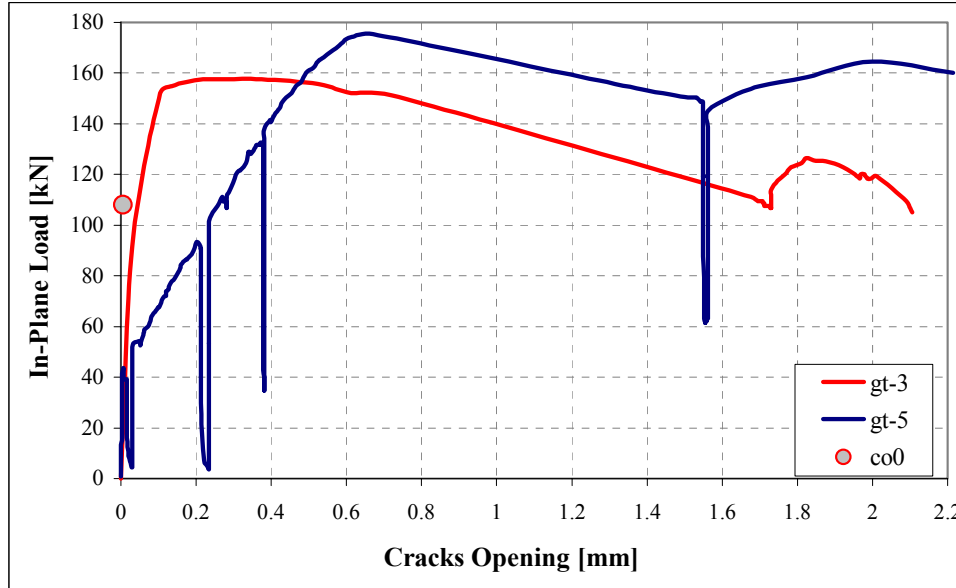


Figure 90. Cracks Opening on the Loaded Diagonal, Front Side

Figures 91 and 92 shows the two specimens after the collapse, that was very similar: for both the walls it is possible to see the slope towards the strengthened side due to the asymmetric and well bonded reinforcement.



Figure 91 Failure of the Wall GT-3(Front Side, Left, Slope of the Wall on the Right)



Figure 92 Failure of the Wall GT-5 (Front Side, Left, Slope on the Right)

Comparison with C-FRP tape

Two specimens, strengthened with 3 and 5 pieces of carbon tape, were tested in a previous research (Grando 02). The carbon tape used had an elastic modulus of 143 GPa (20702 ksi) and an  $\epsilon_u = 0.98\%$ . Table 47 shows the load reached by the four specimens:

Table 47 First Crack Load and Peak Load Reached by Specimens Strengthened with C and G-FRP Tapes

Concrete Walls, strengthened with tapes 45 degree sloped, on one side					
Wall name	# of tapes used	FRP used	Crack load-kN	Peak load-kN	note
CT-3 Grando 02	3	Carbon	<b>124.6</b>	<b>133.5</b>	Shear failure along the loaded diagonal in the unstrengthened side.
CT-5 Grando 02	5	Carbon	<b>98.1</b>	<b>108.5</b>	
GT-3	3	Glass	<b>135.0</b>	<b>157.5</b>	Shear failure along the loaded diagonals in both sides.
GT-5	5	Glass	<b>175.4</b>	<b>175.4</b>	

The following graphs give a comparison between the specimens CT-5 and GT-5. It has been chosen the CT-5 because it was the only one that had the strain gages data.

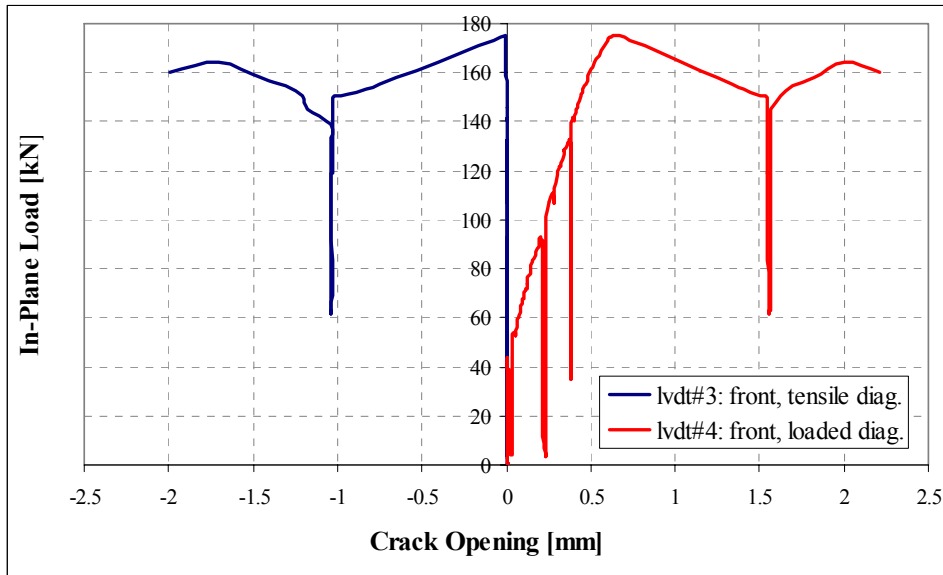


Figure 93 Specimen GT-5, LVDTs on Front Side

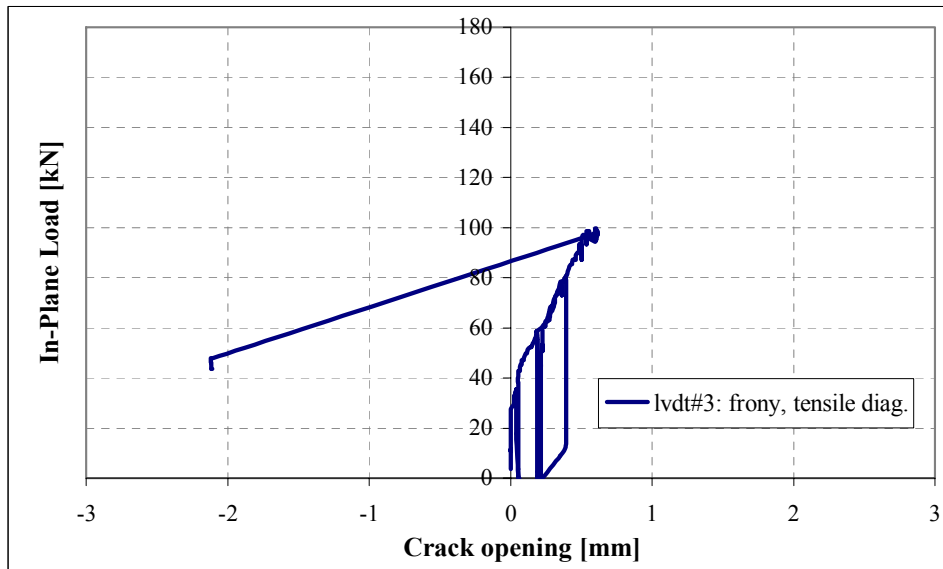


Figure 94 Specimen CT-5, LVDT on Front Side

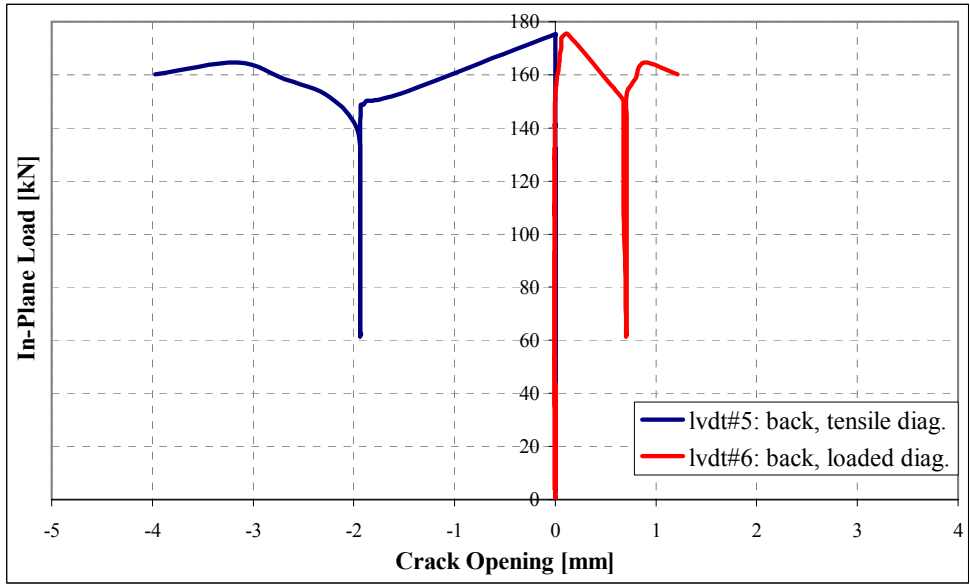


Figure 95 Specimen GT-5, LVDTs on Back Side

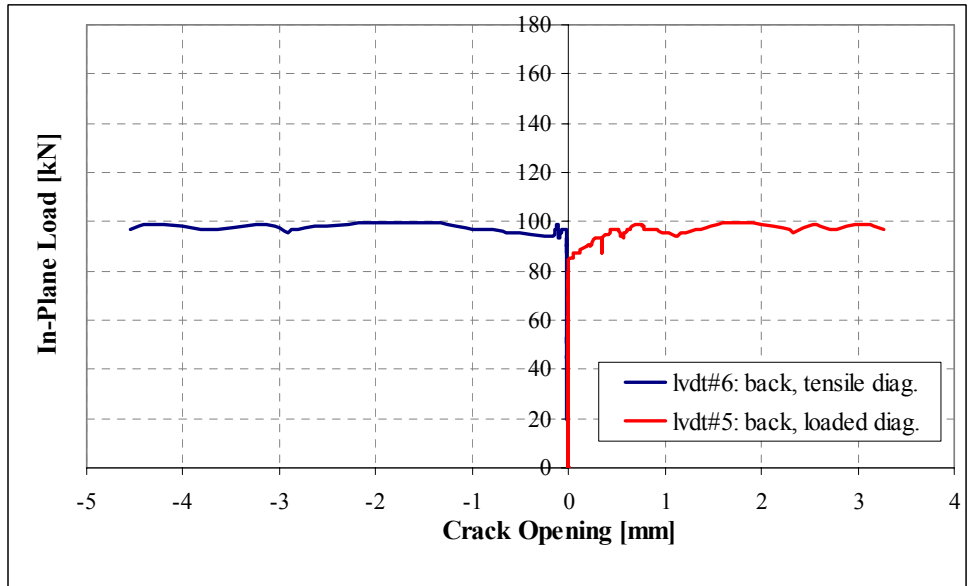


Figure 96 Specimen CT-5, LVDTs on Back Side

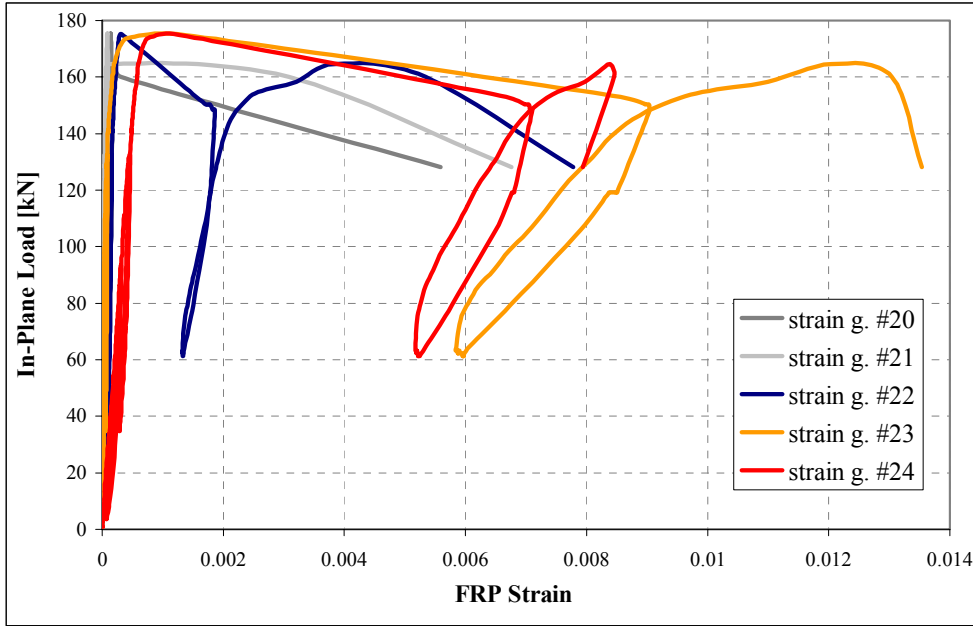


Figure 97 Specimen GT-5, Strain Gages on the Bars (Numbered From Top Left to Down Righth)

note:  $\epsilon_u=0.025$

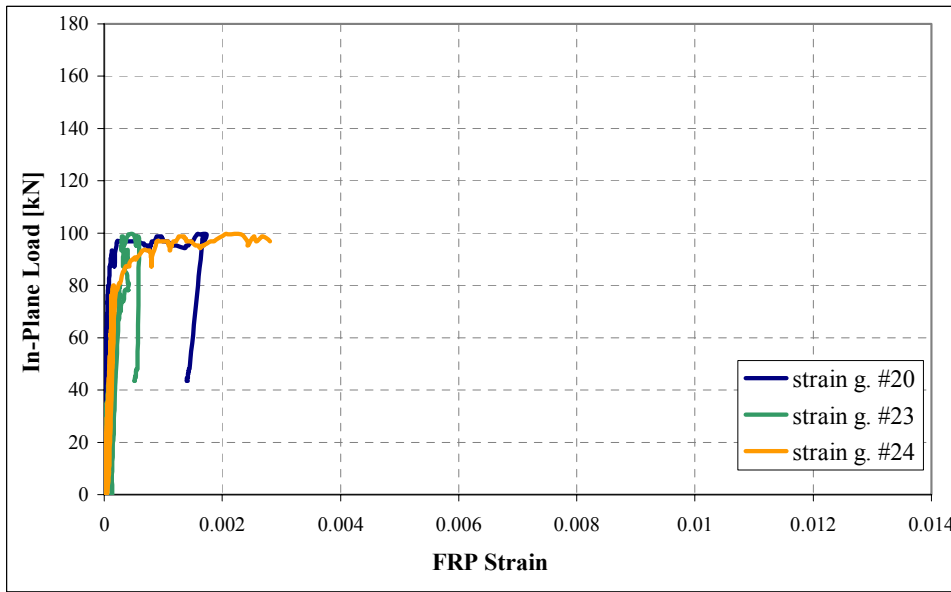


Figure 98 Specimen CT-5, Strain Gages on the Bars (Numbered From Top Left to Down Righth)

note:  $\epsilon_u=0.010$

Considerations upon the rectangular cross section bars.

The rectangular bars have shown an excellent bond behavior (but it should be taken into consideration that it needs a deep groove, that it is not so easy to do and, especially, it may render more brittle the wall) that however can be exploited just with the glass-FRP; the carbon one is probably too stiff and it causes a increase of load eccentricity.

Carbon Tape: The average maximum strain in the carbon bars has reached 0.17% ( $0.174 \epsilon_u$ ) and, compared to the control one the improvement in terms of shear capacity was 24% for the wall CT-3 and 0% for the CT-5.

Glass Tape: The average maximum strain in the glass bars has reached 0.83% ( $0.332 \epsilon_u$ ) and, compared to the control one (Morbin, 01) the improvement in terms of shear capacity was 46% for the wall CT-3 and 62% for the GT-5. In terms of ductility, the improvement is excellent.

#### 4.2.5 Results: GSR-3 and GSR-7

As previously described, these two walls were reinforced with small rods (diameter 5 mm), that have a top coating of an ethylene – acrylic acid copolymer. The purpose was to investigate the bond behavior between the epoxy paste and the smooth surface of the rod.

The two specimens have reached excellent peak loads. Table 48 shows the results.

*Table 48 Test Results for the Specimens Reinforced with the Glass Smooth Bars*

Wall	First Crack load kN (kips)	Peak Load $P$ kN (kips)
C-0-control	108 (24.3)	108 (24.3)
GSR-3	190.4 (42.8)	190.4 (42.8)
GSR-7	241.0 (54.2)	241.0 (54.2)

**Wall GSR-3:** No visible cracks were observed before failure, which was brittle and due to the sliding failure occurred along the unstrengthened mortar joint at the upper course (see figure 99); no bar was debonded or broken. The peak load was reached at 190.4 kN, without showing any ductile behavior. This kind of failure could not be observed in an infill wall, because the frame doesn't allow a sliding failure along a horizontal mortar joint.



*Figure 99 Failure of the Wall WGR-3*

**Wall GSR-7:** No visible cracks were observed before failure, which was brittle and caused by the lack of bonding between concrete units and mortar in the joints. Only one major crack was found after failure running along the loaded diagonal on both sides of the wall. The peak load was reached at 241 kN, without showing any ductile behavior. After the crack, re-loading (the displacement of loaded diagonal was 10 mm) the wall carried still a load equal to 48.9 kN. At the end, just the upper bar was fully debonded (see figure 100, right); no one was broken.



*Figure 100 Wall GSR-7 After Failure*

Figure 101 reports the Applied Load Vs. Crack Opening of the two walls tested and the experimental behavior of the control one.

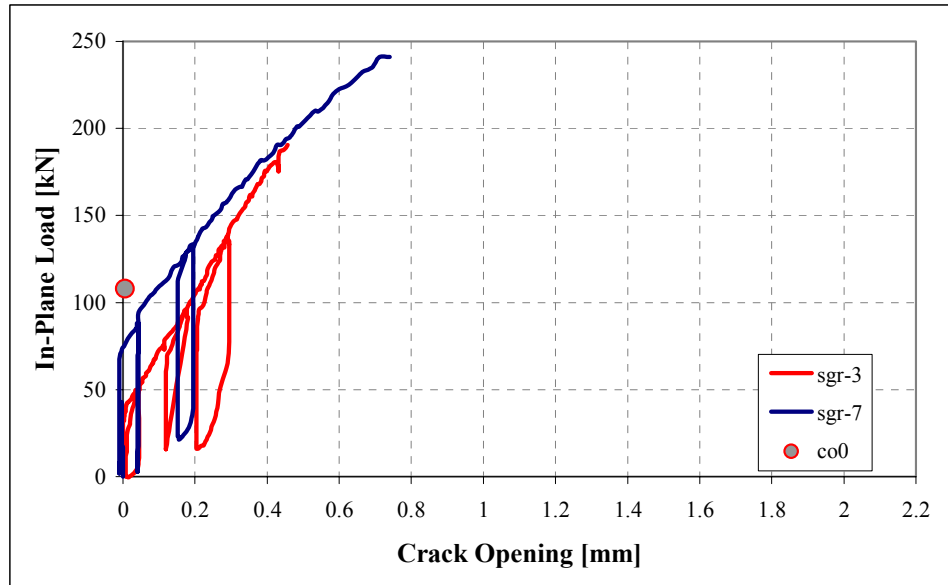
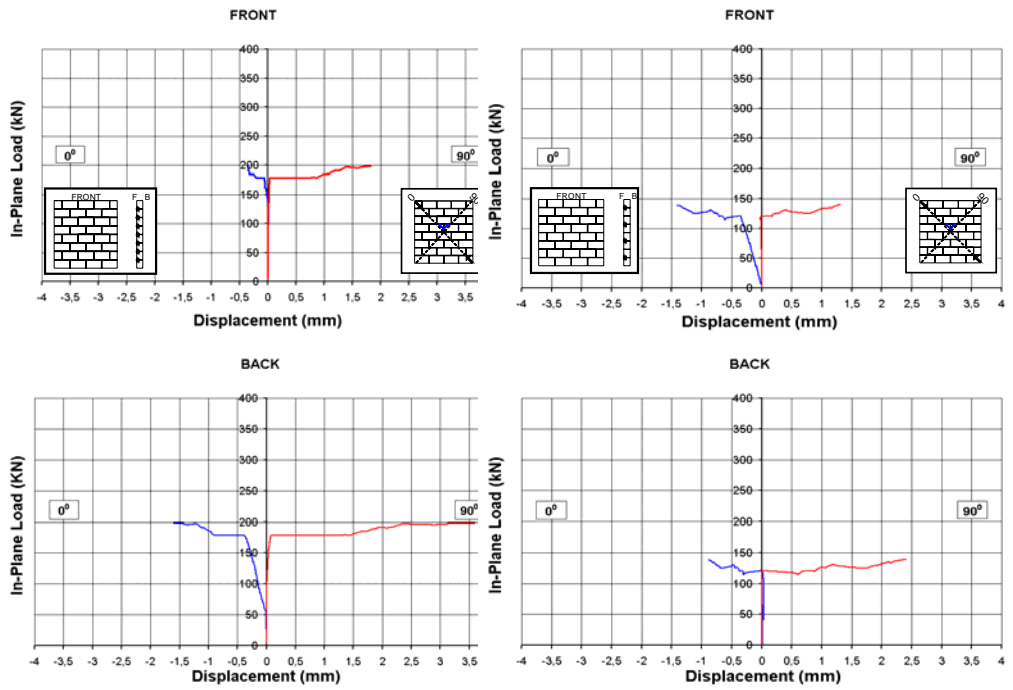


Figure 101 In-Plane Load / Displacement for the Wall Strengthened with Smooth Bars

Considerations upon this glass smooth bar.

This kind of bar, in spite of its smoothness, has exhibited a good bond with the epoxy paste. We did not able to put strain gages on the bars so we can not know its allowable ultimate strain, but, as shown in figure 100, at debonding the bar has not slid on the epoxy paste, but the concrete getting torn. Just to have an idea, other researches, with a similar kind of bar (Pijong 03), have shown a strain at failure about 15%  $\epsilon_u$  if not prestressed, and 30%  $\epsilon_u$  if prestressed, obtaining in both cases peak loads (the test frame was the same) of 180-240 kN (42-54 kips; it depended by the amount of reinforcement).

With these two wall the maximum load overcame the loads recorded by all the previous researches (Morbin 01, see figure 102) with #2 (diameter 6.3 mm) FRP rods along the joints; besides, with the wall GSR-7 we have obtained the highest failure-load since this kind of test has started.



GR-1: rods #2 g-frp every joint

GR-3: rods #2 g-frp every second joint

Figure 102 Test Results of Previous Similar Walls

4.2.6 Summary

All the four walls have exhibited reasonable and good results. Smooth bars proved effective in terms of bond when they are embedded in epoxy paste along the mortar joints, and the tape has indicated its effectiveness when the bar has to be placed in the concrete blocks. While the smooth bars have revealed to can well tolerate asymmetrical reinforcements, the same it is not true for the tape; besides, it should be noted that no walls with both sides reinforced with the tapes were tested because it would be too strong to test, or rather a similar wall would crack in compression and not for shear.

Figure 103 clarifies the load versus the crack opening behavior of the four specimens tested and the control one.

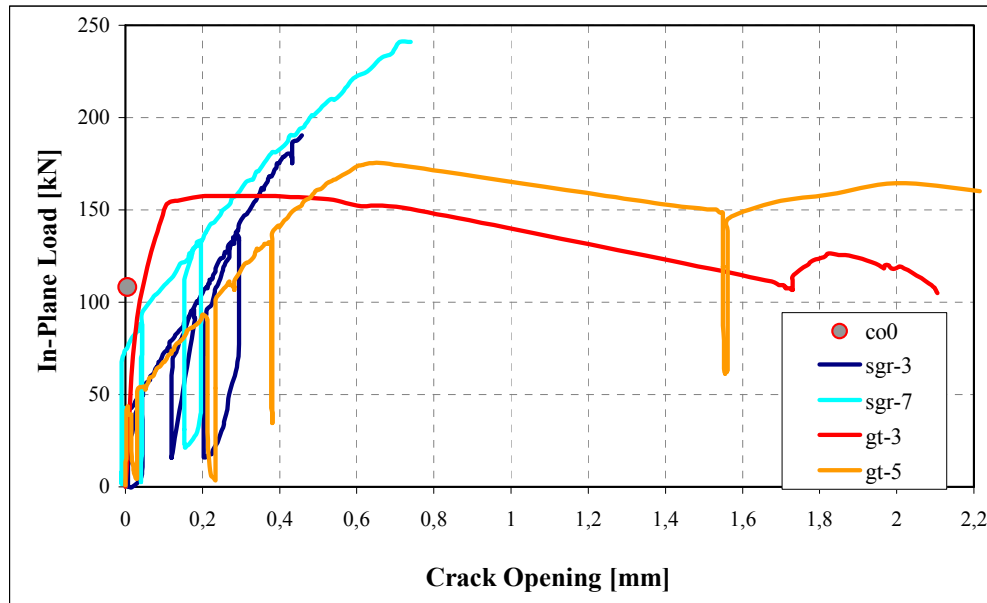


Figure 103 Load / Crack Opening Behavior of the Four Specimens Tested

### 4.3 COMPARISON WITH PREVIOUS TESTS

Like previously anticipated, this work is a sort of conclusion of other works conducted at University of Missouri-Rolla in the last two years, with identical walls, strengthened with G and C FRP laminates, G-FRP circular bars, C-FRP tapes, internal steel wires and stainless steel rods. The results of this work are summarized in the following table 49.

Table 49 Previous Tests Results

Concrete-block Walls					
Wall name	kind of reinforcement used	wall strengthening description	Crack load kN	Peak load $P$ kN	note-failure mode
C-0 Tuliaman 01	nothing	control wall	108.1	108.1	failure mode was brittle, controlled by bonding between the masonry units and mortar
<i>#2 GFRP circular bars</i>					
GR-1 Morbin 01	#2 (d.=6mm) GFRP bars	every horizontal joint, on one side.	180	199.6	Shear failure along the diagonal in the unstrengthened side
GR-2 Morbin 01		every second horiz. joints, on both side, altern.	149	197	Shear failure along diagonals, in both sides
GR-3 Morbin 01		every second horizontal joints, on one side	122	139	failure occurred along the unstrengthened mortar joint at the second course
GR-4 Turco 02		every horizontal joint, on one side, cem.paste	168.1	184.1	Shear failure along the loaded diagonals in both sides
<i>G-FRP Laminates</i>					
GL-1 Morbin 01	10cm (4 in) stripes	four horizontal strips, on one side	135	187	failure was caused by sliding of the second course of the concrete units
GL-2 Morbin 01	10cm (4 in) stripes + #2 GFRP bars	bars every horiz. joint, and four vertical strips, on one side	190	190	progressive debonding of the epoxy from the concrete unit surfaces and partial delamination of the GFRP sheets
GL-3 Grando 02	5 cm (2 in) stripes	at the horizontal joints	89	109.3	Shear failure along diagonals in the unstrengthened side
GL-4 Grando 02	7.5cm (3in) stripes	at the horizontal joints	180.2	208.2	Shear failure along diagonal in both sides
<i>C-FRP Laminates</i>					
CL-1 Grando 02	5 cm (2 in) stripes	at the horizontal joints	63.2	113.0	Shear failure along the diagonal in the unstrengthened side

<i>C-FRP Rectangular Bars</i>					
CT-3 Grando 02	3 bars, one along the diagonal, and two along the diag. at 520.7 mm from the corner		124.6	133.5	Shear failure along diagonals in the unstrengthened side
CT-5 Grando 02	3 bars, one along the main diag., two in the diag. at 749mm from the corner, and two along diag. at 343 mm from the corner.		98.1	108.5	Shear failure along main diagonal in the unstrengthened side
<i>Internal Steel Wires</i>					
IS-1 Grando 02	Internal steel bars	one for every horizontal joint of grout	77.4	208.2	Shear failure along main diagonal
IS-2 Grando 02	#2 GFRP bars + Internal steel bars	bars, every two joints and wires every other joint, altern.; +epoxy	88	160.1	Sliding shear of the first joint on the top
<i>Stainless Steel Rods</i>					
SR-1 Grando 02	Stainless steel rods	every horizontal joint, on one side + epoxy	106.8	122.2	Shear failure along loaded diagonals in both sides
SR-2 Turco 02	stainless steel rods	every horizontal joint, on one side, + cem.paste	219.7	219.7	Shear failure along the diagonals in both sides and opening of the second joint from the top

(note: 1 kN = 0.2248 kips)

## 4.4 ANALYTICAL WORK

It is important to observe that these types of in-plane tests do not reflect real loading conditions. Indeed the interaction of the masonry panel with the surrounding structural frame will modify the masonry panel behavior. Consequently, the following evaluation could give only an indicative idea of the shear strength of reinforced walls.

### 4.4.1 FRP Bars Strengthening Computation

The following process was used to compute the strengthening for the walls reinforced with FRP bars. To estimate the ultimate load for a strengthened wall, it was decided to add the shear contribution from the URM wall and the contribution from the FRP system (adapted from ACI Committee 440, in the case of “externally bonded FRP systems for strengthening concrete structures”):

$$V_n = V_m + V_f$$

where:

- $V_n$  is the overall shear capacity of the system wall-reinforcement
- $V_m$  is the shear capacity provided by the masonry
- $V_f$  is the shear capacity provided by the reinforcement

### 4.4.2 Computation of $V_f$

For the computation of the shear strength contribute given by the reinforcement the following assumptions have to be taken:

- Inclination angle of the shear cracks constant and equal to 45 degrees.
- Constant distribution of bond stresses along the FRP rods at ultimate
- The ultimate bond strength is reached contemporary in all the rods intersected by the crack at ultimate
- The spacing between rods is the layer height

The bond behavior depends on the surface of the rod and on the material in which it is embedded; therefore the assumption of the constant distribution of the stresses may be not appropriate. In this case the bond length has to be calculated solving the differential equation of with the local bond-stress slip relationship of the NSM.

$V_f$  depends on the shear contribution of reinforcing rods developing their full tensile capacity and rods being debonded. Thus, two areas can be identified in a masonry panel.  $L_e$  is defined as the length at which the rod breaks and can be derived from figure 104.

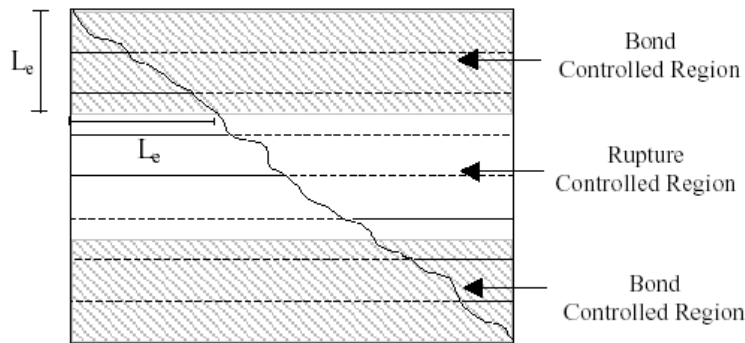


Figure 104 Controlling Areas to Calculate  $V_f$

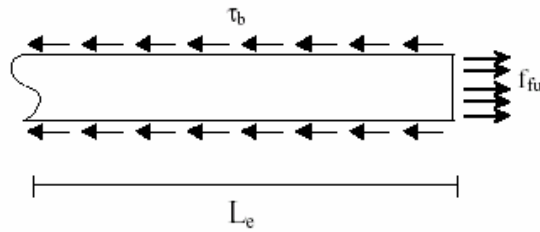


Figure 105 Effective Length  $L_e$

By equilibrium the force given by debonding stress is equal to the force generated by the tensile stresses in the rod (figure 105); thus:

$$\tau_b (\pi d_b L_e) = f_{fu} A_f$$

$$\tau_b (\pi d_b L_e) = f_{fu} \left( \frac{\pi d_b^2}{4} \right)$$

$$L_e = \frac{d_b f_{fu}}{4 \tau_b}$$

Then we may consider the global contribution given by the reinforcement as the sum of the two different types of contribution:

$$V_f = V_b + V_t$$

**Shear in Bond Controlled Region ( $V_b$ )**

The number of the rods in the bond controlled region can be qualified as:

$$r_b = 2 \cdot \frac{L_e}{s}$$

Therefore the value of  $L_{tot}$  is calculated as:

$$L_{tot} = 2s \cdot \sum_{i=1}^{r_b} i$$

The shear force resisted by the FRP rods in this region can be calculated as:

$$V_b = n\pi d_b \tau_b L_{tot}$$

where the know parameters are:

$n$  = number of strengthened sides of the wall

$\tau_b$  = assumed bond stress

$$L_{tot} = r_b \cdot s$$

**Shear in Rupture Controlled Region ( $V_t$ )**

The number of rods ( $r_t$ ) in the rupture controlled region can be calculated as:

$$r_t = r_f - r_b$$

The shear force resisted by the FRP rods in this region can be calculated as:

$$V_t = nr_t A_f f_{fu}$$

Since long-term exposure to various types of environments may reduce properties of the FRP reinforcement, the material properties used in design equations should be reduced based on the environmental exposure condition by an appropriate environmental reduction factor  $C_E$  (ACI-440, 2000). Thus:

$$f_{fu} = C_E f_{fu}^*$$

where  $f_{fu}^*$  is the guaranteed ultimate tensile strength of the FRP bar as reported by the manufacturer.

Since neither debonding nor breaking of the FRP systems were observed, the bond stresses estimated by previous investigations (De Lorenzis) may be reduced with a coefficient “ $k$ ”. Thus:

$$f_{fu} = k \cdot C_E \cdot f_{fu}^*$$

$$\tau_{b1} = k \cdot \tau_b$$

The bond behavior depends on the surface configuration of the rod and on the material used for embedding it. In addition, the behavior of a strengthened wall and, consequently, the ultimate load are influenced by the interaction between the properties of the reinforcement and of the unreinforced wall. As an example, if the difference between the stiffness of the reinforcement and that of the URM wall is too high, the stresses couldn't distribute in uniform way and the reinforcement may be ineffective. Therefore, higher is the difference between the stiffness of the reinforcement (rod+embedding material) and of the URM wall, lower is the reduction factor. Considering these aspects, different empirical values of the factor "k" have been deduced. Tables 52 and 53 report a summary of the calculations.

Finally the shear force resisted by the FRP rods in both regions can be estimated as:

$$V_f = V_b + V_t$$

#### 4.4.3 Computation of $V_m$

The contribution of masonry to the shear strength is computed by the 1997 Unified Building Code (UBC, 1997) as follows:

$$V_m = C_d A_{mv} \sqrt{f'_m}$$

where  $C_d$  = shear strength coefficient estimated as 1.2

$A_{mv}$  = net area [sq-in] for the horizontal section of the wall

$f'_m$  = specified compressive strength of masonry [psi], estimated on the net area.

Using the I.S. units of measurement,  $C_d$  becomes equal to 10, and  $A_{mv}$  is expressed in  $\text{cm}^2$ ,  $f'_m$  in MPa,  $V_m$  in N.

**4.4.4 Theoretical / Experimental Results**

Finally the theoretical shear strength can be evaluated. Table 50 explains the analytical computing scheme adopted, table 51 reports the results of the computations and figure 106 illustrates that the obtained values are reasonable.

Table 50 Analytical Computation Scheme Adopted

$V_n = V_m + V_f$		
$V_m = C_d \cdot (b \times d) \cdot \sqrt{f'_m}$		$V_f = V_b + V_t$
where $b \times d$ is the "Net Area" [sq-in] along the horizontal section, and $f'_m$ is the specified compressive strength of the masonry wall [psi]		$V_b = n \times \pi \times d_b \times \tau_b \times L_t$ n = number of strengthened sides of the walls $\tau_b$ = assumed bond stress (De Lorenzis, 2000) $L_t$ = sum of the bonded lengths of all the rods crossed by the crack, calculated in the most unfavorable crack position
		$V_t = n \times r_t \times A_t \times f_{fu}$ $A_t$ = cross sectional area of a rod $f_{fu}$ = ultimate tensile strength of the FRP rod by $C_E=0.8$
Net Area mm <sup>2</sup> (sq-in)	$f'_m$ MPa (psi)	$V_m$ kN (kips)
1625x152x0.65 (64x6x0.65)	16.73 2429	65.8 (14.8)
$L_e = \frac{d_b \times f_{fu}}{4 \times \tau_b}$		$f_{fu} = \kappa \times C_E \times f_{fu}^*$ $\tau_{b1} = \kappa \times \tau_b$
$\tau_b \times (Perim_f \times L_e) = f_{fu} \times A_f$		

Table 51 Theoretical and Experimental Results

	$\tau_b$ [MPa]	$C_E$	$\kappa$	$L_E$ [mm]	$V_m$ [kN]	$V_b$ [kN]	$V_t$ [kN]	$V_{n,theo.}$ [kN]	$V_{n,exp.}$ [kN]
Control	-	-	-	-	65.8	-	-	<b>65.8</b>	<b>76.4</b>
SGR 3	3.1	0.8	1.0	341	65.8	0	50.8	<b>117.6</b>	<b>134.6</b>
SGR 7				341	65.8	20.1	84.7	<b>170.6</b>	<b>170.5</b>
GT 3	3.1			257	65.8	0	117.1	<b>182.9</b>	<b>111.4</b>
GT 5				257	65.8	0	195.1	<b>260.9</b>	<b>124.0</b>

It is important to note that the  $\tau_b$ , assumed equal to 3.1 MPa for all the four specimens, refers to the results obtained with the bond test in the case of GFRP rods-epoxy paste. This assumption seems to be reasonable, however more accurate values may be calculated in future bond tests.

In addition, for the wall reinforced with the glass-tape 45 degree sloped,  $V_t$  was multiplied by 1.414 to consider the real contribution to the shear.

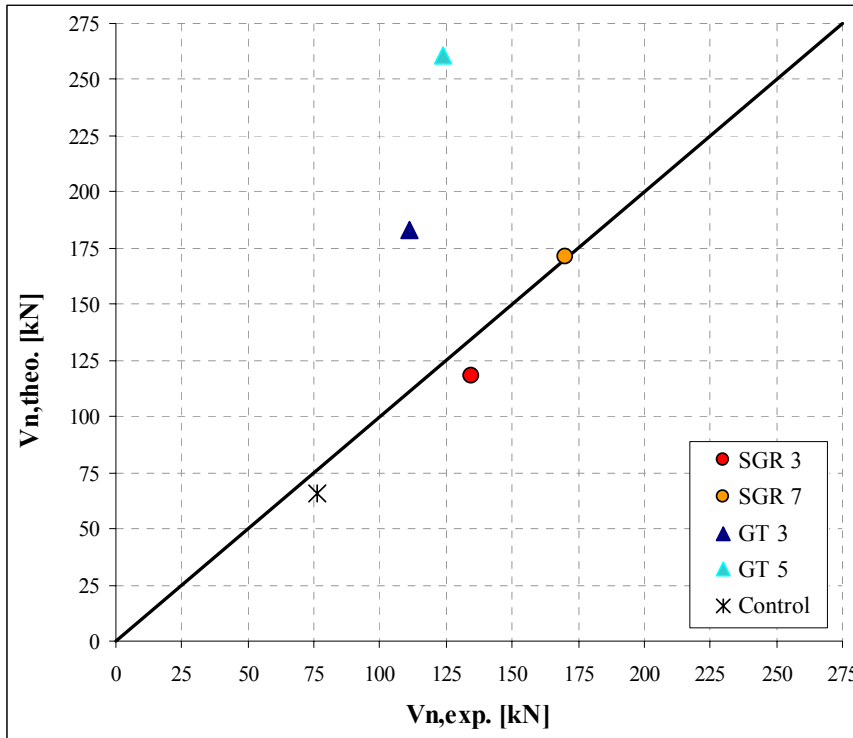


Figure 106 Comparison Between Theoretical and Experimental Results

Figure 106 demonstrates the adequacy of this method to estimate masonry reinforced with the smooth bars, whereas it seems to overestimate the capacity of those strengthened with the tapes. It is important to note that this overestimation is even greater with carbon tape as reinforcement, probably because of its stiffness, just on one side of the wall. This causes high moment/shear ratio that, because of the non-linearity of the Mohr-Coulomb relation, decreases the overall shear capacity.

#### 4.4.5 FRP Laminates Strengthening Computation

In order to better understand also the previous tests on masonry reinforced with FRP-laminates, this method is explained. It adopts the procedure indicated by Triantafillou, which assumes that the contribution to shear reinforcement due to FRP is:

$$V_{FRP} = \rho_{FRP} \times E_{FRP} \times \left( \frac{r \times \varepsilon_{FRP,u}}{\gamma_{FRP}} \right) \times t \times 0.9 \times d$$

where:

- $\rho_{FRP}$  = percentage of FRP Area:  $A_{FRP} / A_M$
- $E_{FRP}$  = Modulus of Elasticity of FRP
- $r$  = reinforcement effectiveness coefficient
- $\varepsilon_{FRP,u}$  = ultimate tensile strain in FRP
- $\gamma_{FRP} = 1.25$
- $d = 0.81$

This equation can be simplified in the next one:

$$V_{FRP} = 0.729 \times \rho_{FRP} \times E_{FRP} \times \varepsilon_{FRP,e} \times b \times t$$

Where  $\varepsilon_{FRP,e}$  = effective strain in FRP

Assuming that “ $r$ ” depends on fracture mechanism, thus

$$\varepsilon_{FRP,e} = r \times \varepsilon_{FRP,u} \quad (\text{P.Salmaso, 2000})$$

Since  $\varepsilon_{FRP,e}$  has not yet been determined, we can say that it depends on the bond length, the minimum length to have a failure in the FRP rather than a debonding. This bond length is proportional to axial strength in the FRP ( $\rho_{FRP} \times E_{FRP}$ ), so we can expect that  $\varepsilon_{FRP,e}$  is proportional in reverse order to  $\rho_{FRP} \times E_{FRP}$ . Thus the stronger and thicker the FRP laminates, the smaller is the effective strain in the FRP.

Triantafillou found a formula to compute  $\varepsilon_{FRP,e}$  in the case of FRP reinforced concrete structures, so we can use even in masonry panels:

$$\varepsilon_{FRP,e} = 0.0119 - 0.0205 \times (\rho_{FRP} \times E_{FRP}) + 0.0104 \times (\rho_{FRP} \times E_{FRP})^2$$

#### 4.4.6 Evaluation of new Coefficients for FRP Systems

Since one of the proposals of this work was to compute new coefficients in the design for FRP systems, it was decided to calculate the values of  $V_f$  for all the walls, not considering the coefficient  $\kappa$  (see table 51). Then, according to the values showed in table 51 the following coefficients were computed:

Table 52 Values for Coefficient  $\kappa$  for the New Materials

FRP SYSTEM	WALL MATERIAL	COEFFICIENT $\kappa$
SMOOTH BARS	Concrete	<b>1.0</b>
G-TAPE	Concrete	<b>0.3</b>

By using these coefficients  $\kappa$ , new theoretical shear capacities are been estimated:

Table 53 Theoretical and Experimental Results

	$\tau_b$ [MPa]	$C_E$	$\kappa$	$L_E$ [mm]	$V_m$ [kN]	$V_b$ [kN]	$V_t$ [kN]	$V_{n,theo.}$ [kN]	$V_{n,exp.}$ [kN]
Control	-	-	-	-	65.8	-	-	<b>65.8</b>	<b>76.4</b>
SGR 3	3.1	0.8	1.0	341	65.8	0	50.8	<b>117.6</b>	<b>134.6</b>
SGR 7				341	65.8	20.1	84.7	<b>170.6</b>	<b>170.5</b>
GT 3	3.1		0.3	257	65.8	0	35.1	<b>100.9</b>	<b>111.4</b>
GT 5				257	65.8	0	58.5	<b>124.3</b>	<b>124.0</b>

\* 1 MPa = 0.1450 ksi; 1 mm = 0.03937 in; 1 kN = 0.2248 kips.

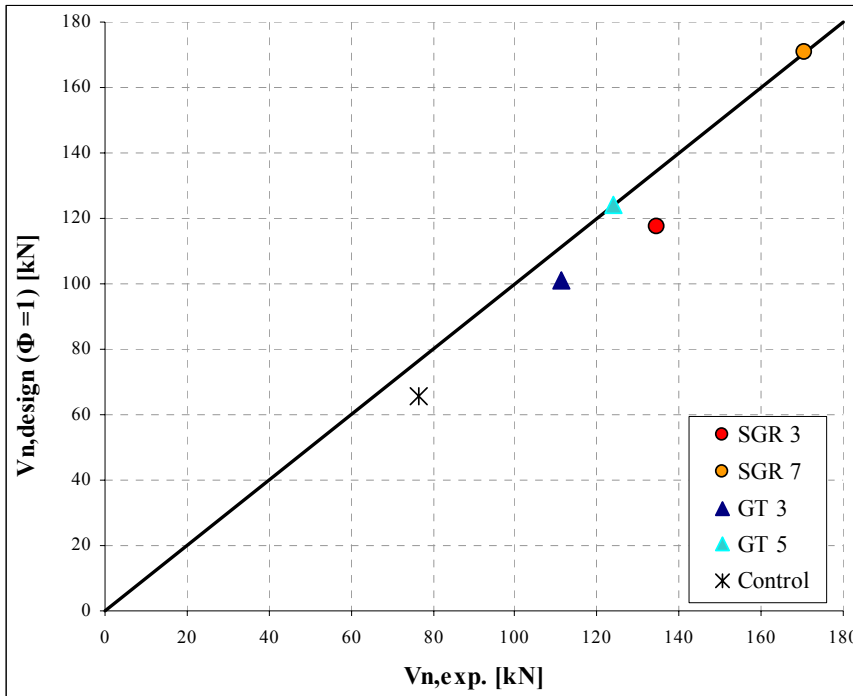


Figure 107 Design Shear Vs. Experimental Reached Shear ( $\Phi=1, \kappa \neq 1$ )

Figure 107 explains that the results obtained are reasonable. Here the safety factor  $\Phi$  was considered to be 1. Figure 108 adds previous results.

Tables 54 and 55 reassume the results obtained with walls (same size and materials) reinforced with sandcoated circular bars (diameter 6.35 mm), and with carbon tape. In particular, table 54 explains the coefficients proposed and table 55 the theoretical and experimental results using these coefficients.

Table 54 Values for Coefficient  $\kappa$  for Other Materials

FRP SYSTEM	WALL MATERIAL	COEFFICIENT $\kappa$
SANDCOATED CIRC. BARS	Concrete	0.5
C-TAPE	Concrete	0.1

Table 55 Theoretical and Experimental Results for the Previous Tests

	$\tau_b$ [MPa]	$C_E$	$\kappa$	$L_E$ [mm]	$V_m$ [kN]	$V_b$ [kN]	$V_t$ [kN]	$V_{n,theo.}$ [kN]	$V_{n,exp.}$ [kN]
Control	-	-	-	-	65.8	-	-	<b>65.8</b>	<b>76.4</b>
GR 1	3.1	0.8	0.5	320	65.8	12.5	52.0	<b>130.3</b>	<b>141.1</b>
GR 2				320	65.8	12.5	52.0	<b>130.3</b>	<b>139.3</b>
GR 3				320	65.8	12.5	20.8	<b>99.1</b>	<b>98.3</b>
GR 4	2.76			360	65.8	11.1	52.0	<b>128.9</b>	<b>130.2</b>
CT 3	3.1	0.8	0.05	324	65.8	0	7.4	<b>73.2</b>	<b>94.4</b>
CT 5				324	65.8	0	12.3	<b>78.1</b>	<b>76.7</b>

It is important to take into account that the dependence of experimental data from the test conditions. Thus, future experimental program may be able to show more accurate values for the factor “ $\kappa$ ”.

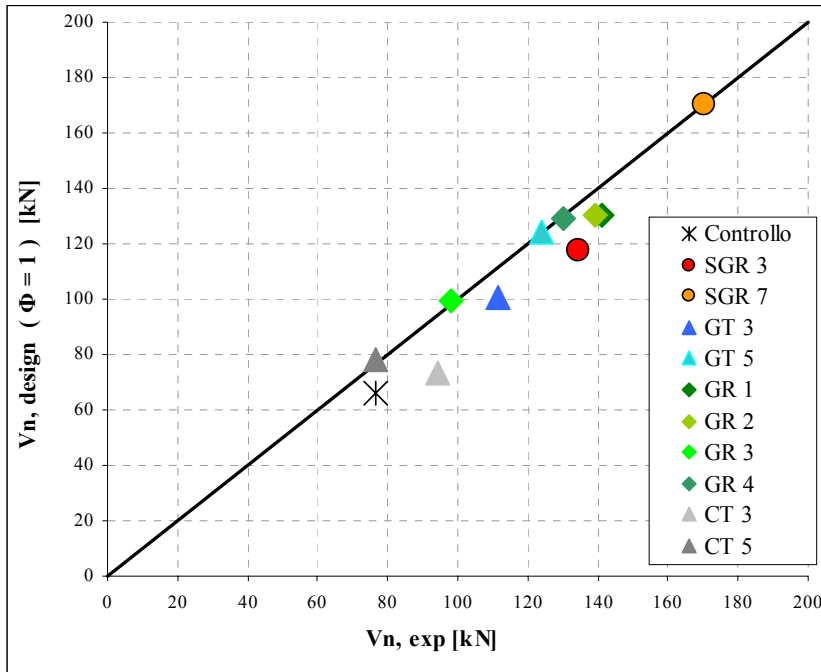


Figure 108 Previous Tests: Design Shear Vs. Experimental Reached Shear ( $\Phi=1, \kappa \neq 1$ )

#### 4.4.7 Comparison Based on Pseudo-Ductility

To obtain a better comparison between the different types of FRP and reinforcing systems, we can use the Pseudo-Ductility they are able to perform. This test setup configuration did not allow estimating pseudo-ductility as conventionally done ( $\mu = \delta_u / \delta_y$ ), where  $\delta_u$  and  $\delta_y$  are the horizontal displacements at ultimate and “yielding” caused by the In-Plane load.

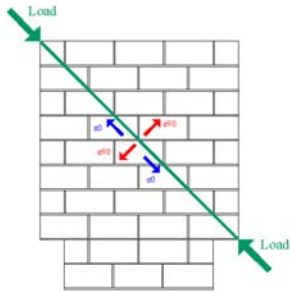
Thus, the pseudo-ductility “ $\mu$ ” was quantified as the ratio  $\mu = \frac{\gamma_u}{\gamma_y}$

“ $\gamma_u$ ” is the shear strain at ultimate and “ $\gamma_y$ ” is the shear strain corresponding to the point where the load vs. shear strain curve tends to be flat. Considering the strains generated by the diagonal load as principal strains, the maximum shear strain is expressed as

$$\gamma = |\varepsilon_{90}| + |\varepsilon_0|$$

in which “ $\varepsilon_0$ ” and “ $\varepsilon_{90}$ ” are the strains associated to the wall diagonals.

Their computation was made with the following relation:



$$\varepsilon_0 = \frac{1}{2} x \frac{(TenseFront + TenseBack)}{d}$$

$$\varepsilon_{90} = \frac{1}{2} x \frac{(Compressed Front + Compressed Back)}{d}$$

These formulas have been chosen according with the Mohr Theory (see figure 107) about deformations: the maximum Shear Strain can be computed as  $\frac{\gamma_{max}}{2} = \frac{\varepsilon_{90} - \varepsilon_0}{2}$ . In this type of

experimentation,  $\varepsilon_{90} \geq 0, \varepsilon_0 \leq 0$  or vice-versa, so  $\frac{\gamma_{max}}{2} = \pm \frac{|\varepsilon_{90}| + |\varepsilon_0|}{2} \Rightarrow \gamma_{max} = \pm (|\varepsilon_{90}| + |\varepsilon_0|)$ .

This is for the bidirectional case.

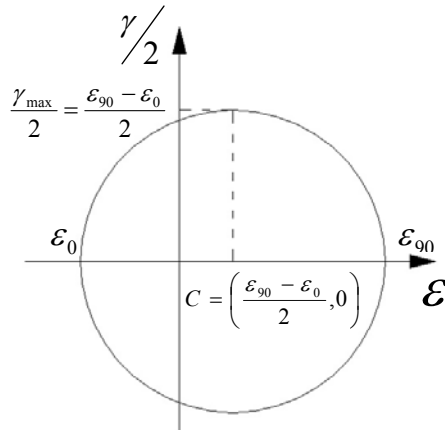


Figure 109 Mohr Theory for  $\epsilon_0$  and  $\epsilon_{90}$

In the three-directional case, the strain tensor must be considered and main deformations needs to be worked out: they coincide with the eigenvalues of the strain matrix. As these values are computed, we need to calculate the directions over which the shear strain is maximum in a generic direction displacement. At the end of this work we have:

$$\frac{\gamma_{i,max}}{2} = \frac{\epsilon_i - \epsilon_j}{2}, \text{ where } i,j = 1, 2, 3 \text{ and } \epsilon_i, \epsilon_j \text{ are the main displacements.}$$

The Pseudo-Ductility was computed using a diagonal length  $d = 2208.78$  mm (86.96 in), between the two points used to attach the diagonal pipes to the wall) to calculate “ $\epsilon_0$ ” and “ $\epsilon_{90}$ ”.

Summarizing:

$$\gamma = |\epsilon_{90}| + |\epsilon_0|; \quad \epsilon_0 = \frac{1}{2}x \frac{(TenseFront + TenseBack)}{d}; \quad \epsilon_{90} = \frac{1}{2}x \frac{(CompressedFront + Compressed Back)}{d}$$

Table 56 Pseudo-ductility

Specimen	Load $P_u$ kN (kips)	$\gamma_y$	$\gamma_u$	$\mu$
W 0	108.1 (24.3)	0.09	0.09	1.00
W-GT-3	157.5 (35.4)	0.104	6.25	60
W-GT-5	175.4 (39.4)	0.18	2.135	11.9
W-GSR-3	190.4 (42.8)	nd	nd	nd
W-GSR-7	241.1 (54.2)	nd	nd	nd

As shown in the previous table, the walls reinforced with the rectangular bars have exhibited a great increment in term of ductility, also better than all the previous. For the walls with smooth bars, failure was unexpected and brittle. Table 57 shows the pseudo-ductility indexes for the previous experimental programs.

Table 57 Comparison of Pseudo-ductility for Concrete Walls (Grando 02)

Specimen	Load <sub>u</sub> kN (kips)	$\gamma_y$	$\gamma_u$	$\mu$
GR-1	200 (45.0)	0.13	1.71	13.1
GR-2	195 (43.8)	0.09	1.82	20.2
GR-3	137 (30.8)	0.17	0.94	5.5
GR-4	184 (41.4)	0.0063	0.1322	20.9
CT-3	134 (30.0)	0.0558	0.952	17.06
CT-5	108 (24.4)	0.116	1.082	9.32
GL-1	189 (42.5)	0.08	0.40	5.0
GL-2	191 (42.9)	0.14	0.72	5.1
GL-3	111 (25.0)	0.036	0.34	9.44
GL-4	208 (46.8)	0.0311	0.611	19.67
CL-1	113 (25.4)	0.145	1.294	8.8
IS 1	212 (47.6)	0.0505	1.075	22.28
IS 2	160 (36.0)	0.037	0.11	2.97
SR-1	126 (28.4)	0.0845	0.213	2.5
SR-2	220 (49.4)	Acquisition data system not working		

As it is showed, the best performances are from the walls where the reinforcement had a symmetric shape, or a not too high stiffness. This allowed the wall itself to make use of the pseudo ductility and increase the ultimate capacity.

Instead the walls that performed the worst results were the one with an overabundant amount of reinforcement or with a too stiff strengthening.

Here is showed a table with a comparison between the different types of reinforcements and their increase in terms of Ultimate Load and Pseudo-Ductility

*Table 58 Comparison of Increases for Concrete Walls*

Reinforcement	$\mu / \mu_0$		Increase in Load <sub>u</sub>	
	minimum	maximum	minimum	maximum
GFRP Smooth Rods	-	-	76%	123%
GFRP Tape	11.9	60.0	46%	62%
Internal Mortar Net	-	22.3	-	96%
Laminates	8.8	19.7	5%	83%
GFRP Rods	13.0	20.2	29%	93%
CFRP Tape	9.3	17.1	0%	23%
Stainless Steel Rods	2.5	21.0	16%	103%

The walls where the failure was due to a Sliding Shear were not considered.

## 4.5 DESIGN

### 4.5.1 Shear Strength Design

The ultimate allowed shear force ( $V_u$ ) must be:

$$V_u \leq \Phi V_n$$

where  $V_n$  is the shear strength calculated in section 4.4.1 and  $\Phi$  is a safety reduction factor equal to 0.8. This value is suggested by the UBC (1997), when the nominal shear strength is larger than the shear corresponding to the development of nominal flexural strength. For masonry structures strengthened with FRP rods, it is suggested to maintain the previously described reduction factor and to apply a supplemental conservative factor equal to 0.8 to the FRP contribution.

Thus the previous equation may be written as following:

$$V_u \leq \Phi_1 (V_m + \Phi_2 V_f)$$

Where the two safety factor may both be assumed equal to 0.8:

$$\Phi_1 = \Phi_2 = 0.8$$

### 4.5.2 Example of Calculation of Nominal Shear Strength

The validation of the calculations for the four walls tested in this experimental program is here presented. It is important to note that the calculations have been made in U.S. units and then translated in the S.I units because some coefficients refer to values expressed in U.S. units (ACI 440).

#### Computation of $V_m$ :

$V_m$  was given by the:

$$V_m = C_d A_{mv} \sqrt{f'_m}$$

where  $C_d$  = shear strength coefficient estimated as 1.2

$A_{mv}$  = net area [sq-in] for the horizontal section of the wall

$f'_m$  = specified compressive strength of masonry [psi] (net area).

Using the S.I. units of measurement,  $C_d$  becomes 10, and  $A_{mv}$  is expressed in  $cm^2$  and  $f'_m$  in MPa.

The net area of the specimens tested was the 65% of the gross area (see table 16). Then the net area of the horizontal masonry section is:

$$A_{mv} = 64 \cdot 6 \cdot 0.65 = 250in^2 = 1610cm^2$$

The contribution of the masonry to the shear strength is:

$$V_m = C_d A_{mv} \sqrt{f'_m} = 1.2 \cdot (250in^2) \cdot \sqrt{2429psi} = 14785lbs = 14.8kips$$

or, using the I.S. units of measurement:

$$V_m = C_d A_{mv} \sqrt{f'_m} = 10 \cdot (1610cm^2) \cdot \sqrt{16.73MPa} = 65853N = 65.85kN$$

### Computation of $V_f$ :

From  $f_{fu} = \kappa \cdot C_E \cdot f^*_{fu}$  and  $\tau_{bl} = \kappa \cdot \tau_b$ ,  $f_{fu}$  and  $\tau_b$  may be computed:

for the smooth rods:  $f_{fu} = \kappa \cdot C_E \cdot f^*_{fu} = 1.0 \cdot 0.8 \cdot 1038MPa = 830MPa$

$$\tau_b = 1.0 \cdot 3.1MPa = 3.1MPa$$

for the glass tape:  $f_{fu} = \kappa \cdot C_E \cdot f^*_{fu} = 0.3 \cdot 0.8 \cdot 1100MPa = 264MPa$

$$\tau_b = 0.3 \cdot 3.1MPa = 0.93MPa$$

where  $C_E$  is equal to 0.8 for GFRP rods in a closed space environment. Since neither debonding nor breaking of the rods was observed, the wall may be divided in two areas: a “bond controlled” area and a “rupture controlled” area, as explained in Section 4.4.2.

### Calculation of $V_b$ :

The first step is to determine  $L_{tot}$  from:  $\tau_b \times (Perim_f \times L_e) = f_{fu} \times A_f$

then, for the smooth rods:  $L_e = \frac{d_b f_{fu}}{4\tau_b} = \frac{(5.1mm) \cdot (830MPa)}{4(3.1MPa)} = 341mm$

for the glass tape:  $L_e = \frac{A_f f_{fu}}{Perim_f \tau_b} = \frac{(31.3mm^2) \cdot (264MPa)}{34.6mm \cdot (0.93MPa)} = 257mm$

As described in section 4.4.2 it is now easy to determine the number of the rods in the “bond controlled” area: two for the wall GSR-7 and zero for the others.

Then for the wall GSR-7 the shear force carried by the rods in the “bond controlled” region is:

$$V_b = n\pi d_b \tau_b L_{tot} = (1) \cdot (\pi) \cdot (5.1mm) \cdot (3.1MPa) \cdot (203mm + 203mm) = 20.1kN$$

**Calculation of  $V_t$ :**

Using the equation:  $V_t = n \times r_t \times A_t \times f_{fu}$  are been estimated the  $V_t$  for the four walls:

Table 59 Computation of  $V_t$  Scheme

	$n$	$r_t$	$A_f$ [mm <sup>2</sup> ]	$f_{fu}$ [MPa]	$V_t$ [kN]
SGR 3	1	3	20.4	830	50.8
SGR 7	1	5	20.4	830	84.7
GT 3	1	3	31.3	264	35.1
GT 5	1	5	31.3	264	58.5

where for the bars 45 degree sloped the final  $V_t$  value is been multiplied by 1.414 in order to consider the real shear contribution given.

Now it should be easy to calculate  $V_f$  and then  $V_n$  from:

$$V_f = V_b + V_t \text{ and } V_{n(\text{theo})} = V_m + V_f.$$

The results obtained may be compared with the horizontal component of the ultimate carried loads.

For example for the wall SGR-7:

$$V_{n(\text{exp})} = P_{\max} \sin 45^\circ = (241.1 \text{ kN}) \cdot \left( \frac{1}{\sqrt{2}} \right) = 170.5 \text{ kN} \square 65.85 + 20.1 + 84.7 = 170.65 \text{ kN}$$

Applying the safety factors  $\Phi$  (see 4.5.1) the ultimate allowed shear force ( $V_u$ ) for the wall SGR-7 must be:

$$V_u[\text{SGR} - 7] \leq \Phi_1 (V_m + \Phi_2 V_f) = 0.8(65.85 + 0.8 \cdot 104.8) = 119.8 \text{ kN}$$

that is more than two times the one without reinforcement:

$$V_u[\text{Control}] \leq \Phi_1 (V_m) = 0.8(65.85) = 52.7 \text{ kN}$$

## 4.6 PRELIMINARY CONCLUSIONS

The following conclusions can be drawn from this experimental program:

Remarkable improvements of about 100% in shear capacity and pseudo-ductility were registered. These increments can be reached especially if the reinforcement is not asymmetric and too stiff, as in the case of the smooth bars (asymmetric but pliable), or the internal wires (symmetric configuration). When reinforcement was asymmetric, the glass bars have shown to be better than the carbon bars, maybe because large amounts of reinforcement, or reinforcement with a high stiffness (like wall CT 2 or SR 1) causes a reduction of pseudo-ductility.

The glass smooth bar is very effective for strengthening, maybe because of its smooth-coated surface that allows internal creep between the fibers.

Two types of failure were observed: brittle failure by sliding-shear and shear failure along the diagonal (stable and instable).

Two failure phases were identified: In-Plane and Out-of-Plane. The In-Plane component is the most critical and related with the stair-development of the crack, the Out-of-Plane could be observed with the slope of the wall. The Out-of-Plane consequence is pronounced in the walls with an eccentricity in the reinforcement (only one side). Actually the specimens reinforced with rectangular bars have exhibit a dangerous slope at the failure. In a real building, this could procure additional injuries and loss of human lives during seismic events.

The procedure for computing the nominal shear strength of strengthened walls gives conservative and reasonable values and the deduction factor “ $\kappa$ ” has been computed. A design approach has been proposed. It should be however recalled that the analytical model adopted assumes a bond-controlled region and a rupture-controlled region even if during the test were observed no FRP ruptures and just one bar debonded. Besides, the assumption of constant bond stresses at ultimate is not believed adequate.

These tests have doubtless shown an improvement of the shear-capacity of the masonry; however they have also shown their limit: with this test-frame we loose all the data about what happen after the first crack that is when the reinforcement often starts working. Especially with the horizontal bars, we have always seen, after the first crack, kinds of failure not possible in reality (i.e. sliding of a course or lifting of a part of the wall, see figure 111). We hope that future works may consider a more adequate frame (see figure 110).



*Figure 110 Preparation for Tests in Peru' Concerning the Surrounding Frame*



*Figure 111 Lifting of Part of Wall, left, Sliding of a Course, right.*

Future works are not needed, for the moment; in case, they could study masonry already cracked and then strengthened. Probably in that case the reinforcement should start working immediately, and then the results should be closer to the analytical previsions.



## 5. FLEXURAL STRENGTHENING OF MASONRY WALLS

Unreinforced masonry (URM) walls are prone to failure when subjected to out-of-plane loads caused by earthquakes or high wind pressure.

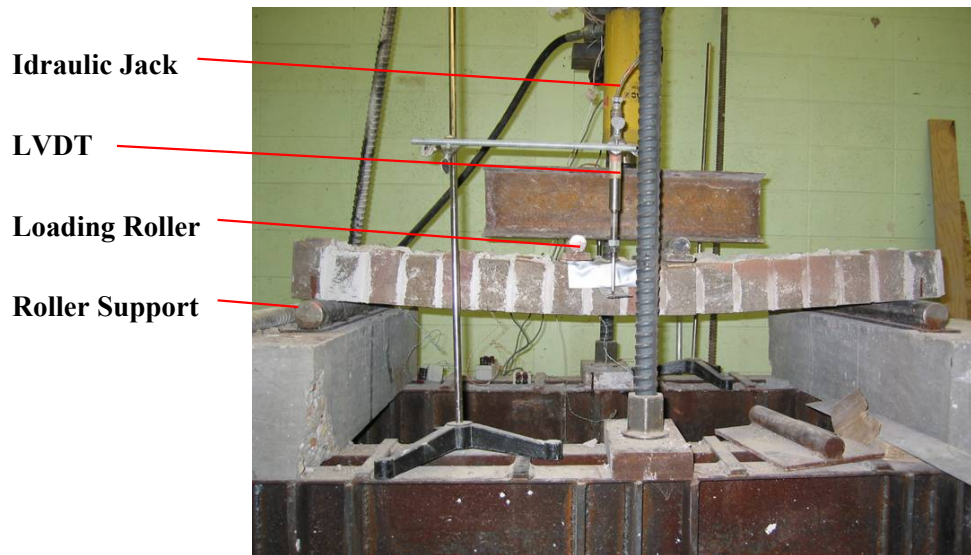


*Figure 112 Test Frame (Wall cl1-gt-2)*

This section presents the results of an experimental program on the flexural behavior of URM walls strengthened with externally bonded (Near Surface Mounted) FRP bars.

## 5.1 INTRODUCTION

Structural weakness, overloading, dynamic vibrations, settlements, and deformations can cause failure of unreinforced masonry (URM) structures. URM buildings have features that, in case of overstressing, can threaten human lives. Organizations such as The Masonry Society (TMS) and the Federal Emergency Management Agency (FEMA) have determined that failures of URM walls result in more material damage and loss of human life during earthquakes than any other type of structural element. Fiber Reinforced Polymer (FRP) composites may provide viable solutions for the strengthening of URM walls subjected to in-plane and out-of-plane loads caused by high wind pressures or earthquakes. As a reflection of retrofitting needs (e.g. approximately 96% of the URM buildings inventoried throughout California needed to be retrofitted) and important advantages (i.e. material characteristics and ease of installation) interest in the use of FRP materials for the strengthening of masonry elements has increased in recent years. To respond to the interest of the engineering community, the American Concrete Institute (ACI) – Committee 440 along with the Existing Masonry Committee of TMS have formed a joint task group to develop design recommendations for the strengthening of masonry elements with FRP materials.



*Figure 113 Out-of-Plane Failure, During the Northridge Earthquake, 94.*

This section of the experimental program consisted of 14 masonry walls reinforced with GFRP rods and tapes and one reinforced with CFRP tapes, using the NSM technique, and subjected to lateral out-of-plane loads. No axial loads were applied on the top and on the bottom of the walls; therefore no arching effect was obtained. It is important to underline that for the flexural analysis arching effect is no more negligible when the slenderness ratio ( $l/t$ ) is less than 20. In that case it is

suggested to consult “Arching effect in masonry walls reinforced with FRP materials” (Galati 02). Arching effect gives also an important contribution in terms of sliding-shear capacity, even if the slenderness ratio is still more than 20.

The parameters investigated were different dimensions kinds of bar, two different filling materials, different groove size and cyclic behavior.

The FRP bars were applied vertically in order to increase the load-carrying capacity of unreinforced masonry walls that are subjected to out-of-plane forces and that had been constructed primarily for carrying vertical loads.

The first objective of this section was to study the proper way of installation of these different bars and to observe the more effective kinds of reinforcement, and then to refine the analytical model. In particular, it has been investigated the different behavior, resistance and failure of walls flexural-reinforced with glass and carbon tape, and glass rods embedded with epoxy and cementitious paste in a big grooves (2.25 times the rod diameter).

The second objective of this section was to compare the results with the issues obtained from previous investigation with walls (same size) strengthened with FRP laminates and rods.

## 5.2 TEST MATRIX

Fifteen masonry walls were manufactured for this experimental program, three built with clay bricks, ten with the 4 in concrete blocks, and two with the 6 in concrete blocks. The dimensions of the walls were 120x60 cm (48x24 in) by the block thickness that was about 93 mm (3.75 in) for the clay bricks walls and for the 4 in thick concrete block walls, and about 143 mm (5.75 in) for the 6 in thick concrete's. The walls were constructed using a Type N mortar; the cores of the clay walls were grouted. All the joints were finished flush with the outside of the block. All specimens were allowed to cure for at least 28 days before testing. The specimens reinforced with repair mortar as embedding material were tested at least 28 days after the reinforcement was applied.

The specimens were strengthened with No. 2 and No. 3 sandblasted deformed GFRP rods and with Glass and Carbon tape using the NSM bars technique.

An epoxy-based paste and a latex modified cementitious-based paste were used as embedding material. The strengthening layout intended to represent URM wall strips with GFRP bars in different amount and at different spacing. The position and the space between two reinforced was chosen taking into account the prescription with the flexural steel-reinforcement and so to have always the same distance if more than one wall would be placed between the other. The bar reinforcements were oriented in the vertical direction to optimize the strength of the rods and were applied only on one side of the wall. Each reinforcement terminated before the reaction point so that the rods would not touch the roller supports used for testing: therefore the length of the bars used was 10 cm (4 in) less the total height of the wall.

Due to the brittle nature of URM and since the specimen could fail due to the weight of the test equipment (i.e. steel beam, hydraulic jack, etc.) no control specimen was tested. However, according to the Masonry Standards Joint Committee, the allowable flexural tension for masonry for a Type N mortar can be taken as 262 kPa (38 psi). Thus, considering that the nominal strength is approximately 2.5 times the allowable one, the nominal moments at cracking for the 143mm thick (6 inches) concrete block specimens can be estimated as 0.31 kNm (0.23 k-ft) , 0.48 kNm (0.35 k-ft) for clay specimens, and 0.23 kNm (0.17 k-ft) for the 92 mm thick (4 inches) concrete block's.

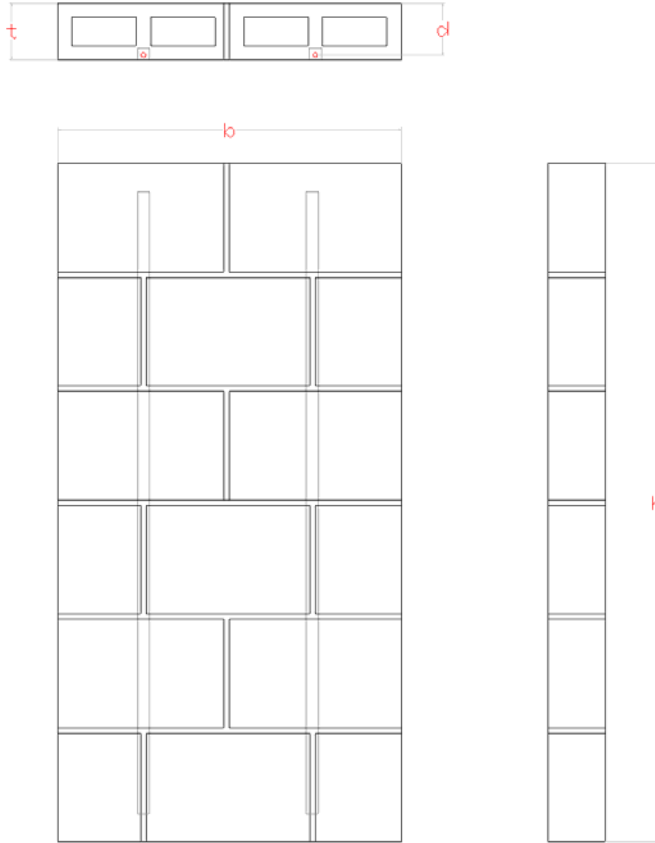


Figure 114 Specimen Characterization

Table 60 presents the test matrix indicating the designation that will be used to identify the specimens, the kind of block used, the wall dimensions and strengthening scheme ( $d$ , shown in figure 114, indicates the values used in the computations).

Table 60 Dimensions and Strengthening Scheme of the Fifteen Specimens

Wall name	Block used	$h \times b \times t$ mm (in.)	type and amount of bars used		groove dim. mm (in.)	infill mater.	$d$ mm (in.)
<b>bcb-gt-1</b>	bcb	1220x600x143 (48x24x6)	glass tape	1	17x3 mm (0.67x0.12)	epoxy	135.3 (5.33)
<b>bcb-gt-2</b>				2			
<b>cl1-gt-1</b>	cl1	1220x600x92 (48x24x4)		1			
<b>cl1-gt-2</b>				2			
<b>cl2-ct-2</b>	cl2		carbon tape	2			85.4 (3.36)

Wall name	Block used	$h \times b \times t$ mm (in.)	type and amount of bar used		groove dim. mm (in.)	infill mater.	$d$ mm (in.)
<b>cob-E2-1b</b>	cob	1220x600x92 (48x24x4)	glass rod #2	1	2.25 times rod diameter:14.3mm 4.5/8 in. (square)	epoxy	83.5 (3.29)
<b>cob-E2-2b</b>				2			
<b>cob-E2-3b</b>				3			
<b>cob-C3-1b</b>			glass rod #3	1	2.25 times rod diameter:21.4mm 6.75/8 in (square)	cement. modified paste	79 (3.11)
<b>cob-C3-2b</b>				2			
<b>cob-C3-3b</b>				3			
<b>cob-E2-1c</b> (bar in joint)			glass rod #2	1	1.5 times rod diameter: 9.5 mm 3/8 in. (square)	epoxy	86.6 (3.41)
<b>cob-E2-2c</b> (bar in joint)				2			
<b>cob-E2-1d</b> (bar in block)				1			
<b>cob-E2-2d</b> (bar in block)				2			

The reason of these choices comes especially from the previous results, which asked for a verification on the bigger groove and on the cementitious modified paste; besides from to have the occasion to test new materials, such as the glass FRP rectangular bar.

### 5.3 SPECIMEN PREPARATION

The preparation of the specimens included: application of strain gages on the FRP bars, cutting of the vertical grooves, positioning and application of the bars.

#### 5.3.1 Application of the Strain Gages

Strain-gages were applied on the surface of the FRP bars prior to their application. The purpose was to monitor the strain distribution along the rod during the test. The strain-gages used had gage lengths of 12.5 mm (1/2 in). They were placed every joint (for the concrete walls): one at midspan, one at 200 mm (8 in) and another at 400 mm (16 in) from each wall end.



*Figure 115 Strain Gages Applied on the Tapes*

#### 5.3.2 Strengthening Procedure

The NSM technique consists of the installation of FRP reinforcing bars in slots grooved in the masonry surface. The strengthening procedure for the tape has been yet explained in section 4.2.2; for the rods it is similar and it is here summarized:

- Grooving of slots diameter (see figure 116.a) and cleaning of surface with an air-blaster
- Application of embedding paste (epoxy-based or latex modified cementitious-based paste) (see figure 116.b)
- Encapsulation of the bars in the joint (see figure 116.c)
- Levelling the filled groove (116.d)

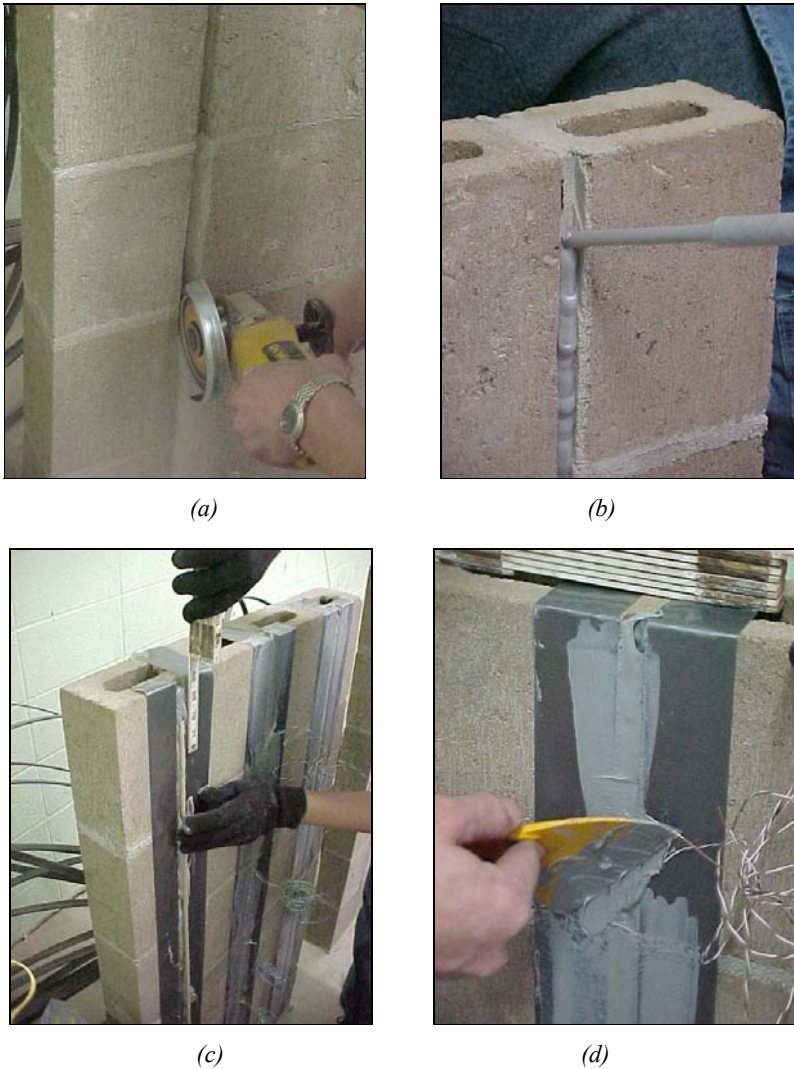


*Figure 116 Specimen Preparation: (a) Cutting of the Groove, (b) Filling the Groove with the Embedding Material, (c) Encapsulation of the Rod, (d) Flushing of the Embedding Material*

If hollow masonry units are present, special care must be taken to avoid the groove depth exceeds the thickness of the masonry unit shell, and local fracture of the masonry occurring. Indeed, using a concrete block about 30 mm thick, the largest groove size can be possibly adopted is believed to be about 21.4 mm (0.84 in). This allows us to use up to a circular bar #3 (diameter=9.5mm) with a groove 2.25 times its diameter (i.e. 2.25x3 eighth in).

## 5.4 TEST SETUP

All specimens were loaded in the test frame shown in figures 117 and 118. Each one was tested as a simply supported beam standing on end. Therefore, the walls were tested under simply supported conditions.

A 12 ton (26.4 kips) capacity hydraulic jack activated by a manual pump was used to load the specimen. The force generated by the hydraulic jack was transferred to the specimen by means of a steel beam supported by two rollers, which applied a load along two lines spaced at 200 mm (8 in). The line loads rested along the full width of the walls.

The load was applied in cycles of loading and unloading. An initial cycle for a low load was performed in every wall to verify that both the mechanical and electronic equipment were working properly.

The instrumentation used consisted of one 89 kN (20 kips) load cell to measure the force from the jack, 2 linear variable differential transducers (LVDTs) in both sides of the specimen to measure deflections at midspan, and strain gages to measure the strain in the rods (see figure 119). The data acquired by the instrumentation were collected by a data acquisition system at a frequency of 1.0 Hz.

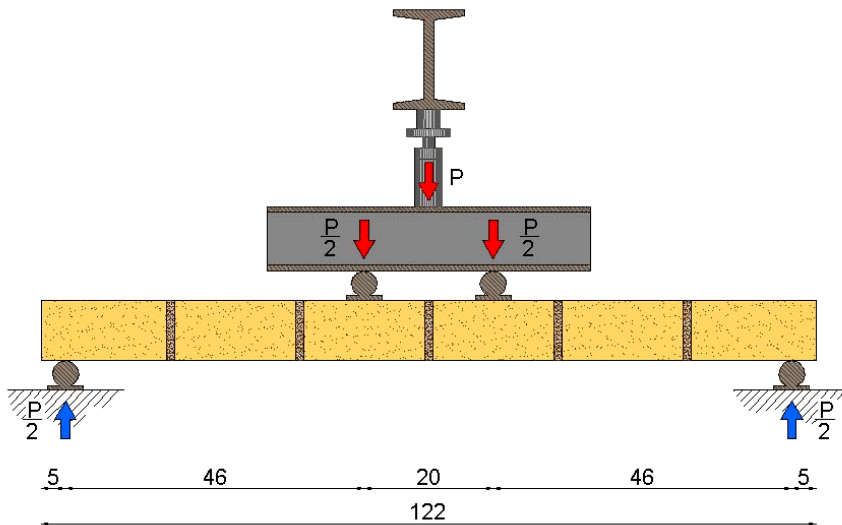
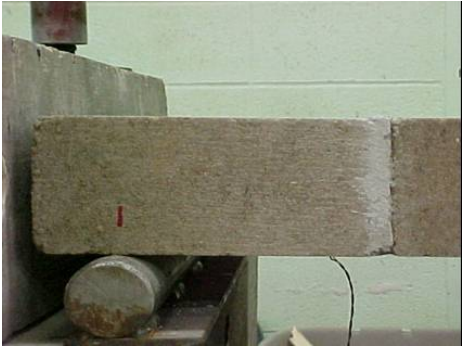


Figure 117 Test Setup Scheme (Dimensions in cm)



(a)



(b) Roller support



(c) Loading Support



(d) Jack and Load Cell



(e) LVDT



(f) Strain Gages

Figure 118 Test Setup

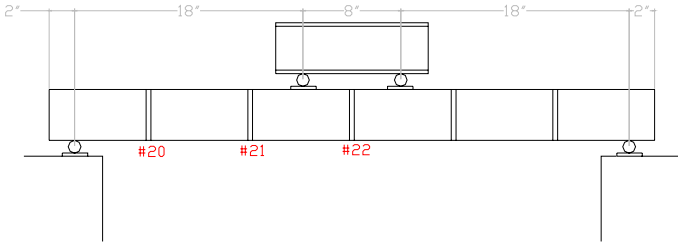


Figure 119 Test Setup Scheme, with the Number of the Strain Gage Channels Used

Figure 119 explains the number of the strain channels used during the test for all the fifteen specimens. In some cases, due to the smallness of the bars, some strain gages did not work.

## 5.5 TEST RESULTS

### 5.5.1 Single used and summary of the main materials

Table 61 presents the meaning of the codes used to identify the specimens that refers to the following parameters: type of block used, type of embedding paste and kind of FRP, number of bars used for reinforcing, and the possible peculiarity of the test. As an example, cob-E2-2b refers to a wall made of concrete 92mm (4 inches) thick blocks having epoxy paste as embedding material and reinforced with 2 GFRP No. 2 (diam.=6.3mm) rods all along the joints.

Table 61 Meaning of the Codes Used to Identify the Walls

type of block used		kind of frp used		amount of bars	type of test	
cl1	clay brick	gt	glass tape		1-2-3	b
cl2	clay brick	ct	carbon tape	c		grooves along the joints
cob	4in concr. block	E2-3	Epoxy+rod #2-3	1-2-3	d	grooves along the blocks
bcb	6in concr. block	C2-3	Cem. + rod #2-3			

Tables 62 and 63 summarize the principal physical properties of the blocks and of the FRP used. More details about the properties are available in chapter 3.

Table 62 Properties of the Blocks Used (from section 3.2)

	$f'_m$ GROSS AREA MPa (ksi)	$f'_m$ NET AREA MPa (ksi)	$E_m$ Young's modulus GPa (ksi)
<b>cl1</b>	19.43 (2.82)	-	13.6 (1973)
<b>cl2</b>	15.78 (2.29)	-	11.0 (1595)
<b>cob</b>	-	9.74 (1.41)	8.8 (1276)
<b>bcb</b>	-	16.74 (2.43)	15.1 (2190)

Table 63 Mechanical Properties of the FRP Used in the Computations (from section 3.4)

	Area mm <sup>2</sup> (sq-in)	Young's modulus GPa (ksi)	Ultimate strain $\epsilon_u$ %	$f_{f,ult}$ MPa (ksi)
<b>C-Tape</b>	31.0 (0.0480)	143 (20702)	0.98	1401
<b>G-Tape</b>	31.3 (0.0485)	44 (6382)	2.50	1100
<b>G-Rod #2</b>	33.2 (0.0515)	46 (6672)	1.70	782
<b>G-Rod #3</b>	84.3 (0.1307)	46 (6672)	1.70	782

The following paragraphs show the results. All the theoretical calculations consider, for simplicity and similarly to the flexural analysis of RC members, the ACI parabolic behavior of  $f_c$  ( $e_c$ ) given for RC and the sections are considered flat (hypothesis true in midspan, but not close to the supports).

### 5.5.2 Glass and Carbon FRP Rectangular Bars

The five specimens have exhibited two failure modes. For the wall cl1-gt-1 and the bcb-gt-2 the failure was caused by the split of the blocks, allowing the bars to go out. For the cl1-gt-2, the bcb-gt-1 and the cl2-ct-2 the failure was due to the sliding of the bars inside the groove. In these cases, after the failure the wall could still carry load (because of the friction epoxy paste-bar). The results, in terms of amount of reinforcement, ultimate load, maximum bending moment and type of failure are summarized in table 64.

Table 64 Test Results

Specimen Name	Amount of Reinforcement $E_f \times A_f$ kN (kips)	Ultimate Load kN (kips)	Maximum Bending Moment kNm (k-ft)	Maximum Displacement in Midspan mm (in)	Type of Failure
<b>bcb-gt-1</b>	1377 (310)	14.7 (3.3)	3.35 (2.47)	16.9 (0.67)	deb. (bar slid.)
<b>bcb-gt-2</b>	2754 (619)	35.1 (7.9)	8.03 (5.92)	19.4 (0.76)	deb. (brick col)
<b>cl1-gt-1</b>	1377 (310)	9.4 (2.1)	2.16 (1.59)	27.3 (1.07)	deb. (brick col)
<b>cl1-gt-2</b>	2754 (619)	16.0 (3.6)	3.66 (2.70)	41.4 (1.63)	deb. (bar slid.)
<b>cl2-ct-2</b>	4433 (997)	25.6 (5.8)	5.86 (4.32)	29.7 (1.17)	deb. (bar slid.)

Figures 120 and 121 explain the carried midspan moment / midspan displacement behavior during the test for the five specimens. According to the Masonry Standards Joint Committee the theoretical capacity of the URM walls have been estimated.

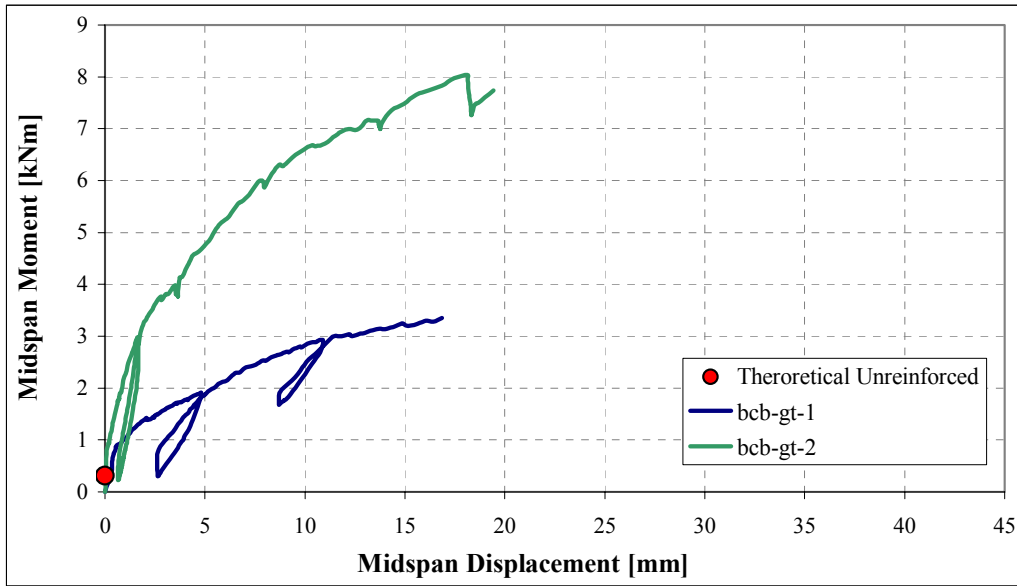


Figure 120 Midspan Moment Versus Deflection in Midspan for the Concrete Walls (Thickness=6 inches)

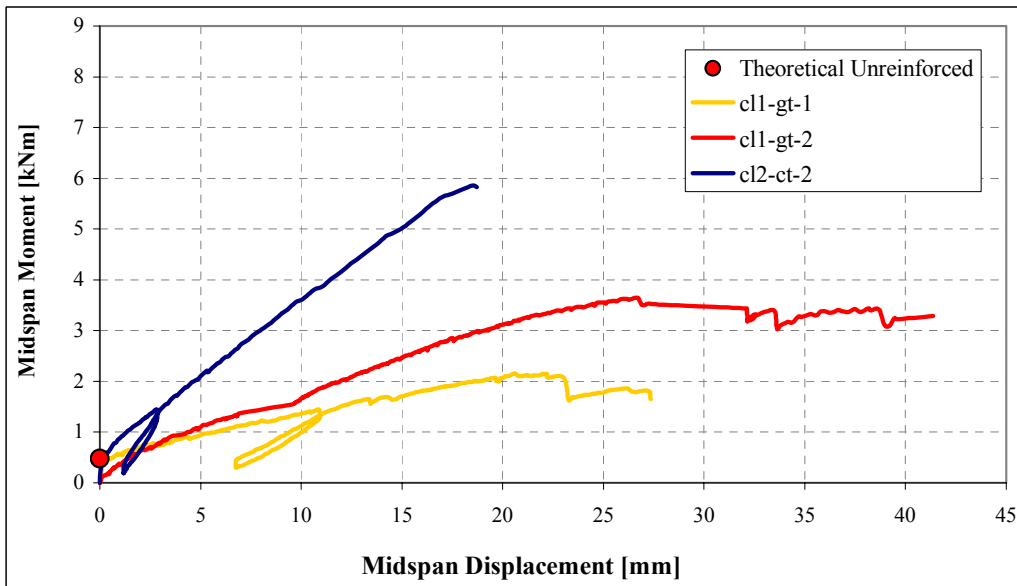


Figure 121 Midspan Moment Versus Deflection in Midspan for the Clay Walls (Thickness=4 inches)



*wall bcb-gt-1: sliding of the bar*



*wall bcb-gt-2: splitting of the concrete block*

*Figure 122 Failures of the 6 in Concrete Block Walls*



*cl-gt-1: splitting of the bricks*



*cl-gt-2: sliding of the bar*

*Figure 123 Failures of the Clay Brick Walls Strengthened with the Glass Tape*

Since the failure for these specimens was due to debonding, it has to be underlined that it occurred ever when the theoretical tension in the reinforcement was between 0.65 to 0.88  $\epsilon_u$  ; and the cl1-gt-2, the one yielded at 0.65  $\epsilon_u$ , probably had the stress in the two bars unbalanced (see strain gages's values, figure 124).

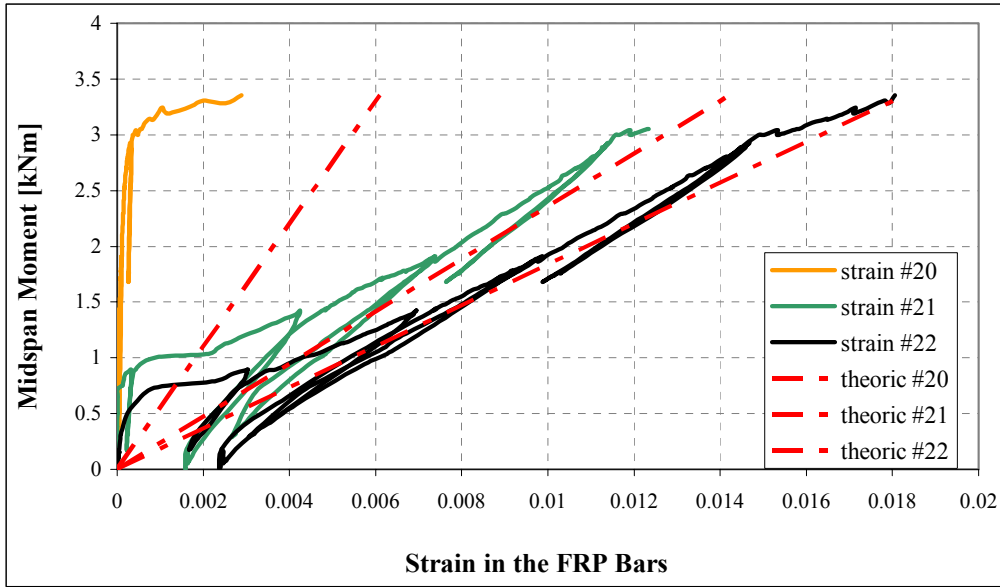


Figure 124 Wall bcb-gt-1: Midspan Moment vs. Theoretical and Experimental Strain in the Bar

As seen in the previous figure, when just one bar is present, the experimental strain behavior in midspan is well described by the theoretical law.

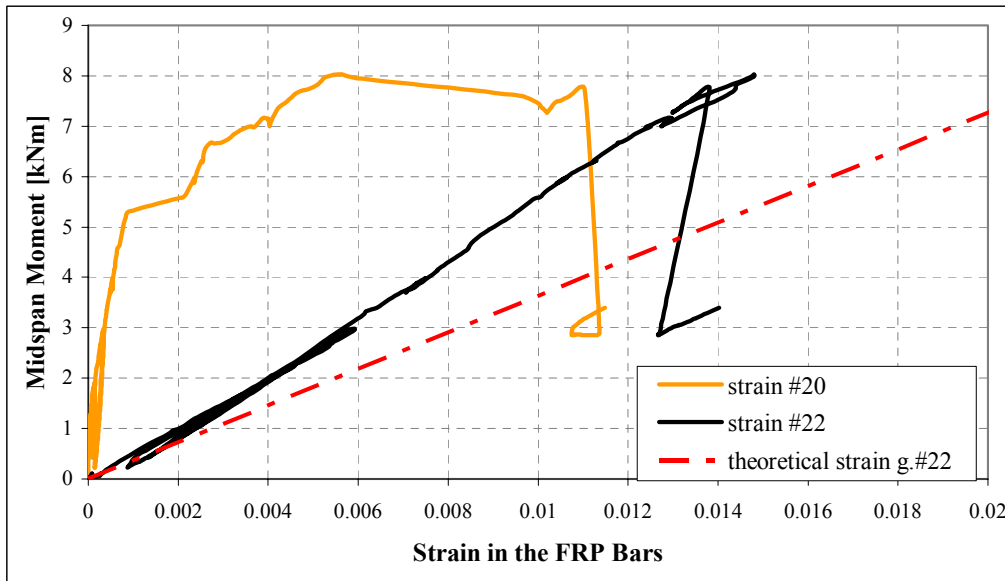


Figure 125 Wall bcb-gt-2 Midspan Moment vs. Theoretical and Experimental Strain in the Bar

When two or more bars are present the theoretical behavior in midspan can err on more or less till 40%, probably because of the surfaces of the wall that are not flat, thus the supports and the loads may weigh just on one side.

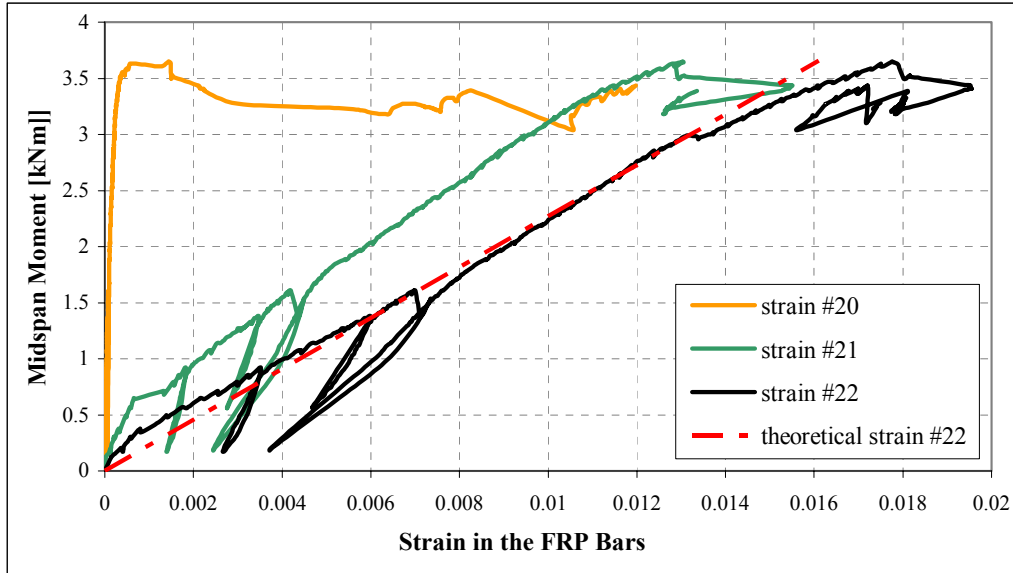


Figure 126 Wall c11-gt-2: Midspan Moment vs. Theoretical and Experimental Strain in the Bar

As shown in figure 125, when the failure is caused by debonding of one or more bars, the bar starts sliding close the loading supports, as well as the strain in the FRP close the roller supports increases: now the cross sections cannot be considered flat.

### 5.5.3 Glass FRP Rods #2 Embedded with Epoxy Paste in a Groove 2.25 Times the Rod Diameter

These three walls were strengthened with G-FRP rod+epoxy but with a groove 2.25 times the rod diameter. During the test they have shown a very stiff behavior till the first noisy cracks in the epoxy paste (the load was around 3.5-7.0 kN).

With all the three specimens the failure was caused by debonding, when the theoretical strain was  $0.64-1.20 \varepsilon_u$ . Also in the case of the wall cob-E2-2b the theoretical strain at failure was so low ( $0.64 \varepsilon_u$ ) probably because the load was not well distributed (in fact the recorded value by the strain gages on the debonded bar was  $0.88 \varepsilon_u$  )

Table 65 Test Results

Specimen Name	Amount of Reinforcement $E_f \times A_f$ kN (kips)	Ultimate Load kN (kips)	Maximum Bending Moment kNm (k-ft)	Maximum Displacement in Midspan mm (in)	Type of Failure
<b>cob-E2-1b</b>	1527 (343)	11.0 (2.5)	2.52 (1.86)	24.3 (0.96)	debonding
<b>cob-E2-2b</b>	3054 (687)	11.5 (2.6)	2.64 (1.95)	28.9 (1.14)	debonding
<b>cob-E2-3b</b>	4582 (1030)	21.6 (4.9)	4.94 (3.64)	28.3 (1.11)	debonding

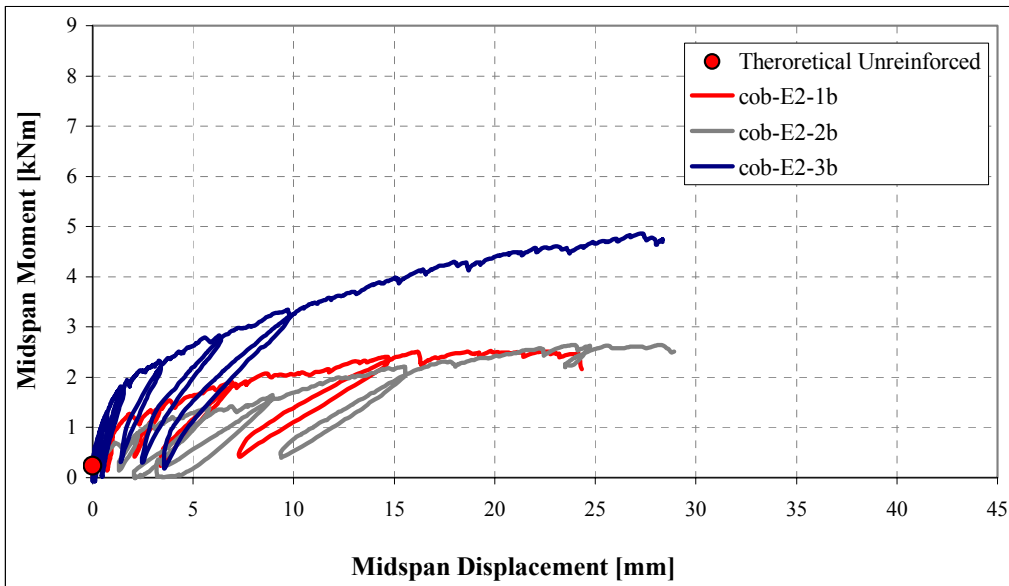


Figure 127 Midspan Moment vs. Deflection in Midspan

The same walls, with a smaller groove, were tested by Turco (02), obtaining the following results:

Table 66 Comparison with Specimens with Smaller Groove (Turco 02)

Specimen name	Max Moment Reached in Midspan kNm (k-ft)		$M_{G=2.25} / M_{G=1.5}$
	Groove=1.5 diam	Groove=2.25diam	
<b>cob-E2 - 1</b>	--	2.52 (1.86)	--
<b>cob-E2 - 2</b>	1.69 (1.24)	2.64 (1.95)	<b>1.56</b>
<b>cob-E2 - 3</b>	2.27 (1.67)	4.94 (3.64)	<b>2.18</b>

**5.5.4 Glass FRP Rods #3 Embedded with Cementitious Modified Paste in a Groove 2.25 Times the Rod Diameter**

These three walls were strengthened with #3 G-FRP rods with cementitious modified paste in a groove 2.25 times the rod diameter. The failure, for all the three specimens, was caused by debonding, when the theoretical strain in the bars was 0.35-0.61  $\epsilon_u$ . While for the first two walls the debonding was plane, for the specimen cob-C3-3b the failure shown also the split of the blocks along the grooves, and especially deep shear cracks, so the type of failure was named “shear”.



Figure 128 Failures of the Three Specimens

Considering the fact that the breakups could depend from the debonding as from the split of the blocks and considering the longitudinal cracks in the blocks at failure, it is seemed clear that this groove poses the deeper possible with concrete this block. It should be remembered that the groove was about 21 mm (6.75 eighth in) deep and the block was about 27-30 mm (8-9 eighth in.) thick.

Table 67 shows the test results.

Table 67 Test Results

Specimen Name	Amount of Reinforcement $E_f \times A_f$ kN (kips)	Ultimate Load kN (kips)	Maximum Bending Moment kNm (k-ft)	Maximum Displacement in Midspan mm (in)	Type of Failure
<b>cob-C3-1b</b>	3879 (872)	13.1 (2.9)	2.99 (2.20)	14.9 (0.59)	debonding
<b>cob-C3-2b</b>	7759 (1744)	15.0 (3.4)	3.43 (2.53)	14.0 (0.55)	debonding
<b>cob-C3-3b</b>	11638 (2616)	26.6 (6.0)	6.07 (4.48)	15.6 (0.61)	shear

The following tables show the results obtained by Turco with the smaller groove and with the epoxy paste.

Table 68 Comparison with Specimens with Smaller Groove (Turco 02)

Specimen name	Max Moment Reached in Midspan kNm (k-ft)		$M_{G=2.25} / M_{G=1.5}$
	Groove=1.5 diam	Groove=2.25diam	
<b>cob-C3 - 1</b>	1.01 (0.74)	2.99 (2.21)	<b>2.97</b>
<b>cob-C3 - 2</b>	1.65 (1.21)	3.43 (2.53)	<b>2.08</b>
<b>cob-C3 - 3</b>	--	6.08 (4.48)	--

Table 69 Comparison with Specimens with Same Amount of Reinforcement, Epoxy Paste, Groove 1.5 Diam (Turco 02)

Specimen name	Max Moment Reached in Midspan kNm (k-ft)		$M_C / M_E$
	Epoxy, groove 1.5 rod diam.	Cement., groove 2.25 rod diam.	
<b>cob-C,E3-1</b>	1.58 (1.16)	2.99 (2.21)	<b>1.89</b>
<b>cob-C,E3-2</b>	3.93 (2.90)	3.43 (2.53)	<b>0.87</b>
<b>cob-C,E3-3</b>	5.58 (4.11)	6.08 (4.48)	<b>1.09</b>

Table 70 Theoretical Strain at Failure  $[\epsilon_u]$  in the Reinforcement

amount of bars	Cement.Paste groove=1.5diam	Epoxy Paste groove=1.5diam	Cement.Paste groove=2.25diam
<b>1 bar #3</b>	0.19	0.30	0.61
<b>2 bars #3</b>	0.16	0.38	0.35
<b>3 bars #3</b>	--	0.37	0.43

We can affirm that a larger groove was necessary for the cementitious modified paste: for the bars #3 a groove 2.25 times the diameter is probably the optimum; greater will mean probably to break the blocks. For the bars #2 a deep of 2.5 the diameter has proved itself to be good.

Unlike the epoxies ones, during the test this three walls have shown a ductile and constant (in terms of stiffness) behavior till the failure; besides the experimental bending behavior is closer to the theoretical behavior, perhaps due to the lower elastic modulus of the paste.

Figure 129 reports the midspan moment versus the midspan displacement, measured during the test, of the three specimens. The displacement is calculated as mean of the two values measured in every side by LVDTs. Figure 130 reports a comparison between the theoretical and the experimental curve. The theoretical was estimated in compliance with the RC analysis (see more in Appendix A).

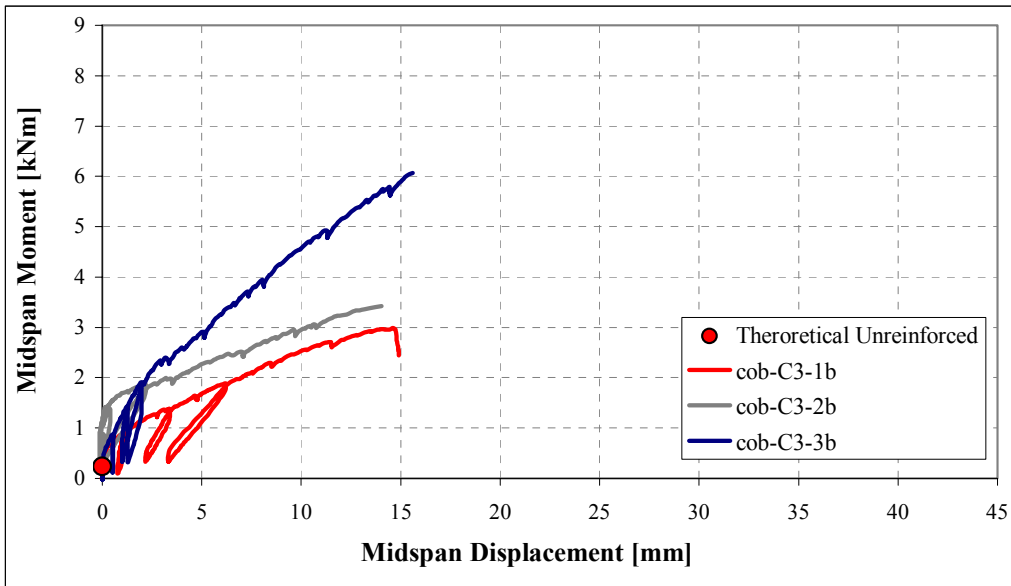


Figure 129 Midspan Moment vs. Deflection in Midspan

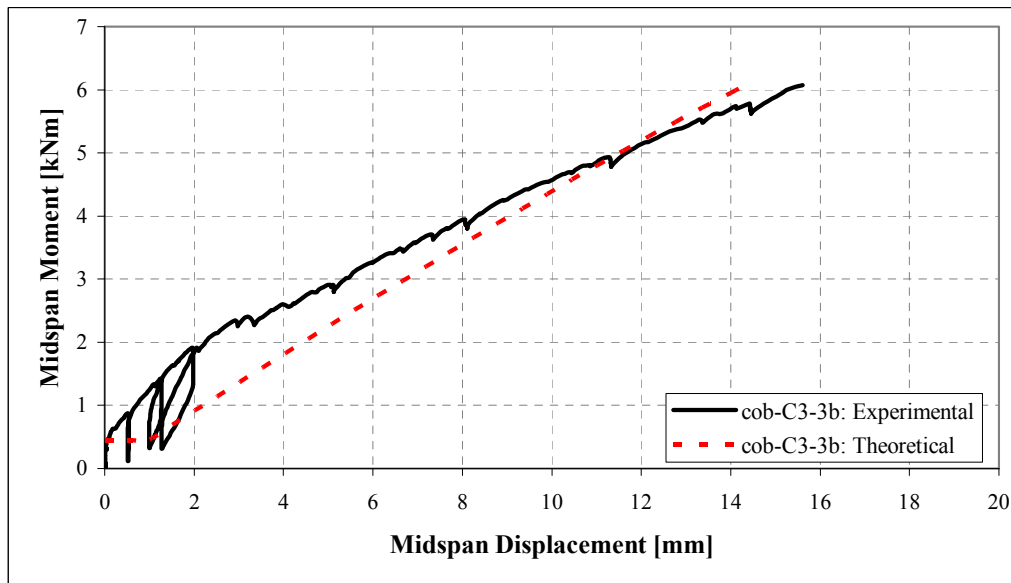


Figure 130 Wall cob-C3-3b: Theoretical and Experimental Displacement in Midspan

Figure 131 shows the strain data concerning the wall cob-C3-3b, where there were three strain gages on one bar (the bar in the centre) and a fourth strain gage in another bar (a side bar, gage just in midspan).

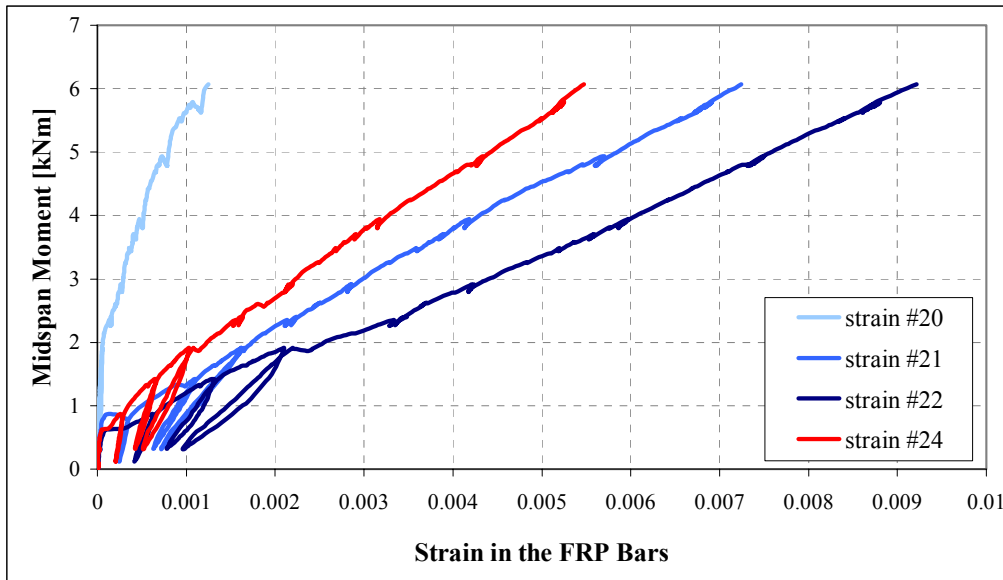


Figure 131 Wall cob-C3-3b: Strain Gages on the Central Bar (20 through 22) and the One in Midspan on the Side Bar(24)

Like said previously, when more bars are present, during the test the stress is not equally distributed on all the bars.

### 5.5.5 Glass FRP Rods #2 Displaced Along the Mortar Joints

These two walls were strengthened with #2 G-rod embedded with epoxy paste (in a groove 1.5 times the rod diameter), along the mortar joints.

The wall strengthened with one bar is yielded very early, when the theoretical strain in the rod was  $0.30 \epsilon_u$ , whereas the one with two rods died very later, when the theoretical strain in the rod was  $0.86 \epsilon_u$ .

The wall cob-E2-1c has exhibit the worst performance, probably because the mortar joint was big and the epoxy bordered on the mortar and not on the concrete blocks, like the second wall. Also if this can be just a hypothesis, it is advisable to groove till the concrete surfaces when rods are placed along the joints.

Figure 132 shows the strengthening scheme for the two specimens, table 71 reports the test results, figure 133 reports the midspan moment versus the midspan displacement and the 132 the midspan moment versus the experimental strain in the FRP bar for the wall cob-E2-1c.

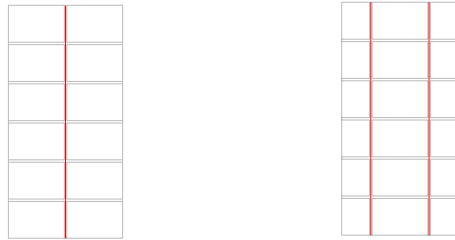


Figure 132 Strengthening Scheme for the Walls cob-E2-1c (left) and ,cob-E2-2c (right)

Table 71 Test Results

Specimen Name	Amount of Reinforcement $E_f \times A_f$ kN (kips)	Ultimate Load kN (kips)	Maximum Bending Moment kNm (k-ft)	Maximum Displacement in Midspan mm (in)	Type of Failure
<b>cob-E2-1c</b>	1527 (343)	2.84 (0.64)*	0.81 (0.60)	7.8 (0.30)	debonding
<b>cob-E2-2c</b>	3054 (687)	16.2 (3.64)	3.43 (2.53)	19.4 (0.76)	debonding

\* because of the low value, a contribution by the wall weight equal to 0.16 kNm was considered.

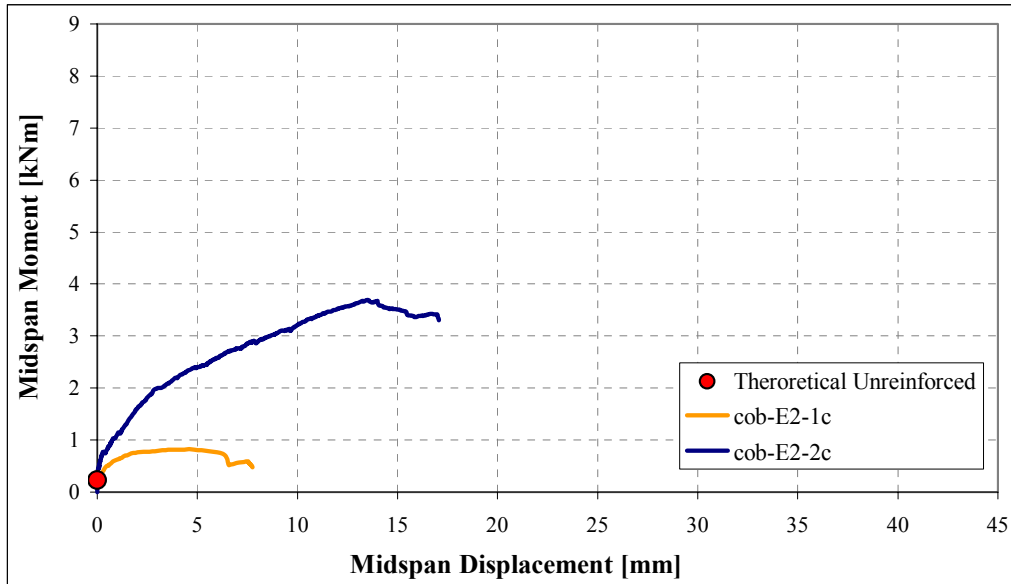


Figure 133 Midspan Moment vs. Deflection in Midspan

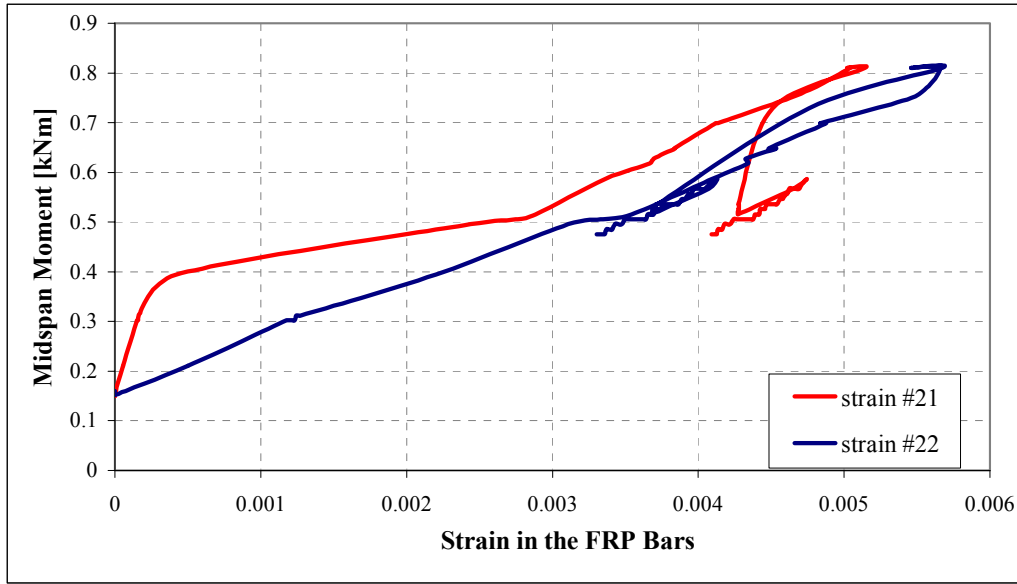


Figure 134 Wall cob-E2-1c: Out-of-Plane Load / Strain in FRP

Figures 135 and 136 show the walls after the failure.



Figure 135 Debonded Rod from the Wall cob-E2-1c

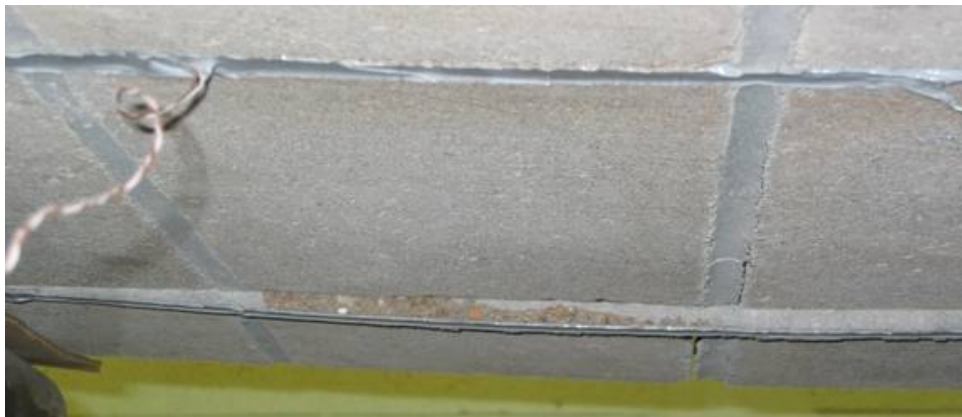


Figure 136 Wall cob-E2-2c: Wall After the Failure

### 5.5.6 Glass FRP Rods #2 Displaced Along the Blocks

These two walls were strengthened with #2 G-FRP rod embedded with epoxy paste in a groove 1.5 times the rod diameter, over along the concrete blocks.

For both the wall the failure was due to the rupture of the bars, when the theoretical strain in the rods was around  $0.88 \epsilon_u$  (considering that applying the strain gages we cut about the 20% the result is considered to be excellent).

Figure 137 shows the strengthening scheme for the two specimens, table 72 reports the test results, and figure 138 the midspan moment versus the midspan displacement.

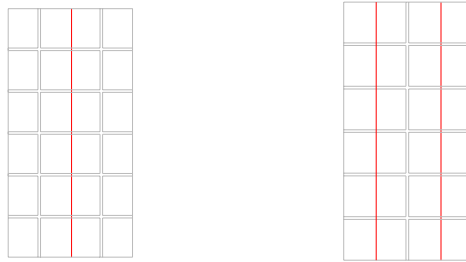


Figure 137 Strengthening Scheme for the Walls cog-E2-1,2d

Table 72 Test Results

Specimen Name	Amount of Reinforcement $E_f \times A_f$ kN (kips)	Ultimate Load kN (kips)	Maximum Bending Moment kNm (k-ft)	Maximum Displacement in Midspan mm (in)	Type of Failure
<b>cob-E2-1d</b>	1527 (343)	8.4 (1.9)	1.91 (1.41)	26.8 (1.06)	FRP rupture
<b>cob-E2-2d</b>	3054 (687)	15.8 (3.5)	3.60 (2.66)	33.3 (1.31)	FRP rupture

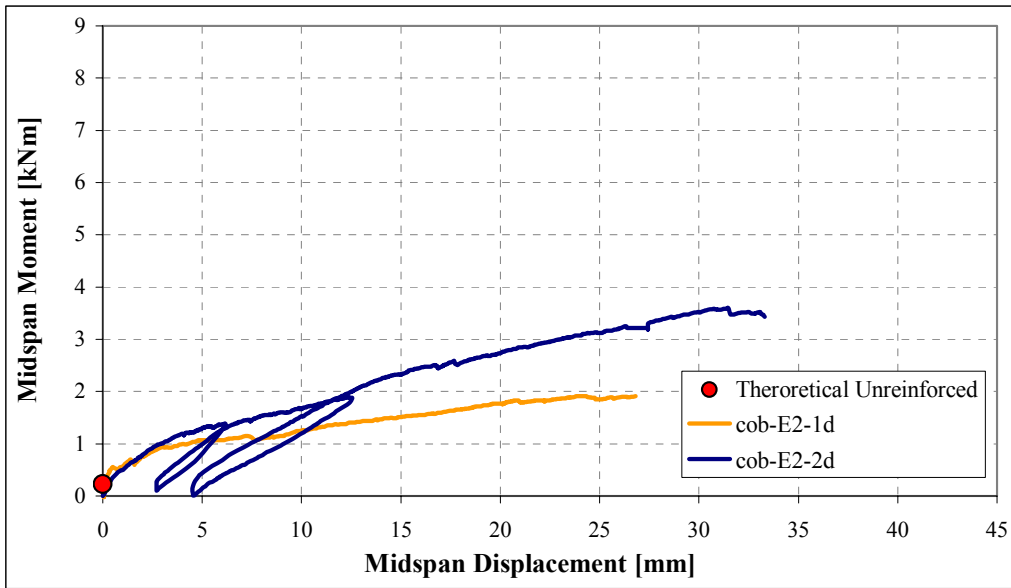


Figure 138 Midspan Moment vs. Deflection in Midspan



Figure 139. Wall cog-E2-2d During the Failure (Rupture of One Bar)

## 5.6 PREVIOUS RESULTS

Tables 73 through 78 report all the previous results in terms of ultimate carried loads, displacement in midspan at failure and type of failure, of tests performed at UMR on identical original walls.

Specimens in the table 73 were strengthened with #2 and #3 (diameter 6.3 and 9.5 respectively) Glass FRP circular bars, embedded with epoxy paste in grooves 1.5 times the rod diameter.

*Table 73 Previous Test Results: Rods #2 and 3 + Epoxy Paste, Groove 1.5 Rod Diameter (Turco 02)*

Specimen Name	Amount of Reinforcement $E_f \times A_f$ kN (kips)	Ultimate Load kN (kips)	Maximum Bending Moment kNm (k-ft)	Maximum Displacement in Midspan mm (in)	Type of Failure
<b>cob-E2-2</b>	3054 (687)	7.38 (1.66)	1.69 (1.25)	27.1 (1.06)	debonding
<b>cob-E2-3</b>	4581 (1030)	9.91 (2.23)	2.27 (1.67)	26.4 (1.04)	sliding shear
<b>cob-E3-1</b>	3879 (872)	6.85 (1.54)	1.57 (1.16)	17.2 (0.68)	debonding
<b>cob-E3-2</b>	7759 (1744)	17.21 (3.87)	3.93 (2.90)	16.9 (0.66)	debonding
<b>cob-E3-3</b>	11638 (2616)	24.36 (5.48)	5.57 (4.11)	18.7 (0.64)	shear

Specimens explained in the next table were strengthened with #2 and #3 (diameter 6.3 and 9.5 respectively) Glass FRP circular bars, embedded with cementitious modified paste (the same product used in this experimental program) in grooves 1.5 or more (specimens identified with a “b”) times the rod diameter.

*Table 74 Previous Test Results: Rods #2 and 3 + Cementitious Paste (Turco 02)*

Specimen Name	Amount of Reinforcement $E_f \times A_f$ kN (kips)	Ultimate Load kN (kips)	Maximum Bending Moment kNm (k-ft)	Maximum Displacement in Midspan mm (in)	Type of Failure
<b>cob-C2-2b</b>	3054 (687)	9.03 (2.03)	1.69 (1.25)	17.8 (0.70)	debonding
<b>cob-C2-3b</b>	4581 (1030)	12.81 (2.88)	2.27 (1.67)	22.7 (0.89)	sliding shear
<b>cob-C3-1</b>	3879 (872)	4.35 (0.98)	1.57 (1.16)	9.7 (0.38)	debonding
<b>cob-C3-2</b>	7759 (1744)	7.16 (1.61)	3.93 (2.90)	10.0 (0.40)	debonding

Next seven specimens were reinforced with G-FRP laminates, with width from 3 up to 12 inches, on not puttied surfaces. Specimen names that have an “r” as last character indicate that the test was repeated two times with two identical walls.

Table 75 Previous Test Results: Concrete Blocks + G-FRP Laminates (Morbin 01)

Specimen Name	Amount of Reinforcement $E_f \times A_f$ kN (kips)	Ultimate Load kN (kips)	Maximum Bending Moment kNm (k-ft)	Maximum Displacement in Midspan mm (in)	Type of Failure
<b>cob-gl-3</b>	2249 (506)	8.66 (1.95)	1.98 (1.44)	20.1 (0.79)	debonding
<b>cob-gl-3r</b>	2249 (506)	11.84 (2.66)	2.71 (2.00)	26.8 (1.06)	debonding
<b>cob-gl-5</b>	3749 (843)	14.15 (3.18)	3.23 (2.38)	22.2 (0.87)	debonding
<b>cob-gl-5r</b>	3749 (843)	14.56 (3.27)	3.33 (2.46)	26.9 (1.06)	debonding
<b>cob-gl-7</b>	5248 (1180)	15.78 (3.55)	3.61 (2.66)	19.0 (0.75)	debonding
<b>cob-gl-9</b>	6748 (1517)	21.95 (4.93)	5.02 (3.70)	18.2 (0.72)	debonding
<b>cob-gl-12</b>	8997 (2023)	25.62 (5.76)	5.86 (4.32)	17.5 (0.69)	shear

Specimens explained in the next table were strengthened with Aramid FRP laminates. The width of the sheets applied is indicated in the last number (inches) of the specimen name.

Table 76 Previous Test Results: Concrete Blocks + A-FRP Laminates (Morbin 01)

Specimen Name	Amount of Reinforcement $E_f \times A_f$ kN (kips)	Ultimate Load kN (kips)	Maximum Bending Moment kNm (k-ft)	Maximum Displacement in Midspan mm (in)	Type of Failure
<b>cob-al-3</b>	2576 (579)	11.69 (2.63)	2.67 (1.97)	22.2 (0.87)	debonding
<b>cob-al-5</b>	4293 (965)	14.83 (3.33)	3.39 (2.50)	23.0 (0.91)	debonding
<b>cob-al-7</b>	6011 (1351)	19.73 (4.44)	4.51 (3.33)	22.1 (0.87)	debonding
<b>cob-al-9</b>	7728 (1737)	22.18 (4.99)	5.07 (3.74)	16.3 (0.64)	shear
<b>cob-al-12</b>	10304 (2317)	26.98 (6.07)	6.17 (4.55)	15.0 (0.59)	shear

Specimens in the tables 77 and 78 were strengthened with Glass and Aramid FRP laminates respectively, but the sheets were applied on clay bricks masonry and the surface was puttied.

Table 77 Previous Test Results: Clay Bricks + G-FRP Laminates (Morbin 01)

Specimen Name	Amount of Reinforcement $E_f \times A_f$ kN (kips)	Ultimate Load kN (kips)	Maximum Bending Moment kNm (k-ft)	Maximum Displacement in Midspan mm (in)	Type of Failure
<b>cl2-gl-3</b>	2249 (506)	15.87 (3.57)	3.63 (2.68)	31.1 (1.22)	debonding
<b>cl2-gl-3r</b>	2249 (506)	15.92 (3.58)	3.64 (2.68)	30.0 (1.18)	debonding
<b>cl2-gl-5</b>	3749 (843)	20.18 (4.54)	4.61 (3.40)	37.0 (1.46)	debonding
<b>cl2-gl-5r</b>	3749 (843)	21.51 (4.84)	4.92 (3.63)	28.5 (1.12)	FRP rupture
<b>cl2-gl-7</b>	5248 (1180)	27.62 (6.21)	6.31 (4.66)	34.2 (1.35)	debonding
<b>cl2-gl-7r</b>	5248 (1180)	29.84 (6.71)	6.82 (5.03)	31.4 (1.24)	debonding
<b>cl3-gl-9</b>	6748 (1517)	29.16 (6.56)	6.67 (4.92)	24.6 (0.97)	sliding shear
<b>cl2-gl-12</b>	8997 (2023)	26.0 (5.85)	5.94 (4.38)	12.8 (0.50)	sliding shear

Table 78 Previous Test Results: Clay Bricks + A-FRP Laminates (Morbin 01)

Specimen Name	Amount of Reinforcement $E_f \times A_f$ kN (kips)	Ultimate Load kN (kips)	Maximum Bending Moment kNm (k-ft)	Maximum Displacement in Midspan mm (in)	Type of Failure
<b>cl2-al-3</b>	2576 (579)	12.02 (2.70)	2.75 (2.00)	23.3 (0.92)	debonding
<b>cl2-al-5</b>	4293 (965)	22.04 (4.95)	5.04 (3.67)	28.5 (1.12)	FRP rupture
<b>cl2-al-7</b>	6011 (1351)	25.91 (5.82)	5.92 (4.31)	23.1 (0.91)	debonding
<b>cl2-al-9</b>	7728 (1737)	35.65 (8.01)	8.15 (5.93)	36.4 (1.43)	FRP rupture
<b>cl2-al-12</b>	10304 (2317)	25.00 (5.62)	5.72 (4.16)	12.5 (0.49)	sliding shear

All these previous results are compared and plotted in figures 146 through 150. Besides, all the section 5.8 considers and investigates these results.

## 5.7 MODES OF FAILURE

As reported in tables 64 through 78 different types of failure were observed:

- FRP debonding. This was the most observed kind of failure in every type of test. Three different debonding-failures were observed:
  - the pulling away of the bar from its groove, the most seen, especially with the rods.
  - the sliding of the bar on the epoxy; it was noted just with the tape.
  - the splitting of the blocks/bricks that allows the bar coming out; it was seen when the groove was deep (tapes or rods #3 in grooves 21mm deep).
- Shear failure. This failure was rare and noted when the amount of reinforcement is high.
- Sliding-shear, i.e. sliding of the first course of bricks. It was seen especially with clay bricks walls when the amount of reinforcement was high.
- Flexural failure, i.e. FRP rupture in midspan: very rare, it was observed when the friction between FRP and the wall was strong.

Indeed weak bond between the mortar and the blocks results in a low tensile strength: the joint, therefore, cracks between the FRP location and the load is redistributed to the FRP rods and to the surrounding regions. A typical noise revealed the progressive cracking of the epoxy paste. The same did not happen with the modified cementitious paste where less cracks were visible up to failure. At the side zone, vertical flexural cracks formed and then sloped going towards the loading supports (figure 140). When the redistribution of the tensile stresses occurred, the cracks developed in the masonry units oriented at  $45^\circ$  or in the head mortar joints. Some of these cracks followed the embedding material and masonry interface causing their debonding and subsequent wall failure (figures 141 and 142).

At the failure, in the specimens with the epoxy paste and with cementitious modified paste if the groove was more than two times the rod diameter, part of concrete block faceshell remained attached to the FRP rods due to the low tensile strength of the masonry compared with the paste. That did not happen when the reinforcement was embedded in the cementitious paste if there was a minimum groove (1.5 times the diameter): in this case, the failure was between it and the masonry because the groove size did not permit the paste to develop enough tensile strength.



Figure 140 Flexural and Shear Crack in the Maximum Moment Region



(a) Specimen Reinforced with Glass Tape



(b) Specimen Reinforced with Glass Rods+Cem.

Figure 141 Develop of the Debonding Cracks



Figure 142 Specimen cob-E2-2c after Failure (Debonding)



Figure 143 Splitting Cracks in the Cover (Specimen C2-3b)

A kind of failure rather common with the clay walls strengthened with FRP sheets, the sliding-shear, was observed just with one concrete wall: the cob-E2-3 (Turco 02, see figures 144 and 145). More considerations about the sliding-shear are presented in the section 5.8.4.



Figure 144 Failure of Specimen E3-2(Sliding-Shear)



(a) Specimen cl2-al-12 (b) Specimen cl2-gl-12  
Figure 145 Failures Caused by Sliding Shear During Previous Tests (Morbin 01)

## 5.8 ANALYTICAL WORK

### 5.8.1 Computation of the maximum moment

The following assumptions and limitations should be adopted:

The strains in the reinforcement and masonry are directly proportional to the distance from the neutral axis.

The maximum usable strain at the extreme compressive fiber  $\varepsilon_{c,u}$  is assumed to be 0.0035 mm/mm (in./in.) for clay masonry and 0.0025 mm/mm (in./in.) for concrete masonry

The tensile strength of masonry is neglected.

The FRP reinforcement has a linear elastic stress-strain relationship up to failure.

For simplicity and similarly to the flexural analysis of RC members, a parabolic distribution is used in the computation of the flexural capacity of the strengthened masonry. Thus:

$$f_m = f'_m \times \left[ 2 \frac{\varepsilon_c}{\varepsilon'_c} - \left( \frac{\varepsilon_c}{\varepsilon'_c} \right)^2 \right]; \quad \alpha \times \beta = \frac{\varepsilon_c}{\varepsilon'_c} - \frac{1}{3} \left( \frac{\varepsilon_c}{\varepsilon'_c} \right)^2; \quad \beta = \frac{4 - \frac{\varepsilon_c}{\varepsilon'_c}}{6 - 2 \frac{\varepsilon_c}{\varepsilon'_c}}$$

Then, in order to satisfy the internal force equilibrium:

$$A_f \times f_f = \alpha \times f'_m \times b \times c \times \beta; \quad f_f = \varepsilon_s \times E_f$$

The effective strain in the reinforcement  $\varepsilon_s$  and the strain in the masonry are related by:

$$\frac{\varepsilon_s}{d - c} = \frac{\varepsilon_c}{c}$$

the theoretical flexural capacity can be estimated by:

$$M_{ext} = A_f \times f_f \times E_f \left( d - \frac{\beta \times c}{2} \right)$$

where  $c$  is:

$$c = \frac{A_f \times f_f}{f'_c \times b \times \alpha \times \beta}$$

And the moment is proportional to the external applied load by the relation:

$$M_{ext} = \frac{P}{2} \times x$$

The analytical model proved effective in the computations. Like other researches suggest (prof. Ayman S. Mosallam, California State Univ.), a different parabolic behavior is been also adopted for the clay brick masonry:

$$\text{for } 0 < \varepsilon_c < \varepsilon'_c: f_m = E_m \varepsilon_c \times \left[ 1 - \frac{1}{n} \left( \frac{\varepsilon_c}{\varepsilon'_c} \right)^{n-1} \right]; \text{ where } n = \frac{E_m \varepsilon'_c}{E_m \varepsilon'_c - f'_m}$$

$$\text{for } \varepsilon'_c < \varepsilon_c < \varepsilon_{c,u}: f_m = f'_m - E_d (\varepsilon_c - \varepsilon'_c); \text{ where } E_d = \frac{0.5 f'_m}{\varepsilon_{c,u} - \varepsilon'_c}$$

where:  $\varepsilon'_c = 0.002$ ,  $\varepsilon_{c,u} = 0.0035$ .

Table 79 shows the maximum moment estimated by the two methods: the results diverge up to 10%, but it has been chosen to use, for simplicity, the ACI - RC parabola.

Table 79 Maximum Moments Estimated by the Two Methods.

	Max Mom. RC [kNm]	Max Mom CL [kNm]	$M_{RC} / M_{LC}$
<b>cl1-gt-1</b>	2.87	2.62	1.09
<b>cl1-gt-2</b>	5.63	5.42	1.04
<b>cl2-ct-2</b>	5.86	6.57	0.89
<b>cl2-gl-3</b>	3.66	3.29	1.11
<b>cl2-gl-5</b>	6.03	5.78	1.04
<b>cl2-gl-7</b>	8.32	7.94	1.05
<b>cl2-gl-9</b>	10.1	9.61	1.05
<b>cl2-gl-12</b>	11.4	10.81	1.05
<b>cl2-al-3</b>	3.72	3.82	0.97
<b>cl2-al-5</b>	6.13	6.60	0.93
<b>cl2-al-7</b>	8.46	8.94	0.95
<b>cl2-al-9</b>	10.6	10.2	1.04
<b>cl2-al-12</b>	12.0	11.4	1.05

Figures 146 through 150 compare the experimental results to the theoretical ones, considering all the tests done till now at UMR. The comparison is based upon the amount of reinforcement  $E_f \times A_f$ . The result seems to be quite satisfactory. Note: the green arrow indicates the specimens broken by this kind of rupture (= rupture of the FRP reinforcement).

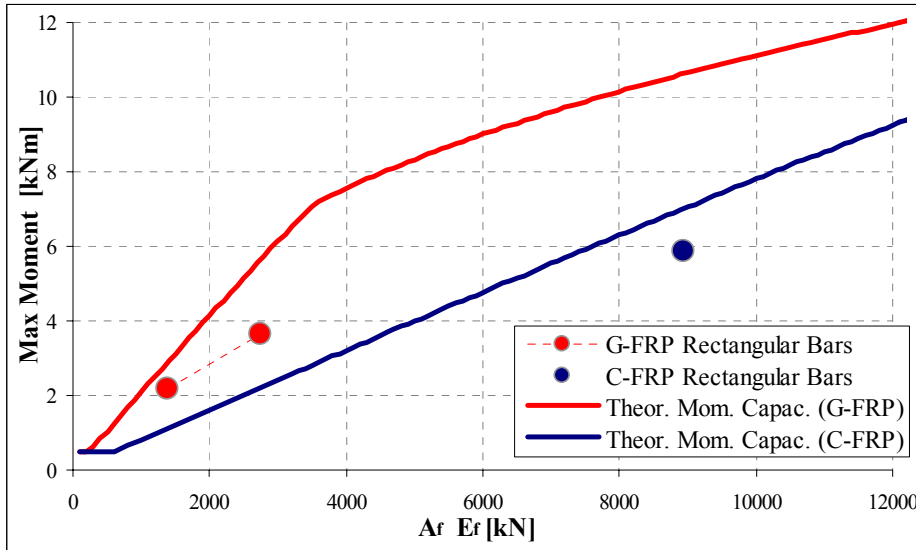


Figure 146 Glass Tape on Clay Walls: Theoretical and Experimental Maximum Moments Carried

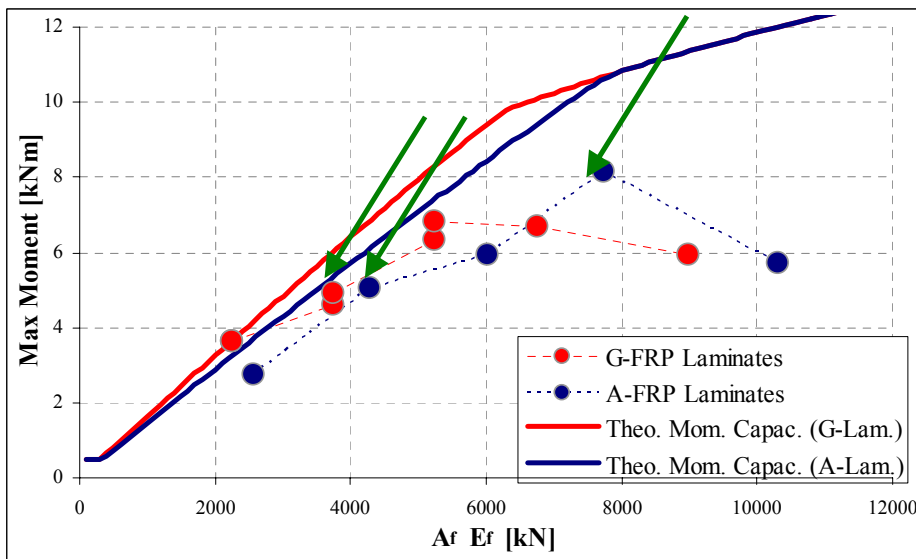


Figure 147 A and G Laminates on Clay Walls: Theoretical and Experimental Maximum Moments Carried

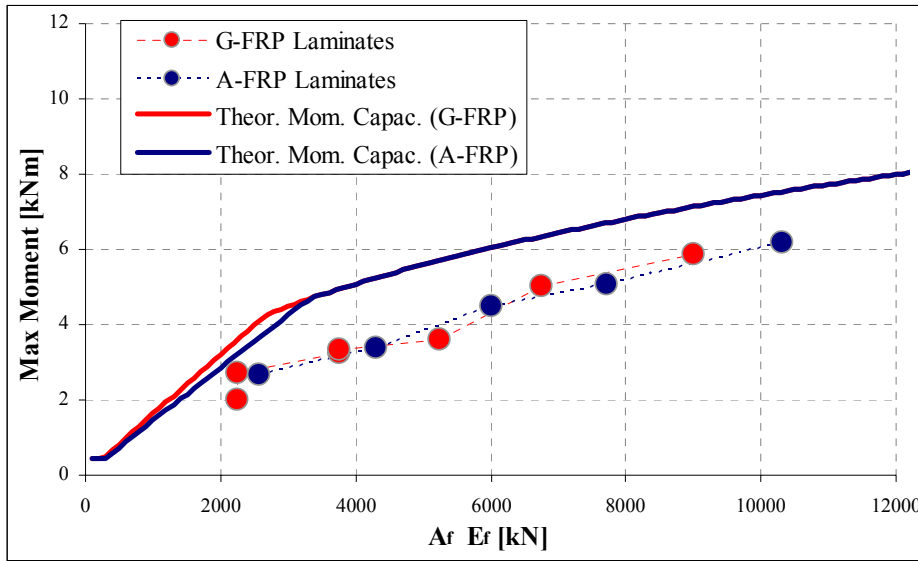


Figure 148 A and G Laminates on Concrete Walls: Theoretical and Experimental Maximum Moments Carried

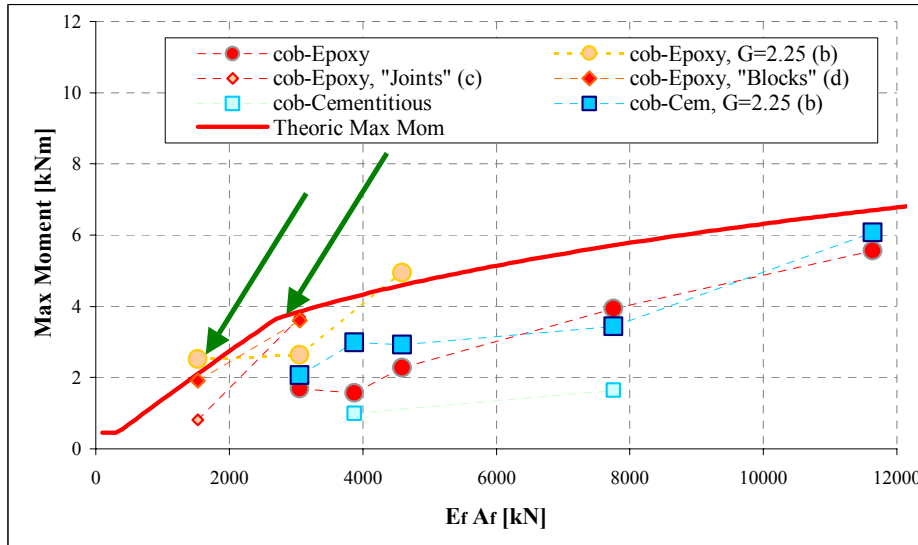


Figure 149 Glass Rods on Concrete Walls: Theoretical and Experimental Maximum Moments Carried

Removing the specimens with the Cementitious Modified Paste and small groove, and the ones with the groove along the mortar joints, the previous graph can be better to be represented as the following:

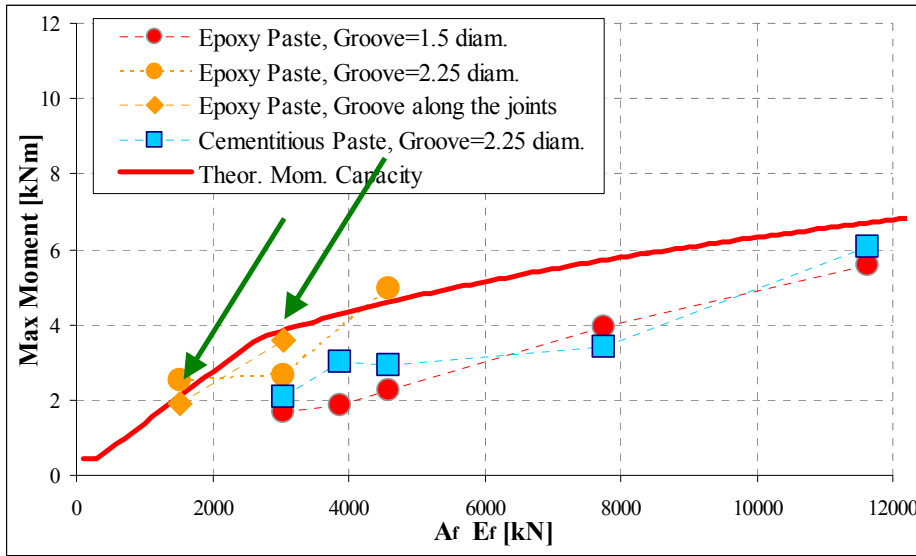


Figure 150 Glass Rods on Concrete Walls: Theoretical and Experimental Maximum Moments Carried

### 5.8.2 Computation of the shear capacity in the blocks

As ACI suggests for RC members, the shear capacity of the concrete/clay is estimated to be:

$$V_{C,ACI[1b]} = 3\sqrt{f'_m} \times b_w \times d ; \quad (V_{C,ACI[N]} = 0.249\sqrt{f'_m} \times b_w \times d \text{ in S.I. units of measurement})$$

where:

- $b_w$  [in] is the total width of concrete or clay in a generic cross section. Table 80 shows the widths used.

Table 80  $b_w$

masonry unit	$b_w$ mm (in)
<b>cl1</b>	230 (9)
<b>cl2</b>	230 (9)
<b>cob</b>	180 (7)
<b>bc</b>	150 (6)

- $f'_m$  [psi] is the maximum compressive strength of the masonry (blocks+mortar)

- $d$  [in] is the distance of the reinforcement's baricentre from the extreme compression fiber

The formula has seemed to be reasonable: actually in our case the problem is often the sliding-shear and not the shear in the blocks (see 5.8.4 - sliding shear). The following tables shows the theoretical and experimental ultimate loads in notable cases, during this experimental program (table 81) or before (82).

Table 81  $V_{th}-V_{exp}$  in this Experimental Program

	$V_{th}$ [kN]	$V_{exp}$ [kN]	failure mode
<b>cl1-gt-1</b>	21.4	4.7	deb. (spitting of the block)
<b>cl1-gt-2</b>	21.4	8.0	deb. (sliding of the bars)
<b>cl2-ct-2</b>	19.3	12.8	deb. (sliding of the bars)
	$V_{th}$ [kN]	$V_{exp}$ [kN]	failure mode
<b>bc-gt-1</b>	21.0	7.3	deb. (sliding of the bars)
<b>bc-gt-2</b>	21.0	17.5	deb.-shear (spitting of the block)*
	$V_{th}$ [kN]	$V_{exp}$ [kN]	failure mode
<b>cob-E2-3b</b>	11.5	10.8	debonding (deb.-shear)*
<b>cob-C3-3b</b>	11.5	13.3	shear*

\* see figures below



Wall bcb-gt-2



Wall cob-C3-3b



Wall cob-E2-3b

Figure 151 Probable Shear Failures Observed

Table 82 Previous Researches: Shear Failures

	$V_{th}$ [kN]	$V_{exp}$ [kN]	failure mode
<b>cob-E3-2</b>	11.5	8.6	sliding-shear
<b>cob-E3-3</b>	11.5	12.2	shear (in the concrete)

	$V_{th}$ [kN]	$V_{exp}$ [kN]	failure mode
<b>cob-gl-9</b>	12.8	11.0	debonding-shear
<b>cob-gl-12</b>	12.8	12.8	shear
<b>cob-al-9</b>	12.8	11.1	shear
<b>cob-al-12</b>	12.8	13.5	shear

	$V_{th}$ [kN]	$V_{exp}$ [kN]	failure mode
cl2-gl-9	22.0	14.6	sliding-shear
cl2-gl-12	22.0	13.0	sliding-shear
cl2-al-9	22.0	17.8	FRP rupture
cl2-al-12	22.0	12.5	sliding-shear

Figures 152 through 155 show the graphs. Green arrows indicate shear ruptures.

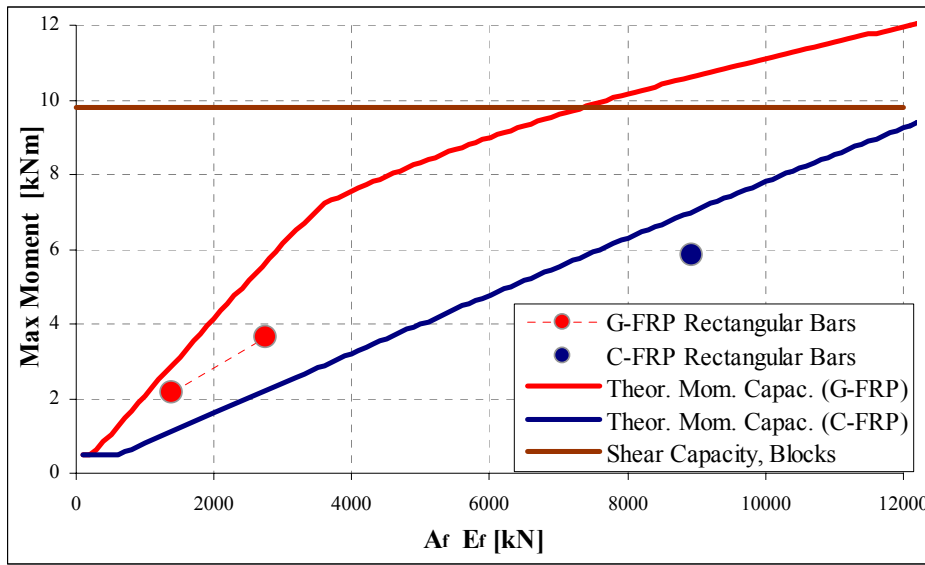


Figure 152 Rectangular Bars on Clay Walls: Theoretical Shear Capacity in the Bricks

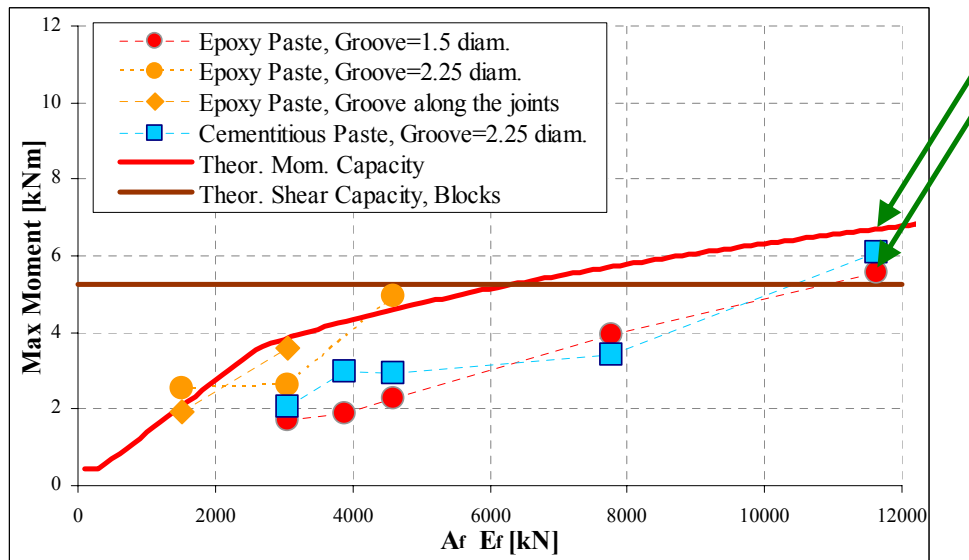


Figure 153 G-FRP Rods on Concrete Masonry: Theoretical Shear Capacity in the Blocks

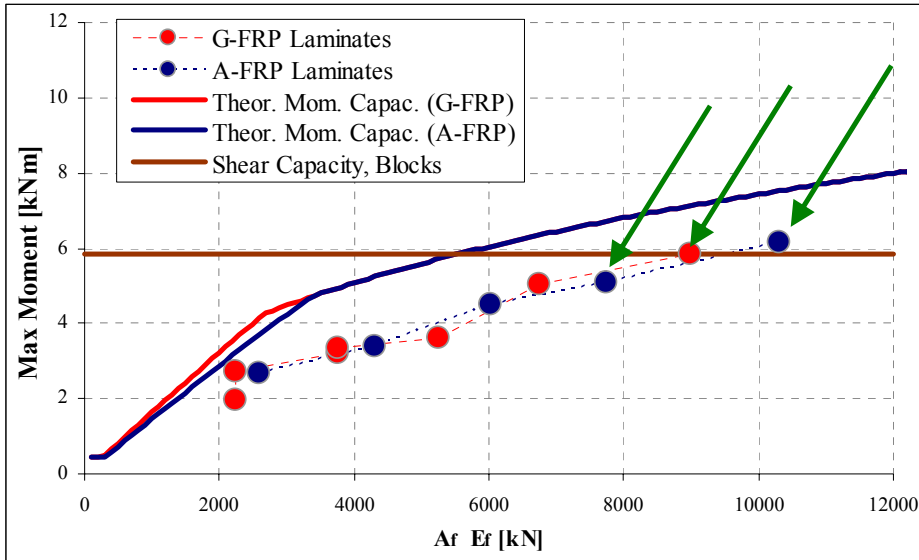


Figure 154 G and A-FRP Laminates on Concrete Masonry: Theoretical Shear Capacity in the Blocks

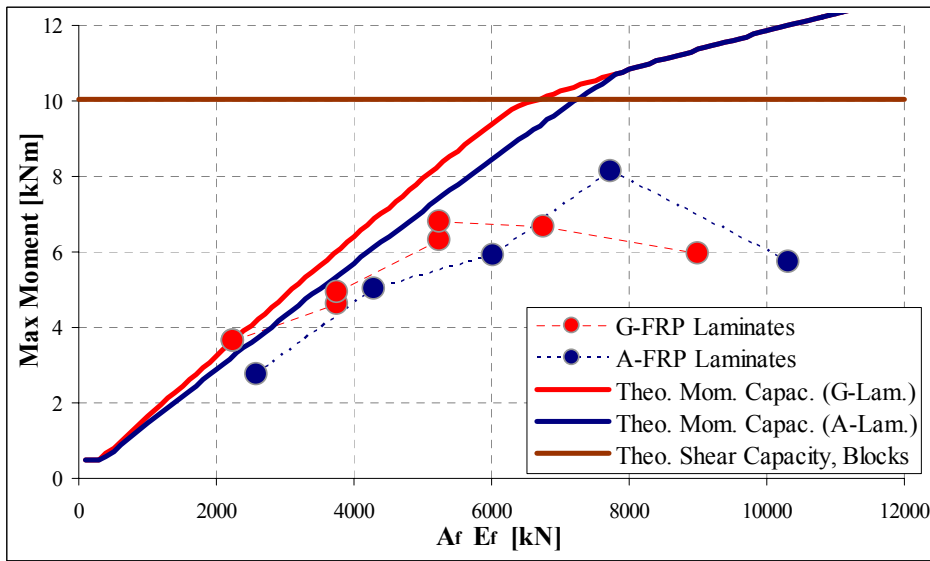


Figure 155 G and A-FRP Laminates on Clay Masonry: Theoretical Shear Capacity in the Bricks

**5.8.3 Estimation of the shear strength in the joints (sliding-shear)**

Since during these tests shear meant often a sliding-shear, and sometimes the debonding of the bars was caused by this kind of shear, in this section an attempt to better understand the sliding-shear has been done.

The analytical sliding-shear capacity could be computed integrating the Mohr-Coulomb relation:

$$\tau = \tau_0 + \mu \sigma_n.$$

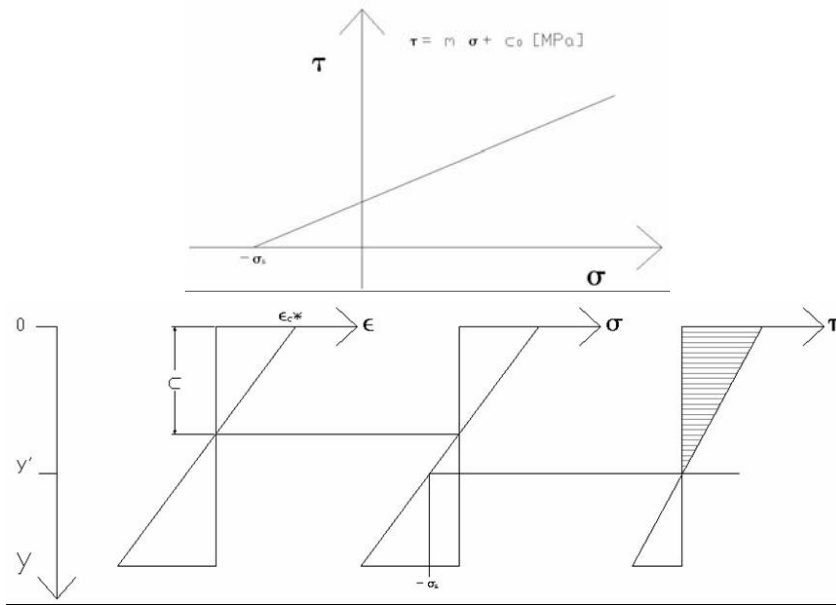


Figure 156 Mohr-Coulomb Relation in Order to Estimate the Sliding-Shear Capacity in the Mortar Joints

$$V_m(x) = \int_0^{y'} \tau \times b \times dy ;$$

$$f'_m(\epsilon_c) : f_m = f'_m \times \left[ 2 \frac{\epsilon_c}{\epsilon'_c} - \left( \frac{\epsilon_c}{\epsilon'_c} \right)^2 \right] \quad \text{and } \epsilon_c(y) : \epsilon_c(y) = \epsilon_c^* \times \frac{y}{c}$$

$$\text{thus: } \sigma(y) = f'_m \times \left[ 2 \frac{\epsilon_c^* \times \frac{y}{c}}{\epsilon'_c} - \left( \frac{\epsilon_c^* \times \frac{y}{c}}{\epsilon'_c} \right)^2 \right] ; \text{ and } \tau(y) = c_0 + m \times f'_m \times \left[ 2 \frac{\epsilon_c^* \times \frac{y}{c}}{\epsilon'_c} - \left( \frac{\epsilon_c^* \times \frac{y}{c}}{\epsilon'_c} \right)^2 \right]$$

integrating  $\tau(y)$  from 0 to  $y'$ , the sliding-shear capacity in the mortar  $V_m$  may be estimated; since  $V_m$  depends by  $\epsilon_c^*$  (strain at the top), then  $V_m$  will depend by the distance mortar joint-support, like shown in the next figure.

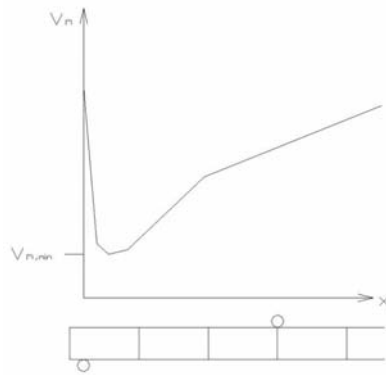


Figure 157 Theoric Sliding-Shear Strength in a Joint Cross Section  $V(x)$

The hypothesis of linearity of the morh-coulomb rule, also for  $\sigma$  high, is not actually true, but like shown in figure 158 it does not affect the evaluation of the minimum shear capacity.

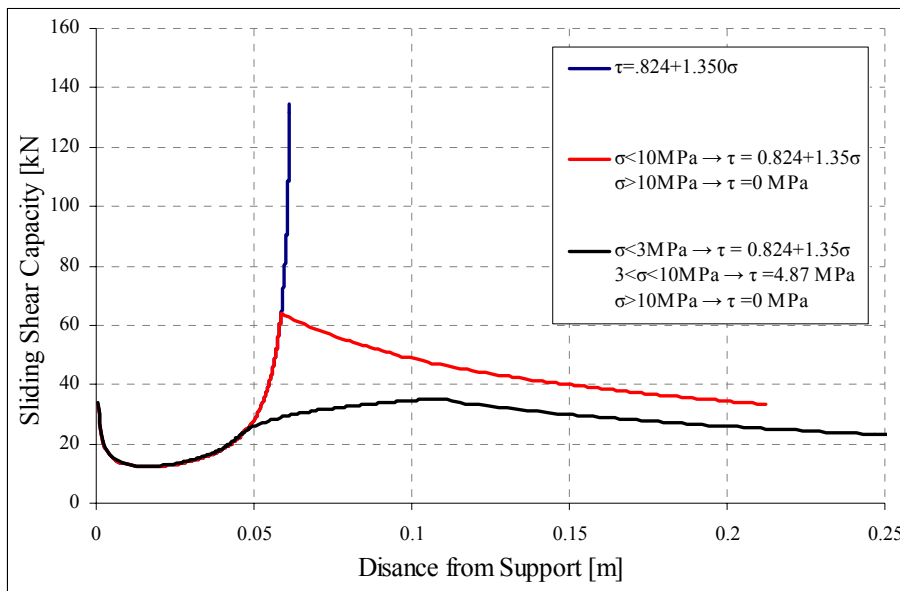


Figure 158 Sliding – Shear Capacity of the Wall c13-al-12 Depending on the Distance from the Support, in Three Different Hypothesis on the Mohr-Coulomb Relation

The resulting theoretical sliding-shear strength is certainly lower than reality for the following reason:

- in this computation the joint is assumed to be at the worst distance from the support
- no shear contribution is assumed to be given by the reinforcement and by the epoxy paste
- strains in the reinforcement and masonry are supposed to be directly proportional to the distance from the neutral axis (the sections are considered flat) and this is not true for high

loads near the supports (see figure 159). As consequence, if the reinforcement is working more that supposed near the supports, then the strain distribution in the mortar joint cross section will be:

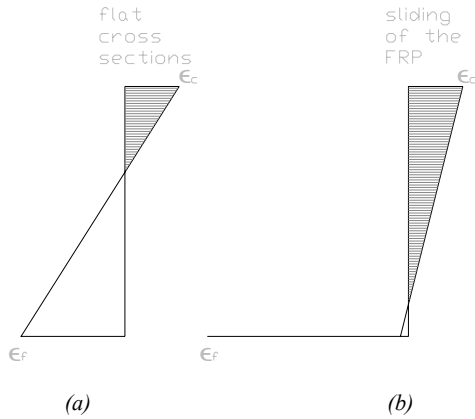


Figure 159 Strain Diagram in a Generic Cross Section near the Supports, Considering the Flat Section Hypothesis (a) or not (b)

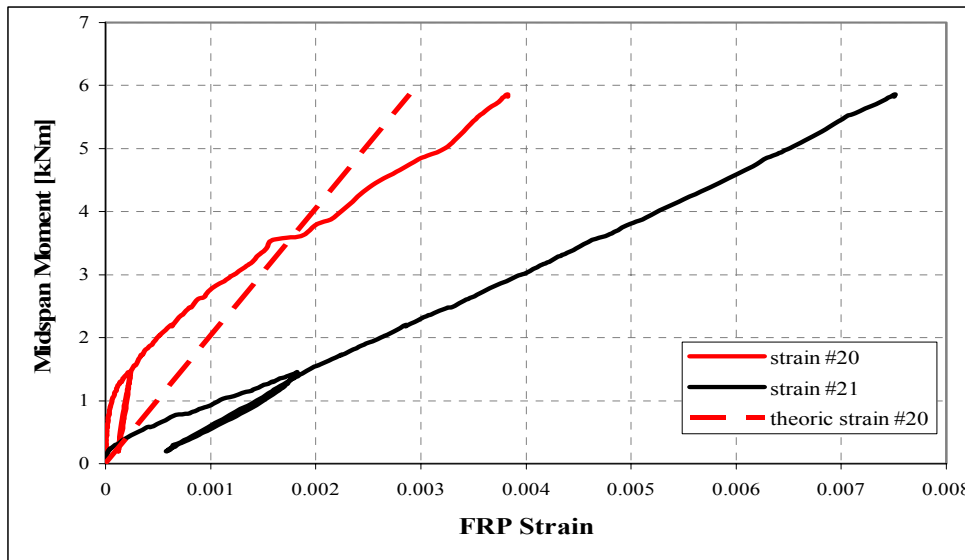


Figure 160 Theoretical (Flat Sections) and Experimental Strain Behavior (Speciman cl-ct2)

Then, the value of the shear capacity obtained, can just represent a minimum and conservative value. Following tables try to estimate the ultimate shear capacity in the first (closest to the supports) mortar joint, using two different equations of Mohr-Coulomb:

(1).....  $\tau = 0.824 + 1.350 \sigma_n$  [MPa] Equation derived by previous researches (Morbin 01) with clay triplets.

(2).....  $\tau = \frac{f'_m}{25} + 0.75 \cdot \sigma$  [MPa] Equation suggested by other researches (“Masonry subjected to combined actions”, Proff Mojsilovic and Marti, Swiss Federal Institute of Technology)

There are reported three different values for the sliding shear strength: two using the two equations to find the strength at the worst distance from the support, and a third one using the equation (2) but imposing a distance of 2 inches (the same distance that in reality).

Table 83 Analytic and Experimental Sliding-Shear Capacity for the Clay-Bricks Specimens

Specimen	$V_{exp}$ [kN]	Failure mode	(1)	(2)	
			$V_{-min}$ [kN]	$V_{-min}$ [kN]	$V_{-2''}$ [kN]
<b>cl1-gt-1</b>	4.72	deb.	4.33	4.08	4.67
<b>cl1-gt-2</b>	8.00	deb.	6.05	5.71	6.53
<b>cl2-ct-2</b>	12.81	deb.	11.61	8.89	10.29
<b>cl2-gl-3</b>	7.94	del.	6.08	5.09	5.61
<b>cl2-gl-3r</b>	7.96	del.	6.08	5.09	5.61
<b>cl2-gl-5</b>	10.1	del.	7.78	6.50	7.17
<b>cl2-gl-5r</b>	10.8	frp rupt.	7.78	6.50	7.17
<b>cl2-gl-7</b>	13.8	deb.	9.12	7.63	8.41
<b>cl2-gl-7r</b>	14.9	deb.	9.12	7.63	8.41
<b>cl2-gl-9</b>	14.6	slid. shear	10.27	8.59	9.46
<b>cl2-gl-12</b>	13.0	slid. shear	11.75	9.83	10.96
<b>cl2-al-3</b>	6.0	del.	6.49	5.43	5.98
<b>cl2-al-5</b>	11.0	frp rupt.	8.29	6.94	7.64
<b>cl2-al-7</b>	13.0	deb.	9.73	8.14	8.97
<b>cl2-al-9</b>	17.8	frp rupt.	10.95	9.16	10.09
<b>cl2-al-12</b>	12.5	slid. shear	12.52	10.47	11.68

For the walls built with clay bricks, where the first mortar joint was 2 inches from the support, the expected ultimate loads were close to the experimental ones where a large amount of reinforcement was used, or better, where the reinforcement was not failing by debonding (c13-gt-9 and 12, c13-al-12).

Table 84 Analytic and Experimental Sliding-Shear Capacity for the Concrete-Blocks Specimens

Specimen	V-Failure [kN]	Failure mode	(2)
			V-min[kN]
<b>bcg-gt-1</b>	7.3	deb.	4.79
<b>bcg-gt-2</b>	17.5	deb.-she.	6.71
<b>cob-E2-1b</b>	5.51	deb.	2.97
<b>cob-E2-2b</b>	5.77	deb.	4.13
<b>cob-E2-3b</b>	10.8	deb.	5.00
<b>cob-C3-1b</b>	6.5	deb.	4.49
<b>cob-C3-2b</b>	7.5	deb.	6.18
<b>cob-C3-3b</b>	13.3	deb.-she.	7.41

Specimen	V-Failure [kN]	Failure mode	(2)
			V-min[kN]
<b>cob-E2-2</b>	3.69	deb.	4.21
<b>cob-E2-3</b>	4.96	deb-sl. shear	5.09
<b>cob-E3-1</b>	3.43	deb.	4.62
<b>cob-E3-2</b>	8.61	slid. shear	6.37
<b>cob-E3-3</b>	12.18	she.	7.65

With the concrete blocks just in one case it was reported a failure due to this kind of rupture, i.e. the cob-E2-3 (Turco 02); and in fact this wall has not a big amount of reinforcement but a good bond (3 bar #2).

In other cases it is not easy to recognize when the failure is due to bedonding and when to this shear (usually when it is debonding the bar is debonded from midspan, when it is shear the bar is debonded just in the last block).

Figures 161 and 162 explain the estimation of the shear capacity in the mortar joints for the clay bricks walls reinforced with sheets and tapes: the blue and red lines represent the maximum flexural capacity changing the amount of reinforcement  $E_f A_f$  in accordance with the RC analysis, the points represent the experimental obtained values and the gray line describes the theoretical shear capacity (the minimum capacity, i.e. computed at the worst distance from the supports) in accordance with the Mohr-Coulomb law.

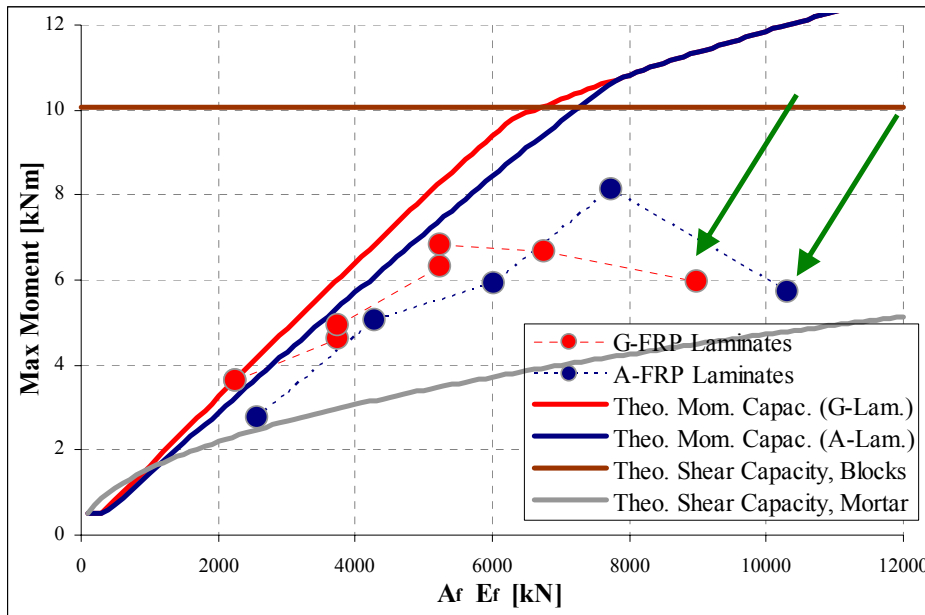


Figure 161 Theoretical Shear Capacity in the Mortar for the Clay Bricks Walls + Sheets

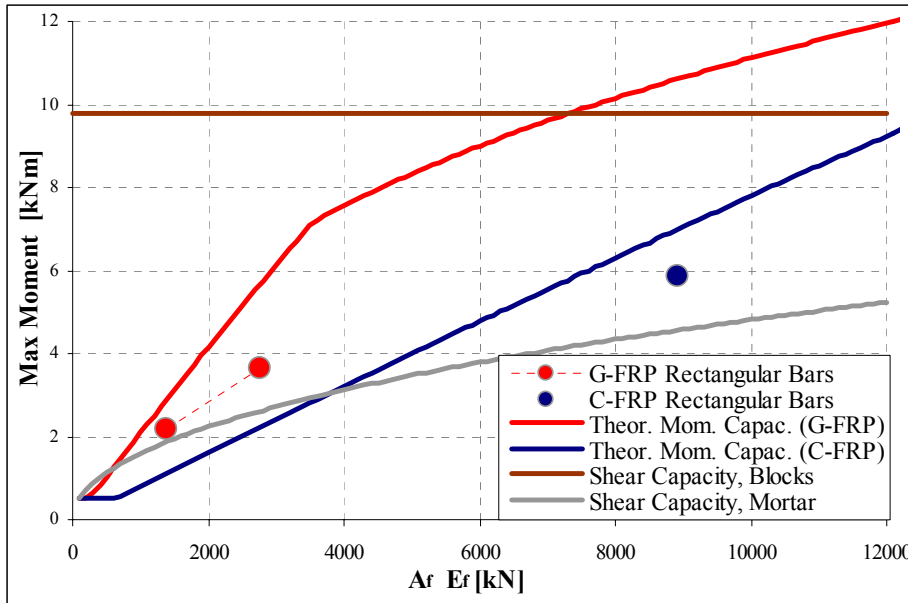


Figure 162 Theoretical Shear Capacity in the Mortar for the Clay Walls + Tapes

Figure 163 and 164 show the same for the concrete blocks walls. The shear capacity is still computed at the worst distance from the support, that is about 1-2 inches, against the true 6 inches. Nonetheless the experimental behavior seems to be well described and a check is suggested.

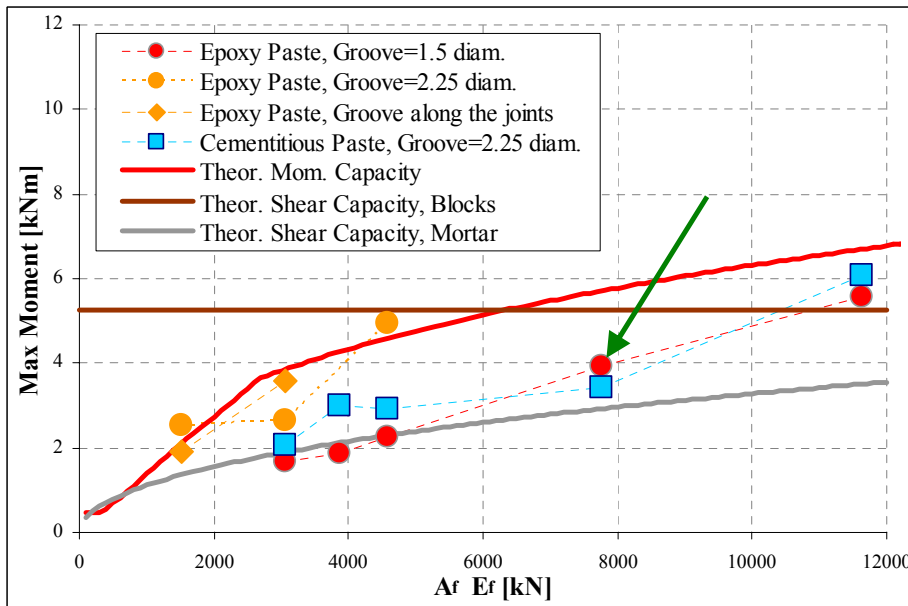


Figure 163 Theoretical Shear Capacity in the Mortar for the Concrete Walls + Rods

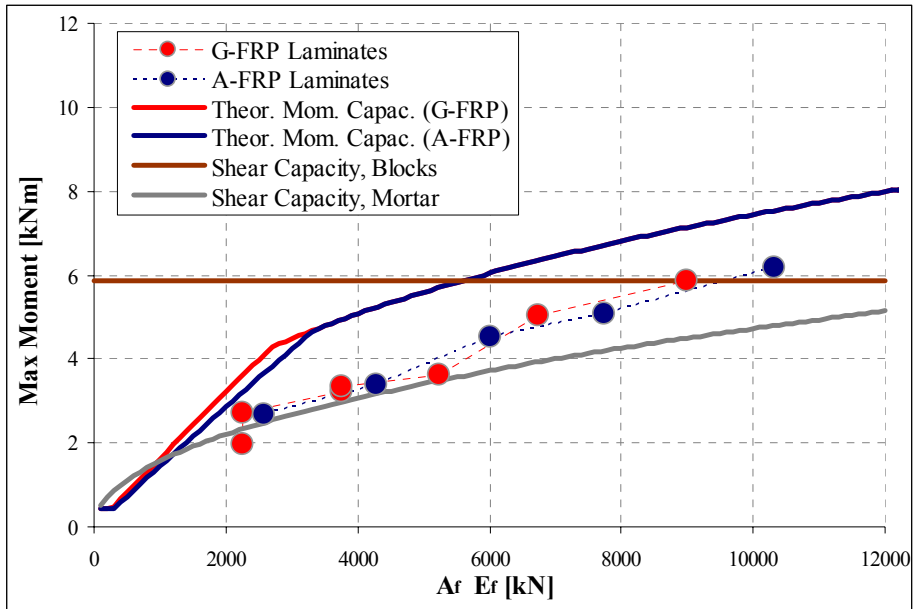


Figure 164 Theoretical Shear Capacity in the Mortar for the Concrete Walls + Sheets

### 5.8.4 Design Method

In this section a study in order to find new coefficients  $k_m$  (bond dependent coefficients) to complete the design method proposed by Tumialan, J.G., N. Galati, and A. Nanni (“FRP Strengthening of URM Walls Subject to Out-of-Plane Loads”) is reported. This method, at the moment the only one adopted by the ACI, proposes to study the reinforced masonry taking as benchmark the reinforcement ratio  $\omega_f$  (indicated also with  $\omega$ ), expressed as:

$$\omega = \frac{\rho_f E_f}{f'_m (h/t)}, \quad \text{or} \quad \omega = \frac{A_f E}{b \cdot t \cdot f'_m \cdot h/t};$$

where:

$$\rho_f = \frac{A_f}{b \cdot t} = \text{ratio of FRP flexural reinforcement}$$

$E_f$  = tensile modulus of elasticity

$f'_m$  = compressive strength of masonry

$(h/t)$  = slenderness ratio (wall height-to-walls thickness)

$\omega$  is an index that intends to capture the key parameters that influence the flexural capacity. These include the FRP flexural reinforcement ratio,  $\rho_f$ , the FRP tensile modulus of elasticity,  $E_f$ , the masonry compressive strength,  $f'_m$ , and the slenderness ratio  $h/t_m$ . This index is intended to represent the ratio of axial stiffness (cross sectional area  $\times$  modulus of elasticity) between FRP and masonry but since the modulus of elasticity of masonry  $E_m$  is directly proportional to  $f'_m$  the latter can replace  $E_m$ . The inclusion of the slenderness ratio  $h/t_m$  has been identified as influential in the out-of-plane behavior of masonry walls.  $h/t_m$  accounts for the ability of the masonry wall behavior to be controlled by flexural capacity rather than shear capacity.  $h/t_m$  and the required out-of-plane load to cause failure are inversely proportional; thus, as the slenderness ratio decreases, the out-of-plane load becomes larger. Since the strength is directly proportional to the compressive strength, then the slenderness ratio and the compressive strength are inversely proportional. Therefore, it is reasonable to express the relation between the compressive strength and the slenderness factor as a product.

Figures 165 through 167 plot the experimental over theoretical bending moments considering the proposed index  $\omega$ , in cases of this experimental program (figure 165), or with previous tests (figures 166 and 167). The theoretical maximum bending moments were calculated using the RC analysis explained in section 5.8.1. A comparison with the same graph but using this design method for the theoretical moment may be seen at the end of this section, figures 169 and 170.

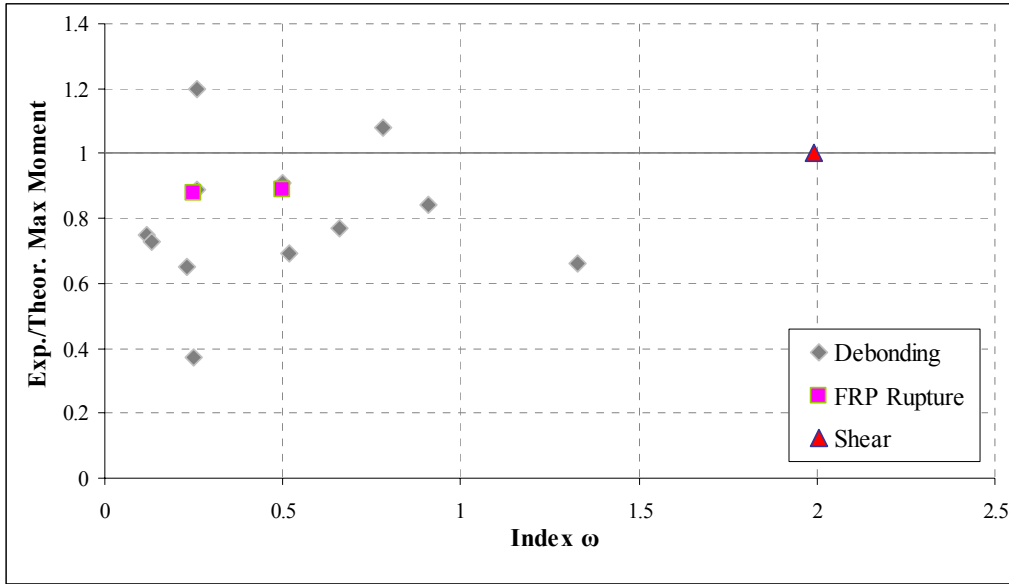


Figure 165 Validation of Design Approach

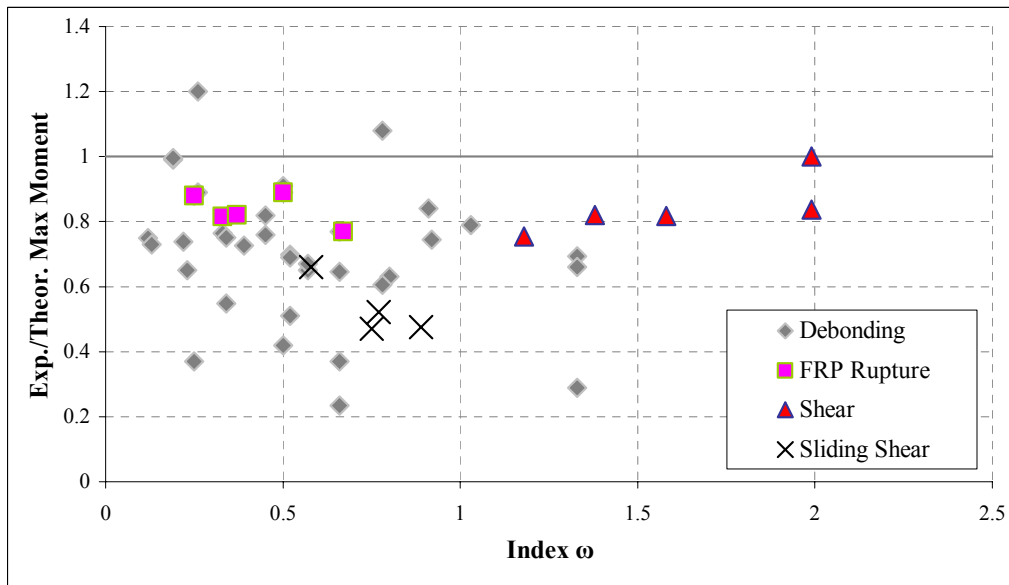


Figure 166 Kinds of Failure of Test of all the Experimental Programs, Considering the Parameter  $\omega$

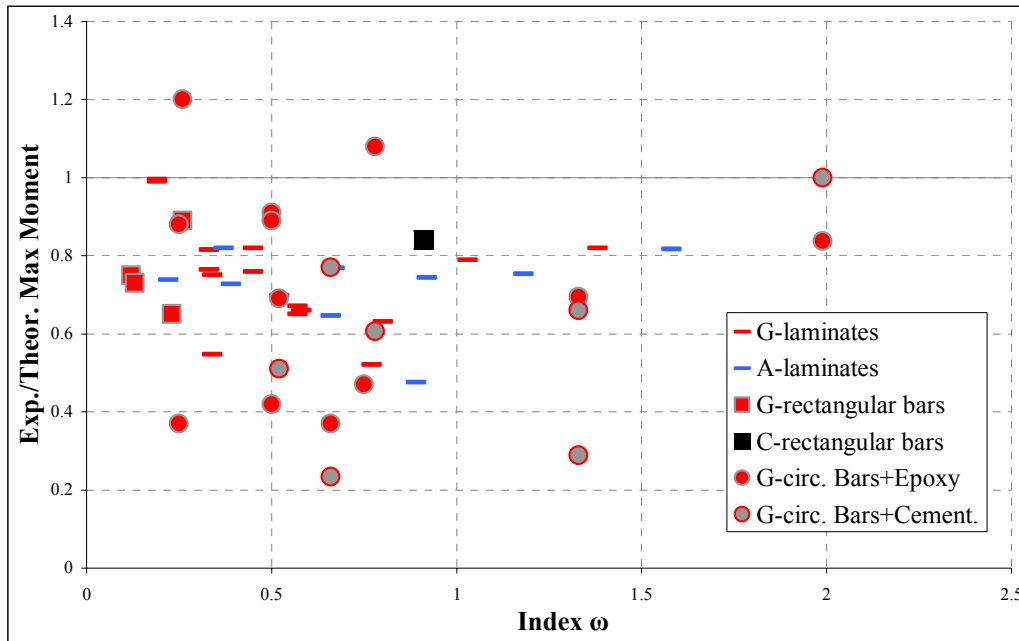


Figure 167 Experimental over Theoretical Maximum Moment Reached Ratio, of all the Tests, Considering the Parameter  $\omega$

The method adopts, as seen in section 5.8.1, the parabolic distribution for compressive stresses in the computation of the flexural capacity of the strengthened walls (like in the section 5.8.1), but some simplifications are assumed:

- the strains in the reinforcement and masonry are directly proportional to the distance from the neutral axis
- the tensile strength of masonry is neglected
- the FRP reinforcement has a linear elastic stress-strain relationship up to failure
- according to MSJC, the maximum usable compressed strain was considered to be 0.0035 mm/mm (in./in.) for clay masonry, and 0.0025 mm/mm (in./in.) for concrete masonry
- for simplicity, both  $\alpha$  and  $\beta$  were assumed to be 0.7
- since the flexural capacity is dependant of the strain developed in reinforcement, it was expressed the effective strain in the laminate,  $\epsilon_f$ , as the product  $k_m \epsilon_u$ , where  $k_m$  is the bond dependent coefficient and  $\epsilon_u$  is the design rupture strain of FRP. These considerations can be taken into account for the implementation of a design methodology
- to account for environmental attack  $\epsilon_u$  is multiplied by a environmental reduction factor  $C_E$ ; table 85 shows different values for  $C_E$  based on the relative durability of each fiber type to different exposure conditions as recommended by the ACI-440.

Table 85 Environmental Reduction Factor  $C_E$  for Various Fibers and Exposure Conditions

Exposure condition	Fiber type	Environmental reduction factor $C_E$
Concrete not exposed to earth and weather	Carbon	1.0
	Glass	0.8
	Aramid	0.9
Concrete exposed to earth and weather	Carbon	0.9
	Glass	0.7
	Aramid	0.8

Thus the Design Moment can be expressed with the following:

$$M = \omega \cdot \kappa_m \cdot C_E \cdot \varepsilon_u \left[ 1 - \frac{\omega \cdot \kappa_m \cdot C_E \cdot \varepsilon_u \cdot h/t}{0.5 \cdot \gamma} \right] b \cdot d^2 \cdot f'_m \cdot h/t$$



Figure 168 Specimen cob-C3-2b After the Failure

Previous researches suggested taking the parameter  $\omega$  ever less than 0.7 in order to avoid brittle failures. During this experimental program, even if  $\omega$  was greater than 1.3, the specimen cob-C3-2b, as shown in the figure above, yielded for debonding of one bar and not for shear like predicted by previous researches. Taking into consideration also the figure 164, it is judged preferable to check what proposed in sections 5.8.2 and 5.8.3 than limit index  $\omega$  to less than 0.7.

Figure 169 plots the experimental reached over the design moments without considering the contribution of safety factor  $\Phi$  (but considering the bond dependent coefficient  $k_m$  and the

environmental reduction factor  $C_E$  explained in table 85). Figure 170 plot the experimental reached moments over the design maximum moments considering the safety factor  $\Phi$ .

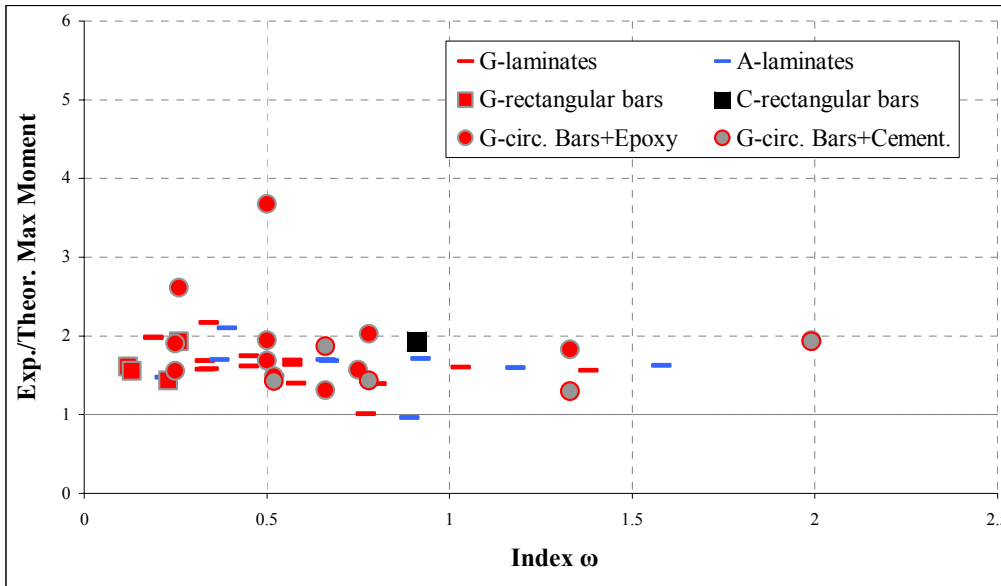


Figure 169 Design Method: Without Considering the Factor  $\Phi$

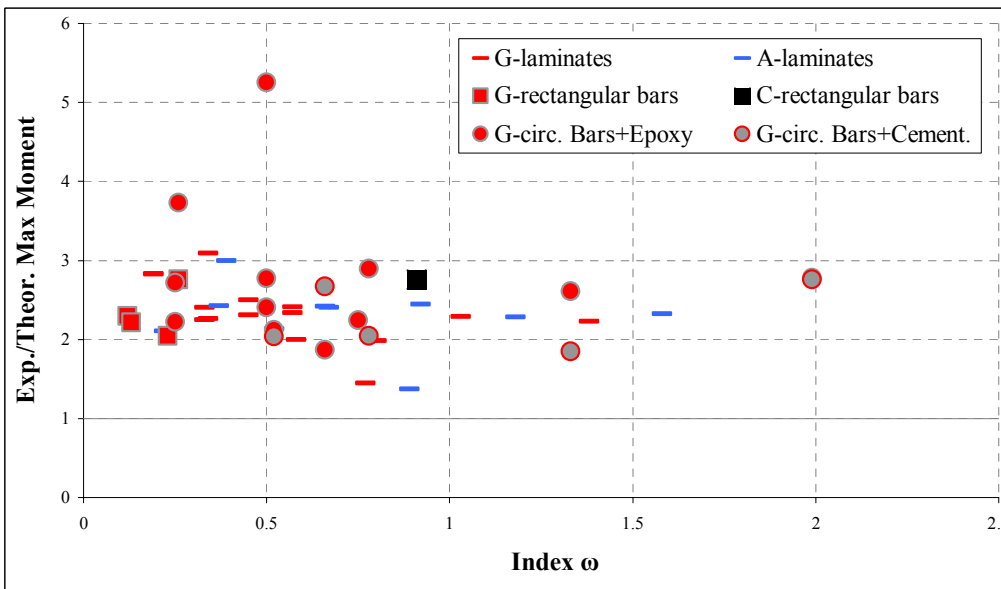


Figure 170 Design Method: Considering the Factor  $\Phi$

Computing the theoretical maximum moment in the previous two figures, it has been considered a environmental reduction factor  $C_E$  to be 0.8, and the bond dependent coefficients  $k_m$  like explained in the following table:

Table 86 Bond Dependent Coefficients  $k_m$  Used

		Clay Bricks	Concrete Blocks
A and G Laminates		0.65	0.45
G and C Tapes		0.6	0.6
G Rods + Epoxy P.	Good Grip*	n.d.	0.3
	Bed Grip		0.6
G Rods + Cem. Paste		n.d.	0.45

\* Bars displaced in a groove 2.25 times the rod diameter, so that the paste touches just the concrete block and not the mortar joint, or bars displaced just along the concrete blocks (i.e. specimens “-d”) are been considered with good grip.

The following tables (87 through 93) report for every wall tested (in this and in previous experimental programs) its index  $\omega$ , its design moment before and after the safety reduction factor  $\Phi$ , and the experimental over design moment ratio. The mean value of this ratio is 2.39, and the standard deviation 0.42. This assures us of the validation of this method.

Table 87 explains the method results for the rectangular bars: here there is good affinity with the experimental data and  $k_m$  may be safely assumed to be 0.6.

Table 87 Carbon and Glass FRP Tape

Wall	$\omega$	Design Moment [kN]		Exp. Mom. [kN]	Exp./Des. Moment
		$k_m=0.6$	$k_m=0.6$ $\Phi=0.7$		
<b>c11-gt-1</b>	0.12	1.34	0.94	2.16	<b>2.30</b>
<b>c11-gt-2</b>	0.23	2.55	1.79	3.66	<b>2.04</b>
<b>c12-ct-2</b>	0.91	3.03	2.12	5.86	<b>2.76</b>
<b>bcg-gt-1</b>	0.13	2.16	1.51	3.35	<b>2.22</b>
<b>bcg-gt-2</b>	0.26	4.16	2.91	8.03	<b>2.76</b>

For the circular bar + epoxy previous researches had given  $k_m = 0.3$ , it seems to be sometimes too conservative, especially with grooves 2.25 times the diameter or with the bar along just the blocks. Therefore it was chosen a  $k_m$  equal to 0.3 in case of bad adherence (small groove or groove along

the mortar joints, see table 88) and to 0.6 in case of good grip (groove 2.25 times the diameter deep or never running along the joints, see table 89).

Table 88 Glass-FRP Rods+Epoxy Paste

Wall	$\omega$	Design Moment [kN]		Exp. Mom. [kN]	Exp./Des. Moment
		$k_m=0.3$	$k_m=0.3$ $\Phi=0.7$		
<b>cob-E2-2</b>	0.50	1.00	0.70	1.69	<b>2.41</b>
<b>cob-E2-3</b>	0.75	1.45	1.02	2.27	<b>2.22</b>
cob-E2-1b	0.26	0.50	0.35	2.52	7.20
cob-E2-2b	0.52	0.96	0.48	2.64	5.50
cob-E2-3b	0.78	1.39	0.97	4.94	5.09
<b>cob-E3-1</b>	0.66	1.20	0.84	1.57	<b>1.87</b>
<b>cob-E3-2</b>	1.33	2.15	1.51	3.934	<b>2.61</b>
<b>cob-E3-3</b>	1.99	2.86	2.00	5.57	<b>2.79</b>
<b>cob-E2-1c</b>	0.25	0.52	0.36	0.65+0.16	<b>2.25</b>
<b>cob-E2-2c</b>	0.50	1.00	0.70	3.69	<b>5.27</b>
cob-E2-1d	0.25	0.52	0.36	1.91	5.31
cob-E2-2d	0.50	1.00	0.70	3.60	5.14

Table 89 Glass FRP Rods+Epoxy Based Paste with good Grip

Wall	$\omega$	Design Moment [kN]		Exp. Mom. [kN]	Exp./Des. Moment
		$k_m=0.6$	$k_m=0.6$ $\Phi=0.7$		
<b>cob-E2-1b</b>	0.26	0.96	0.675	2.52	<b>3.73</b>
<b>cob-E2-2b</b>	0.52	1.78	1.244	2.64	<b>2.12</b>
<b>cob-E2-3b</b>	0.78	2.44	1.707	4.94	<b>2.89</b>
<b>cob-E2-1d</b>	0.25	1.00	0.702	1.91	<b>2.72</b>
<b>cob-E2-2d</b>	0.50	1.85	1.298	3.60	<b>2.77</b>

Also for the circular bars embedded in groove with cementitious modified paste, previous researches had given  $k_m = 0.3$ , that was perhaps enough just restricting  $\omega$  to less than 0.7 (see table 90, specimen cob-C3-2). After these test we can suggest to not use small groove with this type of

paste, but to assure at least a groove 2.25 times the rod diameter deep. In this case it is possible and safe to use a bond dependent coefficients  $k_m$  equal to 0.45.

Table 90 Glass FRP Rods+Cementitious Paste

Wall	$\omega$	Design Moment [kN]		Exp. Mom. [kN]	Exp./Des. Moment
		$k_m=0.3$	$k_m=0.3$ $\Phi=0.7$		
cob-C2-2b	0.52	0.96	0.48	2.064	4.30
cob-C2-3b	0.78	1.39	0.97	2.928	3.02
<b>cob-C3-1</b>	0.66	1.20	0.84	0.994	<b>1.18</b>
<b>cob-C3-2</b>	1.33	2.15	1.51	1.637	<b>1.08</b>
cob-C3-1b	0.66	1.13	0.79	2.99	3.78
cob-C3-2b	1.33	2.01	1.41	3.43	2.43
cob-C3-3b	1.99	2.65	1.85	6.07	3.28

Table 91 larger  $k_m$  for G-FRP Rods+ Cementitious Paste with good Grip

Wall	$\omega$	Design Moment [kN]		Exp. Mom. [kN]	Exp./Des. Moment
		$k_m=0.45$	$k_m=0.45$ $\Phi=0.7$		
<b>cob-C2-2b</b>	0.52	1.45	1.01	2.064	<b>2.04</b>
<b>cob-C2-3b</b>	0.78	2.04	1.43	2.928	<b>2.05</b>
<b>cob-C3-1b</b>	0.66	1.60	1.12	2.99	<b>2.67</b>
<b>cob-C3-2b</b>	1.33	2.65	1.84	3.43	<b>1.86</b>
<b>cob-C3-3b</b>	1.99	3.15	2.20	6.07	<b>2.76</b>

Tables 92 and 93 summarize the previous results obtained with the laminates. Here the difference between the coefficients for two kinds of block used depends if the surfaces are puttied and smooth.

Table 92 Glass and Aramid FRP Laminates on Concrete Blocks

Wall	$\omega$	Design Moment [kN]		Exp. Mom. [kN]	Exp./Des. Moment
		$k_m=0.45$	$k_m=0.45$ $\Phi=0.7$		
<b>cob-gl-3</b>	0.34	1.25	0.88	1.98	<b>2.25</b>
<b>cob-gl-3r</b>	0.34	1.25	0.88	2.71	<b>3.08</b>
<b>cob-gl-5</b>	0.57	1.97	1.38	3.23	<b>2.34</b>

Wall	$\omega$	Design Moment [kN]		Exp. Mom. [kN]	Exp./Des. Moment
		$k_m=0.45$	$k_m=0.45$ $\Phi=0.7$		
<b>cob-gl-5r</b>	0.57	1.97	1.38	3.33	<b>2.41</b>
<b>cob-gl-7</b>	0.80	2.60	1.82	3.61	<b>1.98</b>
<b>cob-gl-9</b>	1.03	3.13	2.19	5.02	<b>2.29</b>
<b>cob-gl-12</b>	1.38	3.76	2.63	5.86	<b>2.23</b>
<b>cob-al-3</b>	0.39	1.27	0.89	2.67	<b>3.00</b>
<b>cob-al-5</b>	0.66	2.00	1.40	3.39	<b>2.42</b>
<b>cob-al-7</b>	0.92	2.63	1.84	4.51	<b>2.45</b>
<b>cob-al-9</b>	1.18	3.17	2.22	5.07	<b>2.28</b>
<b>cob-al-12</b>	1.58	3.80	2.66	6.17	<b>2.32</b>

Table 93 Glass and Aramid FRP Laminates on Clay Bricks

Wall	$\omega$	Design Moment [kN]		Exp. Mom. [kN]	Exp./Des. Moment
		$k_m=0.65$	$k_m=0.65$ $\Phi=0.7$		
<b>cl2-gl-3</b>	0.19	1.84	1.28	3.63	<b>2.84</b>
<b>cl2-gl-3r</b>	0.19	1.84	1.28	3.64	<b>2.84</b>
<b>cl2-gl-5</b>	0.33	2.92	2.05	4.61	<b>2.25</b>
<b>cl2-gl-5r</b>	0.33	2.92	2.05	4.92	<b>2.40</b>
<b>cl2-gl-7</b>	0.45	3.90	2.73	6.31	<b>2.31</b>
<b>cl2-gl-7r</b>	0.45	3.90	2.73	6.82	<b>2.50</b>
<b>cl2-gl-9</b>	0.58	4.77	3.34	6.67	<b>2.00</b>
<b>cl2-gl-12</b>	0.77	5.87	4.11	5.94	<b>1.45</b>
<b>cl2-al-3</b>	0.22	1.87	1.31	2.75	<b>2.10</b>
<b>cl2-al-5</b>	0.37	2.97	2.08	5.04	<b>2.42</b>
<b>cl2-al-7</b>	0.52	3.96	2.71	5.92	<b>2.18</b>
<b>cl2-al-9</b>	0.67	4.84	3.89	8.15	<b>2.10</b>
<b>cl2-al-12</b>	0.89	5.94	4.16	5.72	<b>1.38</b>

## 5.9 PRELIMINARY CONCLUSIONS

The following conclusions can be drawn from this part of the experimental program:

- Flexural strengthening with FRP bars using the NSM technique has been proven to remarkably increase of flexural capacity (up to 26 times) the strength and the pseudo-ductility of URM walls.
- Rectangular bars have proved themselves to be a very good system; their limit is represented by the thickness of the masonry's blocks: by using a tape 15 mm wide, a minimum thick of the masonry of 28-30 mm was requested.
- Latex modified cementitious paste-GFRP rod system has good performances when the size of the groove is approximately 2.25-2.5 times the diameter. A smaller groove size is unadvisable. When latex cementitious paste is the filling material, the increase in amount of FRP does not seem to affect the stiffness: the curves of the load vs. deflection graph are almost parallel when the cross section is cracked. This issue could be addressed to low bond between GFRP rods and repair mortar.
- When epoxy paste is the filling material, an appreciable improvement is obtained by using a greater groove, but loading causes an irregular behavior in terms of stiffness. Then we think this more invasive and expensive operation be not justified.
- Debonding is the predominant mode of failure. When the adherence is improved avoiding mounting the bars in the mortar joints, it has been observed FRP rupture. Shear failure has been observed when large amount of reinforcement was used.
- The flexural behavior of the strengthened masonry seems to be well decrypted by the RC members' analysis. It seems to be valid whether in case of concrete block walls or in case of clay brick walls.
- The shear capacity seems to be greater than what estimated by the previous researches; it may be estimated by the RC-members formula.
- The sliding-shear capacity is well estimated by the Mohr-Coulomb law. Also if an arch-effect, observable in reality, increases this capacity, a check in this way during the design is desirable.
- New coefficients  $k_m$  have been computed for the design method. They have proved themselves to be safe and reasonable.



## 6. CONCLUSIONS AND FUTURE WORKS

This experimental program probed the effectiveness and the benefits of using the NSM rods technique for strengthening URM masonry walls. The reinforced masonry walls showed an increase of strength and ductility: the capacity increased by a factor of 2-3 in the case of shear strengthening and by a factor of 4.5-26 in the case of flexural strengthening.

A wide range of materials have been used in these tests, than the results can be considered well represented. The Glass FRP, in spite of its low elastic modulus, has proved to be a good material in the masonry strengthening: often the performances were better than those obtained by the Carbon FRP.

### SHEAR STRENGTHENING

Shear tests have demonstrated that FRP systems can be good shera-reinforcements in URM masonry, and the analytical model adopted has proved its validity. But we believe there is a limit in this kind of test frame, and regarding previous tests the analytical model proved to be fallacious. We suggest more future tests on better frames or in situ. Then, it should be taken into consideration to reinforce both sides of the masonry with a concrete frame around: as a matter of fact behavior of the infill walls in the presence of the surrounding structural elements (i.e. beams and columns) needs to be studied. This is because the effectiveness of the strengthening may be dangerously overestimated due to premature failures in the masonry or structural elements.

### FLEXURAL STRENGTHENING

Flexural tests have proved to be valid both for the test frame used and for the regularity in terms of results; besides the analytical model adopted it is believed satisfactory. New coefficients  $k$  have been computed for the design method: they have proved themselves to be safe and reasonable. The advice to limit the index  $\omega$  to less than 0.7 is not considered adequate. It is preferable and suggested, until other tests will have better clarify the sliding-shear phenomenon through in situ tests, to check both the design maximum moment proposed in section 5.8.4 and the formulas proposed in sections 5.8.2 (shear) and 5.8.3 (sliding-shear).

More tests for the moment are not believed indispensable, with the same test frame. In case, since strength depends even on the bond between the masonry blocks, walls built with different and representative types of masonry units may be investigated.

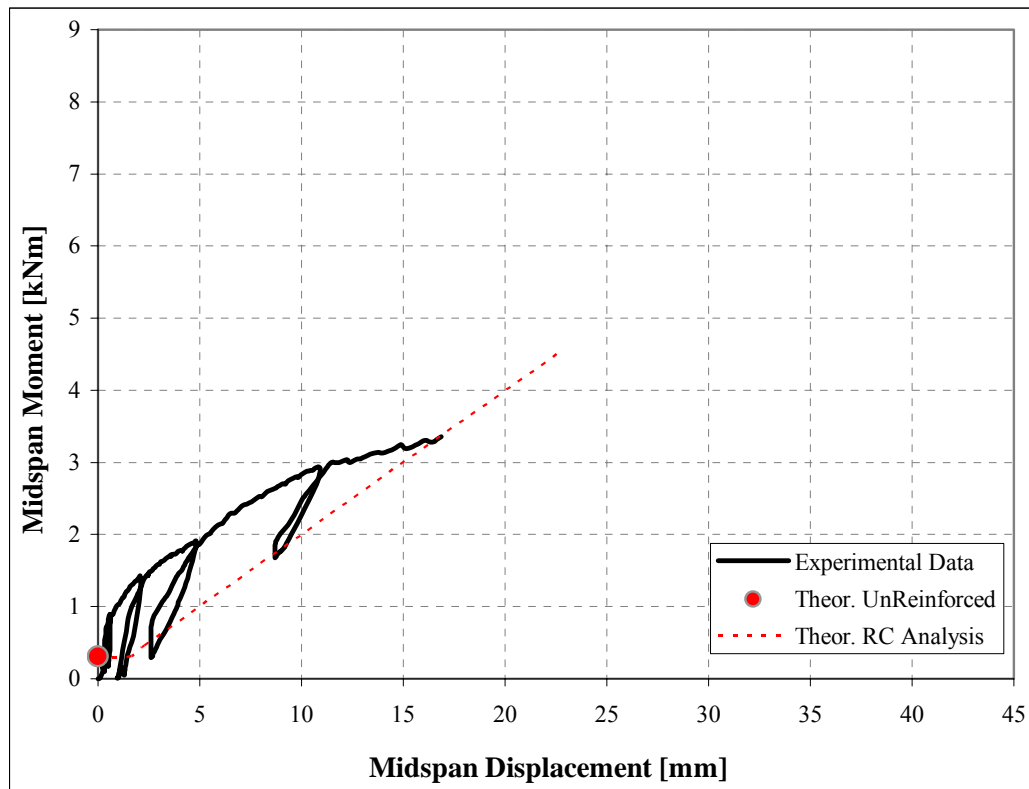


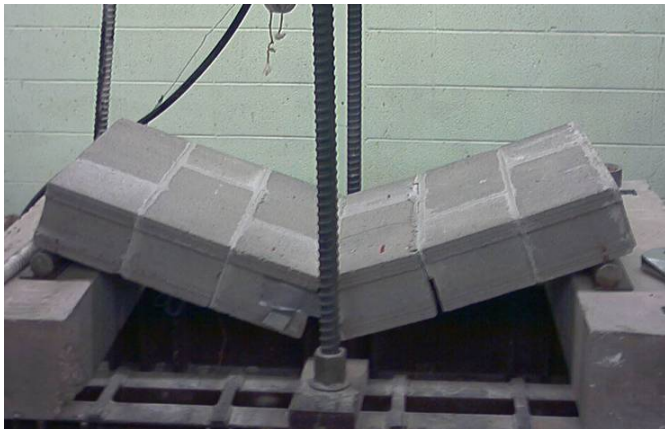
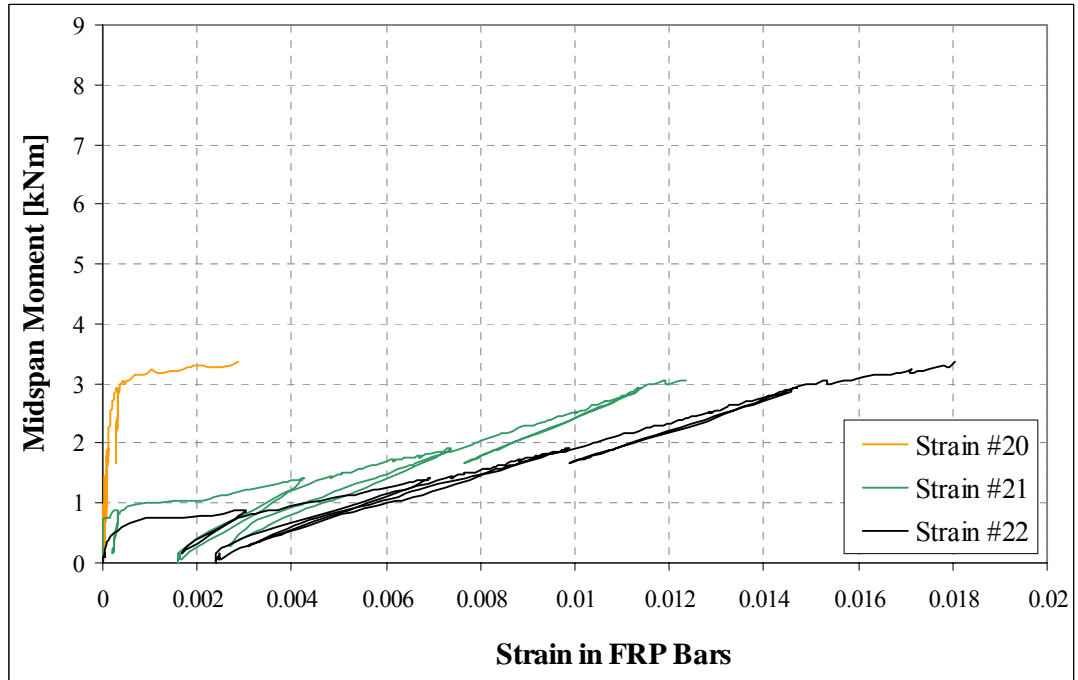
## APPENDIX A: Out-of-Plane Test Results

This appendix presents, for every specimen tested under out-of-plane loads, a summarizing table of results, the midspan moment vs. midspan displacement graph, the midspan moment vs. experimental strain in the reinforcement graph, and some pictures of the wall during or after the test. The table presents in the upper part the experimental recorded results (P was recorded by a load cell, M is estimated to be  $(P/2)/18\text{in}$ , V is estimated to be P/2) and the analytical situation at experimental failure (ACI – RC parabolic  $f_c (e_c)$ ); the second part of the table presents the ultimate theoretical moment (specifying if the collapse would be due to the concrete or to the FRP) and the ratio experimental recorded / theoretical moment.

**bcg-gt-1:**

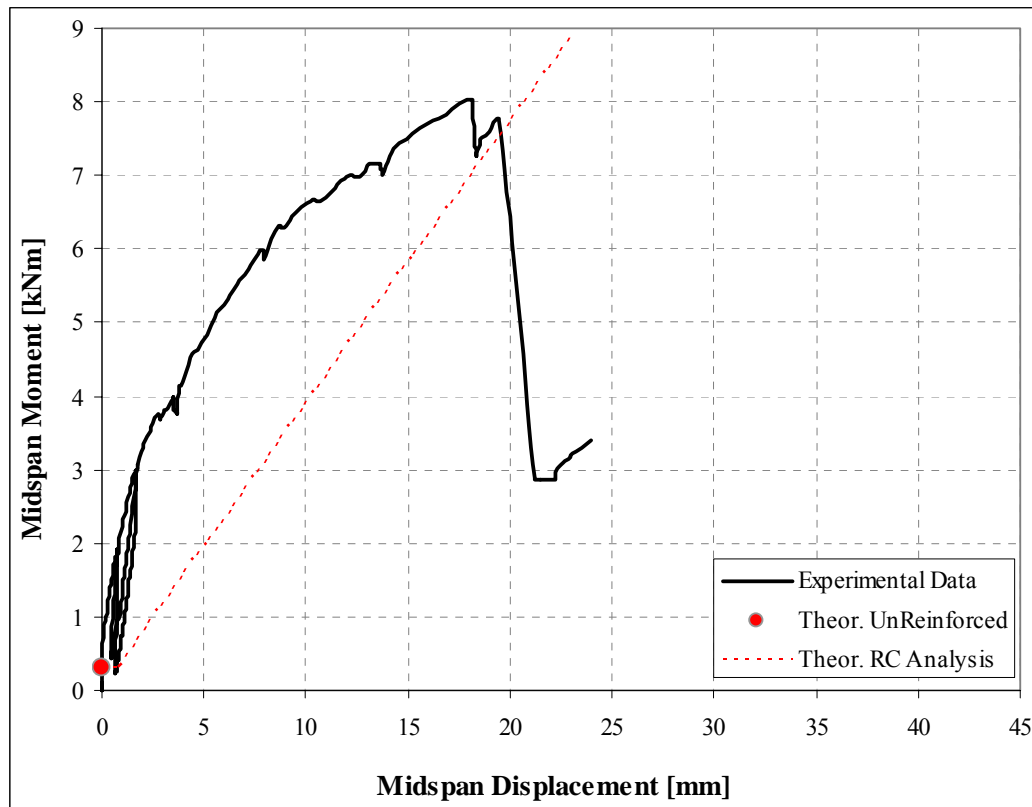
<b>bcg-gt-1</b> As=31.3mm <sup>2</sup> f <sub>c</sub> =16.74MPa	P-failure-exp [kN] =	<b>14.67</b>	M-fail [kNm]	<b>3.35</b>	V-fail [kN]=	<b>7.3</b>
	failure mode	<i>debonding (bar sl.)</i>	<i>theor. ε - c - f - ε/ε<sub>u</sub> at failure</i>	<i>ε<sub>c</sub> = 0.00092</i>	<i>ε<sub>f</sub> = 0.0183</i>	<i>f<sub>f</sub> = 805 MPa</i>
Max theor. Moment [kNm]		<b>4.58</b>	ε <sub>f</sub> = 0.025	ε <sub>c</sub> = 0.0013	M <sub>exp</sub> /M <sub>theor.</sub>	<b>0.73</b>

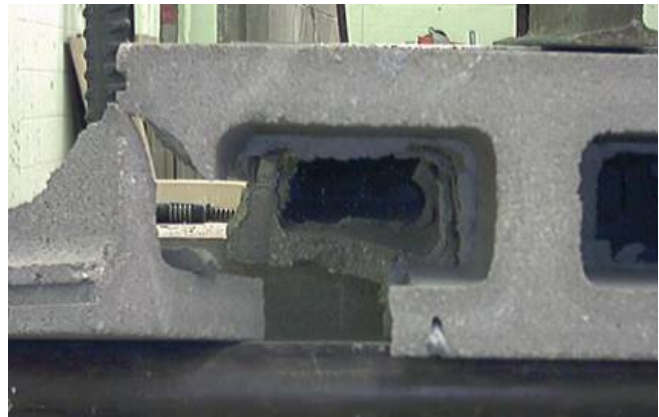
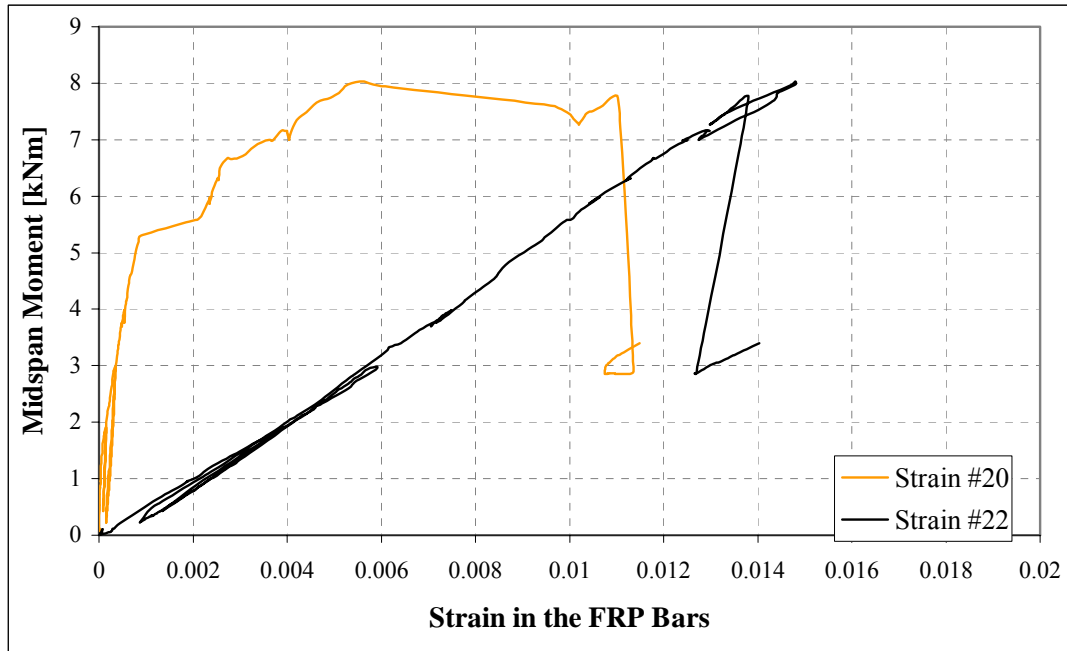




**bcg-gt-2:**

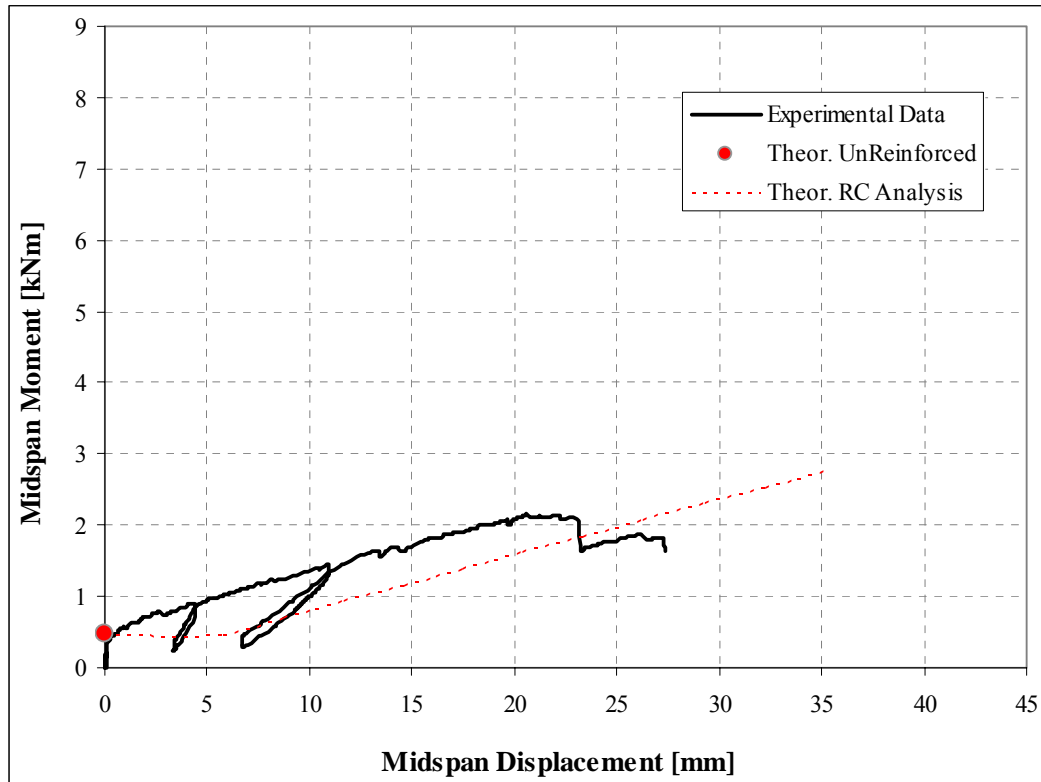
<b>bcg-gt-2</b> As=62.6mm <sup>2</sup> f <sub>c</sub> =16.74MPa	P-failure-exp [kN] =	<b>35.1</b>	M-fail [kNm]	<b>8.03</b>	V-fail [kN]=	<b>17.5</b>
	failure mode	<i>debonding (brick col.)</i>	<i>theor. <math>\epsilon - c - f - \epsilon/\epsilon_u</math> at failure</i>	$\epsilon_c = 0.00174$ $f_f = 974 \text{ MPa}$	$\epsilon_f = 0.0221$ $\epsilon/\epsilon_u = 0.88$	
Max theor. Moment [kNm]		<b>9.05</b>	$\epsilon_f = 0.025$	$\epsilon_c = 0.0020$	M <sub>exp</sub> /M <sub>theor.</sub>	<b>0.89</b>

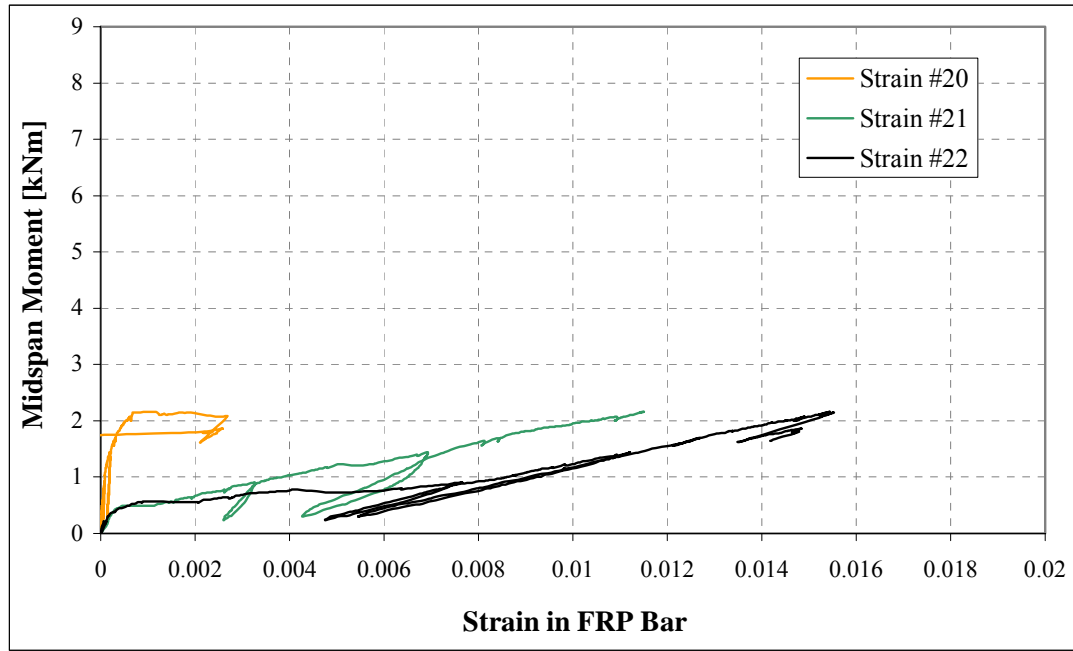




**cl1-gt-1:**

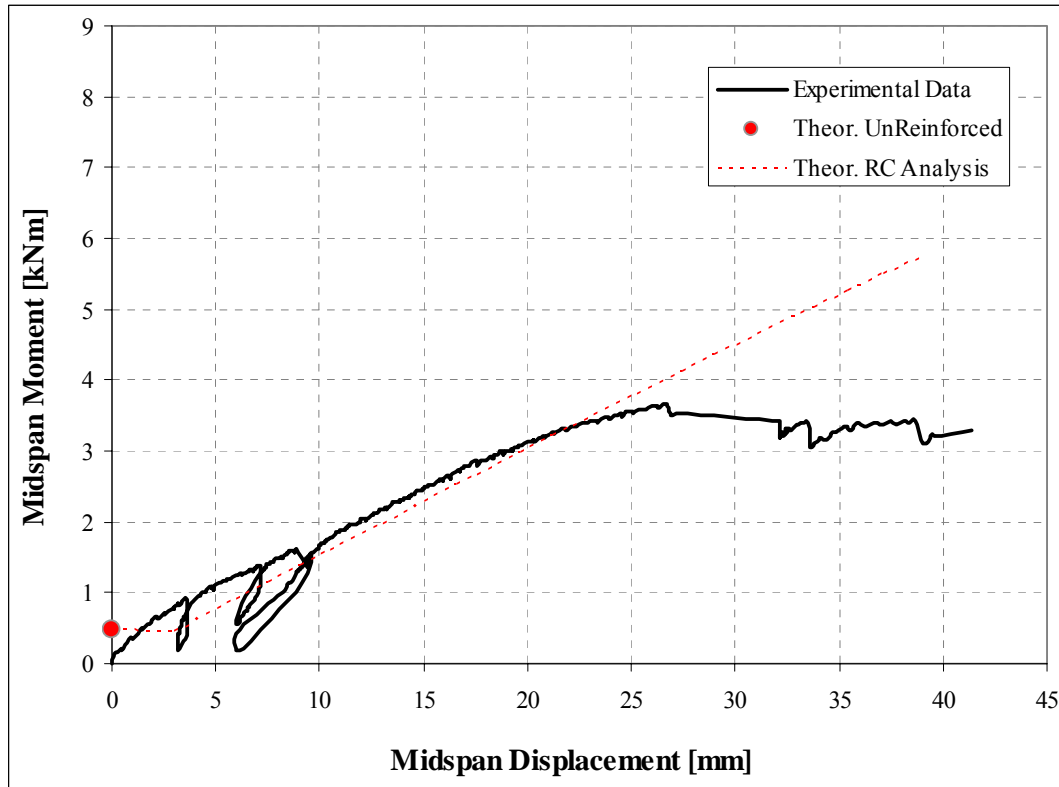
<b>cl1-gt-1</b> $A_s=31.3\text{mm}^2$ $f'_c=17.23\text{MPa}$	P-failure-exp [kN] =	<b>9.43</b>	M-fail [kNm]	<b>2.16</b>	V-fail [kN]=	<b>4.72</b>
	failure mode	<i>debonding (brick col.)</i>	<i>theor. <math>\epsilon - c - f - \epsilon/\epsilon_u</math> at failure</i>	$\epsilon_c = 0.00113$ $f_f = 825 \text{ MPa}$	$\epsilon_f = 0.01874$ $\epsilon/\epsilon_u = 0.75$	
Max theor. Moment [kNm]		<b>2.88</b>	$\epsilon_f = 0.025$	$\epsilon_c = 0.0016$	$M_{\text{exp}}/M_{\text{theor.}}$	<b>0.75</b>

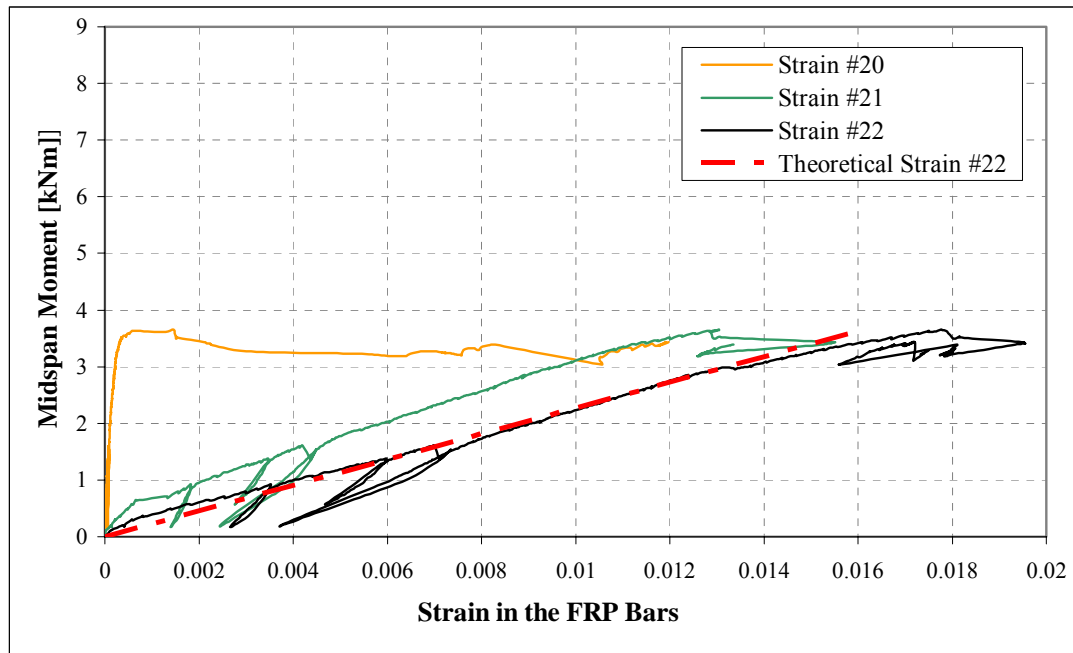




**cl1-gt-2:**

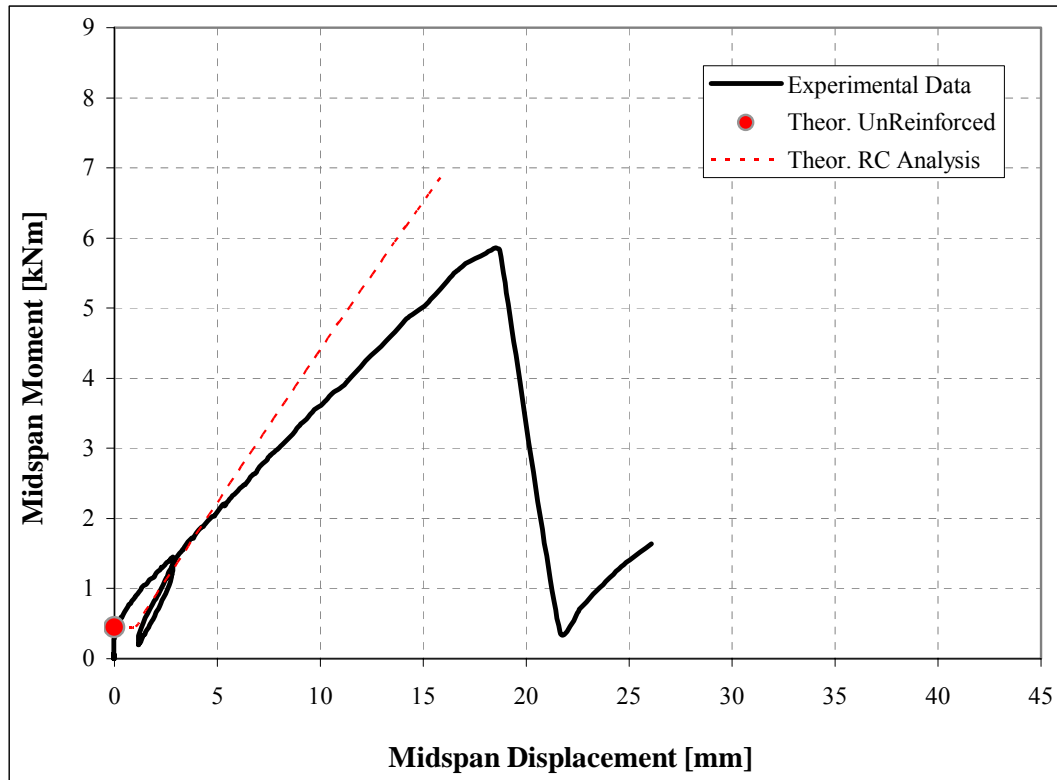
<b>cl1-gt-2</b> As=62.6mm <sup>2</sup> f <sub>c</sub> =17.23MPa	P-failure-exp [kN]=	<b>16.0</b>	M-fail [kNm]	<b>3.66</b>	V-fail [kN]=	<b>8.0</b>
	failure mode	<i>debonding (bar sl.)</i>	<i>theor. <math>\epsilon - c - f -</math> <math>\epsilon/\epsilon_u</math> at failure</i>	$\epsilon_c = 0.00143$ $f_f = 705 \text{ MPa}$	$\epsilon_f = 0.0161$ $\epsilon/\epsilon_u = 0.65$	
Max theor. Moment [kNm]		<b>5.66</b>	$\epsilon_f = 0.025$	$\epsilon_c = 0.0026$	M <sub>exp</sub> /M <sub>theor.</sub>	<b>0.65</b>

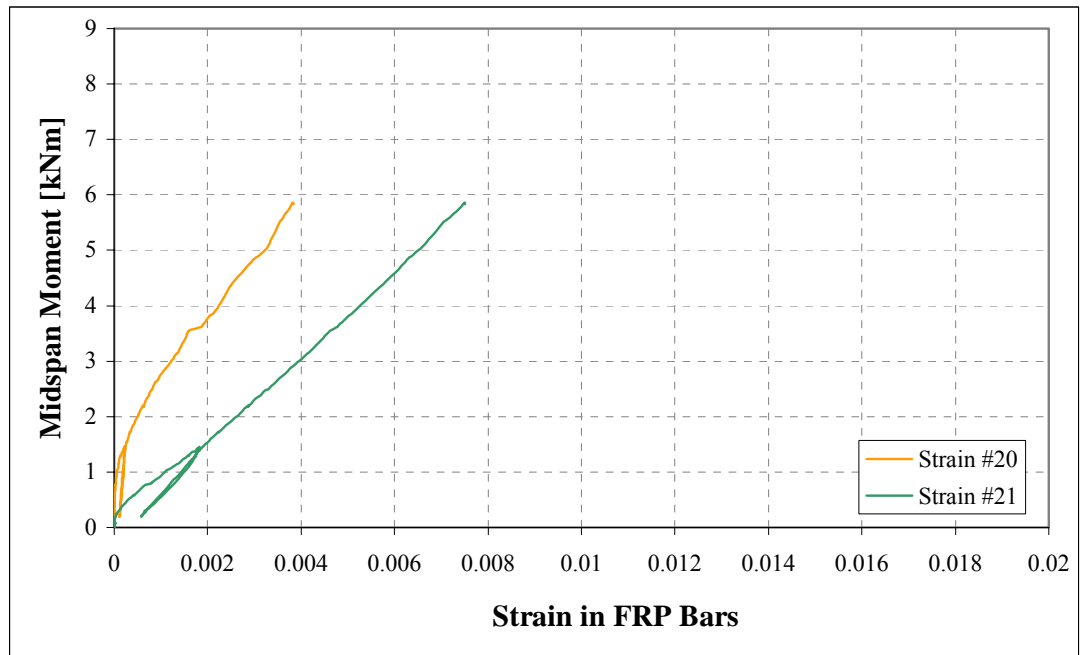




**cl2-ct-2:**

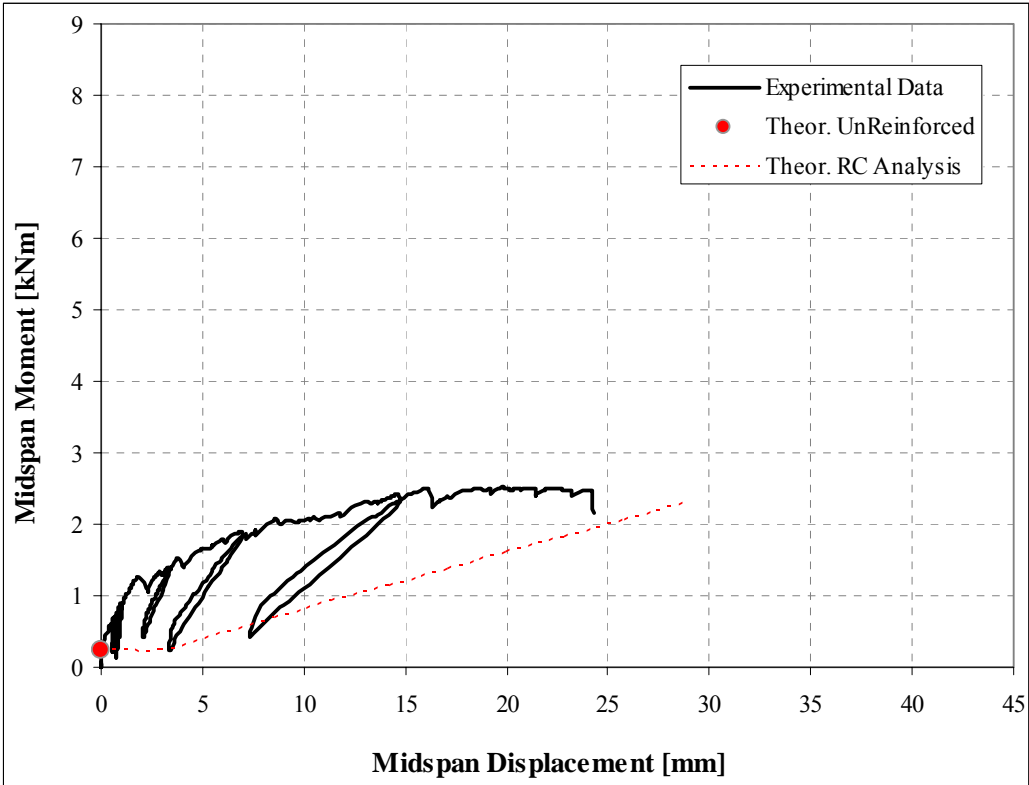
<b>cl2-ct-2</b> As=62.0mm <sup>2</sup> f <sub>c</sub> =15.74 MPa	P-failure-exp [kN] =	<b>25.62</b>	M-fail [kNm]	<b>5.86</b>	V-fail [kN]=	<b>12.8</b>
	failure mode	<i>debonding (bar sl.)</i>	<i>theor. <math>\epsilon - c - f - \epsilon/\epsilon_u</math> at failure</i>	<i><math>\epsilon_c = 0.00154</math></i>	<i><math>\epsilon_f = 0.0082</math></i>	<i><math>f_f = 1172 \text{ MPa}</math></i>
Max theor. Moment [kNm]		<b>6.954</b>	$\epsilon_f = 0.0098$	$\epsilon_c = 0.0019$	M <sub>exp</sub> /M <sub>theor.</sub>	<b>0.84</b>

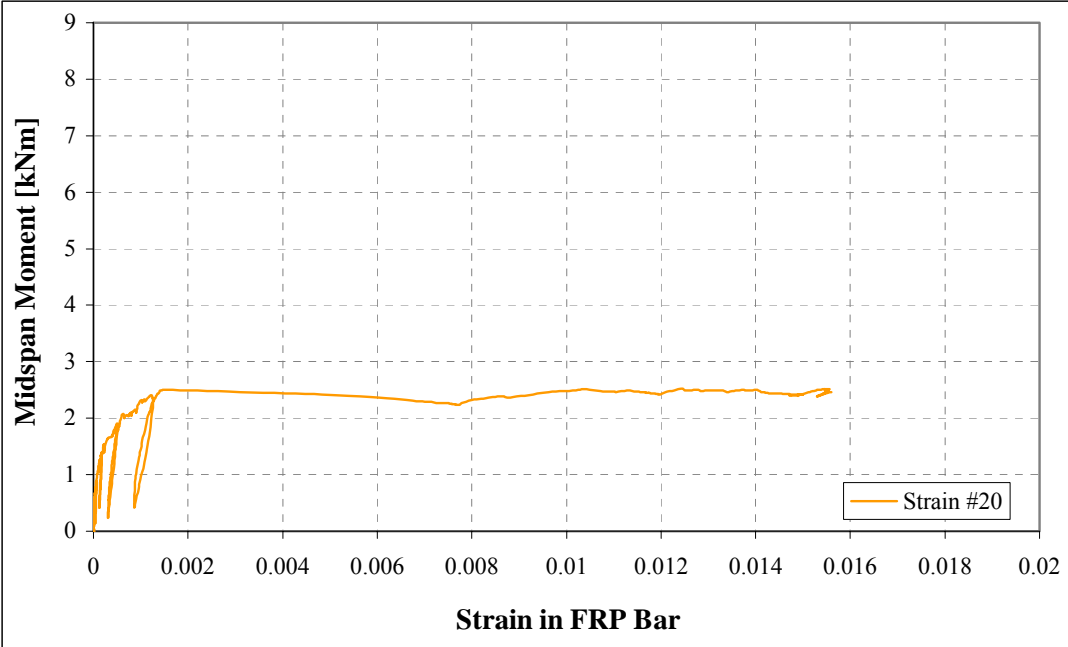




**cob-E2-1b:**

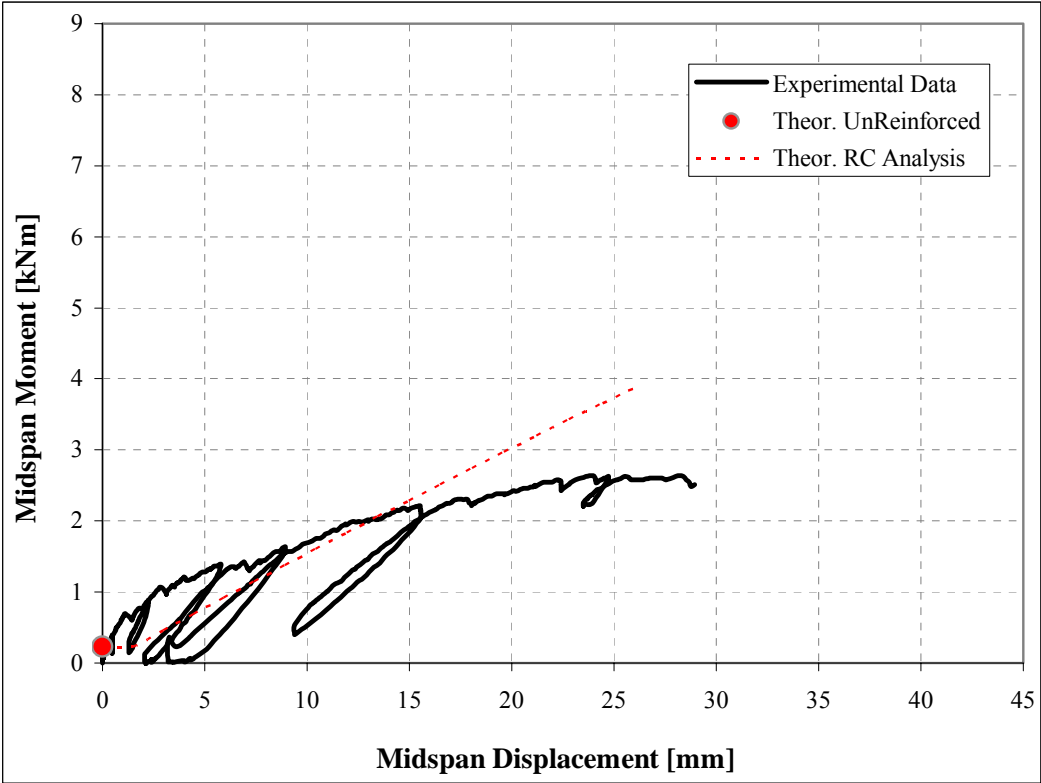
<b>cob-E2-1b</b> As=33.2mm <sup>2</sup> f <sub>c</sub> =9.74MPa	P-failure-exp [kN] =	<b>11.03</b>	M-fail [kNm]	<b>2.52</b>	V-fail [kN]=	<b>5.51</b>
	failure mode	<i>debonding</i>	theor. $\epsilon - c - f -$ $\epsilon/\epsilon_u$ at failure	$\epsilon_c = 0.00212$ $f_f = 943 \text{ MPa}$	$\epsilon_f = 0.0205$ $\epsilon/\epsilon_u = 1.20$	
Max theor. Moment [kNm]		<b>2.10</b>	$\epsilon_f = 0.017$	$\epsilon_c = 0.0017$	M <sub>exp</sub> /M <sub>theor.</sub>	<b>1.20</b>

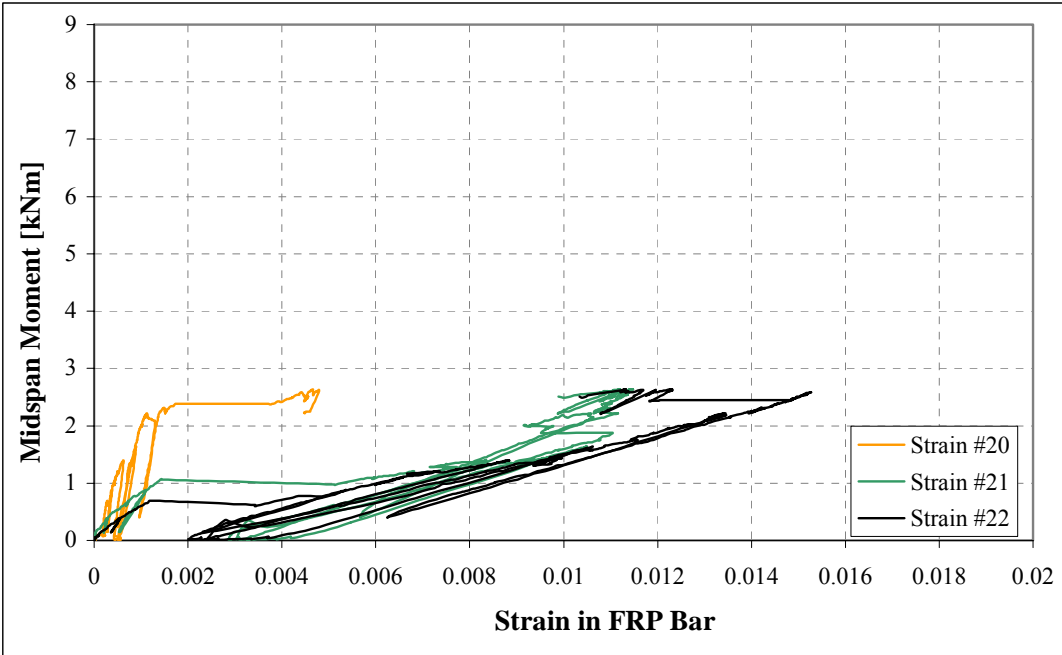




**cob-E2-2b:**

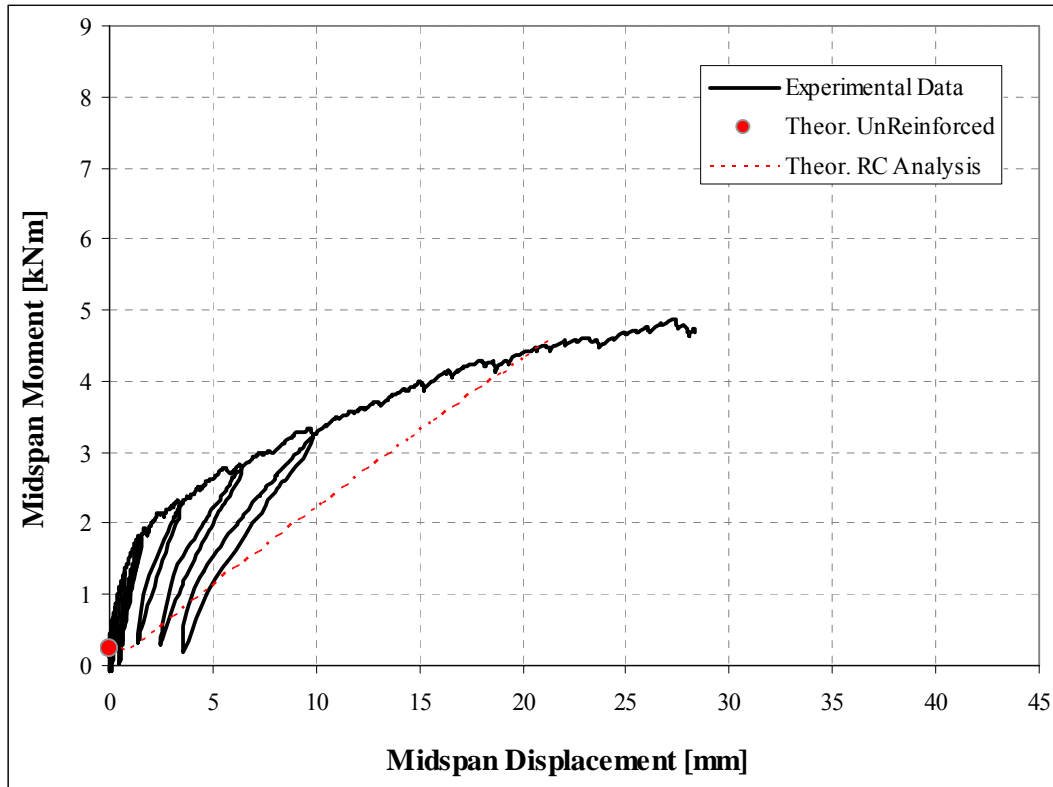
<b>cob-E2-2b</b> As=66.5mm <sup>2</sup> f <sub>c</sub> =9.74MPa	P-failure-exp [kN] =	<b>11.54</b>	M-fail [kNm]	<b>2.64</b>	V-fail [kN]=	<b>5.77</b>
	failure mode	<i>debonding</i>	theor. $\epsilon - c - f - \epsilon/\epsilon_u$ at failure	$\epsilon_c = 0.00149$ $f_f = 498 \text{ MPa}$	$\epsilon_f = 0.0108$ $\epsilon/\epsilon_u = 0.64$	
Max theor. Moment [kNm]	<b>3.83</b>	$\epsilon_f = 0.016$	$\epsilon_c = 0.0025$	$M_{exp}/M_{theor.}$	<b>0.69</b>	

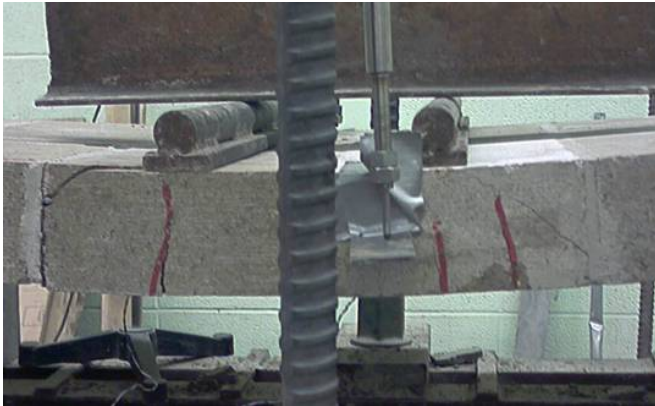
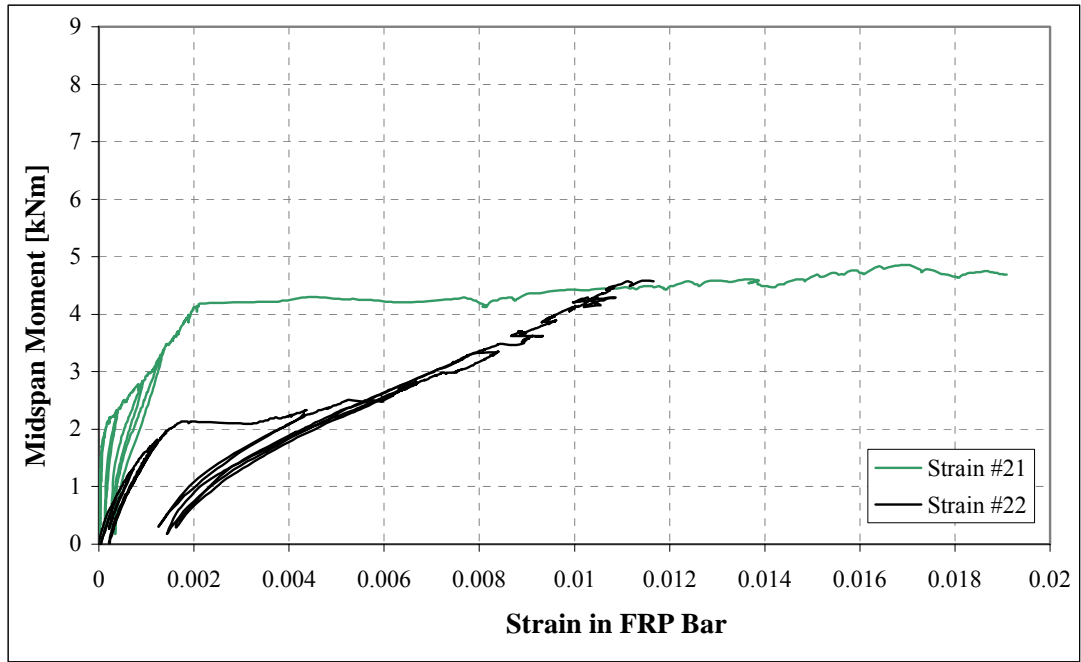




**cob-E2-3b:**

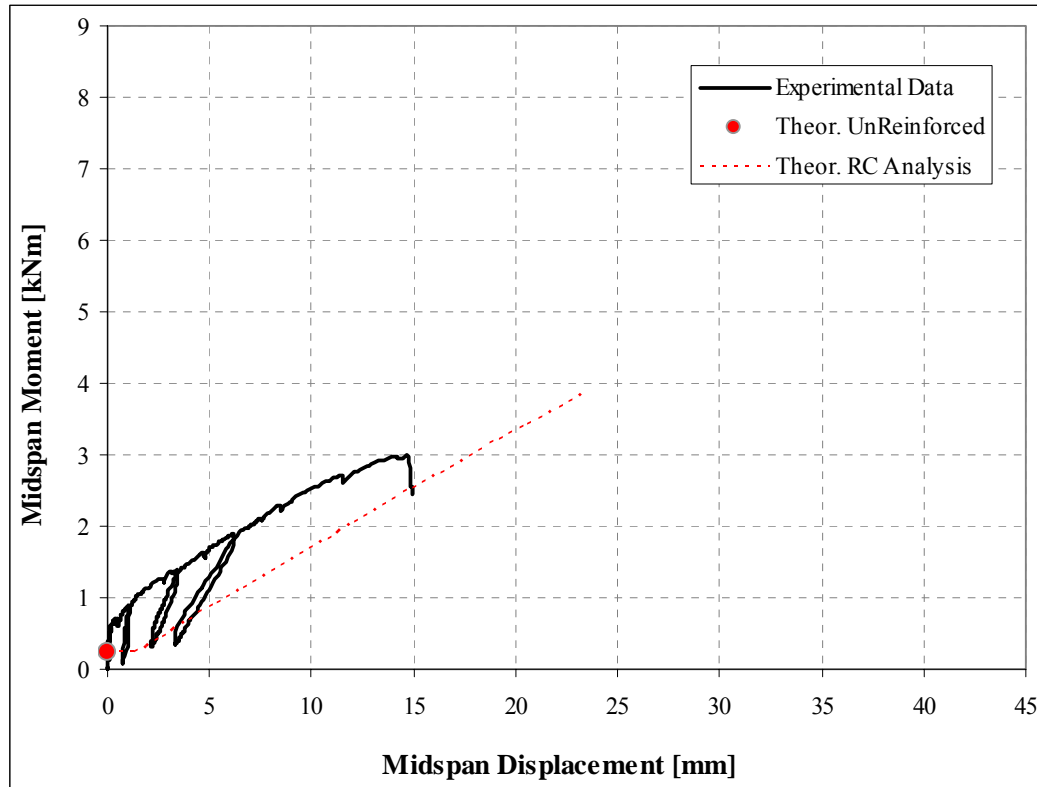
<b>cob-E2-3b</b> As=99.7mm <sup>2</sup> f <sub>c</sub> =9.74MPa	P-failure-exp [kN]=	<b>21.6</b>	M-fail [kNm]	<b>4.94</b>	V-fail [kN]=	<b>10.8</b>
	failure mode	<i>debonding- flex.fail</i>	<i>theor. ε - c - f - ε/ε<sub>u</sub> at failure</i>	<i>ε<sub>c</sub> = 0.00294</i>	<i>ε<sub>f</sub> = 0.0139</i>	<i>f<sub>f</sub> = 640 MPa</i>
Max theor. Moment [kNm]		<b>4.56</b>	ε <sub>f</sub> = 0.013	ε <sub>c</sub> = 0.0025	M <sub>exp</sub> /M <sub>theor.</sub>	<b>1.08</b>

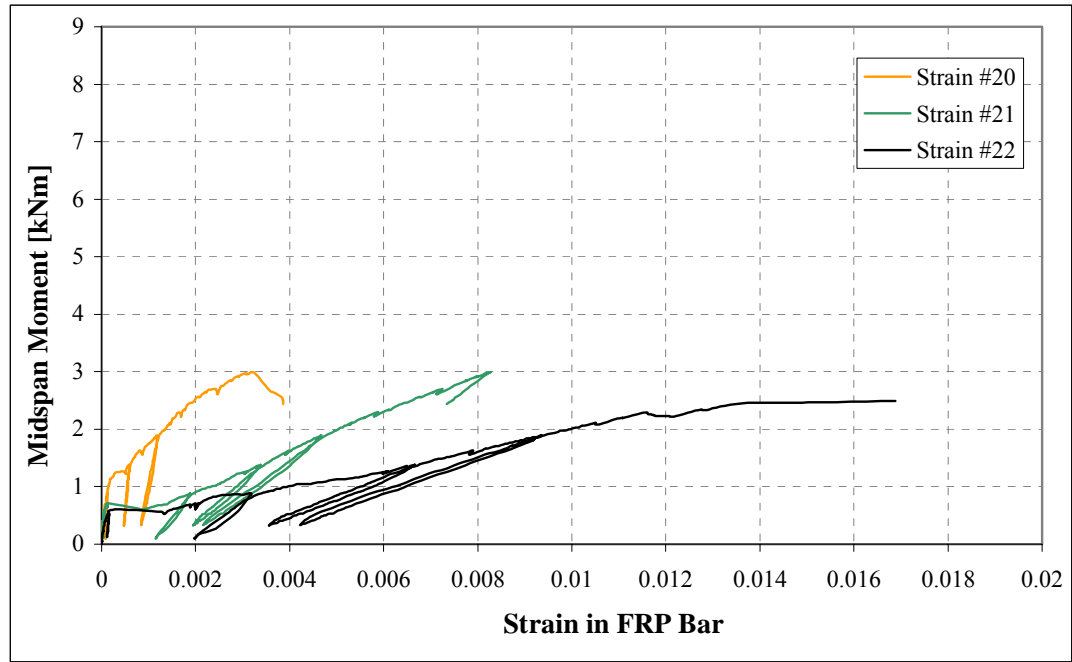




**cob-C3-1b:**

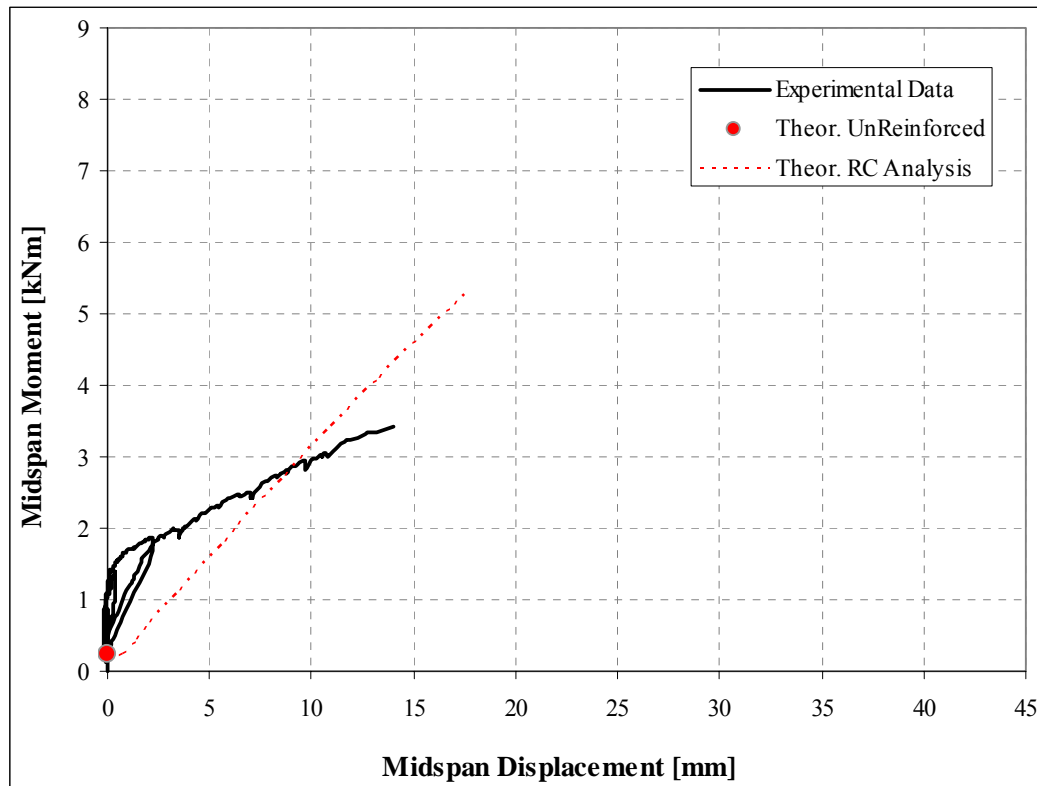
<b>cob-C3-1b</b> As=84.3mm <sup>2</sup> f <sub>c</sub> =9.74MPa	P-failure-exp [kN] =	<b>13.08</b>	M-fail [kNm]	<b>2.99</b>	V-fail [kN]=	<b>6.50</b>
	failure mode	<i>debonding</i>	theor. $\epsilon - c - f - \epsilon/\epsilon_u$ at failure	$\epsilon_c = 0.00170$ f <sub>f</sub> = 474 MPa	$\epsilon_f = 0.0103$ $\epsilon/\epsilon_u = 0.61$	
Max theor. Moment [kNm]		<b>3.893</b>	$\epsilon_f = 0.0135$	$\epsilon_c = 0.0025$	M <sub>exp</sub> /M <sub>theor.</sub>	<b>0.77</b>

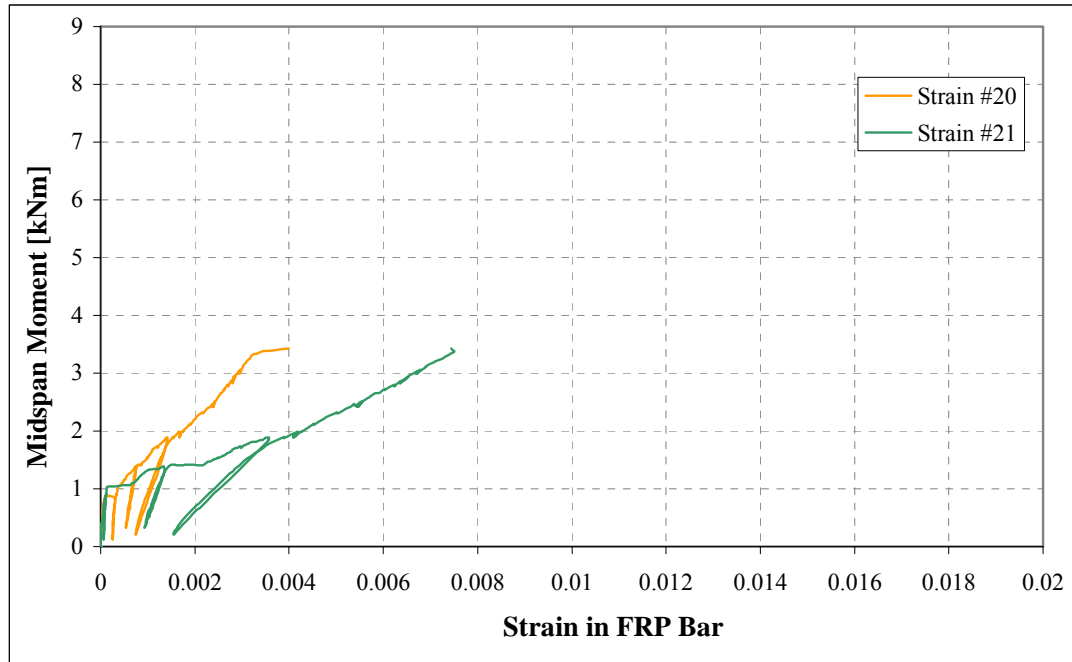




**cob-C3-2b:**

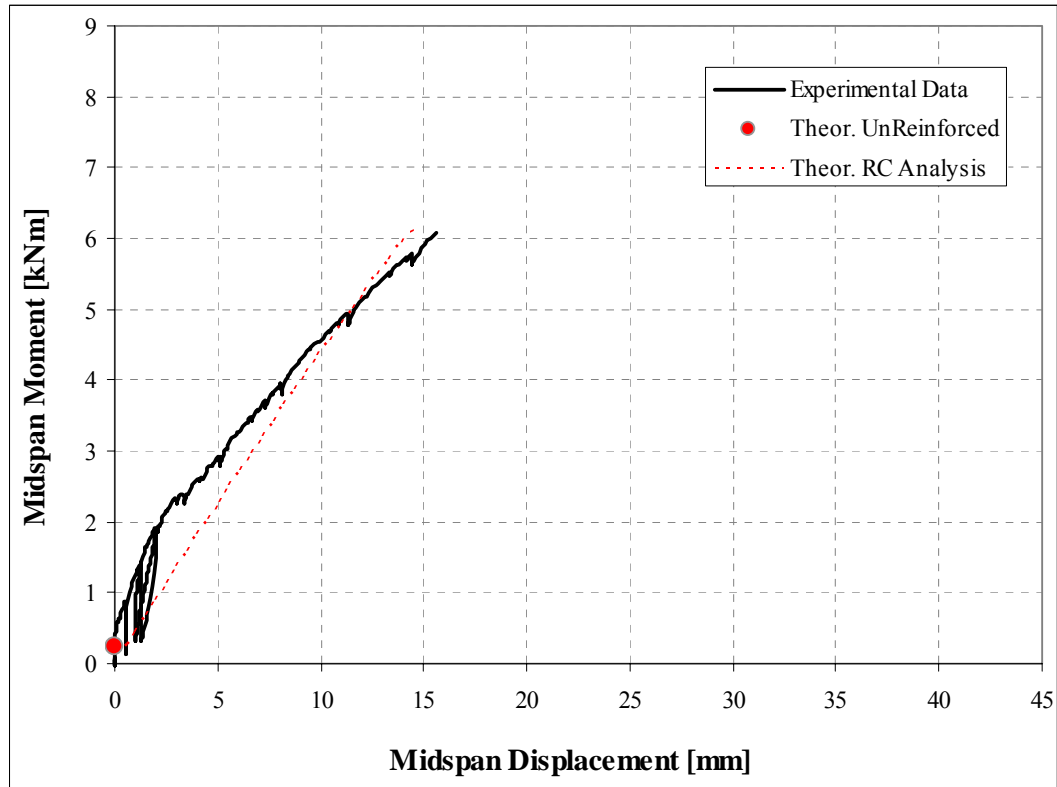
<b>cob-C3-2b</b> As=168.7mm <sup>2</sup> f <sub>c</sub> =9.74MPa	P-failure-exp [kN] =	<b>14.99</b>	M-fail [kNm]	<b>3.43</b>	V-fail [kN]=	<b>7.5</b>
	failure mode	debonding	theor. $\epsilon - c - f - \epsilon/\epsilon_u$ at failure	$\epsilon_c = 0.00140$ $f_f = 276 \text{ MPa}$	$\epsilon_f = 0.0060$ $\epsilon/\epsilon_u = 0.35$	
Max theor. Moment [kNm]		<b>5.19</b>	$\epsilon_f = 0.0092$	$\epsilon_c = 0.0025$	M <sub>exp</sub> /M <sub>theor.</sub>	<b>0.66</b>

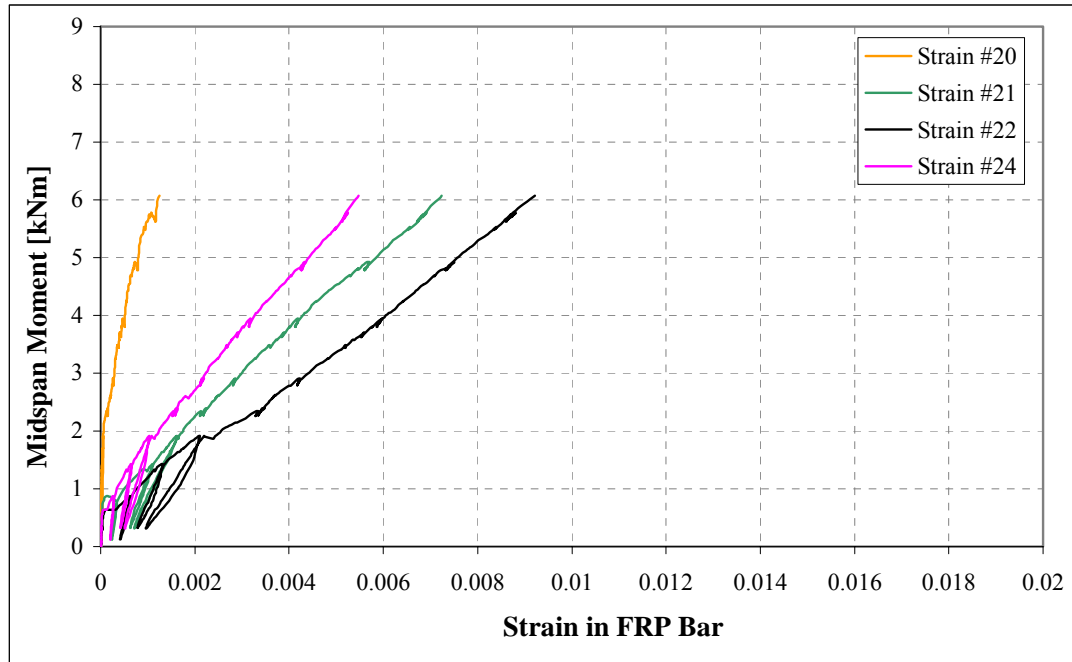




**cob-C3-3b:**

<b>cob-C3-3b</b> As=253.0mm <sup>2</sup> f <sub>c</sub> =9.74MPa	P-failure-exp [kN] =	<b>26.56</b>	M-fail [kNm]	<b>6.07</b>	V-fail [kN]=	<b>13.3</b>
	failure mode	<i>debonding</i>	theor. $\epsilon - c - f -$ $\epsilon/\epsilon_u$ at failure	$\epsilon_c = 0.00249$ $f_f = 337 \text{ MPa}$	$\epsilon_f = 0.0073$ $\epsilon/\epsilon_u = 0.43$	
Max theor. Moment [kNm]		<b>6.08</b>	$\epsilon_f = 0.0074$	$\epsilon_c = 0.0025$	M <sub>exp</sub> /M <sub>theor.</sub>	<b>1.00</b>

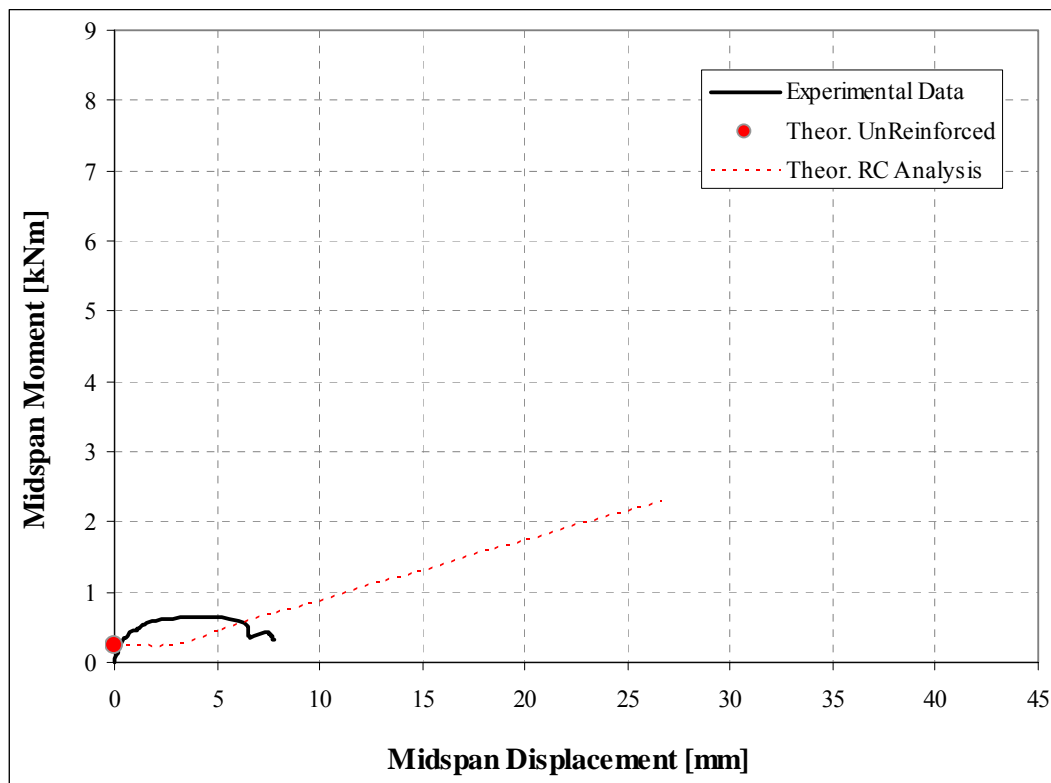


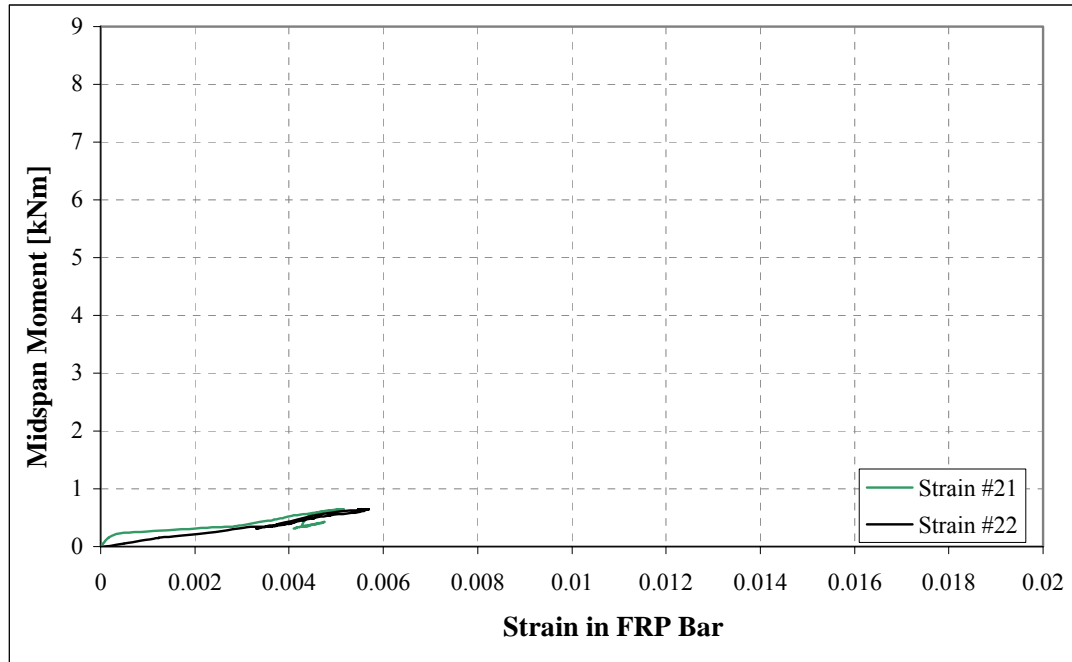


**cob-E2-1c:**

<b>cob-E2-1c</b> As=33.2mm <sup>2</sup> f <sub>c</sub> =9.74MPa	P-failure-exp [kN]=	<b>2.84</b>	M-fail [kNm]	<b>0.65+0.16*</b>	V-fail [kN]=	<b>1.42</b>
	failure mode	debonding	theor. $\epsilon - c - f - \epsilon/\epsilon_u$ at failure	$\epsilon_c = 0.00053$ f <sub>f</sub> = 288 MPa	$\epsilon_f = 0.00625$ $\epsilon/\epsilon_u = 0.37$	
Max theor. Moment [kNm]		<b>2.18</b>	$\epsilon_f = 0.017$	$\epsilon_c = 0.0016$	M <sub>exp</sub> /M <sub>theor.</sub>	<b>0.37</b>

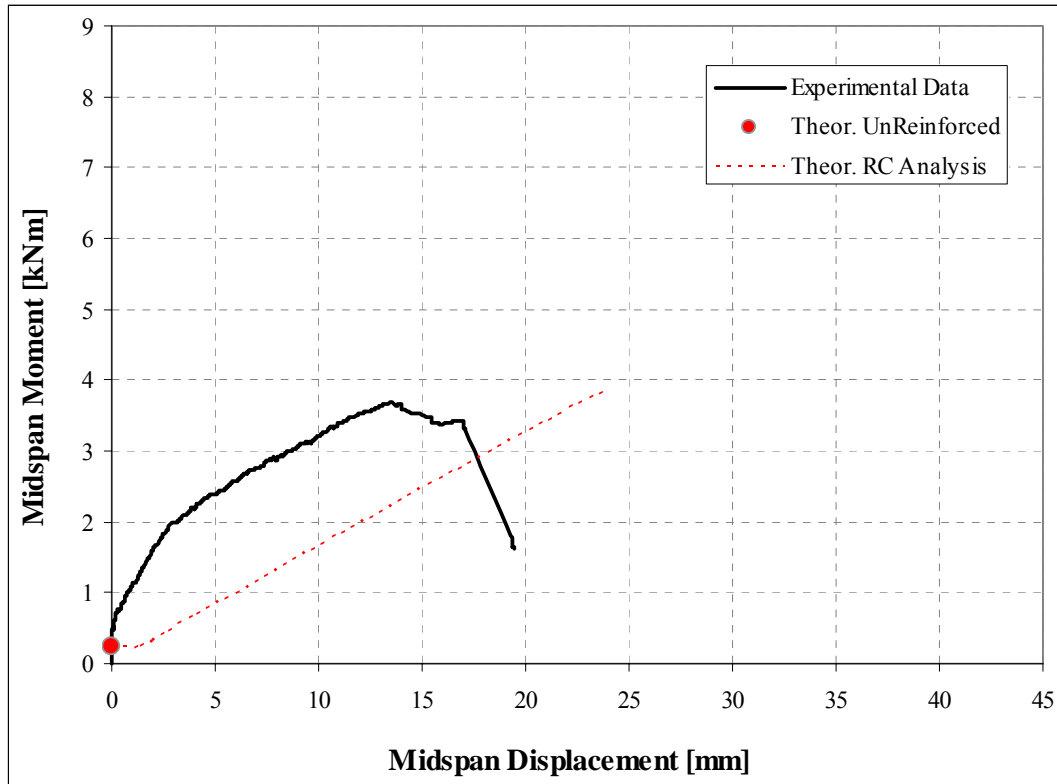
- 0.16 kNm is the estimated moment in midspan due to the own weight

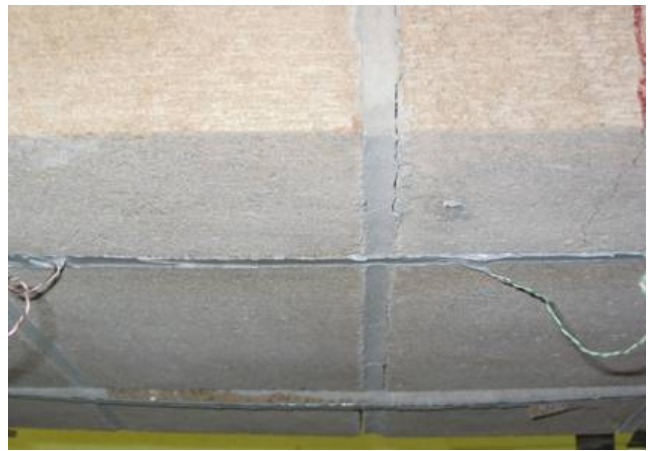
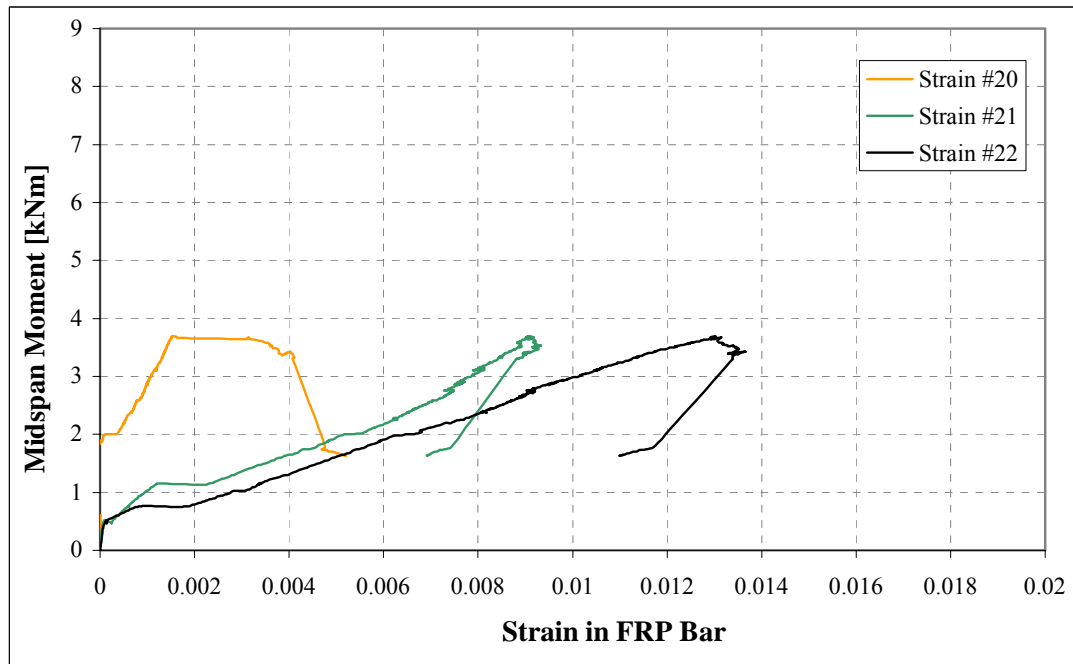




**cob-E2-2c:**

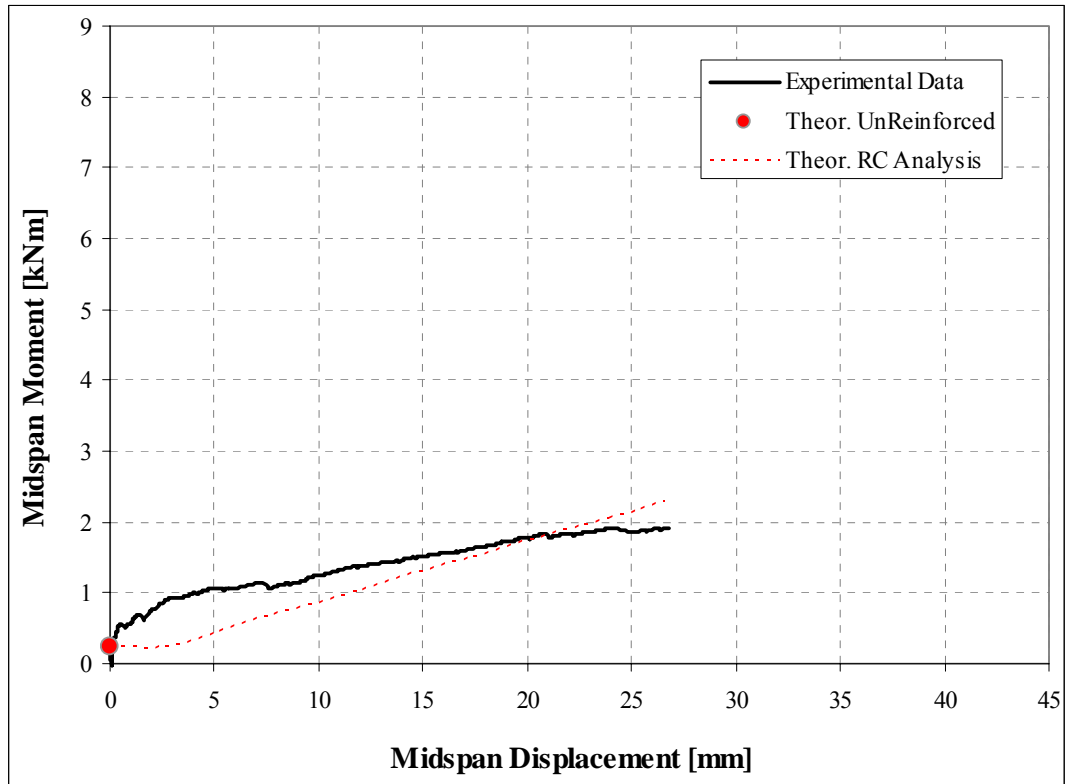
<b>cob-E2-2c</b> As=66.5mm <sup>2</sup> f <sub>c</sub> =9.74MPa	P-failure-exp [KN]=	<b>16.16</b>	M-fail [KNm]	<b>3.69</b>	V-fail [KN]=	<b>8.08</b>
	failure mode	debonding	theor. $\epsilon - c - f - \epsilon/\epsilon_u$ at failure	$\epsilon_c = 0.00216$ f <sub>f</sub> = 675 MPa	$\epsilon_f = 0.0147$ $\epsilon/\epsilon_u = 0.86$	
Max theor. Moment [kNm]		<b>4.05</b>	$\epsilon_f = 0.016$	$\epsilon_c = 0.0025$	M <sub>exp</sub> /M <sub>theor.</sub>	<b>0.91</b>

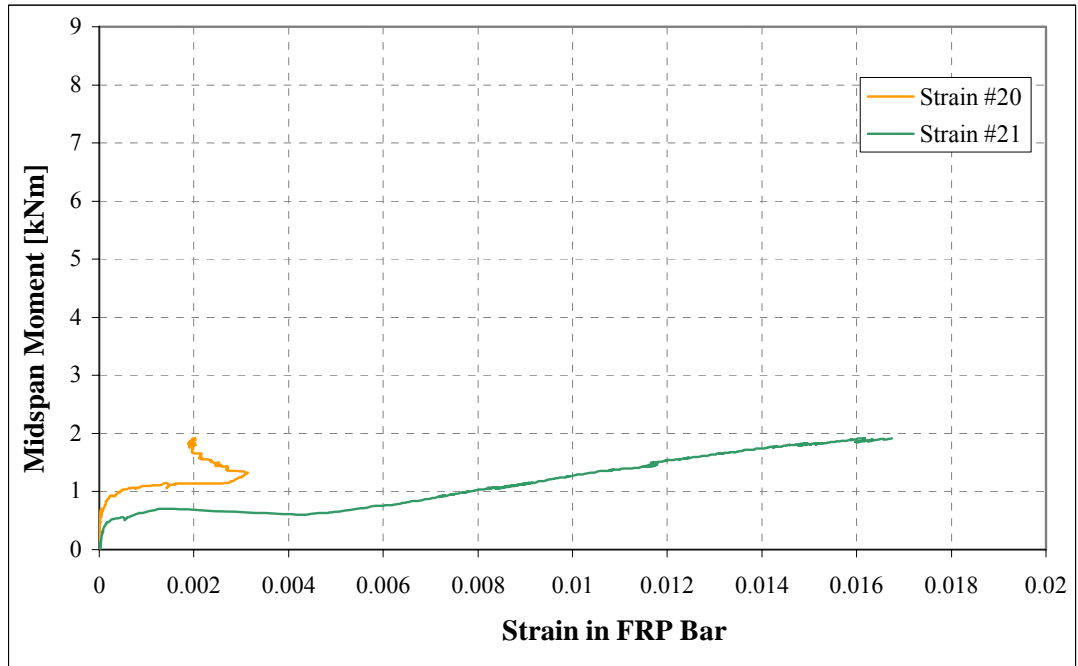




**cob-E2-1d:**

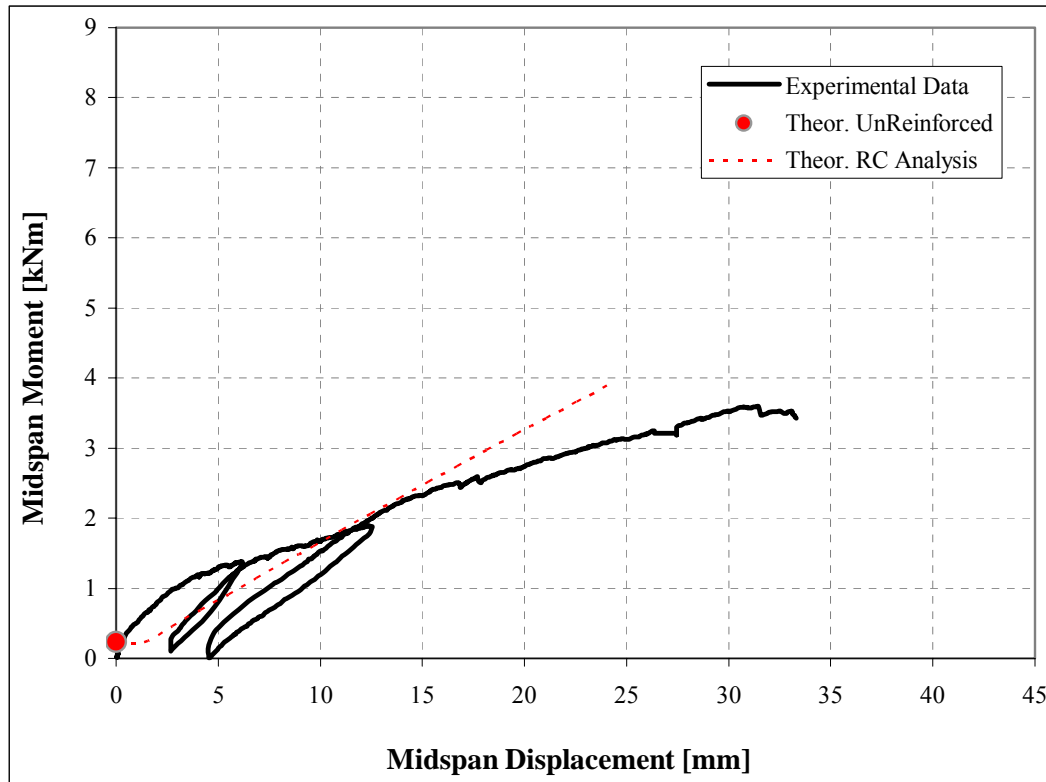
<b>cob-E2-1d</b> As=33.2mm <sup>2</sup> f <sub>c</sub> =9.74MPa	P-failure-exp [kN] =	<b>8.36</b>	M-fail [kNm]	<b>1.91</b>	V-fail [kN]=	<b>4.18</b>
	failure mode	<i>flexural failure (frp)</i>	<i>theor. <math>\epsilon - c - f - \epsilon/\epsilon_u</math> at failure</i>	$\epsilon_c = 0.00138$ $f_f = 685 \text{ MPa}$	$\epsilon_f = 0.0149$ $\epsilon/\epsilon_u = 0.88$	
Max theor. Moment [kNm]		<b>2.18</b>	$\epsilon_f = 0.017$	$\epsilon_c = 0.0016$	M <sub>exp</sub> /M <sub>theor.</sub>	<b>0.88</b>

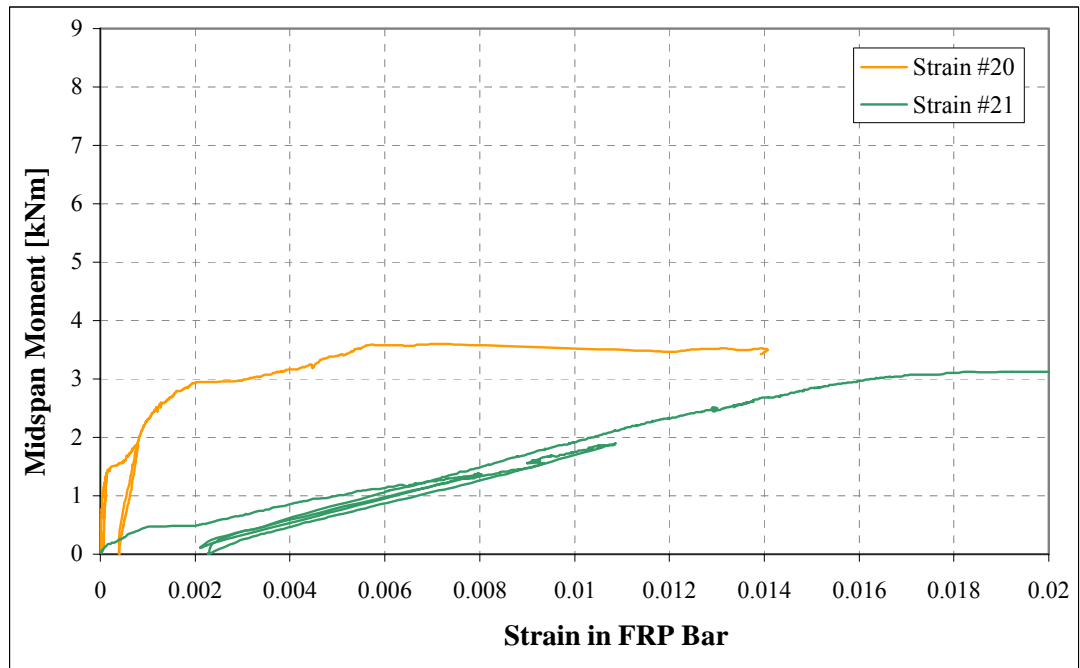




**cob-E2-2d:**

<b>cob-E2-2d</b> As=66.5mm <sup>2</sup> f <sub>c</sub> =9.74MPa	P-failure-exp [kN] =	<b>15.75</b>	M-fail [kNm]	<b>3.60</b>	V-fail [kN]=	<b>7.88</b>
	failure mode	<i>flexural failure (frp)</i>	<i>theor. <math>\epsilon - c - f - \epsilon/\epsilon_u</math> at failure</i>	$\epsilon_c = 0.00208$ $f_f = 658 \text{ MPa}$	$\epsilon_f = 0.0143$ $\epsilon/\epsilon_u = 0.84$	
Max theor. Moment [kNm]		<b>4.05</b>	$\epsilon_f = 0.016$	$\epsilon_c = 0.0025$	M <sub>exp</sub> /M <sub>theor.</sub>	<b>0.89</b>





**Previous tests (Morbin 01, Turco 02):**

Concrete walls strengthened with G-FRP rods embedded in Epoxy Paste

<b>cob-E2-2</b> As=66.5mm <sup>2</sup> f <sub>c</sub> =9.74MPa	P-failure-exp [KN] =	<b>7.38</b>	M-fail [KNm]	<b>1.69</b>	V-fail [KN]=	<b>3.69</b>
	failure mode	<i>debonding</i>	<i>theor. <math>\varepsilon - c - f - \varepsilon/\varepsilon_u</math> at failure</i>	$\varepsilon_c = 0.00083$ $f_f = 306 \text{ MPa}$	$\varepsilon_f = 0.0067$ $\varepsilon/\varepsilon_u = 0.39$	
Max theor. Moment [kNm]		<b>4.05</b>	$\varepsilon_f = 0.016$	$\varepsilon_c = 0.0025$	M <sub>exp</sub> /M <sub>theor.</sub>	<b>0.42</b>
<b>cob-E2-3</b> As=99.7 mm <sup>2</sup> f <sub>c</sub> =9.74MPa	P-failure-exp [KN] =	<b>9.91</b>	M-fail [KNm]	<b>2.27</b>	V-fail [KN]=	<b>4.96</b>
	failure mode	<i>deb.- sl. shear</i>	<i>theor. <math>\varepsilon - c - f - \varepsilon/\varepsilon_u</math> at failure</i>	$\varepsilon_c = 0.00095$ $f_f = 276 \text{ MPa}$	$\varepsilon_f = 0.0060$ $\varepsilon/\varepsilon_u = 0.354$	
Max theor. Moment [kNm]		<b>4.83</b>	$\varepsilon_f = 0.013$	$\varepsilon_c = 0.0025$	M <sub>exp</sub> /M <sub>theor.</sub>	<b>0.47</b>
<b>cob-E3-1</b> As=84.3mm <sup>2</sup> f <sub>c</sub> =9.74MPa	P-failure-exp [KN] =	<b>6.85</b>	M-fail [KNm]	<b>1.57</b>	V-fail [KN]=	<b>3.43</b>
	failure mode	<i>deb.- sl. shear</i>	<i>theor. <math>\varepsilon - c - f - \varepsilon/\varepsilon_u</math> at failure</i>	$\varepsilon_c = 0.00072$ $f_f = 232 \text{ MPa}$	$\varepsilon_f = 0.00504$ $\varepsilon/\varepsilon_u = 0.296$	
Max theor. Moment [kNm]		<b>4.25</b>	$\varepsilon_f = 0.014$	$\varepsilon_c = 0.0025$	M <sub>exp</sub> /M <sub>theor.</sub>	<b>0.37</b>
<b>cob-E3-2</b> As=168.7mm <sup>2</sup> f <sub>c</sub> =9.74MPa	P-failure-exp [KN] =	<b>17.21</b>	M-fail [KNm]	<b>3.934</b>	V-fail [KN]=	<b>8.605</b>
	failure mode	<i>she.+deb.</i>	<i>theor. <math>\varepsilon - c - f - \varepsilon/\varepsilon_u</math> at failure</i>	$\varepsilon_c = 0.00148$ $f_f = 299 \text{ MPa}$	$\varepsilon_f = 0.00651$ $\varepsilon/\varepsilon_u = 0.383$	
Max theor. Moment [kNm]		<b>5.67</b>	$\varepsilon_f = 0.0095$	$\varepsilon_c = 0.0025$	M <sub>exp</sub> /M <sub>theor.</sub>	<b>0.694</b>
<b>cob-E3-3</b> As=253 mm <sup>2</sup> f <sub>c</sub> =9.74MPa	P-failure-exp [KN] =	<b>24.36</b>	M-fail [KNm]	<b>5.569</b>	V-fail [KN]=	<b>12.18</b>
	failure mode	<i>she.+deb.</i>	<i>theor. <math>\varepsilon - c - f - \varepsilon/\varepsilon_u</math> at failure</i>	$\varepsilon_c = 0.00189$ $f_f = 288 \text{ MPa}$	$\varepsilon_f = 0.00627$ $\varepsilon/\varepsilon_u = 0.369$	
Max theor. Moment [kNm]		<b>6.65</b>	$\varepsilon_f = 0.0076$	$\varepsilon_c = 0.0025$	M <sub>exp</sub> /M <sub>theor.</sub>	<b>0.837</b>

Concrete walls strengthened with G-FRP rods embedded in Cementitious Paste

<b>cob-C2-2b</b> As=66.5 mm <sup>2</sup> f <sub>c</sub> =9.74MPa	P-failure-exp [KN] =	<b>9.03</b>	M-fail [KNm]	<b>2.064</b>	V-fail [KN]=	<b>4.46</b>
	failure mode	<i>deb.</i>	<i>theor. <math>\varepsilon - c - f - \varepsilon/\varepsilon_u</math> at failure</i>	$\varepsilon_c = 0.00104$ $f_f = 374 \text{ MPa}$	$\varepsilon_f = 0.00813$ $\varepsilon/\varepsilon_u = 0.478$	
Max theor. Moment [kNm]		<b>4.05</b>	$\varepsilon_f = 0.016$	$\varepsilon_c = 0.0025$	M <sub>exp</sub> /M <sub>theor.</sub>	<b>0.510</b>
<b>cob-C2-3b</b> As=99.7 mm <sup>2</sup> f <sub>c</sub> =9.74MPa	P-failure-exp [KN] =	<b>12.81</b>	M-fail [KNm]	<b>2.928</b>	V-fail [KN]=	<b>6.405</b>
	failure mode	<i>deb.</i>	<i>theor. <math>\varepsilon - c - f - \varepsilon/\varepsilon_u</math> at failure</i>	$\varepsilon_c = 0.00127$ $f_f = 357 \text{ MPa}$	$\varepsilon_f = 0.00777$ $\varepsilon/\varepsilon_u = 0.457$	
Max theor. Moment [kNm]		<b>4.83</b>	$\varepsilon_f = 0.013$	$\varepsilon_c = 0.0025$	M <sub>exp</sub> /M <sub>theor.</sub>	<b>0.606</b>
<b>cob-C3-1</b> As=84.3 mm <sup>2</sup> f <sub>c</sub> =9.74MPa	P-failure-exp [KN] =	<b>4.35</b>	M-fail [KNm]	<b>0.994</b>	V-fail [KN]=	<b>2.175</b>
	failure mode	<i>deb.</i>	<i>theor. <math>\varepsilon - c - f - \varepsilon/\varepsilon_u</math> at failure</i>	$\varepsilon_c = 0.00045$ $f_f = 147 \text{ MPa}$	$\varepsilon_f = 0.00320$ $\varepsilon/\varepsilon_u = 0.188$	
Max theor. Moment [kNm]		<b>4.25</b>	$\varepsilon_f = 0.0139$	$\varepsilon_c = 0.0025$	M <sub>exp</sub> /M <sub>theor.</sub>	<b>0.234</b>
<b>cob-C3-2</b> As=168.7 mm <sup>2</sup> f <sub>c</sub> =9.74MPa	P-failure-exp [KN] =	<b>7.16</b>	M-fail [KNm]	<b>1.637</b>	V-fail [KN]=	<b>3.58</b>
	failure mode	<i>deb.</i>	<i>theor. <math>\varepsilon - c - f - \varepsilon/\varepsilon_u</math> at failure</i>	$\varepsilon_c = 0.00055$ $f_f = 123 \text{ MPa}$	$\varepsilon_f = 0.00268$ $\varepsilon/\varepsilon_u = 0.158$	
Max theor. Moment [kNm]		<b>5.67</b>	$\varepsilon_f = 0.013$	$\varepsilon_c = 0.0025$	M <sub>exp</sub> /M <sub>theor.</sub>	<b>0.289</b>

## Concrete walls strengthened with G-FRP laminates

<b>cob-gl-3</b> As=27.1 mm <sup>2</sup> f <sub>c</sub> =9.74MPa	P-failure-exp [KN] =	<b>8.66</b>	M-fail [kNm]	<b>1.98</b>	V-fail [KN]=	<b>4.33</b>
	<i>failure mode</i>	<i>deb.</i>	<i>theor. <math>\varepsilon - c - f -</math> <math>\varepsilon/\varepsilon_u</math> at failure</i>	$\varepsilon_c = 0.00103$ $f_f = 813 \text{ MPa}$	$\varepsilon_f = 0.00980$ $\varepsilon/\varepsilon_u = 0.544$	
Max theor. Moment [kNm]		<b>3.61</b>	$\varepsilon_f = 0.018$	$\varepsilon_c = 0.0022$	M <sub>exp./M<sub>theor.</sub></sub>	<b>0.548</b>
<b>cob-gl-3r</b> As=27.1 mm <sup>2</sup> f <sub>c</sub> =9.74MPa	P-failure-exp [KN] =	<b>11.84</b>	M-fail [kNm]	<b>2.71</b>	V-fail [KN]=	<b>5.92</b>
	<i>failure mode</i>	<i>deb.</i>	<i>theor. <math>\varepsilon - c - f -</math> <math>\varepsilon/\varepsilon_u</math> at failure</i>	$\varepsilon_c = 0.00148$ $f_f = 1115 \text{ MPa}$	$\varepsilon_f = 0.01344$ $\varepsilon/\varepsilon_u = 0.747$	
Max theor. Moment [kNm]		<b>3.61</b>	$\varepsilon_f = 0.018$	$\varepsilon_c = 0.0022$	M <sub>exp./M<sub>theor.</sub></sub>	<b>0.751</b>
<b>cob-gl-5</b> As=45.2 mm <sup>2</sup> f <sub>c</sub> =9.74MPa	P-failure-exp [KN] =	<b>14.15</b>	M-fail [kNm]	<b>3.23</b>	V-fail [KN]=	<b>7.08</b>
	<i>failure mode</i>	<i>deb.</i>	<i>theor. <math>\varepsilon - c - f -</math> <math>\varepsilon/\varepsilon_u</math> at failure</i>	$\varepsilon_c = 0.00139$ $f_f = 805 \text{ MPa}$	$\varepsilon_f = 0.00970$ $\varepsilon/\varepsilon_u = 0.539$	
Max theor. Moment [kNm]		<b>4.96</b>	$\varepsilon_f = 0.015$	$\varepsilon_c = 0.0025$	M <sub>exp./M<sub>theor.</sub></sub>	<b>0.651</b>
<b>cob-gl-5r</b> As=45.2 mm <sup>2</sup> f <sub>c</sub> =9.74MPa	P-failure-exp [KN] =	<b>14.56</b>	M-fail [kNm]	<b>3.33</b>	V-fail [KN]=	<b>7.28</b>
	<i>failure mode</i>	<i>deb.</i>	<i>theor. <math>\varepsilon - c - f -</math> <math>\varepsilon/\varepsilon_u</math> at failure</i>	$\varepsilon_c = 0.00144$ $f_f = 829 \text{ MPa}$	$\varepsilon_f = 0.01001$ $\varepsilon/\varepsilon_u = 0.556$	
Max theor. Moment [kNm]		<b>4.96</b>	$\varepsilon_f = 0.015$	$\varepsilon_c = 0.0025$	M <sub>exp./M<sub>theor.</sub></sub>	<b>0.671</b>
<b>cob-gl-7</b> As=63.2 mm <sup>2</sup> f <sub>c</sub> =9.74MPa	P-failure-exp [KN] =	<b>15.78</b>	M-fail [kNm]	<b>3.61</b>	V-fail [KN]=	<b>7.89</b>
	<i>failure mode</i>	<i>deb.</i>	<i>theor. <math>\varepsilon - c - f -</math> <math>\varepsilon/\varepsilon_u</math> at failure</i>	$\varepsilon_c = 0.00133$ $f_f = 648 \text{ MPa}$	$\varepsilon_f = 0.00781$ $\varepsilon/\varepsilon_u = 0.434$	
Max theor. Moment [kNm]		<b>5.72</b>	$\varepsilon_f = 0.0125$	$\varepsilon_c = 0.0025$	M <sub>exp./M<sub>theor.</sub></sub>	<b>0.631</b>
<b>cob-gl-9</b> As=81.3 mm <sup>2</sup> f <sub>c</sub> =9.74MPa	P-failure-exp [KN] =	<b>21.95</b>	M-fail [kNm]	<b>5.02</b>	V-fail [KN]=	<b>10.98</b>
	<i>failure mode</i>	<i>deb.-she.</i>	<i>theor. <math>\varepsilon - c - f -</math> <math>\varepsilon/\varepsilon_u</math> at failure</i>	$\varepsilon_c = 0.00176$ $f_f = 708 \text{ MPa}$	$\varepsilon_f = 0.00854$ $\varepsilon/\varepsilon_u = 0.474$	
Max theor. Moment [kNm]		<b>6.36</b>	$\varepsilon_f = 0.0109$	$\varepsilon_c = 0.0025$	M <sub>exp./M<sub>theor.</sub></sub>	<b>0.789</b>
<b>cob-gl-12</b> As=108.4 mm <sup>2</sup> f <sub>c</sub> =9.74MPa	P-failure-exp [KN] =	<b>25.62</b>	M-fail [kNm]	<b>5.86</b>	V-fail [KN]=	<b>12.81</b>
	<i>failure mode</i>	<i>shear</i>	<i>theor. <math>\varepsilon - c - f -</math> <math>\varepsilon/\varepsilon_u</math> at failure</i>	$\varepsilon_c = 0.00184$ $f_f = 627 \text{ MPa}$	$\varepsilon_f = 0.00755$ $\varepsilon/\varepsilon_u = 0.419$	
Max theor. Moment [kNm]		<b>7.15</b>	$\varepsilon_f = 0.0093$	$\varepsilon_c = 0.0025$	M <sub>exp./M<sub>theor.</sub></sub>	<b>0.820</b>

## Concrete walls strengthened with A-FRP laminates

<b>cob-al-3</b> As=21.3 mm <sup>2</sup> f <sub>c</sub> =9.74MPa	P-failure-exp [KN] =	<b>11.69</b>	M-fail [kNm]	<b>2.67</b>	V-fail [KN]=	<b>5.84</b>
	<i>failure mode</i>	<i>deb.</i>	<i>theor. <math>\varepsilon - c - f -</math> <math>\varepsilon/\varepsilon_u</math> at failure</i>	$\varepsilon_c = 0.00135$ $f_f = 1401 \text{ MPa}$	$\varepsilon_f = 0.01158$ $\varepsilon/\varepsilon_u = 0.724$	
Max theor. Moment [kNm]		<b>3.67</b>	$\varepsilon_f = 0.016$	$\varepsilon_c = 0.0020$	M <sub>exp./M<sub>theor.</sub></sub>	<b>0.727</b>
<b>cob-al-5</b> As=35.5 mm <sup>2</sup> f <sub>c</sub> =9.74MPa	P-failure-exp [KN] =	<b>14.83</b>	M-fail [kNm]	<b>3.39</b>	V-fail [KN]=	<b>7.42</b>
	<i>failure mode</i>	<i>deb.</i>	<i>theor. <math>\varepsilon - c - f -</math> <math>\varepsilon/\varepsilon_u</math> at failure</i>	$\varepsilon_c = 0.00137$ $f_f = 1079 \text{ MPa}$	$\varepsilon_f = 0.00891$ $\varepsilon/\varepsilon_u = 0.557$	
Max theor. Moment [kNm]		<b>5.25</b>	$\varepsilon_f = 0.014$	$\varepsilon_c = 0.0025$	M <sub>exp./M<sub>theor.</sub></sub>	<b>0.646</b>

<b>cob-al-7</b> As=49.7 mm <sup>2</sup> f <sub>c</sub> =9.74MPa	P-failure-exp [KN] =	<b>19.73</b>	M-fail [KNm]	<b>4.51</b>	V-fail [KN]=	<b>9.87</b>
	<i>failure mode</i>	<i>deb.-she.</i>	<i>theor. <math>\varepsilon - c - f - \varepsilon/\varepsilon_u</math> at failure</i>	$\varepsilon_c = 0.00163$ $f_f = 1037 \text{ MPa}$	$\varepsilon_f = 0.00857$ $\varepsilon/\varepsilon_u = 0.536$	
Max theor. Moment [kNm]		<b>6.06</b>	$\varepsilon_f = 0.014$	$\varepsilon_c = 0.0025$	M <sub>exp</sub> /M <sub>theor.</sub>	<b>0.744</b>
<b>cob-al-9</b> As=63.9 mm <sup>2</sup> f <sub>c</sub> =9.74MPa	P-failure-exp [KN] =	<b>22.18</b>	M-fail [KNm]	<b>5.07</b>	V-fail [KN]=	<b>11.1</b>
	<i>failure mode</i>	<i>she.</i>	<i>theor. <math>\varepsilon - c - f - \varepsilon/\varepsilon_u</math> at failure</i>	$\varepsilon_c = 0.00165$ $f_f = 913 \text{ MPa}$	$\varepsilon_f = 0.00755$ $\varepsilon/\varepsilon_u = 0.472$	
Max theor. Moment [kNm]		<b>6.72</b>	$\varepsilon_f = 0.010$	$\varepsilon_c = 0.0025$	M <sub>exp</sub> /M <sub>theor.</sub>	<b>0.754</b>
<b>cob-al-12</b> As=85.2 mm <sup>2</sup> f <sub>c</sub> =9.74MPa	P-failure-exp [KN] =	<b>26.98</b>	M-fail [KNm]	<b>6.17</b>	V-fail [KN]=	<b>13.5</b>
	<i>failure mode</i>	<i>she.</i>	<i>theor. <math>\varepsilon - c - f - \varepsilon/\varepsilon_u</math> at failure</i>	$\varepsilon_c = 0.00183$ $f_f = 843 \text{ MPa}$	$\varepsilon_f = 0.00698$ $\varepsilon/\varepsilon_u = 0.436$	
Max theor. Moment [kNm]		<b>7.55</b>	$\varepsilon_f = 0.0086$	$\varepsilon_c = 0.0025$	M <sub>exp</sub> /M <sub>theor.</sub>	<b>0.817</b>

## Clay walls strengthened with G-FRP laminates

<b>cl3-gl-3</b> As=27.1 mm <sup>2</sup> f <sub>c</sub> =17.2 MPa	P-failure-exp [KN] =	<b>15.87</b>	M-fail [KNm]	<b>3.628</b>	V-fail [KN]=	<b>7.94</b>
	<i>failure mode</i>	<i>deb.</i>	<i>theor. <math>\varepsilon - c - f - \varepsilon/\varepsilon_u</math> at failure</i>	$\varepsilon_c = 0.00146$ $f_f = 1479 \text{ MPa}$	$\varepsilon_f = 0.01780$ $\varepsilon/\varepsilon_u = 0.989$	
Max theor. Moment [kNm]		<b>3.66</b>	$\varepsilon_f = 0.018$	$\varepsilon_c = 0.0015$	M <sub>exp</sub> /M <sub>theor.</sub>	<b>0.99</b>
<b>cl3-gl-3r</b> As=27.1 mm <sup>2</sup> f <sub>c</sub> =17.2 MPa	P-failure-exp [KN] =	<b>15.92</b>	M-fail [KNm]	<b>3.64</b>	V-fail [KN]=	<b>7.96</b>
	<i>failure mode</i>	<i>deb.</i>	<i>theor. <math>\varepsilon - c - f - \varepsilon/\varepsilon_u</math> at failure</i>	$\varepsilon_c = 0.00147$ $f_f = 1485 \text{ MPa}$	$\varepsilon_f = 0.0179$ $\varepsilon/\varepsilon_u = 0.994$	
Max theor. Moment [kNm]		<b>3.66</b>	$\varepsilon_f = 0.018$	$\varepsilon_c = 0.0015$	M <sub>exp</sub> /M <sub>theor.</sub>	<b>0.995</b>
<b>cl3-gl-5</b> As=45.2 mm <sup>2</sup> f <sub>c</sub> =17.2 MPa	P-failure-exp [KN] =	<b>20.18</b>	M-fail [KNm]	<b>4.61</b>	V-fail [KN]=	<b>10.1</b>
	<i>failure mode</i>	<i>deb.</i>	<i>theor. <math>\varepsilon - c - f - \varepsilon/\varepsilon_u</math> at failure</i>	$\varepsilon_c = 0.00146$ $f_f = 1136 \text{ MPa}$	$\varepsilon_f = 0.0137$ $\varepsilon/\varepsilon_u = 0.761$	
Max theor. Moment [kNm]		<b>6.03</b>	$\varepsilon_f = 0.018$	$\varepsilon_c = 0.0021$	M <sub>exp</sub> /M <sub>theor.</sub>	<b>0.764</b>
<b>cl3-gl-5r</b> As=45.2 mm <sup>2</sup> f <sub>c</sub> =17.2 MPa	P-failure-exp [KN] =	<b>21.51</b>	M-fail [KNm]	<b>4.92</b>	V-fail [KN]=	<b>10.8</b>
	<i>failure mode</i>	<i>frp rupt.</i>	<i>theor. <math>\varepsilon - c - f - \varepsilon/\varepsilon_u</math> at failure</i>	$\varepsilon_c = 0.00158$ $f_f = 1214 \text{ MPa}$	$\varepsilon_f = 0.0146$ $\varepsilon/\varepsilon_u = 0.811$	
Max theor. Moment [kNm]		<b>6.03</b>	$\varepsilon_f = 0.018$	$\varepsilon_c = 0.0021$	M <sub>exp</sub> /M <sub>theor.</sub>	<b>0.816</b>
<b>cl3-gl-7</b> As=63.2 mm <sup>2</sup> f <sub>c</sub> =17.2 MPa	P-failure-exp [KN] =	<b>27.62</b>	M-fail [KNm]	<b>6.314</b>	V-fail [KN]=	<b>13.8</b>
	<i>failure mode</i>	<i>deb.</i>	<i>theor. <math>\varepsilon - c - f - \varepsilon/\varepsilon_u</math> at failure</i>	$\varepsilon_c = 0.00180$ $f_f = 1122 \text{ MPa}$	$\varepsilon_f = 0.0135$ $\varepsilon/\varepsilon_u = 0.750$	
Max theor. Moment [kNm]		<b>8.32</b>	$\varepsilon_f = 0.018$	$\varepsilon_c = 0.0027$	M <sub>exp</sub> /M <sub>theor.</sub>	<b>0.759</b>
<b>cl3-gl-7r</b> As=63.2 mm <sup>2</sup> f <sub>c</sub> =17.2 MPa	P-failure-exp [KN] =	<b>29.84</b>	M-fail [KNm]	<b>6.82</b>	V-fail [KN]=	<b>14.9</b>
	<i>failure mode</i>	<i>deb.</i>	<i>theor. <math>\varepsilon - c - f - \varepsilon/\varepsilon_u</math> at failure</i>	$\varepsilon_c = 0.00200$ $f_f = 1215 \text{ MPa}$	$\varepsilon_f = 0.0146$ $\varepsilon/\varepsilon_u = 0.811$	
Max theor. Moment [kNm]		<b>8.32</b>	$\varepsilon_f = 0.018$	$\varepsilon_c = 0.0027$	M <sub>exp</sub> /M <sub>theor.</sub>	<b>0.819</b>
<b>cl3-gl-9</b> As=81.3 mm <sup>2</sup> f <sub>c</sub> =17.2 MPa	P-failure-exp [KN] =	<b>29.16</b>	M-fail [KNm]	<b>6.667</b>	V-fail [KN]=	<b>14.6</b>
	<i>failure mode</i>	<i>sl. she.</i>	<i>theor. <math>\varepsilon - c - f - \varepsilon/\varepsilon_u</math> at failure</i>	$\varepsilon_c = 0.00167$ $f_f = 925 \text{ MPa}$	$\varepsilon_f = 0.0112$ $\varepsilon/\varepsilon_u = 0.622$	
Max theor. Moment [kNm]		<b>10.1</b>	$\varepsilon_f = 0.0174$	$\varepsilon_c = 0.0035$	M <sub>exp</sub> /M <sub>theor.</sub>	<b>0.660</b>

<b>cl3-gl-12</b> As=108.4 mm <sup>2</sup> f <sub>c</sub> =17.2 MPa	P-failure-exp [KN] =	<b>26.0</b>	M-fail [kNm]	<b>5.944</b>	V-fail [KN]=	<b>13.0</b>
	<i>failure mode</i>	<i>sl. she.</i>	<i>theor. <math>\varepsilon - c - f - \varepsilon/\varepsilon_u</math> at failure</i>	$\varepsilon_c = 0.00124$ $f_f = 621 \text{ MPa}$	$\varepsilon_f = 0.0075$ $\varepsilon/\varepsilon_u = 0.417$	
Max theor. Moment [kNm]		<b>11.4</b>	$\varepsilon_f = 0.015$	$\varepsilon_c = 0.0035$	M <sub>exp</sub> /M <sub>theor.</sub>	<b>0.521</b>

## Clay walls strengthened with A-FRP laminates

<b>cl3-al-3</b> As=21.3 mm <sup>2</sup> f <sub>c</sub> =17.2 MPa	P-failure-exp [KN] =	<b>12.02</b>	M-fail [kNm]	<b>2.748</b>	V-fail [KN]=	<b>6.0</b>
	<i>failure mode</i>	<i>deb.</i>	<i>theor. <math>\varepsilon - c - f - \varepsilon/\varepsilon_u</math> at failure</i>	$\varepsilon_c = 0.0098$ $f_f = 1424 \text{ MPa}$	$\varepsilon_f = 0.0118$ $\varepsilon/\varepsilon_u = 0.738$	
Max theor. Moment [kNm]		<b>3.72</b>	$\varepsilon_f = 0.016$	$\varepsilon_c = 0.0014$	M <sub>exp</sub> /M <sub>theor.</sub>	<b>0.738</b>

<b>cl3-al-5</b> As=35.5 mm <sup>2</sup> f <sub>c</sub> =17.2 MPa	P-failure-exp [KN] =	<b>22.04</b>	M-fail [kNm]	<b>5.038</b>	V-fail [KN]=	<b>11.0</b>
	<i>failure mode</i>	<i>frp. rupt.</i>	<i>theor. <math>\varepsilon - c - f - \varepsilon/\varepsilon_u</math> at failure</i>	$\varepsilon_c = 0.0131$ $f_f = 1585 \text{ MPa}$	$\varepsilon_f = 0.0131$ $\varepsilon/\varepsilon_u = 0.819$	
Max theor. Moment [kNm]		<b>6.13</b>	$\varepsilon_f = 0.016$	$\varepsilon_c = 0.00195$	M <sub>exp</sub> /M <sub>theor.</sub>	<b>0.820</b>

<b>cl3-al-7</b> As=49.7 mm <sup>2</sup> f <sub>c</sub> =17.2 MPa	P-failure-exp [KN] =	<b>25.9</b>	M-fail [kNm]	<b>5.921</b>	V-fail [KN]=	<b>13.0</b>
	<i>failure mode</i>	<i>deb.</i>	<i>theor. <math>\varepsilon - c - f - \varepsilon/\varepsilon_u</math> at failure</i>	$\varepsilon_c = 0.0153$ $f_f = 1341 \text{ MPa}$	$\varepsilon_f = 0.0111$ $\varepsilon/\varepsilon_u = 0.694$	
Max theor. Moment [kNm]		<b>8.46</b>	$\varepsilon_f = 0.016$	$\varepsilon_c = 0.00253$	M <sub>exp</sub> /M <sub>theor.</sub>	<b>0.699</b>

<b>cl3-al-9</b> As=63.9 mm <sup>2</sup> f <sub>c</sub> =17.2 MPa	P-failure-exp [KN] =	<b>35.65</b>	M-fail [kNm]	<b>8.15</b>	V-fail [KN]=	<b>17.8</b>
	<i>failure mode</i>	<i>frp. rupt.</i>	<i>theor. <math>\varepsilon - c - f - \varepsilon/\varepsilon_u</math> at failure</i>	$\varepsilon_c = 0.0202$ $f_f = 1451 \text{ MPa}$	$\varepsilon_f = 0.0120$ $\varepsilon/\varepsilon_u = 0.750$	
Max theor. Moment [kNm]		<b>10.6</b>	$\varepsilon_f = 0.016$	$\varepsilon_c = 0.00338$	M <sub>exp</sub> /M <sub>theor.</sub>	<b>0.769</b>

<b>cl3-al-12</b> As=85.2 mm <sup>2</sup> f <sub>c</sub> =17.2 MPa	P-failure-exp [KN] =	<b>25.0</b>	M-fail [kNm]	<b>5.715</b>	V-fail [KN]=	<b>12.5</b>
	<i>failure mode</i>	<i>sl-she.</i>	<i>theor. <math>\varepsilon - c - f - \varepsilon/\varepsilon_u</math> at failure</i>	$\varepsilon_c = 0.0111$ $f_f = 762 \text{ MPa}$	$\varepsilon_f = 0.0063$ $\varepsilon/\varepsilon_u = 0.394$	
Max theor. Moment [kNm]		<b>12.0</b>	$\varepsilon_f = 0.0138$	$\varepsilon_c = 0.0035$	M <sub>exp</sub> /M <sub>theor.</sub>	<b>0.476</b>